Fully self-consistent multiparticle-multihole configuration mixing method : applications to a few light nuclei

Caroline Robin

Université Paris-Sud

École Doctorale 517 :
Particules, Noyaux et Cosmos
Laboratoire CEA,DAM,DIF

Discipline : Physique Nucléaire Théorique

Thèse de doctorat

Soutenue le 30 Septembre 2014 par

Caroline Robin

Fully self-consistent multiparticle-multihole configuration mixing method - Applications to a few light nuclei -

Composition du jury :

Directeur de thèse :	Dr. Marcella Grasso	Chargé de recherche CNRS, IPN Orsay
Co-directeur de thèse :	Dr. Nathalie Pillet	Ingénieur-chercheur CEA,DAM,DIF
Président :	Dr. Nguyen Van Giai	Directeur de recherche émérite CNRS, IPN Orsay
Rapporteurs :	Dr. Michael Bender	Directeur de recherche CNRS, CENBG Bordeaux
	Prof. Marek Ploszajczak	Professeur, directeur de recherche CEA, GANIL Caen
Examinateurs :	Dr. Frédéric Nowacki	Directeur de recherche CNRS, IPHC Strasbourg
	Prof. Vladimir Zelevinsky	Professeur, Michigan State University, USA

Remerciements

Je souhaite en premier lieu adresser mes remerciements les plus sincères à Nathalie Pillet, responsable et co-directrice de cette thèse. Je la remercie de m'avoir fait découvrir le domaine de la structure nucléaire théorique ainsi que des nombreuses connaissances qu'elle m'a apporté dans ce domaine. Le sujet de thèse extrêmement intéressant qu'elle m'a proposé m'a permis d'enrichir grandement mes compétences et surtout d'évoluer en tant que scientifique. Je la remercie pour son investissement énorme dans ce travail. Toujours à l'écoute, son implication n'a jamais faibli au cours de ces trois années. Le temps qu'elle a pris pour écouter et discuter des problèmes que j'ai pu rencontrer m'a le plus souvent permis de sortir de l'impasse. Je la remercie de ne pas avoir hésité à prendre sur son temps libre pour m'aider à finaliser mon manuscrit ainsi que ma soutenance, lorsque le stress était au plus haut. Je la remercie pour son dynamisme et son enthousiasme constant pour ce travail, ainsi que pour tous les encouragements qu'elle m'a prodigué. Ce fut pour moi un immense plaisir d'effectuer ces trois années de doctorat sous la responsabilité de Nathalie, en qui je reste extrêmement reconnaissante pour ce travail de thèse ainsi que pour son amitié.

Je remercie également tout particulièrement Daniel Peña Arteaga qui est arrivé en post-doc après ma première année de thèse. Il a été d'une aide immense sur de nombreux problèmes numériques. Également toujours disponible pour discuter de mon travail, il a su faire preuve d'une patience sans faille... ! Je le remercie pour tous ses précieux conseils. Je lui suis également très reconnaissante pour l'aide qu'il m'a apporté dans la finalisation de ma soutenance, même au dernier moment. Ses suggestions m'ont été grandement utiles.

Je souhaite aussi remercier Jean-François Berger qui a été d'un grand secours lors de cette thèse. Ses interventions, peu nombreuses mais d'une efficacité sans égale, m'ont permis de me sortir de situations que l'on pensait sans issue. Je doute que tous les résultats présentés dans cette thèse auraient pu aboutir sans son aide. Je le remercie également pour l'attention particulière qu'il a porté à mon manuscrit de thèse, ainsi que pour ses corrections et commentaires minutieux.

Merci à Julien Le Bloas, mon colocataire de bureau pendant deux ans, qui ne fut jamais remplacé. Il m'a notamment aidé dans mes premiers pas avec la programmation. Toujours de bonne humeur, ce fut un plaisir de travailler à ses côtés. Je le remercie également pour tous les outils qu'il a pu mettre en place durant son travail post-doctoral et qui ont grandement facilité l'aboutissement de certains résultats présentés dans ce manuscrit.

Je souhaite également remercier Marc Dupuis avec qui j'ai collaboré dans le cadre des calculs de réactions. Il a su m'aider efficacement pendant les derniers jours de rédaction de ma thèse pendant lesquels la tension était à son comble. Je le remercie également pour ses commentaires utiles concernant ma présentation de soutenance et sa disponibilité pour répondre à mes questions.

Un grand merci à Marcella Grasso d'avoir si gentiment accepté de remplir le rôle de directrice de thèse officielle. Je la remercie pour sa disponibilité et son soutien.

Je suis tout particulièrement redevable à Vladimir Zelevinsky, sans qui je n'aurais sans doute jamais effectué cette thèse. Je le remercie pour son accueil toujours chaleureux à Michigan State University et pour m'avoir fait profiter de son immense puits de savoir. Je le remercie également d'avoir accepté d'examiner ma thèse et de l'attention minutieuse qu'il y a porté.

Je remercie également les autres membres de mon jury de thèse. Merci à Nguyen Van Giai pour avoir accepté de présider ma soutenance, pour l'intérêt qu'il a porté à mon travail et les discussions que nous avons eu, ainsi que pour sa disponibilité et son aide regardant les formalités administratives. Je remercie Michael Bender et Marek Ploszajczak d'avoir rapporté mon travail ainsi que Frédéric Nowacki de l'avoir examiné. Leurs commentaires et corrections, ainsi que les discussions que l'on a pu avoir, ont été grandement utiles pour finaliser la dernière version de mon manuscrit.

Un grand merci à l'ensemble de mes collègues à Buyères-le-Châtel. Ce fut un plaisir d'y passer ces trois dernières années, dans une ambiance toujours agréable, au sein de thésards, post-docs et permanents, théoriciens, expérimentateurs et autres.

Je remercie évidemment ma famille, mon frère et mes parents pour leurs encouragements.

Pour finir, un grand merci à Sören pour son soutien au cours de ces trois années, et pour les précieux conseils qu'il m'a apporté.

Contents

Chapter I

Introduction

The atomic nucleus is one of the most complex and challenging quantum many-body system. It is composed of two types of nucleons (protons and neutrons), themselves made of internal quarks and gluons, and brings into play no less than three of the four fundamental interactions: the dominating strong force, leading to the binding of nucleons into nuclei, as well as the electromagnetic interaction (mostly the Coulomb force acting between protons) and the weak interaction responsible for the β-decay of some exotic nuclei. As they comprise a rather small number of nucleons ($2 \leqslant A \lesssim 350$), finite-size effects also play a central role in nuclei. Different combinations of proton and neutron numbers can thus lead to very different and rich phenomena in both the structure (shapes, neutron skins, nucleon clusters or halos...) and the excitation modes of nuclei (such as collective vibrations or rotations).
One of the main goal of low-energy nuclear physics is to understand how protons and neutrons interact and bind inside the nucleus, in order to describe and predict different properties of the many-body nuclear system. This task is usually tackled with the use of several assumptions. In particular,

- The typical energy scales of the nucleus are of the order of ~ 10 MeV, which is much lower than the energy necessary to explore the quark structure of the nucleons (~ 1 GeV). Thus, one usually makes use of this "separation of scales" and considers the nucleons as the relevant degrees of freedom for the study of nuclear structure. The protons and neutrons are therefore regarded as point-like particles interacting by means of a nuclear potential which incorporates the effect of the internal structure of the nucleons.

- Since the typical velocities of nucleons in the nucleus are rather small compared to the speed of light $\left(\frac{v}{c}\right)^2 \sim 0.1$, it is of common use to neglect any relativistic effects.

With these hypotheses, the equation governing the structure properties of the many-body system which one aims to describe is the (time-independent) Schrödinger equation,

$$\hat{H} \left|\Psi_M\right\rangle = E_M \left|\Psi_M\right\rangle \ , \tag{I.1}$$

where $\hat{H} = \hat{K} + \hat{V}$ is the many-body Hamiltonian, sum of the non-relativistic kinetic energy $\hat{K}$ and the interaction potential $\hat{V}$. The state $|\Psi_M\rangle$ is an eigenvector of $\hat{H}$, corresponding to a certain nuclear state with energy E_M.
Although the problem appears now quite simple, two major difficulties arise.

- The first one is due to the fact that the nuclear interaction acting between the nucleons is extremely complex and remains today partly unknown.

- The second challenge arises from the mesoscopic nature of atomic nuclei which comprises a number of nucleons that is of intermediate range ($2 \leqslant A \lesssim 350$). This feature prevents in most cases an exact solution of the many-body problem (too many particles), and forbids the use of statistical methods (too few particles).

Since protons and neutrons are composite particles, the inter-nucleon force is interpreted as the residual (colorless) interaction between their constituent quarks and gluons. The interaction between two nucleons in free space has the property of being extremely repulsive at short distance, and for that reason is referred as "hard-core potential". This pathological behavior makes difficult to handle such a "bare interaction" in many-body calculations, and in particular, prohibits the direct application of perturbation theory. An interesting fact is that the nuclear force is deeply modified in the presence of surrounding nucleons. One can incorporate these medium effects into an "effective interaction" which becomes well behaved and more suitable for practical calculations. The last obstacle to an accurate description of low-energy nuclear systems lies in the existence of many-nucleon forces which arise from the approximation of point-like nucleons. The treatment of three-body forces has been proven necessary to reproduce e.g. the triton binding energy (Tjon line) [80] and the saturation properties of nuclear matter. Higher-body forces appear much weaker and are usually not considered in modern approaches. There exists currently many different interactions on the market, bare or effective, microscopic or phenomenological.

Purely phenomenological approaches to bare interactions are based on the symmetry properties of the nucleon-nucleon potential. The analytical form is postulated *a priori* as a sum of terms (central, spin-orbit, tensors...) respecting several invariance properties of nature such as rotational, translational, time-reversal invariances and so on. Such potentials contain parameters that are fitted so that to reproduce nucleon-nucleon scattering data and several properties of the deuteron. For instance the Argonne V18 potential [107] is based on 18 operators and 40 parameters to fit.
Semi-phenomenological potentials based on the meson "theory" of nuclear forces also exist. This concept goes back to Yukawa (1935) who introduced the idea that the force acting between two nucleons would be carried by a meson with non-zero mass [110]. The latter was discovered in 1947 and named as pion (π). Development of realistic interactions based on one

boson-exchange models usually assume the long-range part of the nuclear force to be carried by the pion while heavier mesons contribute to the medium and short range parts. For example, the CD-Bonn potential [68] includes π, ρ, ω and σ mesons with 43 parameters to fit.
Since the discovery of asymptotic freedom in the early 1970's by Politzer, Wilczek and Gross [52, 87, 51], much evidence has been gathered proving that Quantum ChromoDynamics (QCD) is *the* theory of strong interactions. Hence, the goal nowadays is to develop microscopic nuclear forces from the first principles of this theory.

Ideally one could think of deriving the nuclear force directly from QCD, considering quark and gluon degrees of freedom. However due to the confinement properties of QCD, the strong coupling α_S drastically increases in the low-energy regime, where perturbation theory breaks down. Although much progress has been achieved these last few years in the context of non perturbative lattice QCD (see e.g.[95]), this field is currently in its early days and progress will greatly depend on future increase of computer resources.
Nowadays the most fundamental way to derive the nuclear force from first principles is based on Effective Field Theory (EFT), and more particularly Chiral Perturbation Theory [69, 37, 36]. This formalism, first initiated by Weinberg [105], exploits the fact that the relevant degrees of freedom at low energies are hadrons. In this context, nuclear forces are derived from an effective Lagrangian which keeps tracks of all symmetries of the underlying QCD. Spontaneous symmetry breaking of (approximate) chiral symmetry leads to the appearance of (pseudo-) Goldstone bosons, interpreted as pions. The Lagrangian can be expanded in powers of $\frac{Q}{\Lambda_\chi}$ where $Q \sim m_\pi$ represents the soft scale, and $\Lambda_\chi \sim 1$ GeV is the breakdown scale of the theory. One can then derive a NN potential order by order, up to a desired accuracy. Consistent three-body (and higher-body) forces also naturally emerge. In this framework, the high energy degrees of freedom are effectively taken into account via the presence of low-energy constants (LECs). Although these LECs are currently usually extracted from experimental data, the goal will be to derive them from lattice QCD calculations when numerical resources will permit it.

Bare interactions exhibits an extremely strong short-range component which can scatter nucleons into states with very high momentum, and thus can hardly be handled in many-body calculations where basis truncations are often necessary. There exists several ways of properly deriving effective interactions in which the high-momentum hard core has been resumed. Let us cite for instance the Brückner G-matrix theory [22, 27]. This formalism was first introduced to derive an effective interaction which would be suitable for perturbative calculations in nuclear structure. This is achieved by resumming the (non-perturbative) infinite serie of scattering processes onto intermediate states above the Fermi sea (so-called ladder diagrams), into an energy-dependent reaction matrix given by the Bethe-Goldstone equation [9]. This G-matrix can then be used as expansion parameter in e.g. a perturbation expansion of the

ground-state energy. The diagrams of this serie can be ordered according to the number of independent hole lines appearing (this is the so-called "hole expansion"). Alternatively, methods based on the renormalization group approach start from the idea that low-energy observables are not affected by the short-distance details of the potential. Following this idea, the goal is to decouple high and low momentum modes by integrating out these details, allowing for better convergence of many-body calculations. For instance, the $V_{low\,k}$ approach [15, 14] imposes a momentum cut-off Λ and resums the effect of high momentum modes into an effective interaction $V_{low\,k}$ which is obtained by requiring the scattering matrix T to be unchanged while Λ is lowered. This condition leads to an Renormalization Group equation which is integrated using the bare interaction V as initial condition. More recently the Similarity Renormalization Group (SRG) method has been applied to the nuclear interaction [12, 13]. The philosophy of this approach is to transform the Hamiltonian through successive unitary transformations in order to bring non-diagonal terms to zero.

However, deriving effective forces is a difficult task and phenomenological interactions are still widely used in nuclear physics calculations. These interactions are based on a postulated analytic form containing parameters that are fitted to reproduce experimental data within a certain many-body approach. In particular, the zero-range Skyrme interaction [98, 99] and the finite-range Gogny force [29] are the two most employed interactions in self-consistent mean-field calculations. Inspired from the G-matrix theory, their analytical from is taken as density-dependent.

The complexity of the nuclear interaction is only the first difficulty one is confronted with while studying the properties of atomic nuclei. Due to their mesoscopic nature, a unified description of the structure properties (size and deformation of ground states, individual or collective excitation modes...) of all nuclei (stable and exotic, open and closed shell) is extremely difficult to achieve and is yet to be reached. Roughly speaking, the existing many-body methods can be categorized into three classes: *ab-initio* approaches, methods based on the self-consistent mean-field theory and the so-called Shell-Model.

Ab-initio techniques aim to describe the nucleus as accurately as possible using a microscopic two- (and three-) body interaction as only input. Although enormous progress has been achieved the last few years, the most exact approaches, able to handle vacuum forces, are still limited to a small number of nucleons. For example the Green's Function Monte-Carlo (GFMC) [23, 83] can describe system with $A \lesssim 12$. The No-Core Shell-Model [78, 79] based on explicit expansion of the wave function on a large harmonic oscillator basis can now reach $A \simeq 16$. Finally, the more recent development of lattice Effective Field Theory [38], analogous of lattice QCD with nucleons, can tackle nuclei with $A \sim 28$. An *ab-initio* treatment

of heavier systems requires a truncation of the many-body space and thus demands a renormalization of the bare interaction to account for the neglected space. Let us cite for example the Self-Consistent Green's Function (SCGF) [31] method based on the description of nucleon propagators, or the Coupled Cluster (CC) approach [97, 59] which expresses the nuclear wave function as an exponential operator e^S acting on an uncorrelated reference state. Finally the recent In-Medium Similarity Renormalization Group (IMSRG) method [102] directly evolves the bare interaction in the nuclear medium and allows to decouple the uncorrelated reference state from other many-body configurations. These *ab-initio* approaches are currently mostly restricted to light and closed-shell medium mass nuclei. Consequently, the rest of the nuclear chart is usually tackled with methods where approximations and phenomenology enter more drastically. The following two major approaches can be cited.

The Shell-Model [24] belongs to the class of Configuration Interaction (CI) techniques which expand the nuclear wave function on a set of many-body states built on chosen single-particle states. In order to simplify the solution of the Schrödinger equation, the Shell-Model divides the single-particle space into three subspaces: an inert fully occupied core, an active partially filled valence space, and the remaining empty orbitals. The nucleons in the valence space are considered as the relevant degrees of freedom and their interaction fully determines the properties of the nucleus. To make up for such a truncation of the model space, one needs to renormalize the nuclear interaction within this space. Although this can in principle be achieved from the theory of effective operators [92], the interactions used in practical Shell-Model calculations contain a number of matrix elements that are fitted to experimental data. Finally, the diagonalization of the resulting Hamiltonian leads directly to the solutions of the problem: the eigenstates correspond to the nuclear wave functions while the eigenvalues are the energies of the system.

Finally, methods based on the self-consistent mean-field theory starts from the idea that in a first approximation, the nucleons can be considered as evolving independently from each other in an average potential generated by all other nucleons. The wave function can thus be written as a Slater determinant of single-particle states that are the unknown quantities to be determined. Within the Hartree-Fock theory [53, 43], they are obtained by applying a variational principle to the energy of the system. This procedure results in an eigenvalue equation for the Hartree-Fock potential which arises naturally as the two-body interaction folded with the one-body density of the system. Through this density dependence, the average potential is thus related to the single-particle orbitals that are themselves determined in return by the average potential. In this sense, the Hartree-Fock method is a self-consistent problem requiring an iterative solution procedure. As they lead to strong divergences, bare hard-core interactions are impossible to use in self-consistent mean-field methods, which require the use of an effective force. This can be done in the framework of the Brueckner G-matrix described

previously, leading to the Brueckner-Hartree-Fock method. However this approach is very difficult to compute and phenomenological forces, such as Gogny or Skyrme functionals are commonly used.
In order to provide an accurate description of the structure of nuclei, one usually needs to go beyond this 0^{th}-order approximation and account for missing correlations. In particular, pairing correlations are known to play a very important role in the description of open-shell nuclei. In fact this type of correlations can be included into the mean-field using the Hartree-Fock + BCS (Bardeen-Cooper-Schrieffer) [5, 92] or HFB (Hartree-Fock-Bogolyubov) [16, 17] approaches. The wave function is then written as an independent state of quasi-particles. The remaining types of correlations are usually added on top of the mean-field picture. For example the method of the Random Phase Approximation (RPA) [100], or Quasi-particle Random Phase Approximation (QRPA), describes small amplitude collective vibrations of the nucleus as coherent superpositions of individual excitations. Alternatively, the Generator Coordinate Method (GCM) [50] can treat large amplitude collective motion as superpositions of deformed mean-field solutions. Many other methods exist.
Self consistent mean-field solutions usually break a certain number of symmetries. For example, rotational invariance is lost when the Hartree-Fock solution is built on deformed orbitals. The BCS wave function also does not preserve the number of particle in the system. Although these symmetry breakings allow to account for correlations while using simplified wave functions, they need to be restored through the use of projection techniques.

The present work focuses on the development of a many-body approach aiming to describe all types of long-range correlations on the same footing in order to explicitly preserve the most important symmetries of the system, avoiding thus the need for projection techniques. This approach, named "multiparticle-multihole configuration mixing method" (shortly mp-mh method), represents the adaptation of a many-body technique already widely used in the context of atomic physics or quantum chemistry, and known as Multi-Configuration Hartree-Fock (MCHF) [44, 75] or Multi-Configuration Self-Consistent Field (MCSCF) [108, 106] method. While successful results have been obtained in these fields, the application of this approach to the description of nuclear systems present additional difficulties. Namely, the lack of knowledge of the nuclear force contrary to electromagnetic interactions, as well as the presence of two types of particles (protons and neutrons), leading to the collectivity property of nuclei requiring account for a large number of configurations. The multiparticle-multihole configuration mixing method is inspired from both the self-consistent mean-field approach, which optimizes orbitals considering a Slater determinant wave function, and the Shell-model - or more generally configuration interaction techniques - which explicitly treat all correlations in a restricted many-body space built on frozen orbitals. Taking advantage of both philosophies, the mp-mh approach assumes a correlated wave function preserving explicit symmetries, and optimizes at the same time the single-particle states. We thus obtain a set of orbitals reflecting the

correlation content of the nuclear state. In this way, the mp-mh method allows to treat on the same footing long range correlations, beyond a mean-field that is improved as correlations are introduced. First multiconfiguration-type calculations based on Hartree-Fock single-particle states (as opposed to the usual oscillator sates) have been realized in e.g. [85, 91, 18, 76, 61]. The orbitals were however kept frozen. Pioneering work using the full Multi-Configuration Self-Consistent Field approach in the context of nuclear physics has been done a few decades ago [34, 39, 96, 60]. However the applications performed in these studies were restricted to simple analytical cases (Lipkin model). The development of the multiparticle-multihole configuration mixing method at CEA,DAM,DIF started in the early 2000's. So far, the studies that have been performed have not applied the full self-consistent formalism. Recent analysis of the spectroscopy of *sd*-shell nuclei using the Gogny interaction [86, 63] used frozen Hartree-Fock orbitals, while an earlier work [84] applied the mp-mh method to the description of pairing correlations in Sn isotopes making drastic approximations in the equation determining the single-particle states. The goal of this thesis is to pursue the development of the mp-mh approach to be able to apply the full formalism to the description of nuclei. After formal and numerical developments, we are now able to exercise for the first time the completely self-consistent method to a few light nuclei. In particular, the first applications of this work are done for p and sd-shell nuclei using the Gogny interaction.

This thesis is organized as follows.

- In the first chapter we remind of the formalism of the mp-mh configuration mixing approach. For clean understanding and formal analysis of the equations, this formalism is derived from a Hamiltonian operator (without density-dependence). This chapter focuses then on the formal interpretation of the role of the orbital transformation. In particular, we show that the equation determining the single-particle states can be obtained from the Green's function formalism at equal times.

- In the second chapter, we perform a first application of the method using the Gogny force. The density-dependence of this interaction leads to a modification of the formalism which we derive in consequence. Secondly, the procedure used to solve the equations are exposed. Finally, we end by applying the full mp-mh method to a first test case: the ^{12}C nucleus. In particular we test and compare the convergence procedure using two types of truncation of the many-body wave function.

- In the third chapter, a systematic study of *sd*-shell nuclei is performed. The influence of the orbital transformation on the description of ground and excited properties is analyzed.

- Finally, the last chapter is dedicated to first applications of the method for the study of reaction mechanisms. More particularly, transition densities calculated in the framework

of the mp-mh configuration mixing approach are used as input to calculate observables associated with inelastic scattering of electrons and protons from *sd*-shell nuclei.

Chapter II

General Formalism of the mp-mh configuration mixing method

At the crossroads between self-consistent mean-field approaches and Configuration-Interaction techniques, the multiparticle-multihole configuration mixing method exhibits several advantages. The configuration mixing form of the wave function allows to preserve symmetries that are usually broken in mean-field-type approaches. In particular, the number of particles and the angular momentum are explicit good quantum numbers. The Pauli principle, usually slightly violated in RPA-type methods (so-called Quasi-Boson Approximation) is also fully respected here. Moreover, all types of long-range correlations are described on the same footing. Namely, pairing correlations, correlations associated with collective excitations and coupling of these collective states with individual excitations (so-called particle-vibration coupling). Finally ground and excited states of even-even, even-odd and odd-odd nuclei can be described on the same footing. As in self-consistent mean-field methods, the mp-mh approach offers nice and satisfying consistency properties. Even better, the mean-field evolves according to the correlation content of the system, and thus reflects the effect of all types of correlations.

We start this chapter by deriving the formalism of the mp-mh method based on a general two-body Hamiltonian. Secondly, a formal analysis of the role of the orbital optimization is conducted. In particular the link with the Green's function formalism at equal time is established.

II.1 Derivation of the equations

The starting point of the method is to build the trial wave function $|\Psi\rangle$ describing the nuclear state. $|\Psi\rangle$ is taken as a general superposition of direct products of proton (π) and neutron (ν)

Slater determinants $|\phi_\alpha\rangle \equiv |\phi_{\alpha_\pi}\rangle \otimes |\phi_{\alpha_\nu}\rangle$,

$$\begin{aligned} |\Psi\rangle &= \sum_\alpha A_\alpha |\phi_\alpha\rangle \\ &\equiv \sum_{\alpha_\pi \alpha_\nu} A_{\alpha_\pi \alpha_\nu} |\phi_{\alpha_\pi}\rangle \otimes |\phi_{\alpha_\nu}\rangle \ . \end{aligned} \tag{II.1}$$

Each configuration $|\phi_\alpha\rangle$ is a multiparticle-multihole (mp-mh) excitation of a reference state $|\phi\rangle$ obtained by filling the lowest orbitals with the $A = Z + N$ nucleons of the system (see Fig. (II.1)).
That is,

$$\begin{aligned} |\phi_\alpha\rangle &= \prod_i^{M_\alpha} \left(a^\dagger_{p_i} a_{h_i}\right) |\phi\rangle \\ &\equiv |\phi_{\alpha_\pi}\rangle \otimes |\phi_{\alpha_\nu}\rangle = \prod_i^{M_{\alpha_\pi}} \left(a^\dagger_{p_{i_\pi}} a_{h_{i_\pi}}\right) |\phi_\pi\rangle \otimes \prod_j^{M_{\alpha_\nu}} \left(a^\dagger_{p_{j_\nu}} a_{h_{j_\nu}}\right) |\phi_\nu\rangle \ , \end{aligned} \tag{II.2}$$

with,

$$\begin{aligned} |\phi\rangle &= \prod_{i=1}^{A} a^\dagger_i |0\rangle \\ &\equiv |\phi_\pi\rangle \otimes |\phi_\nu\rangle = \prod_{i=1}^{Z} a^\dagger_{i_\pi} |0\rangle \otimes \prod_{j=1}^{A} a^\dagger_{j_\nu} |0\rangle \ . \end{aligned} \tag{II.3}$$

In Eq. (II.2), the indices h (resp. p) stand for "hole" (resp. "particle") and denote occupied (resp. unoccupied) orbitals in $|\phi\rangle$. The highest hole level is known as the Fermi level. $M_\alpha = M_{\alpha_\pi} + M_{\alpha_\nu}$ is called the excitation order of the configuration $|\phi_\alpha\rangle$ and corresponds to the number of p-h excitations applied to $|\phi\rangle$ in order to obtain $|\phi_\alpha\rangle$. The reference state $|\phi\rangle$ obtained from the particle vacuum $|0\rangle$ and characterized by $M_\alpha = 0$ is included in expansion (II.1). It is represented on Fig. (II.1) along with other possible configurations up to 2p-2h configurations.

It is obvious that a wave function as written in Eq. (II.1) explicitly preserves the number of protons and neutrons, Z and N, of the system. Other symmetries, such as the rotational invariance, are preserved by restricting the configuration mixing (II.1) to Slater determinants ensuring the conservation of good quantum numbers.

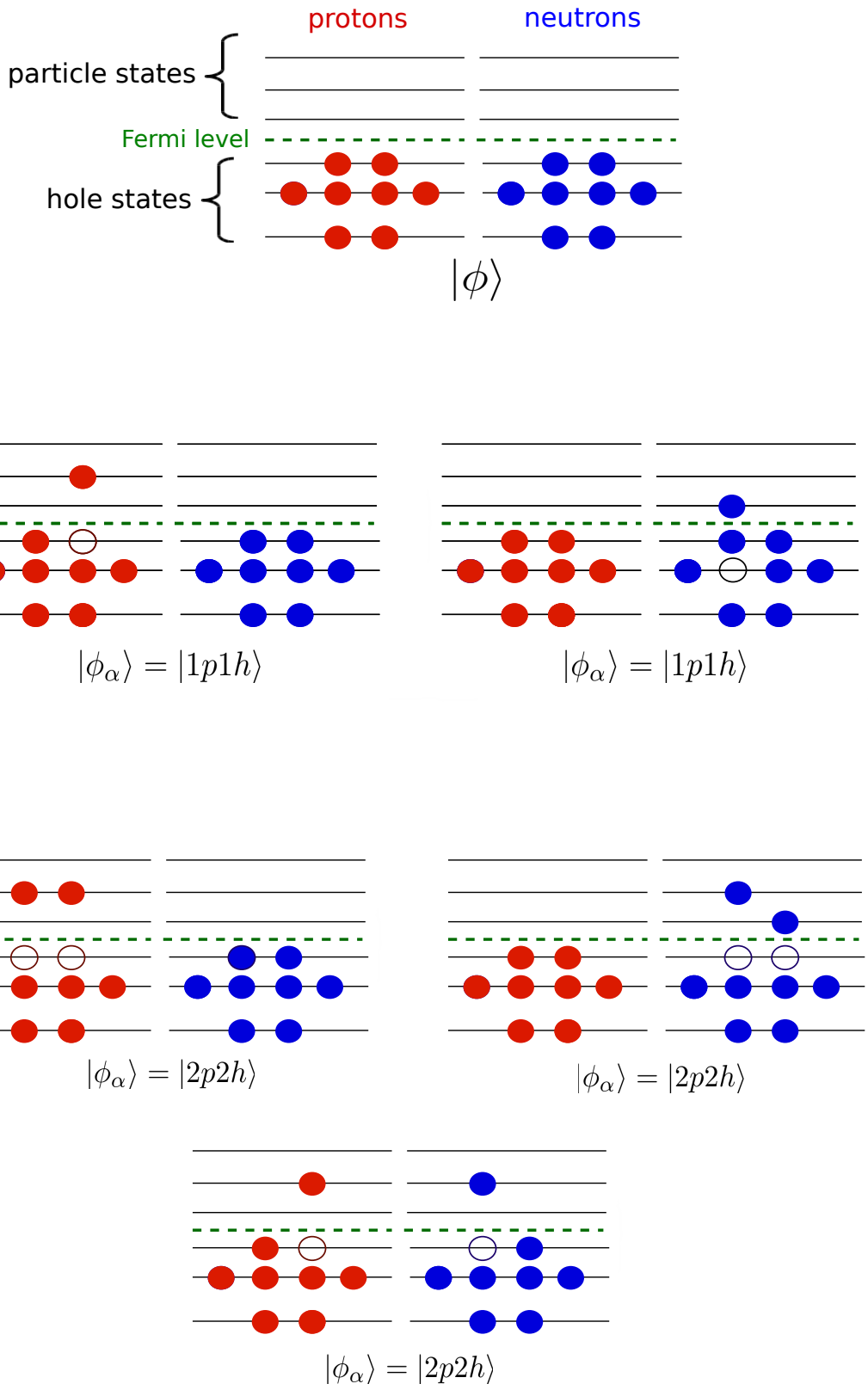

Figure II.1: Examples of multiparticle-multihole excitations.

Ideally the single-particle basis would be infinite so that the many-body configurations $|\phi_\alpha\rangle$ would span the complete Hilbert space $\mathcal{I}$. According to the Ritz variational principle, the exact wave function $|\Psi_{ex}\rangle$ making the energy functional $\mathcal{E}[\Psi_{ex}] = \frac{\langle\Psi_{ex}|\hat{H}|\Psi_{ex}\rangle}{\langle\Psi|\Psi\rangle}$ stationary would then be an eigenstate of the many-body Hamiltonian $\hat{H}$. This wave function would be independent of the nature of the single-particle basis, so that the mixing coefficients A_α would be the only variational parameters to consider.

However, practically, one is forced to consider a finite basis. Thus the trial wave function $|\Psi\rangle$ can only be varied within a subspace $\mathcal{S}$ of the whole Hilbert space $\mathcal{I}$. If one includes in expansion (II.1) all many-body configurations (with good quantum numbers) belonging to $\mathcal{S}$, varying the energy functional with respect to the coefficients A_α leads to finding the exact eigenstates of $\hat{S}^\dagger\hat{H}\hat{S}$, projection of the Hamiltonian on $\mathcal{S}$. These states are not, *a priori*, eigenstates of $\hat{H}$. However, if the one-body basis is large enough, the subspace $\mathcal{S}$ tends to cover an important part of $\mathcal{I}$, so that the trial wave function $|\Psi\rangle$ resembles closely $|\Psi_{ex}\rangle$ and $\mathcal{E}[\Psi] \to \mathcal{E}[\Psi_{ex}]^+$ [67]. The exact solution within $\mathcal{S}$ would then be a satisfactory approximation to the exact solution within $\mathcal{I}$.

However this procedure is usually practically unfeasible. Indeed, roughly speaking, the size of the many-body space $\mathcal{S}$ for N particles on M single-particle states grows combinatorially as $\binom{M}{N} = \frac{M!}{N!(N-M)!}$. Moreover the presence of two types of particles (protons and neutrons) increases drastically the number of possible combinations. Thus, one is usually compelled to restrict the expansion (II.1) to configurations belonging to a subspace $\mathcal{P}$ of $\mathcal{S}$. In this case, the wave function depends significantly on the nature of the single particle basis. The strategy of the multiparticle-multihole configuration mixing approach is thus to determine the single-particle states which optimize at best the subspace $\mathcal{P}$.
Consequently, the two sets of unknown parameters to be determined are,

- **The mixing coefficients** $\{A_\alpha\}$, representing the weight of each configuration in the trial wave function.
- **The single-particle orbitals** $\{\varphi_{i_\tau}(\vec{r},\sigma)\}$ $(\tau = (\pi,\nu), \sigma = (\uparrow,\downarrow))$, or equivalently the creation operators $\{a^\dagger_{i_\tau}\}$[1], used to build the many-body states.

The equation determining the weights $\{A_\alpha\}$ is obtained by requiring the energy functional $\mathcal{E}[\Psi] = \langle\Psi|\hat{H}|\Psi\rangle$ to be stationary with respect to infinitesimal variations δA^*_α of the coeffi-

[1]The orbitals $\{\varphi_{i_\tau}(\vec{r},\sigma)\}$ are related to the creation operators $\{a^\dagger_{i_\tau}\}$ through the relation,

$$\hat{\psi}^\dagger(\vec{r},\sigma,\tau) = \sum_i \varphi_{i_\tau}(\vec{r},\sigma)^* a^\dagger_{i_\tau} \Leftrightarrow a^\dagger_{i_\tau} = \sum_\sigma \int d^3r \hat{\psi}^\dagger(\vec{r},\sigma,\tau)\varphi_{i_\tau}(\vec{r},\sigma)^* \ ,$$

where $\hat{\psi}^\dagger(\vec{r},\sigma,\tau)$ is the field operator creating a nucleon with spin σ and isospin τ at point $\vec{r}$.

cients, while the orbitals are kept fixed. Similarly the orbitals are optimized by fixing the coefficients and minimizing $\mathcal{E}[\Psi]$ with respect to the single-particle states $\{\varphi_{i_\tau}\}$.

This leads to the following system of equations,

$$\begin{cases} \delta_A \mathcal{E}[\Psi] \equiv \sum_\alpha \left.\frac{\partial \mathcal{E}[\Psi]}{\partial A^*_\alpha}\right|_{\{\varphi_i,\varphi_i^*\}\text{ fixed}} \delta A^*_\alpha + \sum_\alpha \left.\frac{\partial \mathcal{E}[\Psi]}{\partial A_\alpha}\right|_{\{\varphi_i,\varphi_i^*\}\text{ fixed}} \delta A_\alpha = 0 & \text{(II.4)} \\ \delta_\varphi \mathcal{E}[\Psi] \equiv \sum_{\varphi_i} \left.\frac{\partial \mathcal{E}[\Psi]}{\partial \varphi^*_i}\right|_{\{A_\alpha,A^*_\alpha\}\text{ fixed}} \delta \varphi^*_i + \sum_{\varphi_i} \left.\frac{\partial \mathcal{E}[\Psi]}{\partial \varphi_i}\right|_{\{A_\alpha,A^*_\alpha\}\text{ fixed}} \delta \varphi_i = 0\,, & \text{(II.5)} \end{cases}$$

where δ_A and δ_φ denote the variations with respect to the expansion coefficients and the orbitals, respectively. Since the mixing coefficients depend on the nature of the single-particle states, and vice versa, the two equations (II.4) and (II.5) are coupled.

In what follows, we show the formalism of the multiparticle-multihole (mp-mh) configuration mixing approach derived from a two-body Hamiltonian with general form,

$$\begin{aligned} \hat{H} &= \hat{K} + \hat{V}^{2N} \\ &= \sum_{ij} K_{ij} a^\dagger_i a_j + \frac{1}{4}\sum_{ijkl} \langle ij|\widetilde{V^{2N}}|kl\rangle\, a^\dagger_i a^\dagger_j a_l a_k\,, \end{aligned} \qquad \text{(II.6)}$$

where $\hat{K}$ is the kinetic energy operator containing the center of mass correction $\left(1-\frac{1}{A}\right)$, and $\widetilde{V^{2N}} \equiv (1-\hat{P}_{12})\hat{V}^{2N}$ is the antisymmetrized two-body interaction. $\hat{P}_{12} = \hat{P}_{r_1r_2}\hat{P}_{\sigma_1\sigma_2}\hat{P}_{\tau_1\tau_2}$ denotes the exchange operator between particle 1 and 2, with $\hat{P}_{r_1r_2}$, $\hat{P}_{\sigma_1\sigma_2}$ and $\hat{P}_{\tau_1\tau_2}$ the space, spin and isospin exchange operators respectively.
The generalization to e.g. a three-body Hamiltonian is straightforward (see. Appendix A).

II.1.1 First variational equation: the mixing coefficients

Let us first consider Eq. (II.4). The mixing coefficients being related through the normalization condition of the wave function,

$$1 = \langle\Psi|\Psi\rangle = \sum_{\alpha\beta} A^*_\alpha A_\beta \langle\phi_\alpha|\phi_\beta\rangle = \sum_\alpha |A_\alpha|^2\,, \qquad \text{(II.7)}$$

we make use of the Lagrange method [2] and introduce a multiplier λ associated to this condition. The new functional to minimize is then,

$$\begin{aligned} \mathcal{F}[\Psi,\lambda] &= \mathcal{E}[\Psi] - \lambda\left(\langle\Psi|\Psi\rangle - 1\right) && \text{(II.8)} \\ &= \sum_{\alpha\beta} A^*_\alpha A_\beta \langle\phi_\alpha|\hat{H}|\phi_\beta\rangle - \lambda\left(\sum_{\alpha\beta} A^*_\alpha A_\beta \langle\phi_\alpha|\phi_\beta\rangle - 1\right) , && \text{(II.9)} \end{aligned}$$

and the equation (II.4) to solve can be rewritten as,

$$\begin{cases} \dfrac{\partial F[\Psi,\lambda]}{\partial A^*_\alpha} = 0, \quad \forall\alpha & \text{(II.10)} \\ \dfrac{\partial F[\Psi,\lambda]}{\partial A_\alpha} = 0, \quad \forall\alpha \ . & \text{(II.11)} \end{cases}$$

Inserting Eq. (II.9) into Eqs. (II.10) and (II.11) we finally get,

$$\boxed{\sum_\beta A_\beta \langle\phi_\alpha|\hat{H}|\phi_\beta\rangle = \lambda A_\alpha, \quad \forall\alpha} \ , \qquad \text{(II.12)}$$

and its equivalent conjugate equation.
Eq. (II.12) represents the diagonalization of the Hamiltonian matrix in the many-body configuration space. This eigenvalue equation is common to all Configuration Interaction-type methods[3]. The nuclear states $|\Psi\rangle$ correspond to the eigenvectors of $\hat{H}$, while the eigenvalues give the energy of the system.

As mentioned earlier the size of the matrix growing combinatorially with the number of particles and the number of single-particle states, one is usually forced to restrict the wave function (II.1) to a subspace $\mathcal{P} \subset \mathcal{S}$ containing certain selected configurations. Thus we have in fact,

$$|\Psi\rangle = \sum_{\alpha\in\mathcal{P}} A_\alpha |\phi_\alpha\rangle \ . \qquad \text{(II.13)}$$

Calling $\mathcal{Q}$ the subspace orthogonal to $\mathcal{P}$ in $\mathcal{S}$, we have

$$\mathcal{P} \oplus \mathcal{Q} = \mathcal{S} \ . \qquad \text{(II.14)}$$

[2] The Lagrange multiplier method states that the extrema of a function $f(x_1,...,x_n)$ constrained to the condition $C(x_1,...,x_m) = 0$ $(m \leqslant n)$, can be obtained by finding unconstrained extrema of the function $g(x_1,...,x_n,\lambda) = f(x_1,...,x_n) - \lambda C(x_1,...,x_m)$.

[3] Since in practical applications we will be using a density-dependent interaction, new terms called "rearrangement terms" will appear, making Eq. (II.12) non-linear and therefore more complicated to solve. See chapter III.

This truncation is schematically shown in Fig. (II.2).

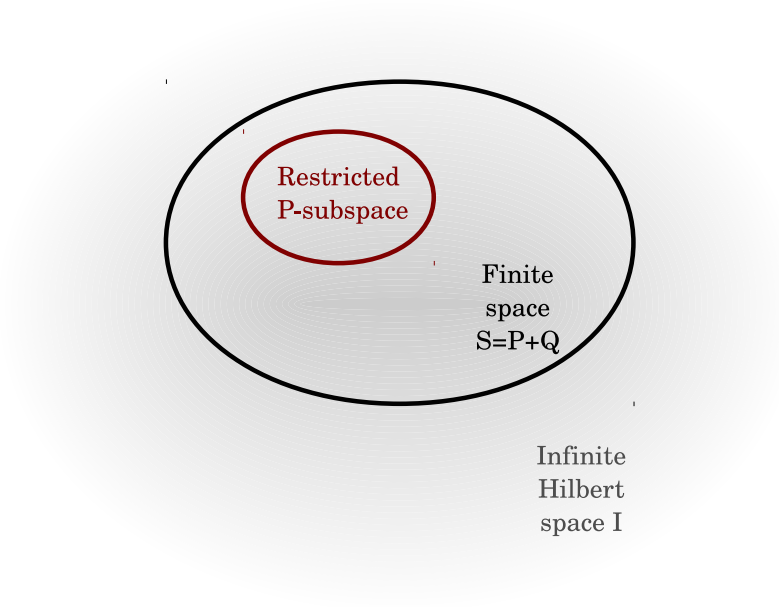

Figure II.2: Truncation of the many-body space.

Neglecting the space outside of $\mathcal{S}$, the projectors $\hat{P}$ and $\hat{Q}$ onto $\mathcal{P}$ and $\mathcal{Q}$ respectively, satisfy the following relations,

$$\begin{aligned} \hat{P}^2 &= \hat{P} \\ \hat{Q}^2 &= \hat{Q} \\ \hat{P}+\hat{Q} &= \hat{1}_{\mathcal{S}} \simeq \hat{1} \\ \hat{P}\hat{Q} = \hat{Q}\hat{P} &= 0\,. \end{aligned} \tag{II.15}$$

The Hamiltonian can then be decomposed into,

$$\begin{aligned} \hat{H} &= \hat{P}\hat{H}\hat{P} + \hat{Q}\hat{H}\hat{Q} + \hat{P}\hat{H}\hat{Q} + \hat{Q}\hat{H}\hat{P} \\ &= \hat{H}_{PP} + \hat{H}_{QQ} + \hat{H}_{PQ} + \hat{H}_{QP}\,, \end{aligned} \tag{II.16}$$

where $\hat{H}_{PP}$ and $\hat{H}_{QQ}$ act within $\mathcal{P}$ and $\mathcal{Q}$ respectively, while $\hat{H}_{PQ}$ and $\hat{H}_{QP}$ represent the couplings between both spaces.

We note that Eq. (II.12) can be rewritten as,

$$\begin{aligned} & \langle\phi_\alpha|\hat{H}-\lambda|\Psi\rangle = 0 \ \ ,\forall\alpha \\ \Leftrightarrow \ & \hat{P}(\hat{H}-\lambda)\,|\Psi\rangle = 0 \qquad\qquad (\text{II.17}) \\ \Leftrightarrow \ & (\hat{1}-\hat{Q})(\hat{H}-\lambda)\,|\Psi\rangle = 0 \\ \Leftrightarrow \ & (\hat{H}-\lambda)\,|\Psi\rangle = \hat{Q}\hat{H}\,|\Psi\rangle \ . \qquad\qquad (\text{II.18}) \end{aligned}$$

Eq. (II.17) expresses nothing but the fact that $|\Psi\rangle$ is the eigenstate of $\hat{H}_{PP}$, projection of $\hat{H}$ onto $\mathcal{P}$, with eigenvalue λ.

Role of the first equation

The first variational equation allows to explicitly build two-body correlations in the wave function of the nucleus. Although these correlations are restricted to a truncated $\mathcal{P}$ space of the complete Hilbert space, they are however of all physical types. Indeed, looking at the elements $\langle\phi_\alpha|\hat{V}|\phi_\beta\rangle$ of the matrix to diagonalize, one sees that different types of vertices can appear according to the difference of excitation order $\Delta M = |M_\alpha - M_\beta|$ of the two Slater determinants ϕ_α and ϕ_β. If $\hat{V}$ is a two-body interaction it can only connect configurations differing by up to $2p-2h$ excitations. Three cases have then to be examined. They are represented in Fig. (II.3).

- Case (a): $\Delta n = 0$. The two top diagrams of the figure correspond to the direct and exchange part of the same matrix element. They represent respectively the scattering and the creation/annihilation of a particle-hole (p-h) pair. This type of vertices are characteristic of RPA-type (Random Phase Approximation-type) correlations. In particular, they correspond to the A-matrix in the ph-RPA approach. These vertices are able to generate the well-known ring diagrams representing collective vibrations of the nucleus. The two bottom diagrams on Fig. (II.3)(a) respectively represent the scattering of a pair of particles and of a pair of holes. These vertices appear for instance in the pp(hh)-RPA or QRPA approaches. They generate pairing vibrations. When particles are in time-reversed states they also occur in BCS (Bardeen-Cooper-Schrieffer) or HFB (Hartree-Fock-Bogolyubov) methods.

- Case (b): $\Delta n = 1$. These diagrams represent the influence of the creation (annihilation) of a ph pair on the propagation of a single particle (hole). They allow to couple collective vibrations of the nucleus to the motion of individual nucleons. This is the so-called "particle-vibration coupling" which is rarely considered in microscopic beyond mean-field approaches. It is however known to play an important role in odd nuclei. In particular these diagrams are expected to lead to a compression of the single-particle spectrum around the Fermi level.

- Case (c): $\Delta n = 2$. These vertices represent the creation (annihilation) of two particle-hole pairs from the uncorrelated reference state. They are essential to introduce correlations in the ground state and appear again in the RPA approach through the B-matrix.

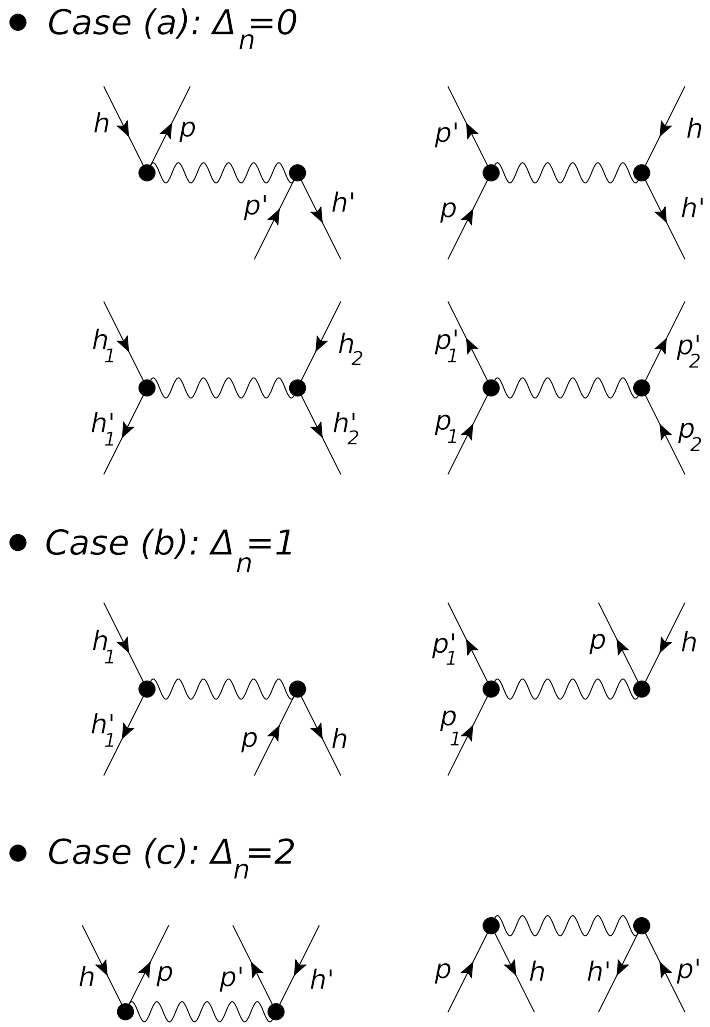

Figure II.3: Different types of vertices appearing in the configuration mixing. See text for explanation.

Finally let us remind that the Hamiltonian appearing in Eq. (II.12) has not been renormalized inside the $\mathcal{P}$-subspace and therefore the first variational equation completely neglects $\mathcal{Q}$. We will see that the second variational equation should partly make up for this truncation.

II.1.2 Second variational equation: the single-particle orbitals

Let us now consider the variation of the energy $\mathcal{E}[\Psi]$ with respect to the single-particle orbitals, while the mixing coefficients are kept fixed. A variation of the creation operators $\{a_i^\dagger\}$ can be

obtained from a general unitary transformation,

$$a_i^\dagger \to e^{i\hat{T}} a_i^\dagger e^{-i\hat{T}} = a_i^\dagger + i\left[\hat{T}, a_i^\dagger\right] - \frac{1}{2}\left[\hat{T}, \left[\hat{T}, a_i^\dagger\right]\right] + \dots , \tag{II.19}$$

where $\hat{T}$ is an infinitesimal hermitian one-body operator $\hat{T} = \sum_{ij} T_{ij} a_i^\dagger a_j$. This leads to the first order variation,

$$\Rightarrow \delta a_i^\dagger = i\left[\hat{T}, a_i^\dagger\right] . \tag{II.20}$$

This transformation of orbitals yields the following variation of the many-body states,

$$\begin{aligned} |\phi_\alpha\rangle = \prod_{i\in\alpha} a_i^\dagger |0\rangle = a_{1_\alpha}^\dagger \dots a_{A_\alpha}^\dagger |0\rangle \quad &\to \quad \left(e^{i\hat{T}} a_{1_\alpha}^\dagger e^{-i\hat{T}}\right) \dots \left(e^{i\hat{T}} a_{A_\alpha}^\dagger e^{-i\hat{T}}\right) |0\rangle \\ &= \quad e^{i\hat{T}} a_{1_\alpha}^\dagger \dots a_{A_\alpha}^\dagger \underbrace{e^{-i\hat{T}} |0\rangle}_{=|0\rangle} \\ &= \quad e^{i\hat{T}} |\phi_\alpha\rangle \ , \end{aligned} \tag{II.21}$$

where we used the unitarity property $e^{-i\hat{T}} e^{i\hat{T}} = \hat{1}$ and the fact that the true vacuum $|0\rangle$ stays invariant under such a transformation.
Expanding the exponential, we get $|\delta\phi_\alpha\rangle = i\hat{T}|\phi_\alpha\rangle$. Similarly the trial wave function varies as $|\delta\Psi\rangle = i\hat{T}|\Psi\rangle$, so that the corresponding first order variation of the energy is,

$$\begin{aligned} \delta_\varphi \mathcal{E}[\Psi] &= \langle\delta\Psi|\hat{H}|\Psi\rangle + \langle\Psi|\hat{H}|\delta\Psi\rangle & \text{(II.22)} \\ &= -i\langle\Psi|\hat{T}\hat{H}|\Psi\rangle + i\langle\Psi|\hat{H}\hat{T}|\Psi\rangle \\ &= i\langle\Psi|\left[\hat{H}, \hat{T}\right]|\Psi\rangle \ . & \text{(II.23)} \end{aligned}$$

The requirement (II.5) for the energy to be stationary amounts then to,

$$\boxed{\langle\Psi|\left[\hat{H}, \hat{T}\right]|\Psi\rangle = 0} . \tag{II.24}$$

This condition is often referred in the literature as "Generalized Brillouin equation" [20, 64]. We show in appendix[4] (A) that the Brillouin equation (II.24) can be recasted as the following generalized inhomogeneous mean-field equation,

$$\boxed{\left[\hat{h}[\rho], \hat{\rho}\right] = \hat{G}[\sigma]} . \tag{II.25}$$

[4]The orbital equation is derived in Appendix (A) for the general case of a three-body Hamiltonian.

In Eq. (II.25) ρ is the one-body density matrix of the correlated state,

$$\rho_{ij} = \langle\Psi|a_j^\dagger a_i|\Psi\rangle \ , \tag{II.26}$$

and σ is the two-body correlation matrix defined by,

$$\begin{aligned} \rho^{[2]}_{ij,kl} &\equiv \langle\Psi|a_j^\dagger a_l^\dagger a_k a_i|\Psi\rangle \\ &= (\rho_{ij}\rho_{kl} - \rho_{il}\rho_{kj}) + \sigma_{ji,lk} \ . \end{aligned} \tag{II.27}$$

We show in appendix (B) that σ can also be expressed as,

$$\begin{aligned} \sigma_{ji,lk} &= \langle\Psi| : a_j^\dagger a_l^\dagger a_k a_i : |\Psi\rangle \\ &\quad - \langle\Psi| : a_j^\dagger a_i : |\Psi\rangle \langle\Psi| : a_l^\dagger a_k : |\Psi\rangle + \langle\Psi| : a_j^\dagger a_k : |\Psi\rangle \langle\Psi| : a_l^\dagger a_i : |\Psi\rangle \ , \end{aligned} \tag{II.28}$$

where :: denotes the normal product taken with respect to the uncorrelated reference state $|\phi\rangle$.
The one-body mean-field Hamiltonian,

$$\begin{aligned} h[\rho]_{ij} &= K_{ij} + \underbrace{\sum_{kl} \langle ik|\widetilde{V}^{2N}|jl\rangle \, \rho_{lk}}_{\Gamma^{2N}_{ij}[\rho]} \\ &\equiv K_{ij} + \qquad\qquad \Gamma^{2N}_{ij}[\rho] \ , \end{aligned} \tag{II.29}$$

represents a generalization of the Hartree-Fock field in the sense that it is built with the density matrix of the correlated system and not an approximated Slater density.
Finally the source term $G[\sigma]$ contains the effect of correlations beyond this mean-field, and is given by,

$$G[\sigma]_{ij} = \frac{1}{2}\sum_{klm} \sigma_{ki,lm}\widetilde{V}^{2N}_{kljm} - \frac{1}{2}\sum_{klm} \widetilde{V}^{2N}_{iklm}\sigma_{jl,km} \ . \tag{II.30}$$

It is easy to show that $G[\sigma]$ is anti-hermitian since it can be rewritten as,

$$G[\sigma] = F[\sigma] - F^\dagger[\sigma] \ , \tag{II.31}$$

where,

$$F[\sigma]_{ij} = \frac{1}{2}\sum_{klm} \sigma_{ki,lm}\widetilde{V}^{2N}_{kljm} \ . \tag{II.32}$$

Eq. (II.24) and (II.25) are two equivalent expressions of the equation determining the optimal orbitals. There exist in fact several other possible ways of deriving and expressing

this equation (see e.g. [73]). For instance, defining the following operator,

$$\hat{O} = \hat{\rho}\hat{h}[\rho] + \hat{F}[\sigma] \, , \tag{II.33}$$

it is straightforward to see that Eq. (II.25) can be recasted into,

$$\hat{O} = \hat{O}^{\dagger} \, . \tag{II.34}$$

This operator $\hat{O}$ is often referred in the literature as the "orbital operator" [45] or "Fock-like operator" [55] (by analogy to the usual Fock operator encountered in the Hartree-Fock theory). Its hermiticity is thus a necessary and sufficient condition for the energy to be stationary with respect to orbital variations.
Continuing this reasoning, this is also equivalent to the fact that the matrix O can be diagonalized by a unitary matrix U as,

$$U^{-1}OU = D \, , \tag{II.35}$$

where D is diagonal and real, and $U^{\dagger}U = 1$. The orbital equation can therefore also be expressed as an eigenvalue problem for the orbital operator $\hat{O}$ [34].

Role of the second equation - Coupling to the $\mathcal{Q}$-subspace

As mentioned previously, the nuclear state built from the first variational equation is in practice restricted to a subspace $\mathcal{P}$ of the full many-body space $\mathcal{S}$. The variation of this state obtained via the variation of the single-particle states can be divided into a part belonging to $\mathcal{P}$ and a part belonging to the orthogonal $\mathcal{Q}$-subspace as,

$$|\Psi\rangle_{\mathcal{P}} \rightarrow |\Psi\rangle_{\mathcal{P}} + |\delta\Psi\rangle \, , \text{ where } \; |\delta\Psi\rangle = |\delta\Psi\rangle_{\mathcal{P}} + |\delta\Psi\rangle_{\mathcal{Q}} \; . \tag{II.36}$$

Thus, the corresponding variation of the energy becomes,

$$\begin{aligned} \delta_{\phi}\mathcal{E}[\Psi] &= {}_{\mathcal{P}}\langle\Psi|\hat{H}\,|\delta\Psi\rangle + \langle\delta\Psi|\hat{H}|\Psi\rangle_{\mathcal{P}} \\ &= {}_{\mathcal{P}}\langle\Psi|\hat{H}\,|\delta\Psi\rangle_{\mathcal{P}} + {}_{\mathcal{P}}\langle\delta\Psi|\hat{H}\,|\Psi\rangle_{\mathcal{P}} + {}_{\mathcal{P}}\langle\Psi|\hat{H}\,|\delta\Psi\rangle_{\mathcal{Q}} + {}_{\mathcal{Q}}\langle\delta\Psi|\hat{H}\,|\Psi\rangle_{\mathcal{P}} \\ &= {}_{\mathcal{P}}\langle\Psi|\hat{P}\hat{H}\hat{P}\,|\delta\Psi\rangle_{\mathcal{P}} + {}_{\mathcal{P}}\langle\delta\Psi|\hat{P}\hat{H}\hat{P}\,|\Psi\rangle_{\mathcal{P}} + {}_{\mathcal{P}}\langle\Psi|\hat{P}\hat{H}\hat{Q}\,|\delta\Psi\rangle_{\mathcal{Q}} + {}_{\mathcal{Q}}\langle\delta\Psi|\hat{Q}\hat{H}\hat{P}\,|\Psi\rangle_{\mathcal{P}} \; . \end{aligned} \tag{II.37}$$

We see from the last two terms on the r.h.s of Eq. (II.37) that couplings between the $\mathcal{P}$- and $\mathcal{Q}$-subspaces are introduced through $\hat{H}_{\mathcal{P}\mathcal{Q}} \equiv \hat{P}\hat{H}\hat{Q}$ and $\hat{H}_{\mathcal{Q}\mathcal{P}} \equiv \hat{Q}\hat{H}\hat{P}$. However propagation into the $\mathcal{Q}$-subspace through $\hat{H}_{\mathcal{Q}\mathcal{Q}} \equiv \hat{Q}\hat{H}\hat{Q}$ is ignored [5].

[5] Since $\hat{H}_{\mathcal{Q}\mathcal{Q}}$ is not taken into account neither in the first nor via the second equation, one of the challenges of the mp-mh approach will be to select an optimal selection criterion of the $\mathcal{P}$-space. That is, find a truncation scheme of the many-body configurations such that the ignored $\mathcal{Q}$-subspace will not impact on the observables

The orbital equation should therefore partly compensate for the truncation made on the wave function. This can be illustrated by the following arguments.
Starting from a certain set of single-particle states $\{a^\dagger\}$, the orbital equation leads to a new set $\{b^\dagger\}$ that can be expressed as,

$$b_i^\dagger = e^{i\hat{\Lambda}} a_i^\dagger e^{-i\hat{\Lambda}} = \sum_j a_j^\dagger \left(e^{i\hat{\Lambda}}\right)_{ji} \equiv \sum_j a_j^\dagger \theta_{ji} \ , \tag{II.38}$$

where the sum runs over all states j (of same symmetry than i in a symmetry-conserving approach), and $\hat{\Lambda} = \sum_{kl} \Lambda_{kl} a_k^\dagger a_l$. Under this transformation, the many-body configurations therefore vary as,

$$\begin{aligned} |\phi_\alpha\rangle \to |\phi'_\alpha\rangle &= e^{i\Lambda}|\phi_\alpha\rangle \\ &= |\phi_\alpha\rangle + \sum_{ij} \Lambda_{ij} a_i^\dagger a_j |\phi_\alpha\rangle + \sum_{ijkl} \Lambda_{ij}\Lambda_{kl} a_i^\dagger a_j a_k^\dagger a_l |\phi_\alpha\rangle + ... \ . \end{aligned} \tag{II.39}$$

The optimization of orbitals thus amounts to creating multiparticle-multihole excitations on top of the existing configurations. These multiparticle-multihole excitations extend to the whole single-particle basis one is considering. Since Λ is a one-body operator, they are always built as products of 1p-1h excitations.

The configurations belonging to the new restricted $\mathcal{P}'$-subspace should therefore take into account the effect of Slater determinants built from the entire starting single-particle basis. Indeed,

$$\begin{aligned} |\phi'_\alpha\rangle &= b_{1_\alpha}^\dagger ... b_{A_\alpha}^\dagger |0\rangle \\ &= \sum_{j_1 \cdots j_A} \theta_{j_1 1_\alpha} ... \theta_{j_A A_\alpha} a_{j_1}^\dagger ... a_{j_A}^\dagger |0\rangle \ , \end{aligned} \tag{II.40}$$

where j_i is in the same symmetry block than i_α but is not restricted to e.g. some type of valence space. Thus,

$$|\phi'_\alpha\rangle = \sum_{\substack{\beta \in \mathcal{P}+\mathcal{Q} \\ \text{with same symmetry} \\ \text{than } \alpha'}} C_{\alpha\beta} \, |\phi_\beta\rangle \tag{II.41}$$

where $C_{\alpha\beta}$ decomposes as product of Λ.

Let us insist on the fact that, since it acts at the one-body level, the transformation of single-particle states does not create additional correlations. It allows however, to optimize

under study (excitation energies, transition probabilities...).

the $\mathcal{P}$-subspace so that the role of the $\mathcal{Q}$-subspace on the description of the nuclear state is minimized.

Hartree-Fock limit Finally let us note that in the limit where only the reference state is included in expansion (II.1), i.e. if $|\Psi\rangle = |\phi\rangle$, the two-body correlation matrix σ cancels and one gets back the usual Hartree-Fock equation $[h[\rho], \rho] = 0$, where ρ reduces to[6],

$$\rho_{ij} = \begin{cases} \delta_{ij}, \text{ if i and j} \leqslant \text{Fermi level}, \\ 0, \text{ otherwise.} \end{cases} \tag{II.42}$$

This equation expresses that the mean-field and the one-body density commute and therefore there exists a common eigenbasis diagonalizing both of theses matrices simultaneously. It is this basis that one usually seeks and takes as optimal set of single-particle states. This commuting property ensures a one to one correspondence between the "canonical" states[7] (eigenstates of the mean field $h[\rho]$) and the "natural" ones (eigenstates of the density ρ). Single-particle energies (eigenvalues of $h[\rho]$) and occupation numbers (eigenvalues of ρ) are therefore both defined simultaneously.
In the general case where one includes several configurations in the wave function (II.1), $[h[\rho], \rho] = G[\sigma] \neq 0$ and this property is lost. The canonical and natural basis do not coincide anymore and one cannot define states with definite single-particle energies and occupations at the same time.

II.1.3 Importance of the consistency between correlations and mean-field description

Most microscopic many-body methods are based on the concept of an existing underlying independent-particle picture. That is, on the idea that in first approximation, the nucleons of the system can be described as evolving independently from each other in an average potential Γ, which generates single-nucleon orbitals organized in shells[8]. The inclusion of correlations arising from the residual interaction $V_{res} = V - \Gamma$ is then accomplished in a second separate stage[9].
On the contrary, the formalism exposed here allows to generate an optimized single-particle picture which reflects and encapsulates part of the correlation content of the system. We see

[6] in the case of a closed sub-shell nucleus.

[7] Here we use the jargon of quantum chemistry where the canonical basis denotes the basis that diagonalizes the mean-field Hamiltonian $h[\rho]$. This definition should not be confused with the one used in HFB theory, where the canonical basis is a special case of a natural basis which also brings the pairing tensor into "canonical" form.

[8] The Shell-model method starts from a schematic potential whereas the Hartree-Fock method optimizes the mean-field self-consistently but considering an independent-particle wave function.

[9] Only pairing correlations can be treated at the mean-field level within HFB or BCS methods.

indeed that the one-body mean-field Hamiltonian $\hat{h}[\rho]$ appearing in the orbital equation,

$$h[\rho]_{ij} = K_{ij} + \Gamma^{2N}[\rho]_{ij} = K_{ij} + \sum_{kl} \langle ik|\widetilde{V}^{2N}|jl\rangle\, \rho_{lk} \ , \tag{II.43}$$

is obtained by averaging the two-body interaction with the *complete* density ρ of the correlated state $|\Psi\rangle$. Thus, contrary to the Hartree-Fock field which averages the interaction of the nucleons over the orbits situated under the Fermi level, the mean potential (II.43) contains contributions from both particle and hole states. It therefore accounts for the scattering of nucleons into orbits that are unoccupied in the reference state $|\phi\rangle$. In the ideal case where ρ is constructed with the exact solution $|\Psi\rangle$ of $H^{2N}\,|\Psi\rangle = E\,|\Psi\rangle$, the mean field (II.43) constitutes the most general mean field that can be constructed from a two-body interaction. In fact, if one considers a M-body force, the average potential is obtained by folding the n-body interactions with the *full* (n-1)-body densities ($1 \leqslant n \leqslant M$) as,

$$\begin{aligned} h_{ij}[\rho, \rho^{[2]}, ..., \rho^{[M-1]}] \ &= \ K_{ij} + \sum_{kl} \langle ik|\widetilde{V}^{2N}|jl\rangle\, \rho_{lk} + \frac{1}{4} \sum_{k_1 l_1 k_2 l_2} \langle ik_1k_2|\widetilde{V}^{3N}|jl_1l_2\rangle\, \rho^{[2]}_{l_1k_1,l_2k_2} \\ &\quad + ... + \frac{1}{(M-1)!^2} \sum_{k_1 l_1 ... k_M l_M} \langle ik_1...k_M|\widetilde{V}^{MN}|jl_1...l_M\rangle\, \rho^{[M-1]}_{l_1k_1,...,l_{M_1}k_{M-1}} \ . \end{aligned} \tag{II.44}$$

See e.g. appendix A for the derivation of h in the case of a three-body force.
Extracted in this way from the correlated many-body solution, the resulting average potential absorbs the mean effect of correlations and partly shields the influence of the latter. The importance of the residual interaction $V_{res} = V - \Gamma[\rho]$ is then minimized and the independent-particle system governed by $h[\rho]$ should therefore be a better approximation to the exact solution then e.g. a Hartree-Fock state.

An expression of such an average potential already appeared in [94]. It was extensively discussed in [4], and more recently in [33] in the context of the definition of single-particle energies ε. It is shown that taking the latter as eigenvalues of the mean-field (II.43),

$$\varepsilon_a = \langle a|h[\rho]|a\rangle = K_{aa} + \sum_{bc} \langle ab|\widetilde{V}^{2N}|ac\rangle\, \rho_{cb} \qquad \text{where} \quad h[\rho]\,|a\rangle = \varepsilon_a\,|a\rangle \ , \tag{II.45}$$

constitutes a "universal" unambiguous definition of the single-nucleon energies, which also coincides with the "experimentalists' definition"[10].
Indeed one can easily show that $h[\rho]$ can also be expressed as (see e.g. [94]),

$$\hat{h}[\rho]_{ij} = \langle\Psi|\left\{\left[a_i, \hat{H}\right], a_j^\dagger\right\}|\Psi\rangle \ , \tag{II.46}$$

[10] Although the notion of single-particle energies can also differ within the experimentalists' community, depending on the mass region under study.

where $[,]$ and $\{,\}$ are the notations for the commutator and anti-commutator respectively. Let us now insert the following closure relations into Eq. (II.46),

$$\hat{1}_{A+1} = \sum_N |\Psi_N^{A+1}\rangle \langle \Psi_N^{A+1}| \ , \qquad \hat{1}_{A-1} = \sum_n |\Psi_n^{A-1}\rangle \langle \Psi_n^{A-1}| \ , \tag{II.47}$$

where N (n) denotes the eigenstates of the neighboring system with A+1 (A-1) nucleons, i.e. the solutions of $\hat{H}\,|\Psi_N^{A+1}\rangle = E_N\,|\Psi_N^{A+1}\rangle$ ($\hat{H}\,|\Psi_n^{A-1}\rangle = E_n\,|\Psi_n^{A-1}\rangle$). We finally obtain,

$$\hat{h}[\rho]_{ij} = \sum_N \langle\Psi|a_i|\Psi_N^{A+1}\rangle\,(E_N - E)\,\langle\Psi_N^{A+1}|a_j^\dagger|\Psi\rangle + \sum_n \langle\Psi|a_j^\dagger|\Psi_n^{A-1}\rangle\,(E - E_n)\,\langle\Psi_n^{A-1}|a_i|\Psi\rangle \ . \tag{II.48}$$

Let us remind that $\hat{H}\,|\Psi\rangle = E\,|\Psi\rangle$ is the problem for the A-particle system one is trying to solve. In the basis $\{a\}$ diagonalizing $h[\rho]$, Eq. (II.48) reads,

$$\varepsilon_a = h_{aa}[\rho] = \sum_N \left|\langle\Psi_N^{A+1}|a_a^\dagger|\Psi\rangle\right|^2 (E_N - E) + \sum_n \left|\langle\Psi_n^{A-1}|a_a|\Psi\rangle\right|^2 (E - E_n) \ . \tag{II.49}$$

We recognize in Eq. (II.49) the observable one-nucleon addition and separation energies, $E_N^+ = E_N - E$ and $E_n^- = E - E_n$ respectively. They correspond to the pole of the complete one-body energy propagator or two-point Green's function. The quantities,

$$\begin{cases} S_{N,a}^+ \equiv \left|\langle\Psi_N^{A+1}|a_j^\dagger|\Psi\rangle\right|^2 \ , & \text{(II.50)} \\ S_{n,a}^- \equiv \left|\langle\Psi_n^{A-1}|a_i|\Psi\rangle\right|^2 \ , & \text{(II.51)} \end{cases}$$

are known as spectroscopic factors. They estimate the validity of approximating the eigenstate N (n) of the A+1 (A-1) system by the ground state of the A-nucleus plus (minus) one nucleon in state a added to it (removed from it).
This analysis allows to extract from Eq. (II.49) the physical meaning of the single-particle energies taken as eigenvalues of the mean field (II.43): they represent the average of the one-nucleon separation energies weighted by the corresponding spectroscopic factors, i.e. they represent the centroid of the observable separation energies.

The theory of the most general mean-field is also extensively exposed in Ref. [11, 93] from the point of view of perturbation theory. It is emphasized that the density ρ used to calculate the potential $\Gamma[\rho]$ must be fully consistent with the correlations σ of the system. More precisely, one can always divide ρ into an uncorrelated part and a correlated one as,

$$\rho = \rho^{(0)} + \rho^{(1)} \ ,$$

where

- $\rho^{(0)} = \langle\phi|\hat{\rho}|\phi\rangle$ is the density of the uncorrelated reference state $|\phi\rangle$. It satisfies the equation $(\rho^{(0)})^2 = \rho^{(0)}$, characteristic of an independent-particle state.
- $\rho^{(1)} = \rho - \rho^{(0)}$ is the contribution to the one-body density arising from the two-body correlations. The presence of this part leads to the loss of the idempotence property: $(\rho)^2 \neq \rho$.

The authors of [11, 93] treat the density and the total energy E in terms of a graph expansion. It is shown that the diagrams for the energy can all be decomposed into sub-diagrams that are categorized into different classes. In particular graphs arising from the two-body correlations are called "irreducible". We denote by Δ their resummed contribution to E. Considering then the total energy as a functional of the average potential $\Gamma[\rho]$, the authors show that the variational condition $\frac{\delta E[\Gamma]}{\delta\Gamma} = 0$ is realized if $\Gamma[\rho]$ is calculated with $\rho^{(1)}$ satisfying,

$$\rho^{(1)} \quad = \quad \frac{\delta}{\delta\Gamma}(\Delta) = \frac{\delta}{\delta\Gamma}(\text{"Irreducible" energy diagrams}) \ . \tag{II.52}$$

It is important to stress that this result stays true in the case where one truncates the infinite summation Δ in the expansion of the energy E, or limits this summation to a certain subclass of diagrams, *as long as* the same graphs are used in (II.52) to calculate $\rho^{(1)}$.
A first application of this method was performed in [81] where the modification of the self-consistent field in the presence of 2p-2h admixtures was studied.

Although the variational principle applied in the multiparticle-multihole configuration mixing method is different (it is based on an explicit expression of the wave function) consistency between the one-body density ρ and the correlation matrix σ is achieved by the fact that they are calculated from the same (approximated) nuclear state $|\Psi\rangle \simeq |\Psi\rangle_{\mathcal{P}}$. A deep link between mean-field description and correlation content is thus ensured.

II.2 Analysis of the orbital equation - Relation to Green's functions

In this section we show that the variational orbital equation can also be obtained using the formalism of Green's functions, and thus constitutes a general equation of Physics. This formalism allows to interpret nicely the renormalization of orbitals in term of a diagrammatic representation.

II.2.1 Reminder of the Green's function formalism

Green's functions (GFs) have been very widely studied and used in all areas of many-body quantum physics. They are discussed in great detail in a large number of textbooks and lecture notes. See e.g. [103, 42, 11, 72]. Here we only recall some definitions and properties of the Green's functions that are needed in order to derive the orbital equation.

Let $a_i^\dagger(t)$ and $a_i(t)$ be the creation and destruction operators of a particle in state i in the Heisenberg picture. They are related to the time-independent operators $a_i^\dagger$ and a_i in the Schrödinger picture as (with $\hbar = 1$),

$$\begin{cases} a_i^\dagger(t) = e^{iHt} a_i^\dagger e^{-iHt} \\ a_i(t) = e^{iHt} a_i e^{-iHt} \ . \end{cases} \tag{II.53}$$

The many-body Green's functions in the representation i are defined as follows,

$$\begin{cases} \mathcal{G}_{ij}^{[1]}(t_1 - t_2) = -i \left\langle \Psi | \mathcal{T} \left(a_i(t_1) a_j^\dagger(t_2) \right) | \Psi \right\rangle \\ \mathcal{G}_{ij,kl}^{[2]}(t_1, t_2; t_3, t_4) = - \left\langle \Psi | \mathcal{T} \left(a_i(t_1) a_j(t_2) a_l^\dagger(t_4) a_k^\dagger(t_3) \right) | \Psi \right\rangle \\ \qquad \vdots \\ \mathcal{G}_{i_1 \dots i_n, j_1 \dots j_n}^{[n]}(t_1 \dots t_n; t'_1 \dots t'_n) = (-i)^n \left\langle \Psi | \mathcal{T} \left(a_{i_1}(t_1) \dots a_{i_n}(t_n) a_{j_n}^\dagger(t'_n) \dots) a_{j_1}^\dagger(t'_1) \right) | \Psi \right\rangle \ , \end{cases} \tag{II.54}$$

where $|\Psi\rangle$ is in principle the exact ground-state of the A-particle system, and $\mathcal{T}()$ is the time-ordering operator which brings the operators taken at latter times on the left of operators taken at earlier times and affects the results by the sign of the corresponding permutation.

◦ **The one-body propagator or two-point Green's function**

Definition According to (II.54), the one-body Green's function is defined as,

$$\begin{aligned} \mathcal{G}_{ij}^{[1]}(t_1 - t_2) &= -i \langle \Psi | \mathcal{T} \left(a_i(t_1) a_j^\dagger(t_2) \right) | \Psi \rangle \\ &= \begin{cases} -i \langle \Psi | a_i(t_1) a_j^\dagger(t_2) | \Psi \rangle \text{ , if } t_1 > t_2 \\ +i \langle \Psi | a_j^\dagger(t_2) a_i(t_1) | \Psi \rangle \text{ , if } t_1 < t_2 \text{ .} \end{cases} \end{aligned} \tag{II.55}$$

When $t_1 > t_2$ the one-body GF gives the probability of finding the system in its initial ground-state after adding a particle in state j at time t_2, letting the system evolve and finally removing a particle in state i at time t_1. It describes therefore the behavior of the system containing one additional particle.
Conversely, when $t_1 < t_2$, the one-body GF gives the probability of finding the system in its ground state after annihilating a particle at time t_1 and creating one at time t_2. The one-body GF for $t_1 < t_2$ thus describes the behavior of the system when removing a particle from it.

Equation of motion Let us start from the equation of motion for the Heisenberg annihilation operator $a_i(t) = e^{i\hat{H}t} a_i e^{-i\hat{H}t}$,

$$\begin{aligned} i\frac{\partial}{\partial t} a_i(t) = [a_i(t), \hat{H}] &= e^{i\hat{H}t} [a_i, \hat{H}] e^{-i\hat{H}t} \\ &= \sum_{kl} K_{kl} e^{i\hat{H}t} [a_i, a_k^\dagger a_l] e^{-i\hat{H}t} + \frac{1}{4} \sum_{jk,lm} \widetilde{V}_{klmn}^{2N} e^{i\hat{H}t} [a_i, a_k^\dagger a_l^\dagger a_n a_m] e^{-i\hat{H}t} \\ &= \sum_{l} K_{il} a_l(t) + \frac{1}{2} \sum_{lmn} \widetilde{V}_{ilmn}^{2N} a_l^\dagger(t) a_n(t) a_m(t) \text{ .} \end{aligned} \tag{II.56}$$

where we have used the following relations,

$$[\hat{A}, \hat{B}\hat{C}] = [\hat{A}, \hat{B}]\hat{C} + \hat{B}[\hat{A}, \hat{C}] = \{\hat{A}, \hat{B}\}\hat{C} - \hat{B}\{\hat{A}, \hat{C}\} \text{ .} \tag{II.57}$$

Multiplying by $a_j^\dagger(t')$ on the right, taking the $\mathcal{T}$-product and the expectation value in $|\Psi\rangle$ of the corresponding expression we obtain,

$$\begin{aligned} i \langle \Psi | \mathcal{T} \left(\frac{\partial}{\partial t} a_i(t) a_j^\dagger(t') \right) | \Psi \rangle &= \sum_l K_{il} \langle \Psi | \mathcal{T} \left(a_l(t) a_j^\dagger(t') \right) | \Psi \rangle \\ &\quad + \frac{1}{2} \sum_{lmn} \widetilde{V}_{ilmn}^{2N} \langle \Psi | \mathcal{T} \left(a_l^\dagger(t) a_n(t) a_m(t) a_j^\dagger(t') \right) | \Psi \rangle \text{ .} \end{aligned} \tag{II.58}$$

On the second line of equation (II.58) appears the four-point Green's function.

The $\mathcal{T}$-product of operators being a distribution it verifies[11],

$$\frac{\partial}{\partial t}\left[\mathcal{T}\left(a_i(t)a_j^\dagger(t')\right)\right] = \Delta\delta(t-t')\delta_{ij} + \mathcal{T}\left(\frac{\partial}{\partial t}(a_i(t)a_j^\dagger(t')\right) \ . \tag{II.59}$$

where $\Delta = 1$ is the module of the distribution's discontinuity in $t = t'$.

Thus we finally get,

$$\boxed{\sum_l \left(i\delta_{il}\frac{\partial}{\partial t} - K_{il}\right)\mathcal{G}^{[1]}_{lj}(t-t') = \delta(t-t')\delta_{ij} + \frac{i}{2}\sum_{lmn}\widetilde{V}^{2N}_{il,mn}\mathcal{G}^{[2]}_{nm,jl}(t,t;t',t^+) \ .} \tag{II.60}$$

This is the equation of motion expressing the one-body propagator $\mathcal{G}^{[1]}$ in terms of $\mathcal{G}^{[2]}$. It is the first step of the infinite Martin-Schwinger hierarchy [71] of coupled equations relating $\mathcal{G}^{[n]}$ to $\mathcal{G}^{[n-1]}$ and $\mathcal{G}^{[n+1]}$.

Similarly one could have started from the equation of motion for the creation operator $a_j^\dagger(t')$. This would have led to the following equivalent equation,

$$\boxed{\sum_k \mathcal{G}^{[1]}_{ik}(t-t')\left(i\frac{\overleftarrow{\partial}}{\partial t'}\delta_{kj} + K_{kj}\right) = -\delta(t-t')\delta_{ij} + \frac{i}{2}\sum_{klm}\mathcal{G}^{[2]}_{im,lk}(t,t'^-;t',t')\widetilde{V}^{2N}_{kl,mj} \ .} \tag{II.61}$$

Free propagator The propagator $\mathcal{G}^{[0]}$ of a free particle is solution of,

$$\sum_l \left(i\delta_{il}\frac{\partial}{\partial t} - K_{il}\right)\mathcal{G}^{[0]}_{lj}(t-t') = \delta(t-t')\delta_{ij} \ , \tag{II.62}$$

or equivalently,

$$\sum_k \mathcal{G}^{[0]}_{ik}(t-t')\left(i\frac{\overleftarrow{\partial}}{\partial t'}\delta_{kj} + K_{kj}\right) = -\delta(t-t')\delta_{ij} \ . \tag{II.63}$$

It is therefore a Green's function in the mathematical sense and solutions of Eq. (II.60) and (II.61) can be written in an integral form as,

$$\mathcal{G}^{[1]}_{ij}(t-t') = \mathcal{G}^{[0]}_{ij}(t-t') + \frac{i}{2}\sum_{klmn}\int \mathrm{d}t_1 \mathcal{G}^{[0]}_{ik}(t-t_1)\widetilde{V}^{2N}_{kl,mn}\mathcal{G}^{[2]}_{nm,jl}(t_1,t_1;t',t_1^+) \ , \tag{II.64}$$

[11] This can be easily shown by writing

$$\mathcal{T}\left(a_i(t)a_j^\dagger(t')\right) = \theta(t-t')a_i(t)a_j^\dagger(t') - \theta(t'-t)a_j^\dagger(t')a_i(t) \ ,$$

differentiating this expression with respect to t and using the anti-commutation rules at equal time $\{a_j^\dagger(t), a_i(t)\} = \delta_{ij}$.

and,

$$\mathcal{G}^{[1]}_{ij}(t-t') = \mathcal{G}^{[0]}_{ij}(t-t') - \frac{i}{2}\sum_{klmn}\int \mathrm{d}t_1 \mathcal{G}^{[2]}_{im,lk}(t,t_1^-;t_1,t_1)\widetilde{V}^{2N}_{kl,mn}\mathcal{G}^{[0]}_{nj}(t_1-t') \;, \tag{II.65}$$

respectively.

∘ The two-body propagator or four-point Green's function

Definition According to (II.54), the two-body GF is defined as,

$$\mathcal{G}^{[2]}_{ij,kl}(t_1,t_2;t_3,t_4) = -\langle\Psi|\mathcal{T}\left(a_i(t_1)a_j(t_2)a^\dagger_l(t_4)a^\dagger_k(t_3)\right)|\Psi\rangle \;. \tag{II.66}$$

Here again different time ordering can be considered: For instance, when $t_1, t_2 > (<) t_3, t_4$ the two-body GF describes the propagation of a pair of particles ("holes"). Whereas it describes the propagation of a particle-hole pair when $t_1, t_3 < t_2, t_4$.

Equation of motion Following the same steps than for the one-body propagator one can derive an equation of motion for the four-point GF, relating $\mathcal{G}^{[2]}$ to $\mathcal{G}^{[1]}$ and $\mathcal{G}^{[3]}$,

$$\begin{aligned}\sum_s\left(i\delta_{is}\frac{\partial}{\partial t_1} - T_{is}\right)\mathcal{G}_{sj,kl}(t_1,t_2;t_3,t_4) &= \delta_{ik}\delta(t_1-t_3)\mathcal{G}_{jl}(t_2-t_4) - \delta_{il}\delta(t_1-t_4)\mathcal{G}_{jk}(t_2-t_3) \\ &\quad -\frac{i}{2}\sum_{srm}\widetilde{V}^{2N}_{is,rm}\mathcal{G}^{[3]}_{mrj,kls}(t_1,t_1,t_2;t_3,t_4,t_1^+) \;. \end{aligned}\tag{II.67}$$

Solutions of Eq. (II.67) can then also be expressed in an integral form in terms of the free propagator $\mathcal{G}^{[0]}$.

Cluster expansion It is also possible to show that $\mathcal{G}^{[2]}$ can be expressed in terms of the complete one-body propagator $\mathcal{G}^{[1]}$ as[12],

$$\mathcal{G}^{[2]}_{ij,kl}(t_1,t_2;t_3,t_4) = \mathcal{G}^{[1]}_{ik}(t_1-t_3)\mathcal{G}^{[1]}_{jl}(t_2-t_4) - \mathcal{G}^{[1]}_{il}(t_1-t_4)\mathcal{G}^{[1]}_{jk}(t_2-t_3) + \mathcal{G}^{[2]C}_{ij,kl}(t_1,t_2;t_3,t_4) \;, \tag{II.68}$$

where $\mathcal{G}^{[2]C}$ denotes the connected part of the two-body GF.

[12] In fact any N-body propagator can be expressed as a sum of an antisymmetrized product of lower-body propagator and a connected N-body part. This cluster decomposition of the GFs is very useful when perturbative methods cannot be used (for instance when dealing with a hard core). One can indeed make a truncation at a certain order in correlations. This amounts to resumming the infinite serie of a certain type of diagrams (partial summation). For instance, the Hartree-Fock approximation is obtained by neglecting two-body correlations, i.e. by setting $\mathcal{G}^{[2]C} = 0$.

◦ **Dyson equation** Defining a quantity Σ which satisfies,

$$\sum_s \int \mathrm{d}t_2 \Sigma_{ks}(t_1 - t_2)\mathcal{G}^{[1]}_{sj}(t_2 - t') = \frac{i}{2}\sum_{lmn} \widetilde{V}^{2N}_{kl,mn}\mathcal{G}^{[2]}_{nmjl}(t_1, t_1; t', t_1^+) \ , \tag{II.69}$$

the equation of motion (II.64) for the one-body propagator can be rewritten as,

$$\mathcal{G}^{[1]}_{ij}(t - t') = \mathcal{G}^{[0]}_{ij}(t - t') + \sum_{ks} \int \mathrm{d}t_1 \int \mathrm{d}t_2 \mathcal{G}^{[0]}_{ik}(t - t_1)\Sigma_{ks}(t_1 - t_2)\mathcal{G}^{[1]}_{sj}(t_2 - t') \ , \tag{II.70}$$

or equivalently,

$$\mathcal{G}^{[1]}_{ij}(t - t') = \mathcal{G}^{[0]}_{ij}(t - t') + \sum_{sn} \int \mathrm{d}t_1 \int \mathrm{d}t_2 \mathcal{G}^{[1]}_{is}(t - t_2)\Sigma_{sn}(t_2 - t_1)\mathcal{G}^{[0]}_{nj}(t_1 - t') \ . \tag{II.71}$$

Eq. (II.70) and (II.71) are two equivalent forms of the well known Dyson equation represented on Fig. (II.4). Σ is the self-energy (also called mass-operator) which contains all information about the one-, two-, three-, ...-body propagators. The self-energy resums all one-particle irreducible diagrams.

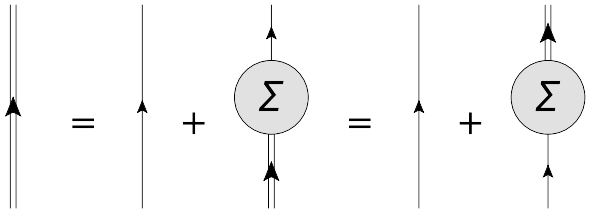

Figure II.4: Graphical representation of the Dyson equation. The simple line represents the free propagator $\mathcal{G}^{[0]}$, while the double line denotes the complete propagator $\mathcal{G}^{[1]}$.

II.2.2 Orbital equation from the Green's function formalism at equal times

Now that the notations and definitions have been recalled, let us show that the second variational equation of the mp-mh approach can be obtained from the Green's function formalism at equal times.

Let us first define,

$$\Omega_{ij}(t, t') = \frac{i}{2}\sum_{klm} \mathcal{G}^{[2]}_{im,lk}(t, t'^{-}; t', t')\widetilde{V}^{2N}_{kl,mj} \tag{II.72}$$

The equations of motion (II.60) and (II.61) can then be written as,

$$\sum_l \left(i\delta_{il}\frac{\partial}{\partial t} - K_{il} \right) \mathcal{G}^{[1]}_{lj}(t - t') = \delta(t - t')\delta_{ij} + \Omega^*_{ji}(t', t) \ , \tag{II.73}$$

and ,

$$\sum_k \mathcal{G}^{[1]}_{ik}(t-t')\left(i\frac{\overleftarrow{\partial}}{\partial t'}\delta_{kj}+K_{kj}\right)=-\delta(t-t')\delta_{ij}+\Omega_{ij}(t,t')\ , \tag{II.74}$$

respectively.
Adding now Eq. (II.73) to Eq. (II.74) eliminates the time derivatives and we get,

$$\sum_k \left(\mathcal{G}_{ik}(t-t')K_{kj}-K_{ik}\mathcal{G}_{kj}(t-t')\right)=\Omega_{ij}(t,t')+\Omega^*_{ji}(t',t)\ . \tag{II.75}$$

Let us now take the equal-time limit $t'\to t^+$ of Eq. (II.75).
It is straightforward to see that the many-body propagators taken at equal times are proportional to the many-body densities. In particular,

$$\begin{aligned}
\lim_{t'\to t^+}\mathcal{G}^{[1]}_{ij}(t-t') &= -i\lim_{t'\to t^+}\langle\Psi|\mathcal{T}\left(a_i(t)a^\dagger_j(t')\right)|\Psi\rangle \\
&= +i\langle\Psi|a^\dagger_j(t)a_i(t)|\Psi\rangle \\
&= +i\langle\Psi|a^\dagger_j(0)a_i(0)|\Psi\rangle \ \text{(translation invariance)} \\
&= +i\rho_{ij}\ ,
\end{aligned} \tag{II.76}$$

and,

$$\begin{aligned}
\lim_{t'\to t^+}\mathcal{G}^{[2]}_{kl,ji}(t,t;t',t') &= -\lim_{t'\to t^+}\langle\Psi|\mathcal{T}\left(a_k(t)a_l(t)a^\dagger_i(t')a^\dagger_j(t')\right)|\Psi\rangle \\
&= -\langle\Psi|a^\dagger_i(0)a^\dagger_j(0)a_k(0)a_l(0)|\Psi\rangle \\
&= -\rho^{[2]}_{likj} \\
&= -\left(\rho_{li}\rho_{kj}-\rho_{lj}\rho_{ki}+\sigma_{il,jk}\right)\ .
\end{aligned} \tag{II.77}$$

Using the cluster decomposition (II.68) of $\mathcal{G}^{[2]}$ we also notice that,

$$\lim_{t'\to t^+}\mathcal{G}^{[2]C}_{kl,ji}(t,t;t',t')=-\sigma_{il,jk}\ . \tag{II.78}$$

We deduce from these properties that,

$$\begin{cases}
\lim\limits_{t'\to t^+}\Omega(t,t')=-i\left(F(\sigma)+\rho\Gamma[\rho]\right) & \text{(II.79)}\\
\lim\limits_{t'\to t^+}\Omega^\dagger(t',t)=i\left(F^\dagger(\sigma)+\Gamma[\rho]\rho\right)\ , & \text{(II.80)}
\end{cases}$$

where $\Gamma[\rho]$ is the average potential given in Eq. (II.29), and $F(\sigma)$ is defined in Eq. (II.32).

Thus, Eq. (II.75) taken at the limit $t' \to t^+$ leads exactly to the orbital equation (II.25),

$$\left[\underbrace{\hat{K} + \hat{\Gamma}[\rho]}_{=\hat{h}[\rho]}, \hat{\rho}\right] = \hat{F}[\sigma] - \hat{F}^\dagger[\sigma] \equiv \hat{G}[\sigma] \ . \tag{II.81}$$

II.2.3 Diagrammatic analysis

Using the cluster decomposition (II.68) of $\mathcal{G}^{[2]}$, Ω can be split into two parts as,

$$\Omega(t,t') = \Omega^1(t,t') + \Omega^C(t,t') \ , \tag{II.82}$$

where,

$$\begin{aligned}
\Omega^1_{ij}(t,t') &= \frac{i}{2}\sum_{klm}\Big(\mathcal{G}_{il}(t-t')\mathcal{G}_{mk}(t'^- - t') - \mathcal{G}_{ik}(t-t')\mathcal{G}_{ml}(t'^- - t')\Big)\widetilde{V}^{2N}_{kl,mj} \\
&= -\sum_{l}\mathcal{G}_{il}(t-t')\sum_{km}\rho_{mk}\widetilde{V}^{2N}_{kl,mj} \\
&= -\sum_{l}\mathcal{G}_{il}(t-t')\Gamma_{lj}[\rho] \ ,
\end{aligned} \tag{II.83}$$

and,

$$\Omega^C_{ij}(t,t') = \frac{i}{2}\sum_{klm}\mathcal{G}^{[2]C}_{im,lk}(t,t'^-;t',t')\widetilde{V}^{2N}_{kl,mj} \ . \tag{II.84}$$

These contributions are diagrammatically represented on Fig. (II.5).

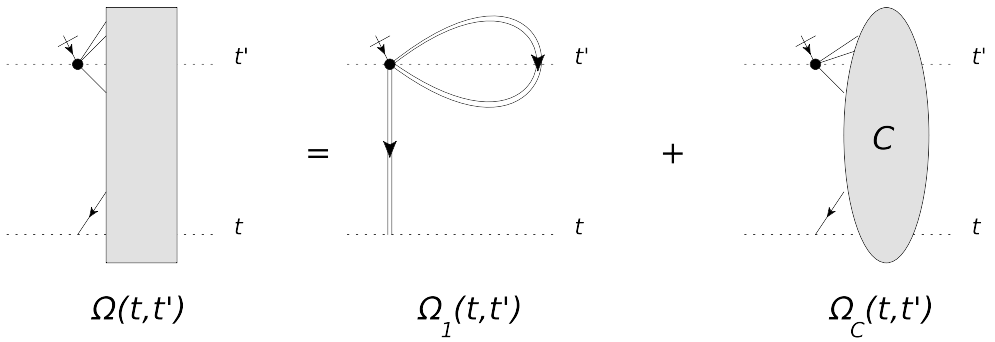

Figure II.5: Graphical representation of $\Omega = \Omega^1 + \Omega^C$. The blob '$C$' denotes the connected part of the two-body GF. The cut leg corresponds to the interaction line that is not attached to $\mathcal{G}^{[2]}$.

The equal-time limit of Ω^1 corresponds to,

$$\lim_{t' \to t^+} \Omega^1(t,t') = -i\rho\Gamma[\rho] \ . \tag{II.85}$$

We see from Eq. (II.83) that $\Gamma[\rho]$ is the part of Ω_1 represented on Fig. (II.5) without the external propagator. It is therefore represented by the diagram on Fig. (II.6).

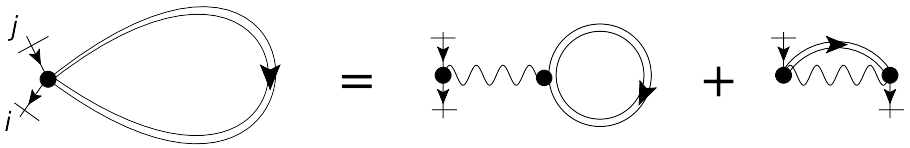

Figure II.6: General diagrams for $\Gamma_{ij}[\rho]$.

It was shown in [4] that the average potential $\Gamma[\rho]$ is in fact the discontinuity of $\Omega(t,t')$ at $t=t'$ which is equal to the discontinuity of $\Omega^1(t,t')$ at $t=t'$. This is easily obtained by subtracting the equation of motion (II.73) taken at $t'=t^+$ from the same equation taken at $t'=t^-$.

The equal-time limit of Ω^C gives,

$$\begin{aligned} \lim_{t'\to t}\Omega^C_{ij}(t,t') &= \frac{i}{2}\sum_{klm}\sigma_{km,li}\widetilde{V}^{2N}_{kl,mj} \\ &= iF_{ij}[\sigma]\ . \end{aligned} \tag{II.86}$$

Thus, we can represent $F[\sigma]$ as shown on Figs. (II.7) and (II.8).

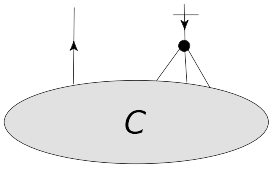

Figure II.7: Graphical representation of $F_{ij}[\sigma]$.

In particular one wees from Fig. (II.8) that $F[\sigma]$ contains resummations of ring and ladder diagrams shown in Fig. (II.9).

Relation to the self energy From this study we can now also establish a relation between the quantities appearing in the orbital equation and the self-energy of the Dyson equation. Using again the cluster decomposition (II.68) for $\mathcal{G}^2$, it is easily shown that $\Sigma(t-t')$ can always be split into a static part proportional to $\delta(t-t')$, which is nothing but the average potential $\hat{\Gamma}$ defined in (II.29), and a dynamical part $\Sigma^{dyn}(t-t')$ which is given by,

$$\Sigma^{dyn}_{ij}(t-t') = -i\int dt_1 \sum_{klmn}\widetilde{V}^{2N}_{ki,lm}\mathcal{G}^{[2]C}_{ml,nk}(t,t;t_1,t^+)\mathcal{G}^{[1]-1}_{nj}(t_1-t')\ . \tag{II.87}$$

From this we can relate the operator $F(\sigma)$, and therefore the source term of the orbital

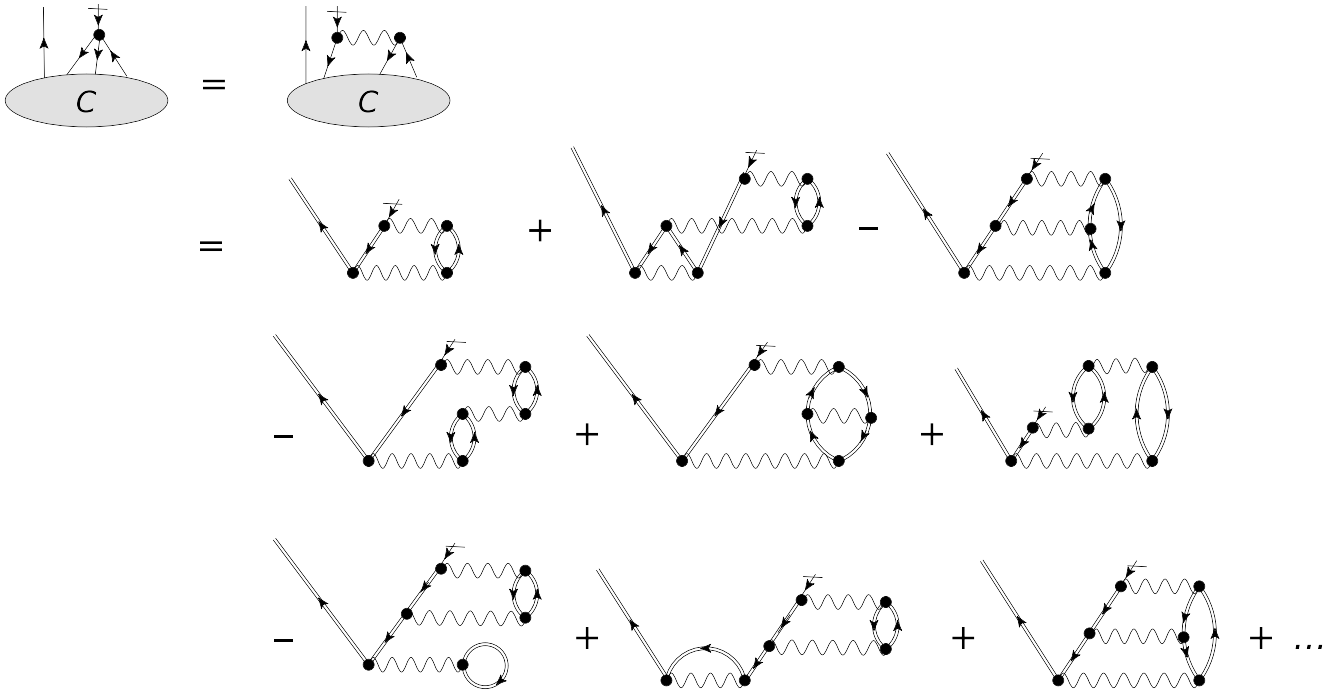

Figure II.8: A few diagrams contained in the expansion of $F_{ij}[\sigma]$.

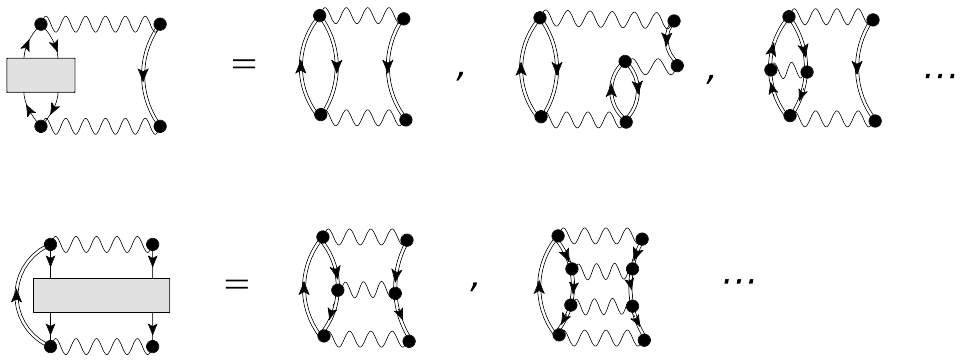

Figure II.9: Resummation of ring (top) and ladder (bottom) diagrams in $F_{ij}[\sigma]$.

equation, to the dynamical part of the self-energy as,

$$\lim_{t_2 \to t^+} \frac{1}{2i} \sum_j \int \mathrm{d}t' \Sigma^{dyn}_{ij}(t-t') \mathcal{G}^{[1]}_{js}(t'-t_2) = \frac{1}{2} \sum_{klm} \widetilde{V}^{2N}_{ki,lm} \sigma_{kl,sm} = (F^\dagger)_{is} \ . \tag{II.88}$$

The previous analysis allowed us to improve our understanding of the second variational equation of the mp-mh method. In particular the relation to Green's function led to a diagrammatic interpretation of the renormalization of the orbitals. In the next chapters, we apply the mp-mh configuration mixing formalism to the description of a few nuclei. The im-

pact induced by the inclusion of correlations into the mean-field, as well as the role of the "dynamical" correlations (via the source term $G[\sigma]$) will be analyzed.

Chapter III

Application to the Gogny force

Although the multiparticle-multihole configuration mixing approach could in principle be applied to any effective nuclear interaction, the applications realized in this work are performed using the phenomenological effective Gogny force D1S. Although the density-dependence of this interaction prevents any precise and formal link with the analysis made in the previous chapter, the qualitative discussions should stay valid.
We start the present chapter with a short presentation of the Gogny interaction. In the second part, we derive the formalism applied to a density-dependent force. As we will see, this property leads to the appearance of new terms complicating the resolution of the variational equations. In the third part, we describe in detail the procedure adopted to practically solve the equations. Finally, the last part applies the self-consistent procedure to a first test case: the ^{12}C nucleus.

III.1 A few words about the Gogny force

The first version D1 of the Gogny interaction dates back to the 1970's [29]. At that time effort was being made in order to go beyond the Hartree-Fock description of nuclei by adding the treatment of pairing correlations. D1 was originally introduced in this context in order to realize Hartree-Fock-Bogolyubov (HFB) [92] calculations in which the mean-field and the pairing correlations were derived in a fully self-consistent manner from the same interaction.

As effective interaction, the analytical form of the Gogny force was taken as density-dependent. This property can be derived from the G-matrix theory [22, 27] and reflects the fact that the actual force felt by a nucleon depends on the density of its neighboring particles, and therefore on its position in the nucleus. The parameters of this phenomenological force were then adjusted in order to reproduce some nuclear properties at the lowest Hartree-Fock order, although the fitting procedure was done in the perspective of allowing reasonable extensions beyond this approximation such as the inclusion of pairing correlations. To make this possi-

ble, the introduction of finite ranges in part of the interaction was crucial in order to avoid pathologies when high relative momenta appear[1]. However one should always keep in mind that such a phenomenological approach causes the loss of any link with perturbation theory, making impossible any clear higher-order correction.

The analytical form of the Gogny force was postulated as,

$$\begin{aligned} V_{\vec{r},\vec{x}}[\rho] &= \sum_{j=1,2} (W_j + B_j P_\sigma - H_j P_\tau - M_j P_\sigma P_\tau)\, e^{-\frac{\vec{x}^2}{\mu_j^2}} \\ &\quad + t_3\,(1 + x_0 P_\sigma)\delta(\vec{x})\rho^\alpha(\vec{r}) \\ &\quad + i\,W_{LS}\,\overleftarrow{\nabla}_{12}\delta(\vec{x}) \times \overrightarrow{\nabla}_{12}.(\sigma_1 + \sigma_2) \\ &\quad + (1 + 2\tau_{1_z})(1 + 2\tau_{2_z})\frac{e^2}{|\vec{r_1} - \vec{r_2}|}\ . \end{aligned} \tag{III.1}$$

where,

$$\begin{cases} \vec{r} &= \frac{\vec{r_1}+\vec{r_2}}{2} \quad \text{is the center of mass of the particles 1 and 2,} \\ \vec{x} &= \vec{r_1} - \vec{r_2} \quad \text{is the relative coordinate .} \end{cases} \tag{III.2}$$

The first line in Eq. (III.1) represents the finite range central part of the interaction. P_σ and P_τ are the spin and isospin exchange operators respectively. The form factor is taken as two Gaussian functions with respective ranges $\mu_1 = 0.7$ fm and $\mu_2 = 1.2$ fm, allowing explicit treatment of middle and long-range correlations. Short-range correlations associated with the hard core of the interaction are implicitly taken into account via the zero-range density-dependent term on the second line of Eq. (III.1), which also accounts for many-body effects. The third and fourth line of Eq. (III.1) respectively represent a zero-range spin-orbit interaction and the Coulomb interaction acting between protons (with $\tau_z = \frac{1}{2}$). The coefficients W_j, B_j, H_j, M_j, μ_j $(j = 1, 2)$ as well as t_3, x_0, α and W_{LS} are the 14 parameters to be determined.

The D1 interaction led to successful results concerning the description of static properties of nuclei within the HFB approach [29, 47], as well as the description of vibrational collective modes within the RPA method (see e.g. [10, 48]). However, spectroscopy results obtained using the 5DCH approach [30] were not found in adequacy with experiment: Ref. [46] shows unsatisfactory description of rotational and vibrational bands. This disagreement was mostly

[1] In the Hartree-Fock approximation the use of a zero-range interaction is not catastrophic since it only involves relative momenta up to twice the Fermi momentum k_F.

attributed to the pairing content of the force whose intensity was slightly too high. The D1 interaction was also tested on the description of nuclear fission [7] which revealed unrealistic shapes of the second barrier. The D1S version of the Gogny interaction [8] was created at the beginning of the 1980's, in order to correct these discrepancies. Since then, this parametrization has been successful in reproducing many properties of nuclei within reasonable extensions of the mean-field such as HFB, RPA, GCM as well as projection techniques (see e.g. [30, 88, 89, 90]).

The D1S interaction The D1S version of the Gogny force uses the following set of parameters,

j	μ_j (fm)	W_j (MeV)	B_j (MeV)	H_j (MeV)	M_j (MeV)
1	0.7	-1720.30	1300.00	-1815.53	1397.60
2	1.2	103.639	-163.483	162.812	-223.933

and,

t_3 (MeV.fm^3)	x_0	α	W_{LS} (MeV)
1390.60	1.0	$\frac{1}{3}$	-130.00

The ranges (μ_1, μ_2) were fixed *a priori*. The exponent α of the density-dependence was chosen equal to 1/3 in order to fit at best different properties such as the binding energy per nucleon E/A and the incompressibility of nuclear matter K_∞. The coefficient x_0 was taken equal to one so that the density-dependent part of the interaction would be of proton-neutron type only, in order to avoid the appearance of density-dependent terms in the particle-like pairing fields. The spin-orbit intensity W_{LS} was also determined independently of the other parameters in order to reproduce the $p^{3/2} - p^{1/2}$ splitting in ^{16}O. Regarding the other free parameters, they have been fitted so as to reproduce some properties of nuclear matter as well as,

- Global properties such as binding energies and charge radii of a few nuclei,
- Pairing properties by constraining matrix elements in the singlet-even component of the interaction,
- Isospin properties by constraining the energy difference between the neutron and the proton $2s_{1/2}$ states in ^{48}Ca.

Note on the use of the D1S Gogny force in the mp-mh configuration mixing approach As stated previously, the Gogny interaction was originally created in order to achieve mean-field calculations, leaving room for RPA and GCM-type extensions. Although it showed success in certain beyond-mean-field extensions, there is no clear way of calculating higher order corrections and it might not be adapted to the treatment of all kind of correlations

such as in the mp-mh configuration mixing approach. Moreover, the question of which density is to be used in the interaction remains open when going to correlated system (density of the uncorrelated reference state, density of the correlated state...). In the following we use the density built with the correlated wave function $|\Psi\rangle$ (this simplifies the orbital equation since only one density appears). However there is no physical justification for that, and since the phenomenological nature of the Gogny force makes impossible to disentangle what effects are already included in the interaction, uncontrolled over-counting effects might occur.
Nevertheless, as seen throughout this work, the results obtained in the present studies are generally satisfactory and no pathological behaviour is obtained.
There exist in fact more recent parametrizations of the Gogny force such as D1N [25] or D1M [49] improving the equation of state in nuclear matter, as well as the description of nuclear states within the GCM method. One of the challenges in the development of the multiparticle-multihole configuration mixing method, is to be able to use, at some point, an interaction containing only finite-range components and adjusted to new constraints associated with the proton-neutron $T = 0$ channel. Since none of the existing parametrizations of the D1 interaction satisfy to this new criteria, and seem to lead to similar satisfying results, the choice has been made to develop the multiparticle-multihole configuration mixing method using the most tested and thus reliable version, that is D1S. Parallely to this project, work is in progress in order to develop an interaction satisfying the new requirements [26, 82].

III.2 Modification of the variational equations due to the density dependence of the interaction

Let us now present the formalism of the multiparticle-multihole configuration mixing method applied to a density dependent interaction. In the following, for the sake of simplicity, we omit the $\vec{r}, \vec{x}$ indices, so that $\hat{V}[\rho] \equiv \hat{V}_{\vec{r},\vec{x}}[\rho]$. The density dependence of the interaction can also be understood as a dependence in the mixing coefficients $\{A_\alpha\}$ and the single-particle orbitals $\{\varphi_i(\vec{r})\}$. This leads to the appearance of new terms while deriving the variational equations. They are explicitly described in the following.

III.2.1 First variational equation: the mixing coefficients

Varying the Lagrange functional $\mathcal{F}[\Psi,\lambda] = \langle\Psi|\hat{H}[\rho]|\Psi\rangle - \lambda\left(\langle\Psi|\Psi\rangle - 1\right)$ with respect to the expansion coefficients $\{A_\alpha\}$ now leads to,

$$\begin{aligned} 0 &= \frac{\partial\mathcal{F}[\Psi,\lambda]}{\partial A^*_\alpha} \ ,\forall\alpha \\ &= \frac{\partial}{\partial A^*_\alpha}\Big(\langle\Psi|\hat{H}[\rho]-\lambda|\Psi\rangle\Big) \\ &= \frac{\partial}{\partial A^*_\alpha}\left(\sum_{\beta\beta'} A^*_{\beta'}A_\beta\,\langle\phi_{\beta'}|\hat{H}[\rho]-\lambda|\phi_\beta\rangle\right) \\ &= \sum_\beta A_\beta\,\langle\phi_\alpha|\hat{H}[\rho]-\lambda|\phi_\beta\rangle + \langle\Psi|\frac{\partial\hat{H}[\rho]}{\partial A^*_\alpha}|\Psi\rangle \ , \end{aligned} \tag{III.3}$$

where,

$$\frac{\partial\hat{H}[\rho]}{\partial A^*_\alpha} = \frac{\partial\hat{V}[\rho]}{\partial A^*_\alpha} = \int d^3r'\frac{\delta V[\rho]}{\delta\rho(\vec{r'})}\frac{\partial\rho(\vec{r'})}{\partial A^*_\alpha} \ . \tag{III.4}$$

The local density $\rho(\vec{r'})$ can be expressed as,

$$\begin{aligned} \rho(\vec{r'}) &= \langle\Psi|\hat{\rho}(\vec{r'})|\Psi\rangle \\ &= \sum_{\sigma,\tau}\sum_{i_\tau j_\tau}\varphi^*_{i_\tau}(\vec{r'},\sigma)\varphi_{j_\tau}(\vec{r'},\sigma)\,\langle\Psi|a^\dagger_{i_\tau}a_{j_\tau}|\Psi\rangle \ , \end{aligned} \tag{III.5}$$

so that,

$$\frac{\partial\rho(\vec{r'})}{\partial A^*_\alpha} = \sum_{\sigma,\tau}\sum_{i_\tau j_\tau}\varphi^*_{i_\tau}(\vec{r'},\sigma)\varphi_{j_\tau}(\vec{r'},\sigma)\sum_\beta A_\beta\,\langle\phi_\alpha|a^\dagger_{i_\tau}a_{j_\tau}|\phi_\beta\rangle \ . \tag{III.6}$$

Therefore the last term on the r.h.s. of Eq. (III.3) reads,

$$\langle\Psi|\frac{\partial\hat{H}[\rho]}{\partial A^*_\alpha}|\Psi\rangle = \sum_\beta A_\beta\,\langle\phi_\alpha|\hat{R}[\rho,\sigma]|\phi_\beta\rangle \ , \tag{III.7}$$

where we have defined,

$$\begin{aligned} \hat{R}[\rho,\sigma] &= \sum_\tau\sum_{i_\tau j_\tau} R^\tau_{ij}[\rho,\sigma]a^\dagger_{i_\tau}a_{j_\tau} \\ &= \sum_\tau\sum_{i_\tau j_\tau}\int d^3r'\sum_\sigma\varphi^*_{i_\tau}(\vec{r'},\sigma)\varphi_{j_\tau}(\vec{r'},\sigma)\,\langle\Psi|\frac{\delta V[\rho]}{\delta\rho(\vec{r'})}|\Psi\rangle\,a^\dagger_{i_\tau}a_{j_\tau} \\ &= \int d^3r'\,\langle\Psi|\frac{\delta V[\rho]}{\delta\rho(\vec{r'})}|\Psi\rangle\,\hat{\rho}(\vec{r}) \ . \end{aligned} \tag{III.8}$$

This type of operator due to the density-dependence of the Gogny force is called "rearrangement term". Although one-body operator, this rearrangement term introduces a dependence on the correlation matrix σ through,

$$\begin{aligned}\langle\Psi|\frac{\delta V[\rho]}{\delta\rho(\vec{r'})}|\Psi\rangle &= \frac{1}{4}\sum_{klmn}\langle kl|\frac{\delta V[\rho]}{\delta\rho(\vec{r'})}|\widetilde{mn}\rangle\,\langle\Psi|a_k^\dagger a_l^\dagger a_n a_m|\Psi\rangle \\ &= \frac{1}{4}\sum_{klmn}\langle kl|\frac{\delta V[\rho]}{\delta\rho(\vec{r'})}|\widetilde{mn}\rangle\,(\rho_{mk}\rho_{nl}-\rho_{ml}\rho_{nk}+\sigma_{km,ln})\ , \end{aligned} \tag{III.9}$$

and thus requires the construction of this connected two-body quantity. Defining now $\hat{\mathcal{H}}[\rho,\sigma]$ as,

$$\hat{\mathcal{H}}[\rho,\sigma] \equiv \hat{H}[\rho] + \hat{R}[\rho,\sigma]\ , \tag{III.10}$$

the first variational equation (III.3) can be expressed as,

$$\boxed{\sum_\beta A_\beta\,\langle\phi_\alpha|\mathcal{H}[\rho,\sigma]|\phi_\beta\rangle = \lambda A_\alpha,\quad\forall\alpha}\ , \tag{III.11}$$

representing the diagonalization of the modified Hamiltonian matrix $\mathcal{H}[\rho,\sigma]$ in the many-body configuration space. It is important to remind that the dependence of $\mathcal{H}$ on the one- and two-body densities of the system renders Eq. (III.11) non-linear. Solving this equation thus requires an iterative procedure and therefore is more complicated to solve than the usual diagonalization performed in Configuration-Interaction-type methods. Finally let us note that the eigenvalues λ of this Hamiltonian no longer correspond to the energies of the nucleus under study. In fact we have $E[\Psi_N] = \langle\Psi_N|\hat{H}[\rho]|\Psi_N\rangle = \lambda_N - \langle\Psi_N|\hat{R}[\rho,\sigma]|\Psi_N\rangle$.

III.2.2 Second variational equation: the single-particle orbitals

Similarly, additional terms appear when minimizing the energy functional with respect to the single-particle orbitals. Eq. (II.22) is modified as,

$$0 = \langle\delta\Psi|\hat{H}[\rho]|\Psi\rangle + \langle\Psi|\hat{H}[\rho]|\delta\Psi\rangle + \langle\Psi|\delta\hat{H}[\rho]|\Psi\rangle\ , \tag{III.12}$$

where,

$$\delta\hat{H}[\rho] = \delta\hat{V}[\rho] = \int d^3r'\frac{\delta\hat{V}[\rho]}{\delta\rho(\vec{r})}\delta\rho(\vec{r})\ . \tag{III.13}$$

Considering a transformation $a_i^\dagger \to e^{i\hat{T}} a_i^\dagger e^{-i\hat{T}}$ of the orbitals, leading to a variation $|\delta\phi_\alpha\rangle = i\hat{T}\,|\phi_\alpha\rangle$ of the many-body configurations, we get,

$$\begin{aligned}
\delta\rho(\vec{r}) &= \delta\left(\langle\Psi|\hat{\rho}(\vec{r})|\Psi\rangle\right) \\
&= \delta\left(\sum_{\alpha\beta} A_\alpha^* A_\beta \,\langle\phi_\alpha|\hat{\rho}(\vec{r})|\phi_\beta\rangle\right) \\
&= \sum_{\alpha\beta} A_\alpha^* A_\beta \left(\langle\delta\phi_\alpha|\hat{\rho}(\vec{r})|\phi_\beta\rangle + \langle\phi_\alpha|\hat{\rho}(\vec{r})|\delta\phi_\beta\rangle\right) \\
&= i\,\langle\Psi|[\hat{\rho}(\vec{r}),\hat{T}]|\Psi\rangle \ . \qquad \text{(III.14)}
\end{aligned}$$

The third term on the r.h.s of Eq. (III.12) therefore reads,

$$\begin{aligned}
\langle\Psi|\delta\hat{H}[\rho]|\Psi\rangle &= i\int d^3r'\,\langle\Psi|\frac{\delta\hat{V}[\rho]}{\delta\rho(\vec{r})}|\Psi\rangle\,\langle\Psi|[\hat{\rho}(\vec{r}),\hat{T}]|\Psi\rangle \\
&= i\,\langle\Psi|\left[\hat{R}[\rho,\sigma],\hat{T}\right]|\Psi\rangle \ , \qquad \text{(III.15)}
\end{aligned}$$

where we recognized the expression of the rearrangement term defined in Eq. (III.8). According to Eq. (II.23) the first two terms on the r.h.s of Eq. (III.12) are equal to $i\,\langle\Psi|\left[\hat{H}[\rho],\hat{T}\right]|\Psi\rangle$. The second variational equation (III.12) therefore reads,

$$\boxed{\langle\Psi|\left[\hat{\mathcal{H}}[\rho,\sigma],\hat{T}\right]|\Psi\rangle = 0}\,, \qquad \text{(III.16)}$$

where $\hat{\mathcal{H}}[\rho,\sigma] = \hat{H}[\rho] + \hat{R}[\rho,\sigma]$ is the Hamiltonian modified by rearrangement terms as defined in Eq. (III.10).

Following the same procedure than in Appendix (A), it can then easily be shown that this variational equation can be recasted into,

$$\boxed{\left[\hat{h}[\rho,\sigma],\hat{\rho}\right] = \hat{G}[\sigma]}\,, \qquad \text{(III.17)}$$

where ρ and σ are respectively the one-body and connected two-body densities as previously. The mean-field Hamiltonian $\hat{h}[\rho,\sigma]$ is modified by rearrangement terms as,

$$\begin{aligned} h[\rho,\sigma]_{ij} &= K_{ij} + \sum_{kl} \langle ik|\hat{V}[\rho]|\widetilde{jl}\rangle\, \rho_{lk} + \frac{1}{4}\sum_{klmn} \langle kl|\frac{\partial \hat{V}[\rho]}{\partial \rho_{ji}}|\widetilde{mn}\rangle\, \langle\Psi|a_k^\dagger a_l^\dagger a_n a_m|\Psi\rangle \\ &= \underbrace{K_{ij} + \sum_{kl} \langle ik|\hat{V}[\rho]|\widetilde{jl}\rangle\, \rho_{lk}}_{\Gamma_{ij}[\rho]} + \underbrace{\frac{1}{4}\sum_{klmn} \langle kl|\frac{\partial \hat{V}[\rho]}{\partial \rho_{ji}}|\widetilde{mn}\rangle\, (\rho_{mk}\rho_{nl} - \rho_{ml}\rho_{nk} + \sigma_{km,ln})}_{R_{ij}[\rho,\sigma]} \ . \end{aligned} \tag{III.18}$$

The one-body Hamiltonian $h[\rho,\sigma]$ now directly depends on the two-body correlation matrix[2] σ. The expression of the source term $G[\sigma]$ stays unchanged,

$$G[\sigma]_{ij} = \frac{1}{2}\sum_{klm} \sigma_{ki,lm}\, \langle kl|\hat{V}[\rho]|\widetilde{jm}\rangle - \frac{1}{2}\sum_{klm} \langle ik|\hat{V}[\rho]|\widetilde{lm}\rangle\, \sigma_{jl,km} \ . \tag{III.19}$$

Let us note however that if an explicit three-body force is used, the source term contains additional terms in $\rho\sigma$ and χ, where χ denotes the three-body correlation matrix (see Appendix A).

III.3 Solution techniques

III.3.1 Global self-consistent procedure

Since the mixing coefficients $\{A_\alpha\}$ depend on the choice of orbitals $\{a_i^\dagger\}$, and vice-versa, both variational equations (III.11) and (III.17) are coupled and therefore can be solved using the following iterative procedure.

1. Start from a set of pure Hartree-Fock orbitals $\{a_i^{(0)}\}$ obtained by solving $\left[\hat{h}[\rho^{(0)}], \hat{\rho}^{(0)}\right] = 0$, i.e. by solving Eq. (III.17) with $|\Psi^{(0)}\rangle = |\phi^{(0)}\rangle$ and therefore $\sigma^{(0)} = 0$.

2. Build the many-body configurations $|\phi_\alpha^{(0)}\rangle$ on this first set of orbitals, and calculate the matrix elements $\mathcal{H}_{\alpha\beta}[\rho^{(0)}, \sigma^{(0)} = 0] = H[\rho^{(0)}]_{\alpha\beta} + R[\rho^{(0)}, \sigma^{(0)} = 0]_{\alpha\beta}$. At this stage, the density used in the interaction is the density $\rho^{(0)}$ of the uncorrelated state $|\phi^{(0)}\rangle$. The rearrangement terms are also calculated at the Hartree-Fock level using $(\rho^{(0)}, \sigma^{(0)} = 0)$. Solve then Eq. (III.11) to obtain a first set of mixing coefficients $\{A_\alpha^{(1)}\}$, that is, a first correlated state $|\Psi^{(1)}\rangle$.

[2] Although the density dependence of the Gogny interaction effectively takes into account various many-body effects, we note the similarity between the expression of this mean-field and the one derived from a real three-body interaction in Appendix A.

3. Calculate the one-body density matrix $\rho^{(1)}$ and the two-body correlation matrix $\sigma^{(1)}$ as,

$$\rho_{ij}^{(1)} = \langle \Psi^{(1)} | a_j^{\dagger(0)} a_i^{(0)} | \Psi^{(1)} \rangle \ ,$$

and,

$$\sigma_{ij,kl}^{(1)} = \langle \Psi^{(1)} | a_i^{\dagger(0)} a_k^{\dagger(0)} a_l^{(0)} a_j^{(0)} | \Psi^{(1)} \rangle - \rho_{ji}^{(1)} \rho_{lk}^{(1)} + \rho_{jk}^{(1)} \rho_{li}^{(1)} \ ,$$

respectively.

4. From this, calculate the mean-field $h[\rho^{(1)}, \sigma^{(1)}]$ and the source term $G[\sigma^{(1)}]$, and solve Eq. (III.17) to obtain a new set of single particle states $\{a_i^{(1)}\}$.

5. Go back to step 2 and calculate $\mathcal{H}[\rho^{(1)}, \sigma^{(1)}]$ using correlated densities. Solve Eq. (III.11) to obtain new mixing coefficients $\{A_\alpha^{(2)}\}$.

6. Calculate $\rho^{(2)}$ and $\sigma^{(2)}$ as,

$$\rho_{ij}^{(2)} = \langle \Psi^{(2)} | a_j^{\dagger(1)} a_i^{(1)} | \Psi^{(2)} \rangle \ ,$$

and,

$$\sigma_{ij,kl}^{(2)} = \langle \Psi^{(2)} | a_i^{\dagger(1)} a_k^{\dagger(1)} a_l^{(1)} a_j^{(1)} | \Psi^{(2)} \rangle - \rho_{ji}^{(2)} \rho_{lk}^{(2)} + \rho_{jk}^{(2)} \rho_{li}^{(2)} \ .$$

7. Calculate $h[\rho^{(2)}, \sigma^{(2)}]$ and $G[\sigma^{(2)}]$, and solve Eq. (III.17) to obtain a new set of single particle states $\{a_i^{(2)}\}$.

8. And so on... until convergence.

This procedure is represented on Fig. (III.1).
In principle, convergence of both the mixing coefficients and the orbitals, or equivalently of both the one-body density ρ and the two-body correlation matrix σ, must be reached. In practice however, we only verify the convergence of the one-body density[3], that is,
$|\rho_{ij}^{(N)} - \rho_{ij}^{(N-1)}| \leqslant \eta$, $\forall i, j$, where η is the convergence parameter.

Let us now detail the solution techniques used to solve each variational equation.

III.3.2 First equation

Eq. (III.11) involves the diagonalization of the matrix $\mathcal{H}$ which is achieved numerically using a Lanczos algorithm. More precisely, we use the very efficient techniques for large-scale Shell-Model calculations developed by the group in Strasbourg, and in particular E. Caurier [24]. Because of the density-dependence of the Gogny interaction, the matrix $\mathcal{H} = \mathcal{H}[\rho, \sigma]$ depends

[3]This being said, we notice in practice that whenever ρ has converged to the required accuracy, the two-body density is then also converged to a similar accuracy.

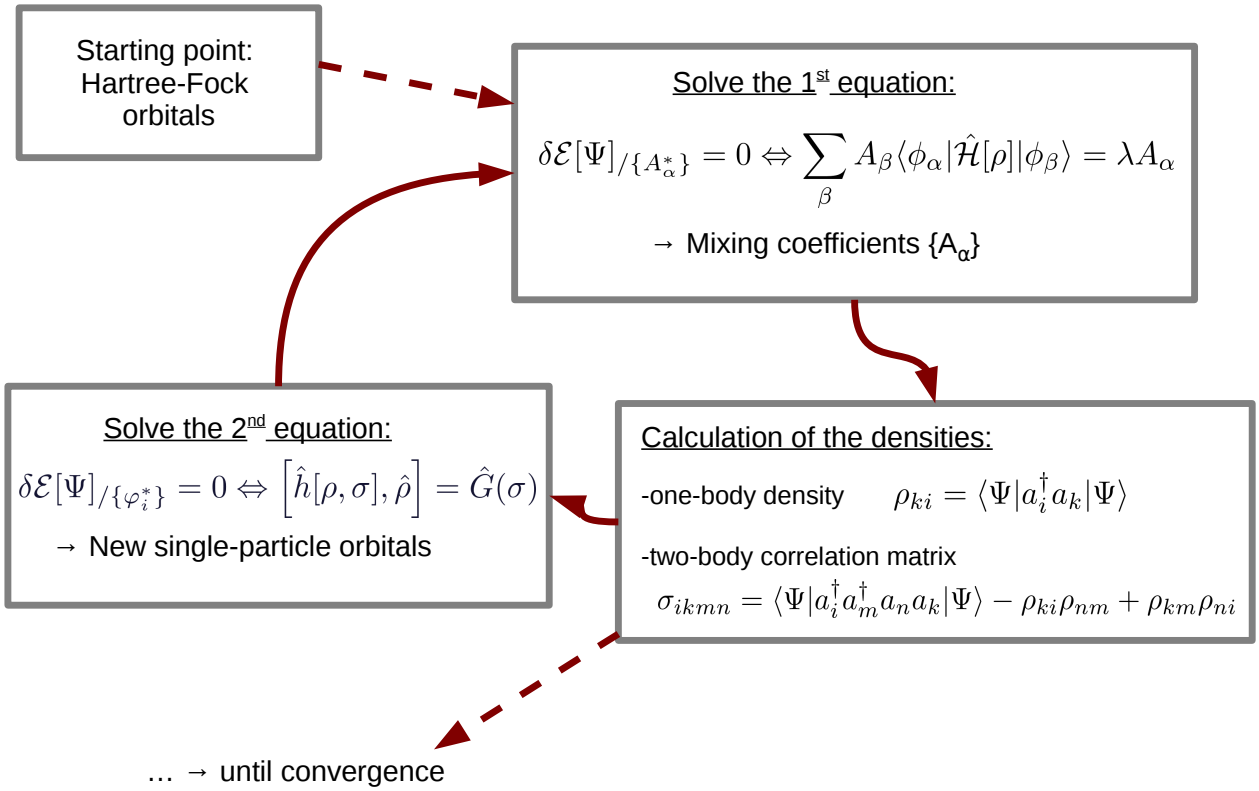

Figure III.1: Global convergence procedure

on the one- and two-body densities of the system, and this equation therefore becomes non-linear. One could thus iterate the diagonalization of the matrix until the mixing coefficients are converged, before solving the orbital equation. However, because the size of the matrix $\mathcal{H}$ can rapidly explode (see the application done in the next section), this step can become very time consuming, and since this convergence is destroyed when moving to the second equation, we choose not to perform this sub-convergence process.

III.3.3 Second equation

Contrary to the uncorrelated Hartree-Fock case, the presence of the source term $G[\sigma]$ in Eq. (III.17) forbids the existence of a basis diagonalizing both the mean-field $h[\rho,\sigma]$ and the one-body density ρ. *A priori* one could either choose to work in the eigenbasis of ρ (natural basis) or in the eigenbasis of $h[\rho,\sigma]$ (canonical basis). However, in order to build the many-body configurations during the self-consistent procedure, one needs to be able to create and destroy (dressed) particles. This can only be done in the natural basis where occupation numbers are

defined. We therefore consider as unknown of Eq. (III.17) the set of single-particle states that are eigenstates of the matrix ρ satisfying $[h[\rho,\sigma],\rho] = G[\sigma]$. As discussed in chapter II one can then define the single-particle energies as the eigenvalues of the mean-field $h[\rho,\sigma]$.
Solving Eq. (III.17) is far from being an easy task. Unlike in the Hartree-Fock case, the presence of the source term $G[\sigma]$ does not allow a clear interpretation of the equation. The idea followed here is therefore to find a way to rewrite Eq. (III.17) in a homogeneous form, where the source term is expressed as a commutator with ρ. This is done using the following reasoning [6].

The orbital equation in an homogeneous form

Let $\{|\alpha\rangle\}$ denote an arbitrary single-particle basis (e.g. a Hartree-Fock or harmonic oscillator basis). As symmetric matrix, ρ can be diagonalized using an orthogonal matrix U as,

$$\sum_{\alpha\beta}(U^T)_{\mu\alpha}\,\rho_{\alpha\beta}\,U_{\beta\nu} = n_\mu\delta_{\mu\nu}\ , \tag{III.20}$$

where $UU^T = U^TU = \hat{I}$ and $n_\mu \in \mathbb{R}$.
Let us now write the orbital equation (III.17) in the natural basis $\{\mu\}$ (we omit for now the σ- and ρ-dependencies to lighten the notations),

$$\left[\hat{h},\hat{\rho}\right] = \hat{G} \ \Rightarrow\ h_{\mu\nu}(n_\nu - n_\mu) = G_{\mu\nu}\ . \tag{III.21}$$

- If there is no degeneracy,

$$n_\nu = n_\mu \Rightarrow \nu = \mu \Rightarrow G_{\mu\nu} = G_{\mu\mu} = 0\ ,$$

  because G is skew-symmetric [4]. Eq. (III.21) is then automatically fulfilled.

- In fact, degeneracies $n_\nu = n_\mu$ for $\mu \neq \nu$ can happen

  - Because of the symmetries (rotational invariance $\nu = (n_\mu, l_\mu, j_\mu, \Omega_\nu)$, time-reversal invariance $\nu = \overline{\mu}$ ...) of the Hamiltonian. In this case, the explicit conservation of these symmetries in the multiparticle-multihole configuration mixing method leads to $G_{\mu\nu} = 0$.

  - If one chooses to select the many-body configurations of the nuclear state by defining

[4] As shown in section II.1.2 it is anti-hermitian since $G = F - F^\dagger$. We also assume the system to be invariant under complex conjugation transformation $\hat{K} = \hat{T}\hat{\Pi}_2^{-1}$, where $\hat{T}$ denotes the time-reversal operator and $\hat{\Pi}_2 = e^{-i\pi\hat{J}_y}$ is the operator of signature with respect to the y-axis. All matrices are therefore real.

a core + valence space + empty orbitals. In that case,

$$\begin{cases} n_\mu = n_\nu = 1 \text{ , if } \mu, \nu \in \text{ core,} \\ n_\mu = n_\nu = 0 \text{ , if } \mu, \nu \in \text{ empty states.} \end{cases}$$

Looking at the expression of the source term,

$$G_{\mu\nu} = \frac{1}{2} \sum_{\mu_1\mu_2\mu_3} \sigma_{\mu_1\mu,\mu_2\mu_3} \widetilde{V}_{\mu_1\mu_2,\nu\mu_3} - \frac{1}{2} \sum_{\mu_1\mu_2\mu_3} \widetilde{V}_{\mu\mu_1,\mu_2\mu_3} \sigma_{\nu\mu_2,\mu_1\mu_3} \ , \tag{III.22}$$

one sees that $G_{\mu\nu}$ is non-zero if at least one index among μ and ν belongs to the valence space. Indeed the correlations being restricted to this valence space, if both μ and ν belong to the core (or the empty orbitals) then all elements of σ occurring in (III.22) are zero and $G_{\mu\nu}$ vanishes.

Therefore in both cases, Eq. (III.21) is automatically satisfied.

Let us now define the following quantity,

$$Q_{\mu\nu} = \begin{cases} \frac{G_{\mu\nu}}{n_\nu - n_\mu} & \text{if } n_\nu \neq n_\mu \\ 0 & \text{otherwise.} \end{cases} \tag{III.23}$$

In fact, in the degenerate case when $n_\mu = n_\nu$, the orbital equation being trivially fulfilled, the corresponding elements $Q_{\mu\nu}$ can be taken equal to any arbitrary real value. In particular they can be taken equal to zero.

Eq. (III.21) can then be written as,

$$(h - Q)_{\mu\nu}(n_\nu - n_\mu) = 0 \ . \tag{III.24}$$

That is, in any single-particle basis,

$$\boxed{\Big[h[\rho,\sigma] - Q[\rho,\sigma], \rho\Big] = 0} \ . \tag{III.25}$$

The orbital equation expressed as (III.25) can then be solved as some sort of Hartree-Fock equation where the mean-field h is constrained by the "correlation field" Q. The latter introduces modification of the mean-field coming from the inclusion of two-particle correlations, in particular those associated with the scattering of two nucleons from core orbitals into valence states, taking also into account the rearrangement effect due to the density dependence of the effective interaction.

Solution of the orbital equation

Eq. (III.25) tells us that the modified mean-field $\widetilde{h}[\rho,\sigma] \equiv \hat{h}[\rho,\sigma] - \hat{Q}[\rho,\sigma]$ and the density $\hat{\rho}$ are commuting operators and therefore can be diagonalized simultaneously[5]. The common basis of eigenvectors is the optimal single-particle basis we seek. Since $\widetilde{h}[\rho,\sigma]$ depends on the solution of the equation (the one-body density ρ), this is of course a non-linear problem which requires an iterative solution procedure.

Let us note that during this sub-iterative process the wave function $|\Psi\rangle$, output of the first variational equation, is fixed. Thus, the correlations contained in σ do not evolve while solving the orbital equation. We therefore omit the σ-dependence of the quantities in the following. We refer to the number of global iterations by capital letters N and to the number of "local" sub-iterations by small letters n. The solution procedure for the second variational equation consists then in,

1. Start from a given density $\rho^{(N),(n=0)}$ which is given by the solution of the first variational equation:
$$\rho^{(N),(n=0)} \equiv \rho^{(N)} = \langle \Psi^{(N)} | a^{\dagger(N-1)} a^{(N-1)} | \Psi^{(N)} \rangle \ .$$
2. Diagonalize $\rho^{(N),(n=0)}$ to obtain the occupation numbers $\{n_\mu\}$ and the natural states $\{|\mu\rangle\}$.
3. Calculate the mean-field $h[\rho^{(N),(n=0)}]$ and the correlation field $Q[\rho^{(N),(n=0)}]$.
4. Diagonalize $\widetilde{h}[\rho^{(N),(n=0)}] = h[\rho^{(N),(n=0)}] - Q[\rho^{(N),(n=0)}]$ to obtain its eigenstates $\{|i\rangle\}$ and eigenvalues $\{\widetilde{\varepsilon}_i\}$.
5. Construct the new density $\rho^{(N),(n=1)}$ by imposing it to be diagonal on the basis $|i\rangle$. That is,
$$\rho_{ij}^{(N),(n=1)} = n_i \delta_{ij} \ . \tag{III.26}$$
6. Go back to step 2 ... and so on, until the density matrix ρ has converged, i.e. until $|\rho_{ij}^{(N),(n)} - \rho_{ij}^{(N),(n-1)}| \leqslant \eta_2, \ \forall i,j$. Where η_2 is the convergence parameter of this sub-process.

Let us emphasize once again that this sub-convergence process takes place inside a global one. We represented on Fig. (III.2) the detailed global self-consistent procedure.
Finally, let us note that in principle the formalism gives different orbitals for different many-body eigenstates of $\mathcal{H}$. However, solving the orbital equation for each eigenvalue would be very difficult to achieve. The approach adopted in this work consists in calculating the source term and solving the orbital equation using the densities of the ground-state. The resulting single-particle basis is then also used to expand the excited states.

[5] they are both diagonalizable because symmetric.

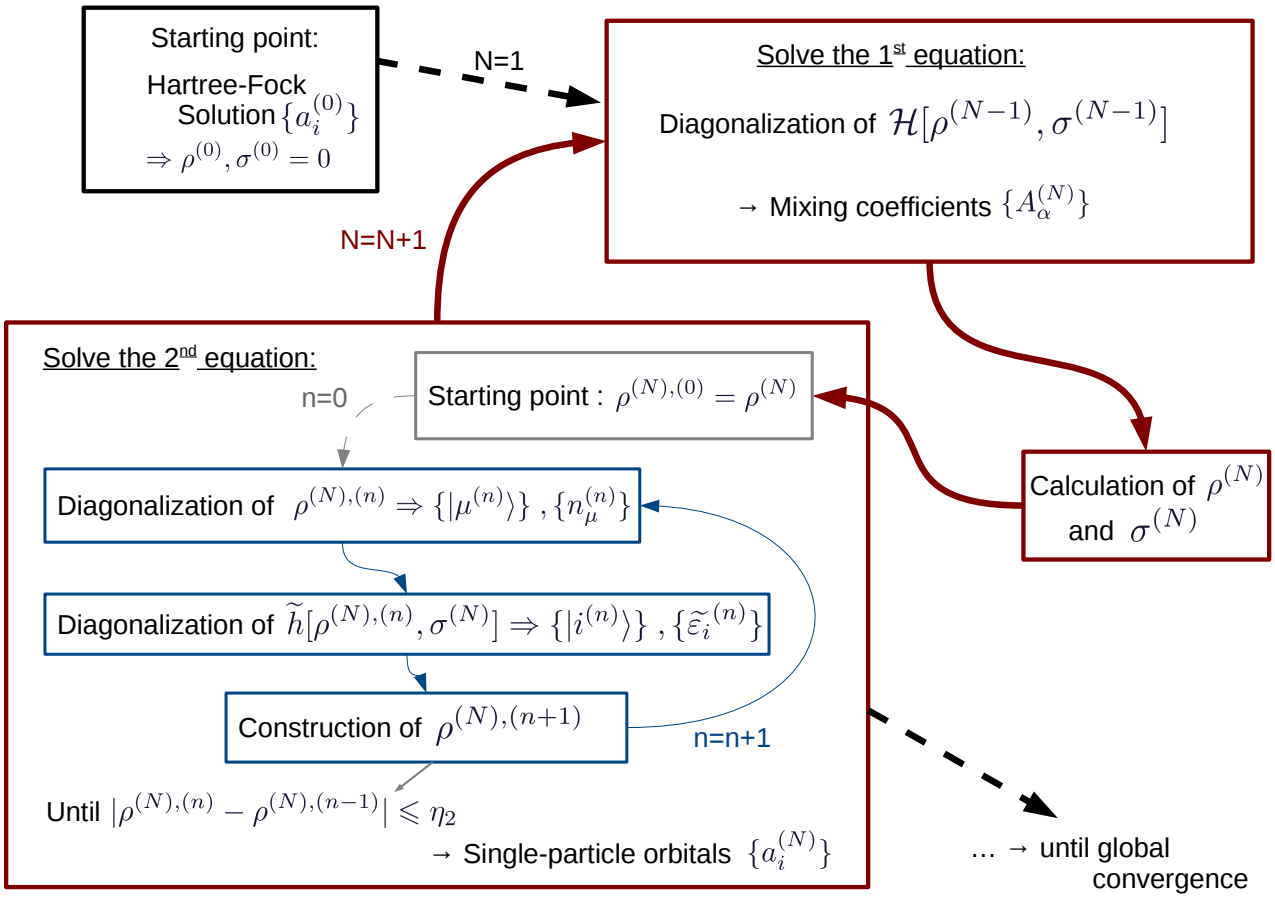

Figure III.2: Detailed global convergence procedure.

III.4 Example of convergence in the case of the ^{12}C ground state

In this part we want to apply the solution procedure described previously to a test-case nucleus. The idea is to compare the convergence process and the effect induced by the orbital optimization when adopting different types of criteria for selecting the many-body configurations $|\phi_\alpha\rangle$ included in the nuclear state $|\Psi\rangle$. Such configurations can indeed be chosen using different truncation schemes, e.g.,

- A "Shell-model-type" truncation involving the separation of the single-particle orbits in three different blocks: a filled core, a partially filled valence space where particle are distributed according to their interaction, and a block of remaining empty orbits.
- A selection of the configurations according to their excitation order (1p-1h, 2p-2h, ...) in the full available single-particle space, respecting rotational invariance.
- A selection of the configurations according to their excitation energy $E_\alpha^* = E_\alpha - E_\phi$ from

the uncorrelated ground reference state $|\phi\rangle$.

The third type of truncation generally breaks spherical symmetry and special care needs to be applied in this case. In fact, an ideal criterion may be to e.g. select the configurations according to their excitation order M and impose a cut-off energy that is chosen different for each order M. This type of truncation is however very complicated to set up and we do not attempt to use it in this work. We therefore restrict our comparative study to the first and second criteria. This test analysis is applied to the ground-state of the ^{12}C nucleus composed of $Z = 6$ protons and $N = 6$ neutrons. This rather small number of particles allows us to perform these tests without having to deal with too enormous matrices and calculation times.

A few technical details

Let us first give some details about the tools used in practical calculations.

- Single-particle states are expanded on axially deformed harmonic oscillator states, so that many-body states are explicitly characterized by a good projection $K \equiv J_z$ of the angular momentum J (so-called m-scheme). In order to obtain solutions with a good J, the calculations are done at the spherical point. That is, the perpendicular and longitudinal oscillator frequencies are taken equal: $\omega_\perp = \omega_z \equiv \omega$. The self-consistent property of the spherical symmetry ensures then its preservation along the convergence process.

- The values of the oscillator frequency ω, as well as the number of major shells N_0 are optimized at the Hartree-Fock level. This leads to, $\hbar\omega = 15.50$ and $N_0 = 5$ shells.

- The criteria ensuring convergence of the one-body density matrix during the global and local iterative procedures are both taken equal to $\eta = \eta_2 = 10^{-4}$.

Conventions

In what follows we denote by,

- $i, j, k...$ the single-particle states used to build the configurations during the convergence procedure at a given global iteration N. They correspond therefore to the basis diagonalizing simultaneously $\rho^{(N-1)}$ and $\widetilde{h}[\rho^{(N-1)}, \sigma^{(N-1)}]$. ($i = (\alpha_i, \Omega_i)$ where $\alpha_i = (n_i, l_i, j_i)$ denotes a spherical sub-shell.) During the first iteration, the i-basis is the Hartree-Fock one.

- $a, b, c...$ the eigenstates of the mean-field $h[\rho, \sigma]$.

- $\mu, \nu...$ the optimal orbitals we seek, diagonalizing simultaneously $\rho^{(N_F)}$ and $\widetilde{h}[\rho^{(N_F)}, \sigma^{(N_F)}]$ (N_F denoting the last global iteration), when the process has converged and both variational equations are simultaneously satisfied.

The ^{12}C nucleus

The understanding of ^{12}C has always attracted much interest. The presence of a 0^+ Hoyle state at 7.654 MeV, exhibiting a structure of three alpha particles, is necessary for the existence of many other stable elements. A recent experiment [70] also reported evidence that the ^{12}C ground-state displays an equilateral triangular structure.

Fig. (III.3) displays the potential energy curve (PEC) and potential energy surface (PES) provided by Hartree-Fock-Bogolyubov calculations performed with the D1S Gogny force. Two distinct minima appear. The ground-state minimum exhibits a strong oblate shape, characterized by an axial deformation parameter $\beta \sim -0.65$. The second minimum is characterized by a prolate shape with $\beta \sim 0.45$. This deformed nucleus is thus expected to incorporate a great correlation content where shell effects play an important role. Fig. (III.4) displays the evolution of the proton and neutron single-particle spectra with deformation β. One notices the evolution of the gaps at the Fermi level, while β varies. Moreover, we note a crossing of the $0p_{1/2}$ sub-shell with the $d_{5/2}$ at $\beta \sim 0.6$ and $\beta \sim -0.7$. The latter shell should thus play a role at high deformations.

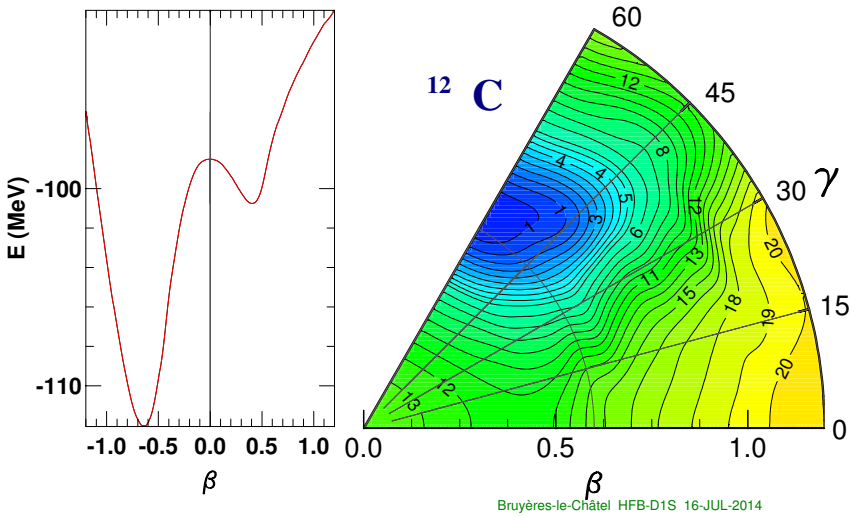

Figure III.3: Hartree-Fock-Bogolyubov Potential Energy Curve (left) and Surface (right) for the ^{12}C nucleus.

III.4.1 First truncation scheme: ^{4}He core + p-shell valence space

We first apply the multiparticle-multihole configuration mixing method using a "Shell-model-type" truncation to select the many-body Slater determinants. The single-particle states are divided into a core of ^{4}He and a valence space taken as a full oscillator shell corresponding

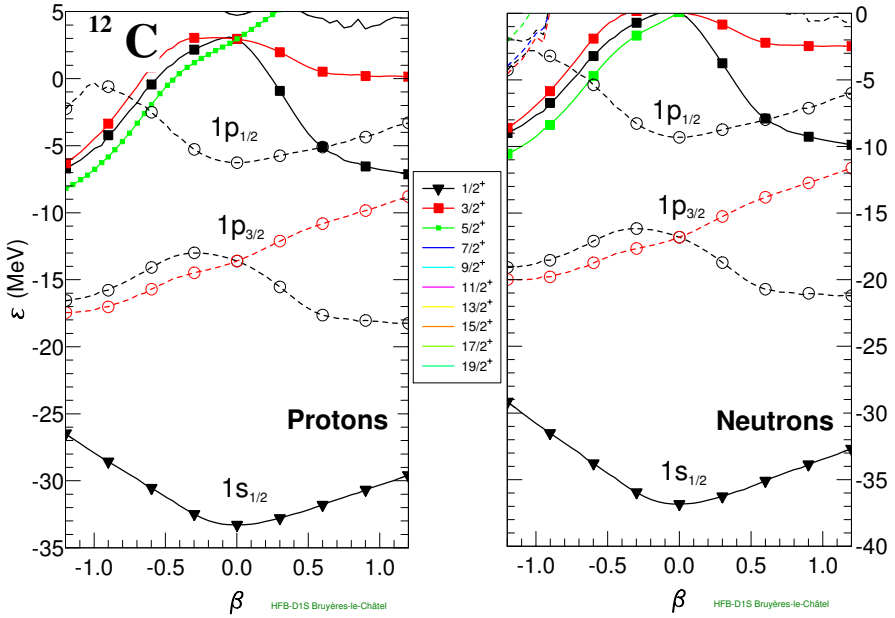

Figure III.4: Evolution of HFB single-particle spectra as a function of axial deformation β.

here to the $0p$-shell. The remaining orbitals are considered empty. This is represented on Fig. (III.5).

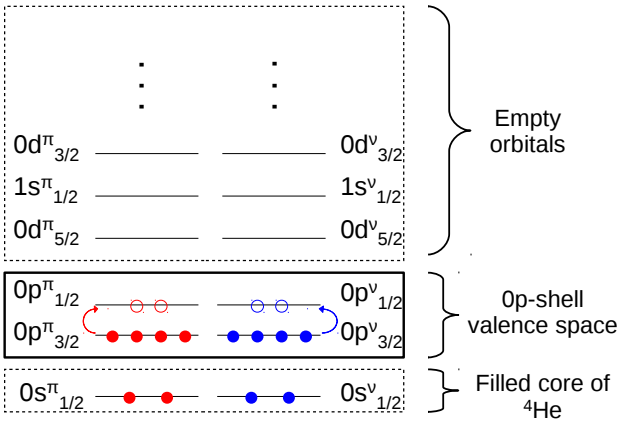

Figure III.5: Schematic separation of the single-particle states.

All excitations of the valence nucleons in the $0p$-shell are considered. The correlated wave function $|\Psi\rangle$ is then built as a superposition of all possible configurations in this model space,

$$|\Psi\rangle = \sum_{\alpha} A_\alpha |\phi_\alpha\rangle \qquad \text{with,} \quad |\phi_\alpha\rangle = \prod_{i_\alpha \in 0p\text{-shell}} a^\dagger_{i_\alpha} |^4\text{He}\rangle \ . \tag{III.27}$$

This choice of truncation scheme defines the $\mathcal{P}$ and $\mathcal{Q}$ subspaces from chapter II and their

respective projectors $\hat{P}$ and $\hat{Q}$ as,

$$\hat{P} = \sum_{\alpha \in \text{model space}} |\phi_\alpha\rangle \langle\phi_\alpha| \ , \qquad \hat{Q} \simeq \hat{1} - \hat{P} \ .$$

Correlations in the restricted valence shell are explicitly treated by the diagonalization of the many-body Hamiltonian matrix $\mathcal{H}[\rho, \sigma]$, while the rest of the space is ignored and considered frozen at that stage. However, optimizing the single-nucleon states by solving the second variational equation will result in a mixing of the three orbital blocks (core/valence shell/empty states). Thus, none of these blocks remain frozen and this procedure should allow to partly account for configurations built outside of the initial model space. This will be illustrated in the following. With this truncation scheme the convergence of the one-body density is reached in 15 global iterations. In fact we can easily reach a convergence up to a precision of $\Delta\rho \leqslant 10^{-6}$ in 30 iterations.

Step 1: Building the configurations

At the first global iteration $N = 1$, the Slater determinants are built on Hartree-Fock single-particle states. As explained in more detail in appendix C, the nuclear states are characterized in practice by a good parity π and a good projection $K = J_z$ of the total angular momentum J on the z-axis (so-called m-scheme). By considering all possible configurations in the $0p$-shell, we ensure the conservation of spherical symmetry, and thus J is also a good quantum number. Since we focus here on the description of the ground state of the even-even nucleus ^{12}C, we have $J = K = 0$. The configurations $|\phi_\alpha\rangle = |\phi_{\alpha_\pi}\rangle \otimes |\phi_{\alpha_\nu}\rangle$ are classified into blocks of projections $(K_{\alpha_\pi}, K_{\alpha_\nu} = K - K_{\alpha_\pi})$ and organized by increasing excitation orders (0p-0h, 1p-1h, 2p-2h...). Time reversal invariance allows to deduce the configuration blocks with $(K_{\alpha_\pi} > 0)$ from the ones characterized by $(K_{\alpha_\pi} < 0)$. The former are therefore never explicitly built and the size of the matrix $\mathcal{H}[\rho, \sigma]$ to diagonalize is drastically reduced (factor ~ 2).
Following this procedure, we obtain here 38 configurations from 0p-0h to 4p-4h excitations, organized in three blocks:

- $K_{\alpha_\pi} = K_{\alpha_\nu} = 0$,
- $K_{\alpha_\pi} = -1$, $K_{\alpha_\nu} = 1$,
- $K_{\alpha_\pi} = -2$, $K_{\alpha_\nu} = 2$,

which are schematically represented on Fig. (III.6), (III.7) and (III.8) respectively. On these figures the $0p_{3/2}$ sub-shell has been virtually split into two degenerate levels corresponding to the projections $|\Omega| = |j_z| = \frac{1}{2}, \frac{3}{2}$. Pure proton or neutron multiparticle-multihole excitations of the reference state (the 0p-0h configuration) are denoted by $(\text{mp-mh})_\tau$ $(\tau = \pi, \nu)$, while excitations of proton-neutron nature are referred as $(\text{mp-mh})_{\pi\nu}$.

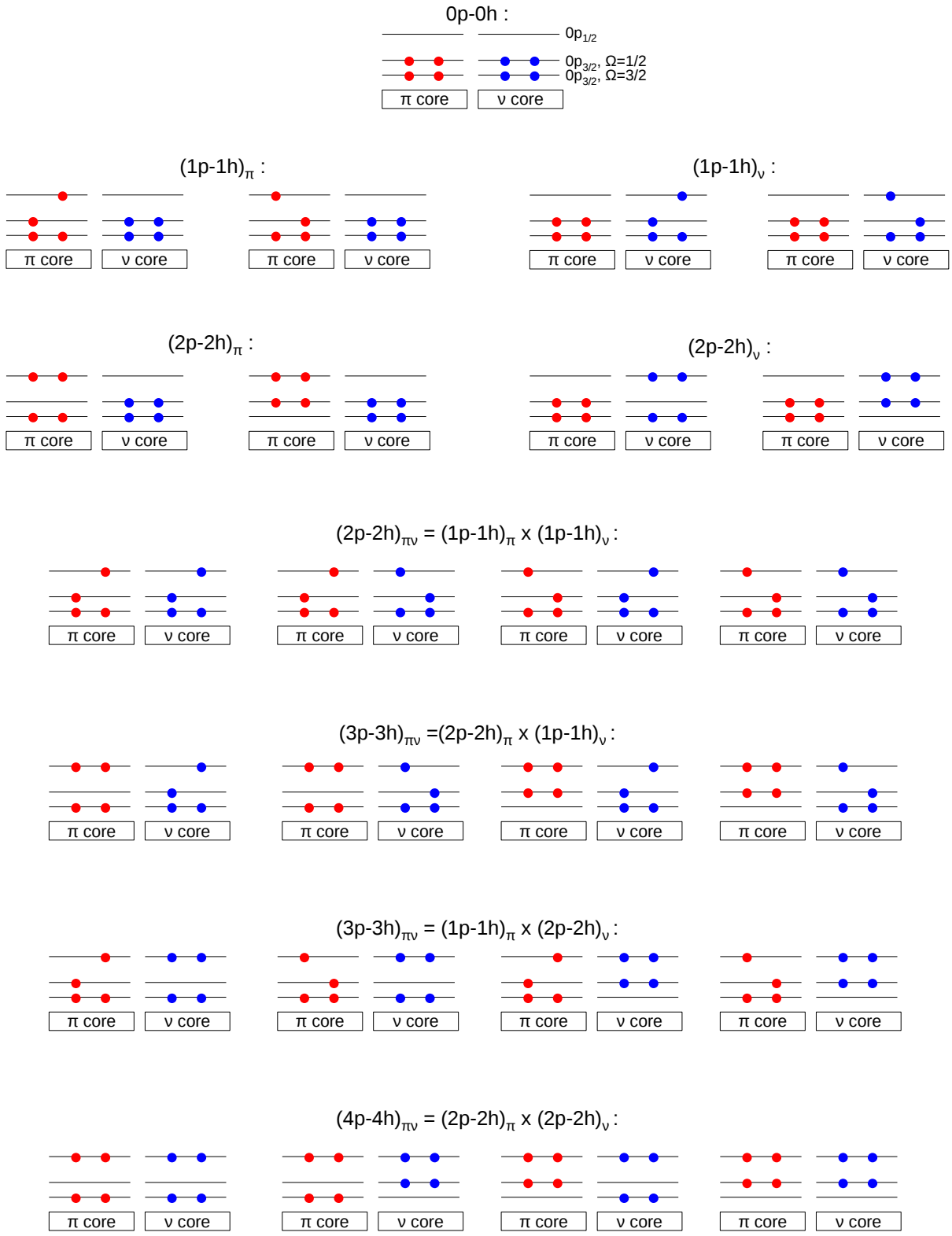

Figure III.6: Block of configurations $|\phi_\alpha\rangle$ characterized by $(K_{\alpha_\pi} = K_{\alpha_\nu} = 0)$.

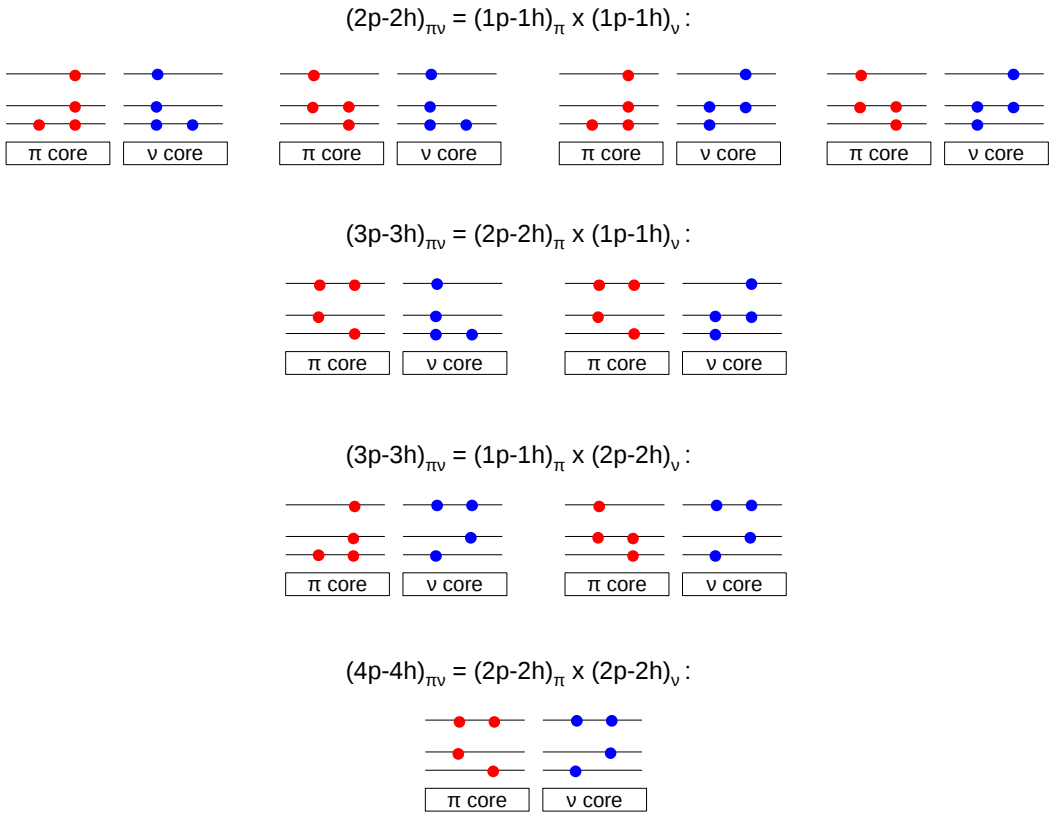

Figure III.7: Block of configurations $|\phi_\alpha\rangle$ characterized by $(K_{\alpha_\pi} = -1,\ K_{\alpha_\nu} = 1)$.

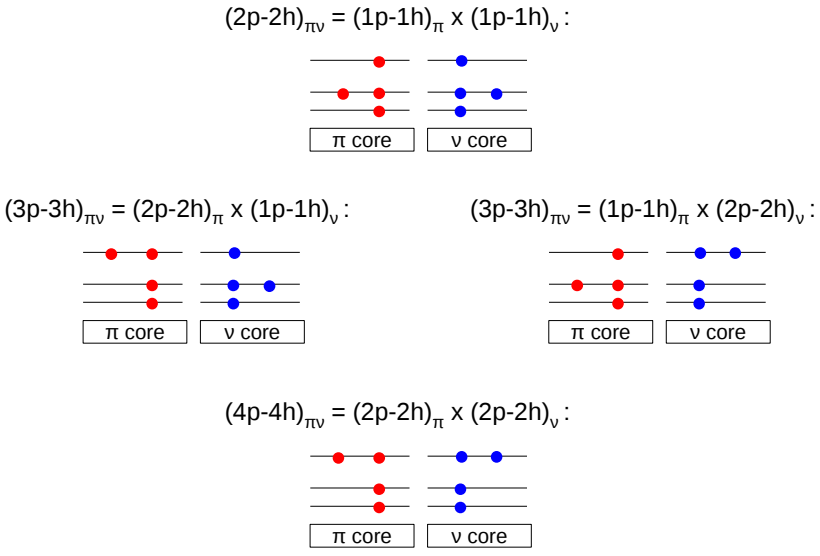

Figure III.8: Block of configurations $|\phi_\alpha\rangle$ characterized by $(K_{\alpha_\pi} = -2,\ K_{\alpha_\nu} = 2)$.

Step 2: Calculation of the correlation matrix σ.
Diagonalizing the Hamiltonian matrix $\mathcal{H}[\rho,\sigma]$ in the $\mathcal{P}$ configuration space leads to the determination of the weight of each mp-mh excitation in the correlated wave function and allows us to calculate the two-body correlation matrix σ.
We plotted on Fig. (III.9) all non-zero elements $\sigma(I)=\sigma_{ij,kl}$ of the (non recoupled in J) proton and neutron correlation matrices (they are found very similar since $N=Z$). I is a linear index corresponding to a certain quadruplet of single-particle states (i,j,k,l). The graphs are organized as follows,

- The indices $I=1\rightarrow 10$ correspond to quadruplet of single-particle states (i,j,k,l) which are all different.
  - The two main peaks $\sigma(I)\simeq 0.19$ at $I=9,10$ correspond to correlations of pairing type, and more precisely to the scattering of a pair of protons (neutrons) from the $0p_{3/2}$ to the $0p_{1/2}$ sub-shell. This process is represented by the diagram (III.10a).
  - Elements $\sigma(I=2,3,4)\simeq 2\times 10^{-2}$ reflect the propagation of a particle-hole pair, as shown on diagram (III.10b). This corresponds to RPA-type correlations.
  - Elements $\sigma(I=5\rightarrow 8)\simeq 1\times 10^{-2}$ reflect particle-vibration couplings (III.10c).
  - Finally $\sigma(I=1)\simeq 5\times 10^{-2}$ corresponds to the destruction of a pair of time-reversed protons (neutrons) on e.g. the $\Omega=\frac{3}{2}$-level of the $0p_{3/2}$ sub-shell, followed by the creation of a pair on the $\Omega=\frac{1}{2}$-level of the same spherical sub-shell.
- The indices $I=11\rightarrow 45$ represents "diagonal" elements of σ, i.e., elements of the type $\sigma_{ii,jj}=\langle\Psi|a_i^\dagger a_j^\dagger a_j a_i|\Psi\rangle-\rho_{ii}\rho_{jj}+\rho_{ij}\rho_{ji}$. They are globally of order $\sim 5\times 10^{-2}-1\times 10^{-1}$
- Finally, $\sigma(I=46\rightarrow 56)\lesssim 2\times 10^{-2}$ represent elements of the correlation matrix with two equal indices, i.e. of the type $\sigma_{kk,ij}=\langle\Psi|a_k^\dagger a_i^\dagger a_j a_k|\Psi\rangle-\rho_{kk}\rho_{ji}+\rho_{ki}\rho_{jk}$, where e.g. $j,k\in 0p_{3/2}$ and $i\in 0p_{1/2}$. They reflect therefore a particular case of particle-vibration coupling.

Similarly, correlations of proton-neutron type $\sigma_{i_\pi l_\pi,j_\nu k_\nu}=\langle\Psi|a_{i_\pi}^\dagger a_{j_\nu}^\dagger a_{k_\nu}a_{l_\pi}|\Psi\rangle-\rho_{li}^\pi\rho_{kj}^\nu$ are shown on Fig. (III.11). They appear to be more important than correlations of pure proton (or neutron) nature.

- As previously, on the first part of the graph ($I=1\rightarrow 89$) are represented the "non-diagonal" part of the correlation matrix, i.e. $\sigma_{i_\pi l_\pi,j_\nu k_\nu}$ with $(i_\pi\neq l_\pi, j_\nu\neq k_\nu)$.
  - The biggest peaks $\sigma(I)\simeq 0.166$ at $I=73,88$ and $\sigma(I)\simeq 0.118$ at $I=17,63$ correspond again to pairing-type correlations, where a proton-neutron pair with $J_z^{pair}=0$ is scattered from the $p_{3/2}^\pi\otimes p_{3/2}^\nu$ sub-shell to the $p_{1/2}^\pi\otimes p_{1/2}^\nu$ one.
  - $\sigma(I)\simeq 9\times 10^{-2}$ at $I=3,8,76,85$ reflects the propagation of a particle-hole pair.

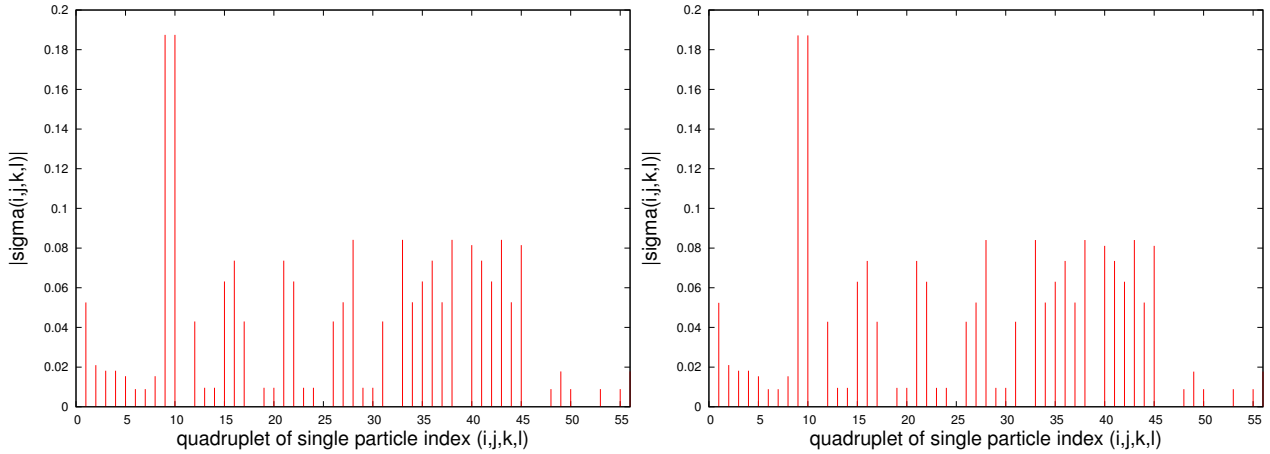

Figure III.9: Absolute value of the proton (left) and neutron (right) two-body correlation matrices. The two main peaks at $\alpha = 9, 10$ correspond to the scattering of a pair of proton (neutron) from the $p_{3/2}$ to the $p_{1/2}$ sub-shell.

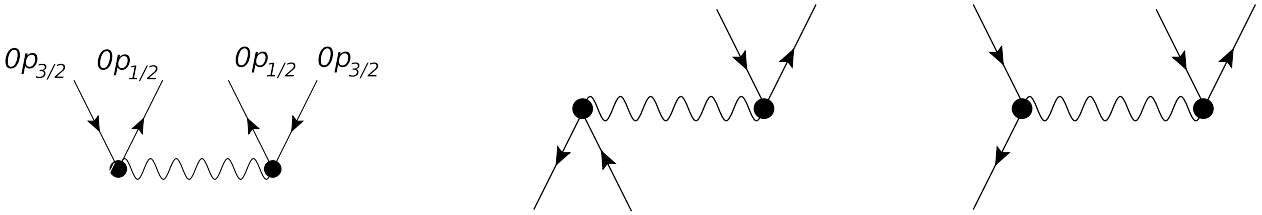

(a) Pairing-type correlations.

(b) Propagation of a particle-hole pair.

(c) Particle-vibration coupling.

Figure III.10: Different types of correlations involved in the two-body correlation matrix σ.

- Finally $\sigma(I = 9, 18) \simeq 8 \times 10^{-2}$ correspond to the destruction (or creation) of two particle-hole pairs.

- The rest of the graph shows $\sigma_{ij,kl}$ with one or two couples of equal indices.

In conclusion, pairing correlations inducing scattering from the Fermi level onto the $0p_{1/2}$ sub-shell seem to be the most important in this case.

Step 3: Calculation of the source term $G[\sigma]$ and the correlation field $Q[\rho, \sigma]$.
The previous correlation matrices are now used to calculate the source term $G[\sigma]$ appearing in the orbital equation. Let us first look more closely at the analytical expression of this term,

$$G[\sigma]_{ij} = \frac{1}{2}\sum_{klm}\sigma_{ki,lm}\widetilde{V}^{2N}_{kljm} - \frac{1}{2}\sum_{klm}\widetilde{V}^{2N}_{iklm}\sigma_{jl,km} \ . \tag{III.28}$$

We note that $G[\sigma]_{ij} \neq 0$ if there exists at least one triplet (k, l, m) of single-particle states such that $\sigma_{ki,lm} \neq 0$ or $\sigma_{jl,km} \neq 0$. Since σ reflects the correlations that have been explicitly

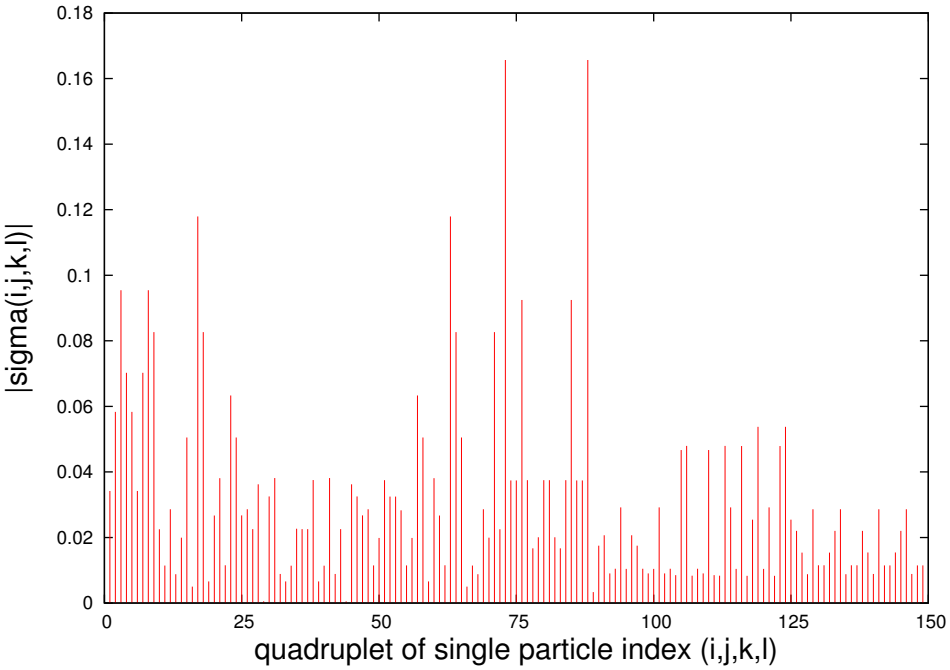

Figure III.11: Proton-neutron two-body correlation matrix. The main peaks corresponds to the scattering of a proton-neutron pair of from the $p^{\pi}_{3/2} \otimes p^{\nu}_{3/2}$ to the $p^{\pi}_{1/2} \otimes p^{\nu}_{1/2}$ shells.

introduced in the wave function, $\sigma_{ki,lm} \neq 0$ if (k, i, l, m) all belong to the valence $0p$-shell. The source matrix $G[\sigma]_{ij}$ therefore has at least one external index (i or j) belonging to the valence space. The second index being attached to the matrix element of the interaction $\widetilde{V}^{2N}$, it can belong to the whole single-particle basis. The source term is therefore able to couple the active valence space to the rest of the orbitals that were previously considered as inert. Thus, it has the role of propagating the effect of correlations on the full single-particle basis by establishing a communication between the three blocks (core/valence/empty states).
Because of explicit symmetry conservations imposed in this study, the source term can only couple states of same parity π and angular momentum j. In the present test case, it therefore couples the $0p_{3/2}$ and $0p_{1/2}$ sub-shells to the $1p_{3/2}$ and $1p_{1/2}$ ones respectively. We obtain the following values,

$$\begin{cases} G^{\pi}[\sigma]_{p_{3/2}} \equiv |G^{\pi}[\sigma]_{0p_{3/2},1p_{3/2}}| \simeq 0.226 \text{ MeV} & \text{(III.29)} \\ G^{\pi}[\sigma]_{p_{1/2}} \equiv |G^{\pi}[\sigma]_{0p_{1/2},1p_{1/2}}| \simeq 0.456 \text{ MeV} , & \text{(III.30)} \end{cases}$$

and,

$$\begin{cases} G^{\nu}[\sigma]_{p_{3/2}} \equiv |G^{\nu}[\sigma]_{0p_{3/2},1p_{3/2}}| \simeq 0.207 \text{ MeV} & \text{(III.31)} \\ G^{\nu}[\sigma]_{p_{1/2}} \equiv |G^{\nu}[\sigma]_{0p_{1/2},1p_{1/2}}| \simeq 0.416 \text{ MeV} . & \text{(III.32)} \end{cases}$$

This is shown on Fig. (III.12) where we represented the proton and neutron source terms (calculated at iteration $N = 1$) in a matrix form $G^{\pi}[\sigma]_{\alpha_i,\alpha_j}$ and $G^{\nu}[\sigma]_{\alpha_i,\alpha_j}$ where α_i denotes a spherical sub-shell (n_i, l_i, j_i).

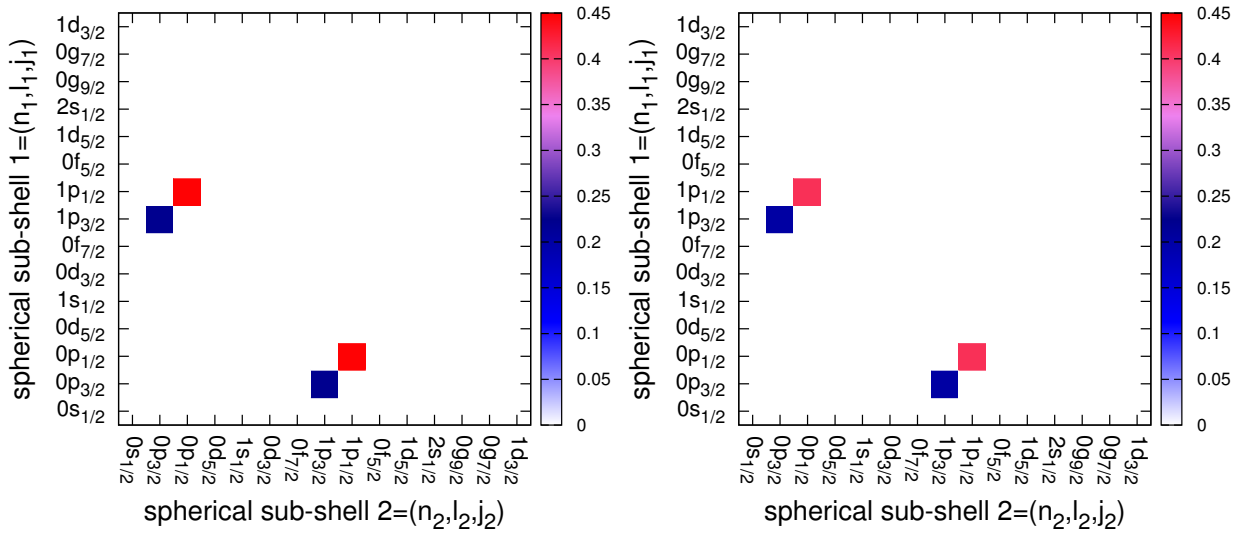

Figure III.12: Proton (left) and neutron (right) source terms $G[\sigma]_{\alpha_i,\alpha_j}$ calculated at the first global iteration $N = 1$. The x and y-axis correspond to the different spherical sub-shells $\alpha_i = (n_i, l_i, j_i)$ ordered by increasing energy. We note the coupling between the $0p_{3/2}$ and $1p_{3/2}$ sub-shells, as well as the coupling between the $0p_{1/2}$ and $1p_{1/2}$ sub-shells.

Since the valence space only contains sub-shells with different angular momentum, the basis $\{i\}$ used to construct the many-body configurations (at this stage the original Hartree-Fock basis) already diagonalizes the one-body density matrix: $\rho_{ij} = n_i\delta_{ij}$. We can therefore express the correlation field Q in this basis as,

$$Q_{ij}[\rho,\sigma] = \begin{cases} \frac{G_{ij}[\sigma]}{n_j - n_i} & \text{, if } n_i \neq n_j \\ 0 & \text{, otherwise,} \end{cases} \tag{III.33}$$

so that the only non zero elements are,

$$\begin{cases} Q^{\tau}[\rho,\sigma]_{1p_{3/2},0p_{3/2}} = Q^{\tau}[\rho,\sigma]_{0p_{3/2},1p_{3/2}} = \dfrac{G^{\tau}[\sigma]_{0p_{3/2},1p_{3/2}}}{n_{1p_{3/2}} - n_{0p_{3/2}}} = -\dfrac{G^{\tau}[\sigma]_{0p_{3/2},1p_{3/2}}}{n_{0p_{3/2}}} & \text{(III.34)} \\ Q^{\tau}[\rho,\sigma]_{1p_{1/2},0p_{1/2}} = Q^{\tau}[\rho,\sigma]_{0p_{1/2},1p_{1/2}} = \dfrac{G^{\tau}[\sigma]_{0p_{1/2},1p_{1/2}}}{n_{1p_{1/2}} - n_{0p_{1/2}}} = -\dfrac{G^{\tau}[\sigma]_{0p_{1/2},1p_{1/2}}}{n_{0p_{1/2}}} \ . & \text{(III.35)} \end{cases}$$

We find at iteration $N = 1$,

$$\begin{cases} Q^{\pi}[\rho,\sigma]_{p_{3/2}} \equiv |Q^{\pi}[\rho,\sigma]_{0p_{3/2},1p_{3/2}}| \simeq \dfrac{0.226 \text{ MeV}}{0.870} \simeq 0.260 \text{ MeV} & \text{(III.36)} \\ Q^{\pi}[\rho,\sigma]_{p_{1/2}} \equiv |Q^{\pi}[\rho,\sigma]_{0p_{1/2},1p_{1/2}}| \simeq \dfrac{0.456 \text{ MeV}}{0.260} \simeq 1.754 \text{ MeV} \ , & \text{(III.37)} \end{cases}$$

and,

$$\begin{cases} Q^{\nu}[\rho,\sigma]_{p_{3/2}} \equiv |Q^{\nu}[\rho,\sigma]_{0p_{3/2},1p_{3/2}}| \simeq \dfrac{0.207 \text{ MeV}}{0.870} \simeq 0.238 \text{ MeV} & \text{(III.38)} \\ Q^{\nu}[\rho,\sigma]_{p_{1/2}} \equiv |Q^{\nu}[\rho,\sigma]_{0p_{1/2},1p_{1/2}}| \simeq \dfrac{0.416 \text{ MeV}}{0.259} \simeq 1.606 \text{ MeV} . & \text{(III.39)} \end{cases}$$

To establish their importance, these values can be compared to the values of the mean field $h[\rho,\sigma]$. We find,

$$\begin{cases} h^{\pi}[\rho,\sigma]_{p_{3/2}} \equiv |h^{\pi}[\rho,\sigma]_{0p_{3/2},1p_{3/2}}| \simeq 10.33 \text{ MeV} & \text{(III.40)} \\ h^{\pi}[\rho,\sigma]_{p_{1/2}} \equiv |h^{\pi}[\rho,\sigma]_{0p_{1/2},1p_{1/2}}| \simeq 8.03 \text{ MeV} , & \text{(III.41)} \end{cases}$$

and,

$$\begin{cases} h^{\nu}[\rho,\sigma]_{p_{3/2}} \equiv |h^{\nu}[\rho,\sigma]_{0p_{3/2},1p_{3/2}}| \simeq 10.48 \text{ MeV} & \text{(III.42)} \\ h^{\nu}[\rho,\sigma]_{p_{1/2}} \equiv |h^{\nu}[\rho,\sigma]_{0p_{1/2},1p_{1/2}}| \simeq 8.24 \text{ MeV} . & \text{(III.43)} \end{cases}$$

Clearly the constraint that couples the $p_{1/2}$ states are not negligible compared to the mean field value.

Again because of symmetry conservations, the orbital equation can be solved separately for each block of states with same angular momentum and parity (j,π) [6]. Thus, we have (omitting the ρ- and σ-dependency of the quantities),

$$\begin{cases} \left[h^{\frac{3}{2}^-}, \rho^{\frac{3}{2}^-}\right] = G^{\frac{3}{2}^-} \Leftrightarrow \left[h^{\frac{3}{2}^-} - Q^{\frac{3}{2}^-}, \rho^{\frac{3}{2}^-}\right] = 0 , & \text{(III.44)} \\ \left[h^{\frac{1}{2}^-}, \rho^{\frac{1}{2}^-}\right] = G^{\frac{1}{2}^-} \Leftrightarrow \left[h^{\frac{1}{2}^-} - Q^{\frac{1}{2}^-}, \rho^{\frac{1}{2}^-}\right] = 0 , & \text{(III.45)} \\ \left[h^{j^\pi}, \rho^{j^\pi}\right] = 0 \quad \text{, for } j^\pi \neq \dfrac{1}{2}^- , \dfrac{3}{2}^- . & \text{(III.46)} \end{cases}$$

The states characterized by different quantum numbers j^π than the ones present in the valence space are therefore not affected by source term $G[\sigma]$. They are however still renormalized through Eq. (III.46) by the fact that the mean-field $h[\rho,\sigma]$ is much richer than a pure Hartree-Fock field. These states are indeed influenced by the two-body correlations,

- Indirectly through the fact that the average potential $\sum_{kl} \widetilde{V}^{2N}_{ik,jl}\rho_{lk}$ in $h[\rho,\sigma]$ is built with the correlated one-body density ρ.
- Directly through the rearrangement terms $R[\rho,\sigma]$ that introduce an explicit dependence of the mean-field $h[\rho,\sigma]$ on the two-body correlation matrix σ.

[6] In practice, the equations are solved in an axial formalism (i.e. the orbital equation is solved for each (Ω,π) blocks) at the spherical point. The spherical symmetry being self-consistently conserved, couplings between states of different j are indeed found to be zero.

Step 4: Modification of the one-body density via the orbital optimization.
A first manifestation of the effect induced by the orbital equation can be seen on the evolution of the one-body density matrix ρ.
Before looking at the results, it is important to remind the following. In the previous section, we mentioned the density ρ calculated from the output of the first variational equation, i.e. calculated as,

$$\rho_{ij} = \sum_{\alpha\beta} A^*_\alpha A_\beta \langle \phi_\alpha | a^\dagger_j a_i | \phi_\beta \rangle \ ,$$

and the density resulting from the second variational equation, i.e. solution of $[h, \rho] = G$. Formally these two densities should correspond to the same quantity. However, at the beginning of the procedure, when convergence has not been yet reached, they are not identical. This is illustrated on Fig. (III.13), where we show the evolution of the neutron density along the convergence process (since $N = Z$ the behavior of the proton density shows a similar behavior). To emphasize the effect of the orbital equation, we plotted the difference $\Delta\rho_{\alpha_i,\alpha_j} \equiv |\rho_{\alpha_i,\alpha_j} - \rho^{HF}_{\alpha_i,\alpha_j}|$ between the correlated density and the density of a Hartree-Fock state (being equal to unity under the Fermi level and to zero above), in the original Hartree-Fock basis.

In Fig. (III.13a) we show the matrix $\Delta\rho$ obtained at the first global iteration $N = 1$, resulting from the solution of the first equation only (i.e. when the mixing coefficients have been calculated with fixed Hartree-Fock orbitals). As expected, the density is only modified in the valence space, where explicit correlations have been introduced.

In Fig. (III.13b) is represented $\Delta\rho$ obtained at $N = 1$, after solving the orbital equation. We see that optimizing the single-particle states has modified the density in the whole basis and introduced non-diagonal elements $\rho_{\alpha_i\alpha_j}$. As stated before, couplings between positive-parity states also appear, even though they have not been introduced in the configuration mixing (and thus are not affected by $G[\sigma]$).

in Fig. (III.13c) we show $\Delta\rho$ at the global iteration $N = 2$ after solving the first variational equation. At this stage we redefined the p-shell valence space on the new single-particle basis. We note that the density kept trace of the orbital mixing and is starting to look similar to the density resulting from the orbital equation.
In fact, as expected, we observe that the density matrices from the first and second variational equations converge to the same quantity at the end of the procedure. This is shown on Fig. (III.14) where we plotted both densities at different stages of the convergence process. We see that they tend to align themselves on the $y = x$ line after a few iterations.

Finally we show on Fig. (III.13d) the matrix $\Delta\rho$ obtained at the end of the convergence procedure (at iteration $N = 15$). We see that the difference to the Hartree-Fock density has

generally increased. Let us note that mixing the orbitals not only allows to introduce non-diagonal couplings in the density (which in this case would be nonexistent if only the first equation was solved), it also modifies the diagonal elements of ρ. More precisely it allows in principle to partially empty the core and populate the initially empty states. In this test case, the biggest effect concerns the initial Hartree-Fock $0s$-shell of the core which is emptied up to 1.43×10^{-3} in the case of protons and 1.48×10^{-3} in the case of neutrons. The initially empty $1s$-shell is populated at 1.22×10^{-3} and 1.27×10^{-3} respectively. In this test case, the effect is thus quite weak and not visible on the figures. However, it could in principle become more drastic when e.g. using a different truncation scheme to build the wave function (see next section).

Evolution of the source term

We previously showed on Fig. (III.12) the source matrix $G_{ij}[\sigma]$ obtained at the first iteration $N = 1$ (in the starting Hartree-Fock basis). It is now interesting to look at the evolution of this term after the convergence procedure. The source term $G[\sigma]$ reflects the residual correlations beyond the mean field $h[\rho, \sigma]$. Since the latter absorbs the average effect of the correlation content of the system and thus becomes more and more refined, one could expect the intensity of G to decrease. The results obtained in this test case are however not so straightforward. We show on Fig. (III.15) the proton and neutron source terms expressed in the final basis μ. We note that if the coupling between the $p_{1/2}$ sub-shells has indeed decreased to,

$$\begin{cases} G^{\pi}[\sigma]_{p_{1/2}} \simeq 0.356 \text{ MeV} & \text{(III.47)} \\ G^{\nu}[\sigma]_{p_{1/2}} \simeq 0.328 \text{ MeV} , & \text{(III.48)} \end{cases}$$

the coupling between the $p_{3/2}$ sub-shells has increased to,

$$\begin{cases} G^{\pi}[\sigma]_{p_{3/2}} \simeq 0.307 \text{ MeV} & \text{(III.49)} \\ G^{\nu}[\sigma]_{p_{3/2}} \simeq 0.283 \text{ MeV} . & \text{(III.50)} \end{cases}$$

It seems that both final couplings tend to resemble each other. This behavior will also be encountered in the next section where another truncation scheme of the wave function is used. The occupation of single-particle states are only slightly modified at the end of the convergence procedure. Thus the behavior for the correlation field $Q[\rho, \sigma]$ is similar to the one observed for $G[\sigma]$. Finally, the corresponding values of the mean-field $h[\rho, \sigma]$ in the optimized basis remain roughly unchanged along the convergence process.

Evolution of the single-particle energies

The single-particle energies (SPEs) ε_a are defined as eigenvalues of the mean-field $h[\rho, \sigma]$. In order to appreciate the modification induced by the correlations on the single-particle spectrum, we plotted on Fig. (III.16) the difference between these SPEs and Hartree-Fock

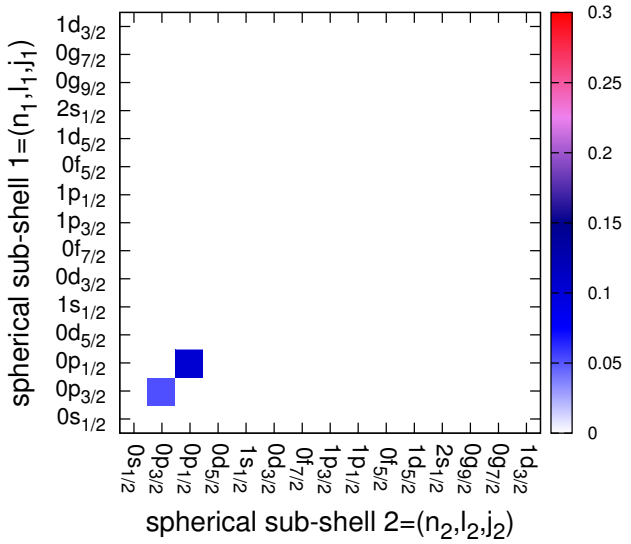

(a) $\Delta\rho$ after solving the first variational equation at the first global iteration $N = 1$. The density is modified in the valence space only.

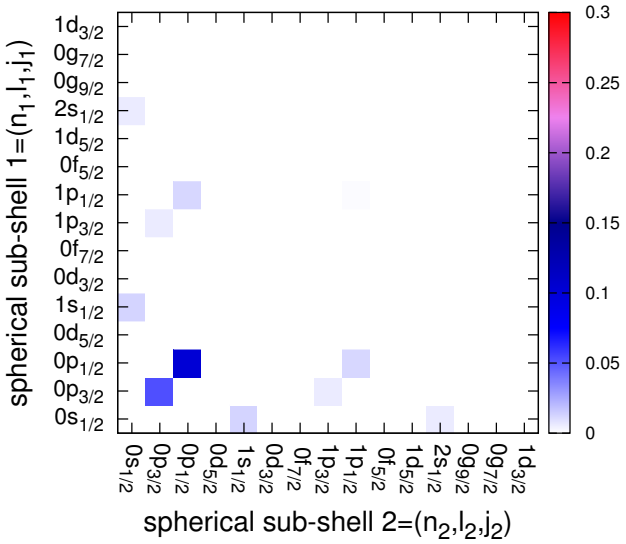

(b) $\Delta\rho$ after solving the second variational equation at the first global iteration $N = 1$. The density is modified in the whole basis. Positive-parity states are also affected.

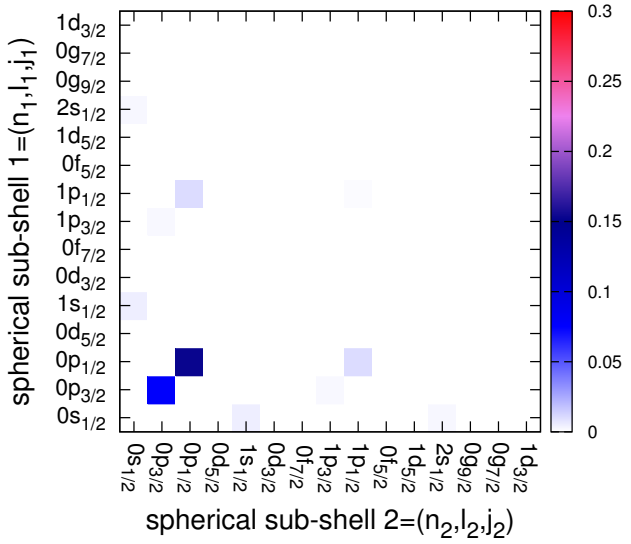

(c) $\Delta\rho$ after solving the first variational equation at the second global iteration $N = 2$. The density in the valence space has kept trace of the orbital transformation.

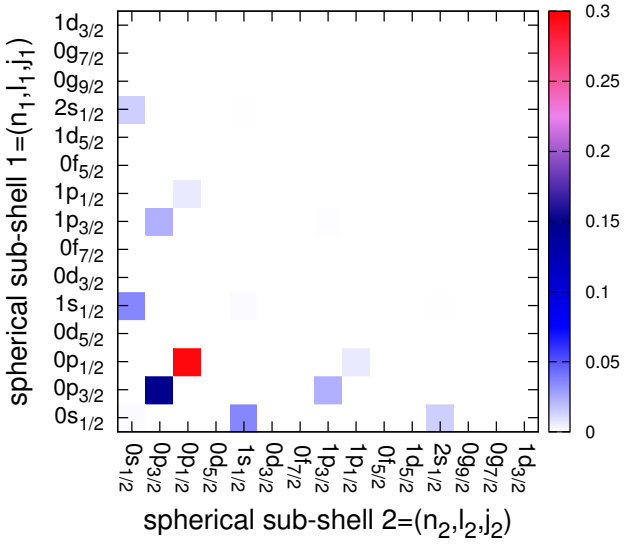

(d) $\Delta\rho$ at the end of the convergence procedure $N = 15$. The density given by the first and the second variational equations have become identical, and the difference to the Hartree-Fock density has increased.

Figure III.13: Evolution of the neutron one-body density along the convergence process. The difference between the correlated density and a pure Hartree-Fock density $\Delta\rho = |\rho - \rho_{HF}|$ is represented in a matrix form, in the original Hartree-Fock basis.

ones (eigenvalues of the Hartree-Fock field). We arrive to similar conclusions concerning both types of nucleons: the account for correlations in the mean-field leads to a global compression of the single-particle spectra. The energy difference between the lowest shell ($0s$) and the

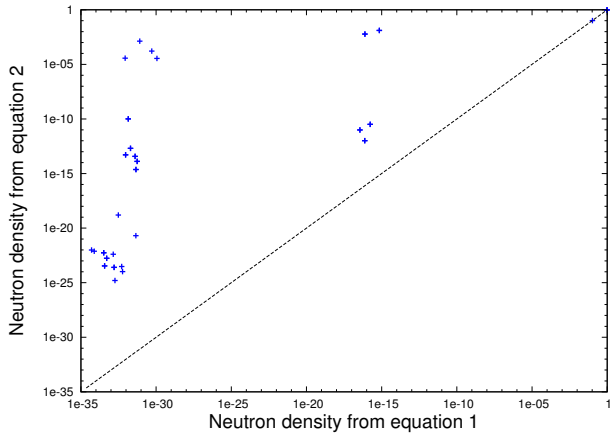

(a) Iteration $N = 1$.

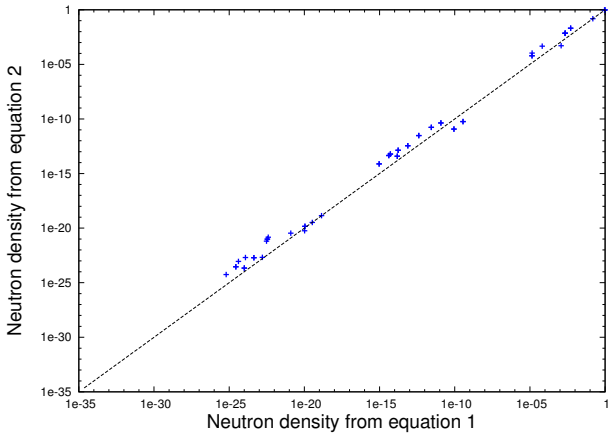

(b) Iteration $N = 2$.

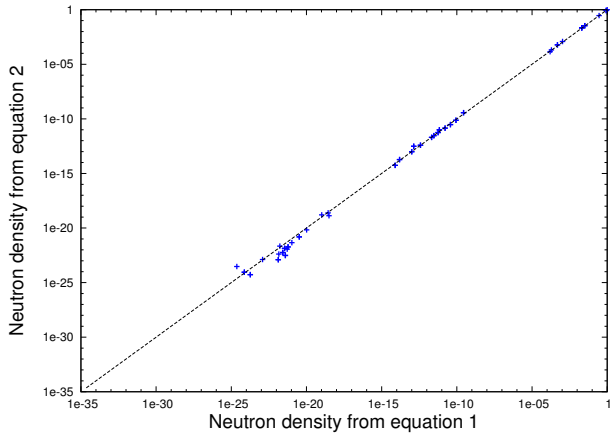

(c) Iteration $N = 10$.

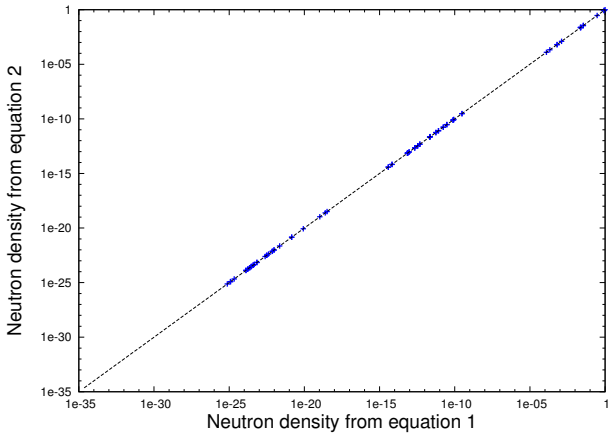

(d) Iteration $N = 15$, convergence reached.

Figure III.14: Comparison between the neutron density matrices given by the first and second variational equations at different stages of the convergence process.

highest one ($1d_{3/2}$ in this case) is decreased by ~ 2.5 MeV. In particular the gap at the Fermi level between $\varepsilon_{0p_{3/2}}$ and $\varepsilon_{0p_{1/2}}$ is reduced. The $0p_{3/2}$-level is increased by ~ 0.74 MeV in both cases. The $0p_{1/2}$-level is lowered by $\sim$ 0.18 MeV in the case of protons, whereas is stays almost unchanged in the case of neutrons. Let us also note the important effect induced on the $0s_{1/2}$-shell which is shifted up by more than 2 MeV for both types of particles.

Effect on the description of the ground-state

Let us now look at the effect caused by the orbital optimization on the energy and the composition of the ground state wave function. For a complete comparison and in order to isolate the effect of the second equation alone, we calculate these quantities at three levels:

- After solving the first variational equation (Eq. (III.11) denoted by Eq. 1 in the following tables) without rearrangement terms, i.e. after simple diagonalization of the Hamiltonian matrix $H[\rho_{HF}]$ constructed with the uncorrelated Hartree-Fock density.
- After solving the first variational equation (Eq. (III.11) denoted by Eq. 1) with rear-

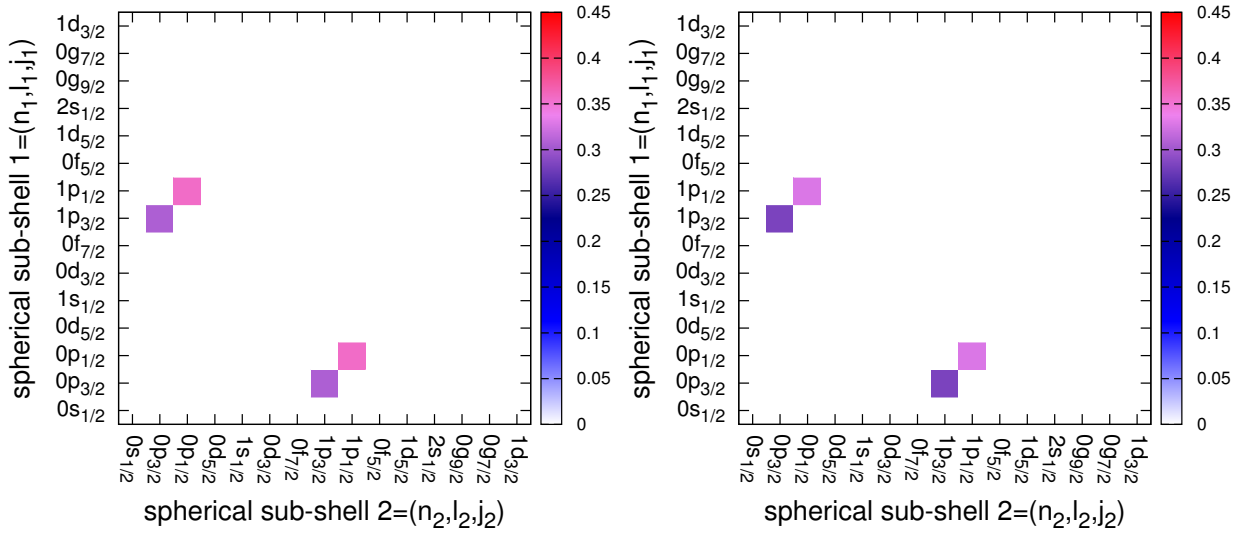

Figure III.15: Proton (left) and neutron (right) source term at the end of the convergence procedure $N = 15$.

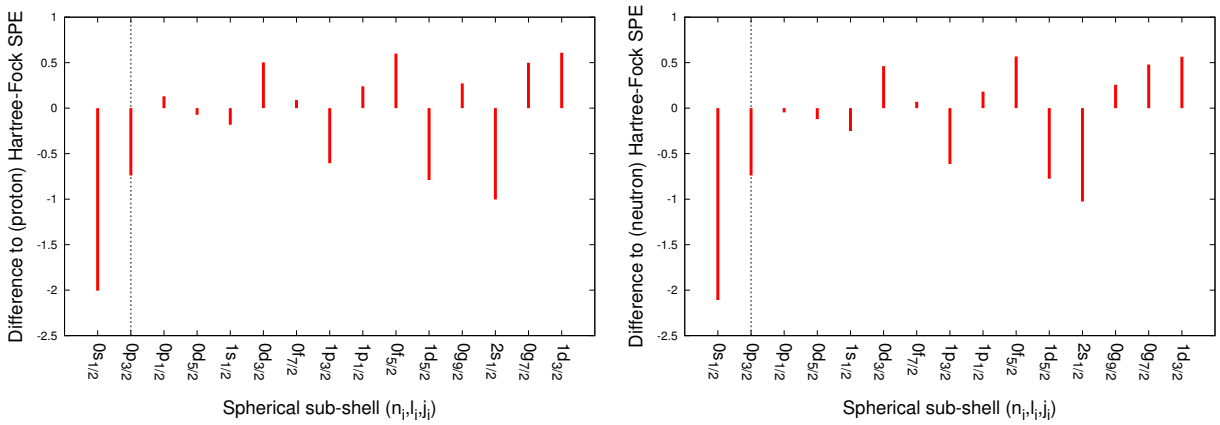

Figure III.16: Difference $\Delta\varepsilon = \varepsilon^{HF} - \varepsilon[\rho, \sigma]$ between single-particle energies taken as eigenvalues of the Hartree-Fock field and single-particle energies taken as eigenvalues of the improved mean-field $h[\rho, \sigma]$, for protons (left) and neutrons (right). The Fermi level is marked by a dashed line.

rangement terms, i.e. by iterating the diagonalization of $\mathcal{H}[\rho, \sigma] = H[\rho] + R[\rho, \sigma]$. This allows to identify the effect generated by the nucleus' medium.

- After the whole self-consistent procedure, when both variational equations (Eq. (III.11) and Eq. (III.17) denoted by Eq. 1 and Eq. 2 respectively in the following tables) are simultaneously satisfied.

We first show the correlation energy, difference between ground state and spherical Hartree-Fock energies, $E_{corr} = E_{HF} - E_0$, obtained in these three cases:

Correlation energy		
Eq. 1 with $R = 0$	Eq. 1 with $R \neq 0$	Eqs. 1 and 2 satisfied
5.1	6.22	6.56

The major effect with the D1S Gogny force, is produced by the inclusion of the rearrangement terms which increases the correlation energy by $\sim$ 1.12 MeV. The optimization of orbitals allows to gain additional 340 keV. Although the effect is small, the variational aspect of the orbital equation is indeed found on these results.

Regarding now the composition of the wave function, we show in the next table the weight of the most important configurations *built on original Hartree-Fock orbitals*. In fact, to calculate the latter after the self-consistency process, one has to perform the following procedure. Denoting by $b^\dagger_\mu$ the optimized single-particle states, the final self-consistent wave function can be written as,

$$|\Psi^{SC}\rangle = \sum_\alpha A^{SC}_\alpha \, |\phi^{SC}_\alpha\rangle \qquad \text{where,} \qquad |\phi^{SC}_\alpha\rangle = \prod_{\mu\in\alpha} b^\dagger_\mu \, |0\rangle \ . \tag{III.51}$$

The weight B^0_β of a configuration $|\phi^0_\beta\rangle = \prod_{i_\beta} a^\dagger_i \, |0\rangle$ built on Hartree-Fock orbitals $a^\dagger_i$, in $|\Psi^{SC}\rangle$ reads,

$$B^0_\beta = \langle\phi^0_\beta|\Psi^{SC}\rangle = \sum_\alpha A^{SC}_\alpha \, \langle\phi^0_\beta\phi^{SC}_\alpha\rangle \ , \tag{III.52}$$

and is thus obtained by calculating overlaps of the Slater determinants, themselves equal to the determinant of the overlaps of their occupied orbitals.

Configurations built on HF basis	Eq. 1 with $R = 0$	Eq. 1 with $R \neq 0$	Eqs. 1 and 2 satisfied
0p-0h (spherical HF state)	64.42%	53.95%	47.65%
$(2p\text{-}2h)_{\pi\nu}$	15.68%	19.05%	29.26%
$(2p\text{-}2h)_{\pi}$	7.03%	8.94%	9.74%
$(2p\text{-}2h)_{\nu}$	7.08%	8.90%	9.76%

The weight of the spherical Hartree-Fock component is lowered by $\sim$ 10% after adding the rearrangement effects. It keeps decreasing with the orbital optimization to reach a final value $\sim$ 48%. The Hartree-Fock reference state therefore represents less than half of the correlated wave function at the end of the self-consistent procedure, underlying the importance of correlations in the ^{12}C nucleus. In fact, we note that the second major configuration is a 2p-2h excitation of proton-neutron type, indicating the necessity of accounting for correlations between protons and neutrons in this case. The weight of this configuration increases to $\sim$ 19% after including rearrangement terms.

Finally it is also of interest to compare the final weights of these configurations (the ones built on HF orbitals) to the weights of configurations built on optimized orbitals μ. We therefore show on the next table the main components of the wave function obtained when both variational equations are solved.

Configurations built on optimized basis	Eqs. 1 and 2 satisfied
0p-0h (optimized reference state)	48.20%
$(2p\text{-}2h)_{\pi\nu}$	20.84%
$(2p\text{-}2h)_{\pi}$	9.85%
$(2p\text{-}2h)_{\nu}$	9.87%

We note that the weight of the new reference state is slightly higher than the weight of the pure Hartree-Fock state. Although the difference is small in this case, this is a sign that the optimized 0p-0h excitation is "better" than the HF state, in the sense that it contains more physics. The $(2p\text{-}2h)_{\pi\nu}$ configurations is here again very important since it has reached a weight of almost 21%.

III.4.2 Second truncation scheme: excitation order of the configurations in the full single-particle space

We apply now the formalism of the multiparticle-multihole configuration method using a second scheme for selecting the many-body configurations. They are now chosen according to their excitation order. We decide to include all possible proton and neutron configurations up to 2p-2h. This generates A-body states $|\phi_\alpha\rangle = |\phi_{\alpha_\pi}\rangle \otimes |\phi_{\alpha_\nu}\rangle$ with an excitation order $M_\alpha \leqslant 4$. In other words, all nucleon excitations of the following types are considered: (0p-0h), $(1p\text{-}1h)_\pi$, $(1p\text{-}1h)_\nu$, $(2p\text{-}2h)_\pi$, $(2p\text{-}2h)_\nu$, $(2p\text{-}2h)_{\pi\nu}$, $(3p\text{-}3h)_{\pi\nu}$ and $(4p\text{-}4h)_{\pi\nu}$. This type of truncation scheme ensures explicit conservation of spherical symmetry.
Since no use of a core is made, all particles are considered active and the number of Slater determinants expands very rapidly. In the case of ^{12}C, when single-particle states are expanded on $N_0 = 5$ oscillator shells we obtain a total of

26 401 700 configurations to build,

in the $J = K = 0$ component, making use of the time-reversal invariance. Convergence of the one-body density with a precision $\eta \leqslant 10^{-4}$ is reached after 14 global iterations.

Two-body correlation matrices
We show on Fig. (III.17) all elements of the proton, neutron and proton-neutron correlation matrices. They appear much more fragmented than in the previous case.

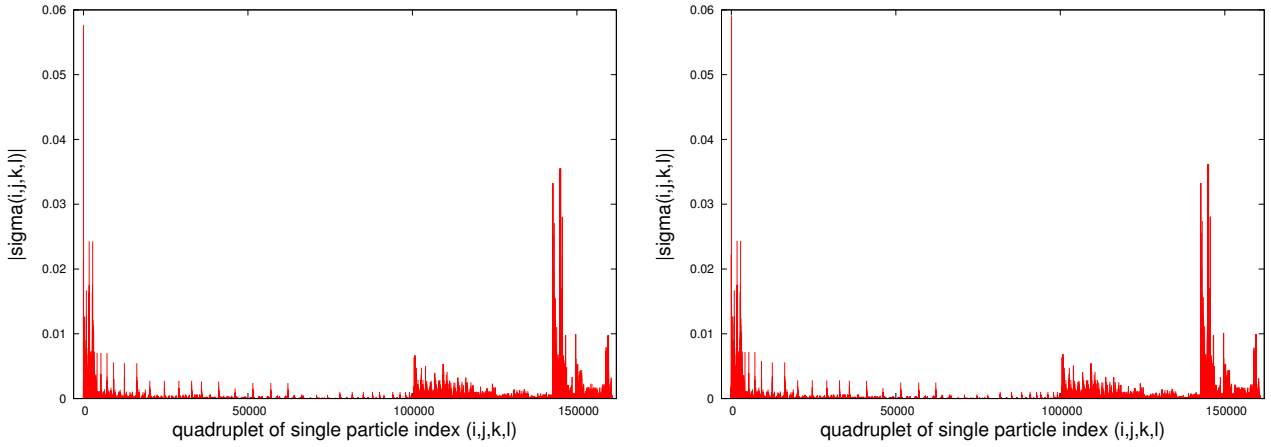

(a) Proton correlation matrix

(b) Neutron correlation matrix

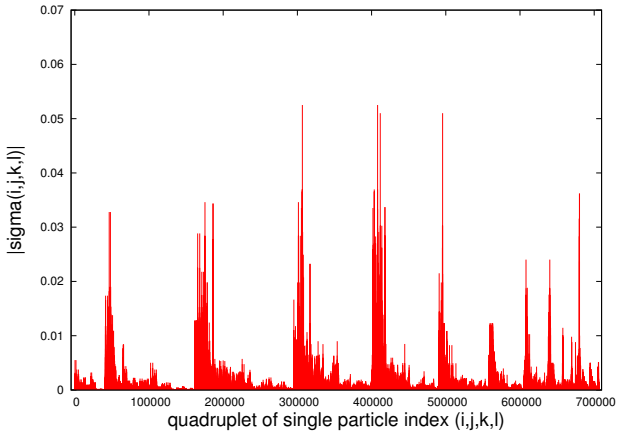

(c) proton-neutron correlation matrix

Figure III.17: Correlation matrices at iteration $N = 1$.

In the case of pure proton or neutron correlations, more than 160 000 elements appear. If most of them are of very small intensity, several distinguishable peaks appear, mostly reflecting correlations of pairing type.

- The biggest one at $I = 6$, and characterized by $\sigma(6) \simeq 5.8 \times 10^{-2}$, corresponds to the scattering of a pair of protons (neutrons) on the $0p_{3/2}$ sub-shell itself (from one projection $\Omega = j_z$ to another).
- The elements $\sigma(I = 4, 5) \simeq 2.2 \times 10^{-2}$ reflect the scattering of a pair from the $0s$ sub-shell to the $0p_{3/2}$ one.
- Scattering between the $0p_{3/2}$ and the $0p_{1/2}$ is contained in $\sigma(I = 142713, 142714) \simeq 3.33 \times 10^{-2}$.
- Scattering between the $0s$ and the $0p_{1/2}$ is contained in $\sigma(I = 142712) \simeq 2.03 \times 10^{-2}$.

Correlations between protons and neutrons appear again more intense. More than 700 000 elements are represented on Fig. (III.17). The strongest ones are again of pairing type. For

instance the element at $\sigma(I = 306734) \simeq 5.3 \times 10^{-2}$ reflects pair scattering between the $0p_{3/2}$ sub-shell and the $1d_{5/2}$ one.
Let us remind that these correlations matrices are not recoupled in J and therefore it is difficult to compare the intensity of the couplings between different shells. It is interesting however to see how these correlations evolve after the process has converged.

Hence, we show on Fig. (III.18) the same correlation matrices at iteration $N = 14$, when convergence is reached. We note a decrease of some elements of the correlation matrices of same isospin. This behaviour is coherent with the interpretation of the role of the orbital equation. The mean-field is indeed supposed to absorb as much effect of the correlations as possible and thus reduce the intensity of the latter. However, we note that this is not true concerning the proton-neutron correlation matrix $\sigma^{\pi\nu}$, which even has a tendency to slightly increase. In a shell-model context, it is often argued that this type of correlations is at the origin of deformation in nuclei. Perhaps the behaviour of $\sigma^{\pi\nu}$ is thus due to the fact that the spherical symmetry stays explicitly conserved in our approach, and therefore this type of correlations cannot be incorporated into the mean-field. They remain correlations of "dynamical" type. Hence, it would be very informative to perform the same study while allowing for deformation, i.e. by working in the intrinsic frame of the nucleus. The main drawback of such an approach would however be the need to project the final solution in order to obtain a state characterized by a good angular momentum J.

Source term
We show on Fig. (III.19) the proton and neutron source terms at the beginning and end of the convergence procedure. Since all orbitals participate to the configuration mixing, many more couplings appear in the source matrix G_{ij}, than in the previous case, where a valence space was considered. However, this source term seems to evolve in the same manner as before. That is, some kind of "harmonization" of the different couplings seems to appear: the strongest ones decrease while the weakest ones increase.

One-body density
We also show on Fig. (III.20) the evolution of the one-body density (in fact its difference to a Hartree-Fock-state density) in the starting Hartree-Fock basis.
Since no use of a valence space is made, the correlated density calculated at the end of the first variational equation at the global iteration $N = 1$ already contains non-diagonal couplings in this basis. Again, the densities obtained via both variational equations tend to resemble each other along the convergence procedure. In fact they become identical up to $\sim 10^{-3}$, as seen from Fig. (III.21). It is important to state that this also means that the non-diagonal elements of the density ρ calculated via the first equation *in the final optimal basis* μ go to zero.
Finally a stronger modification of the diagonal elements of the density are observed, compared

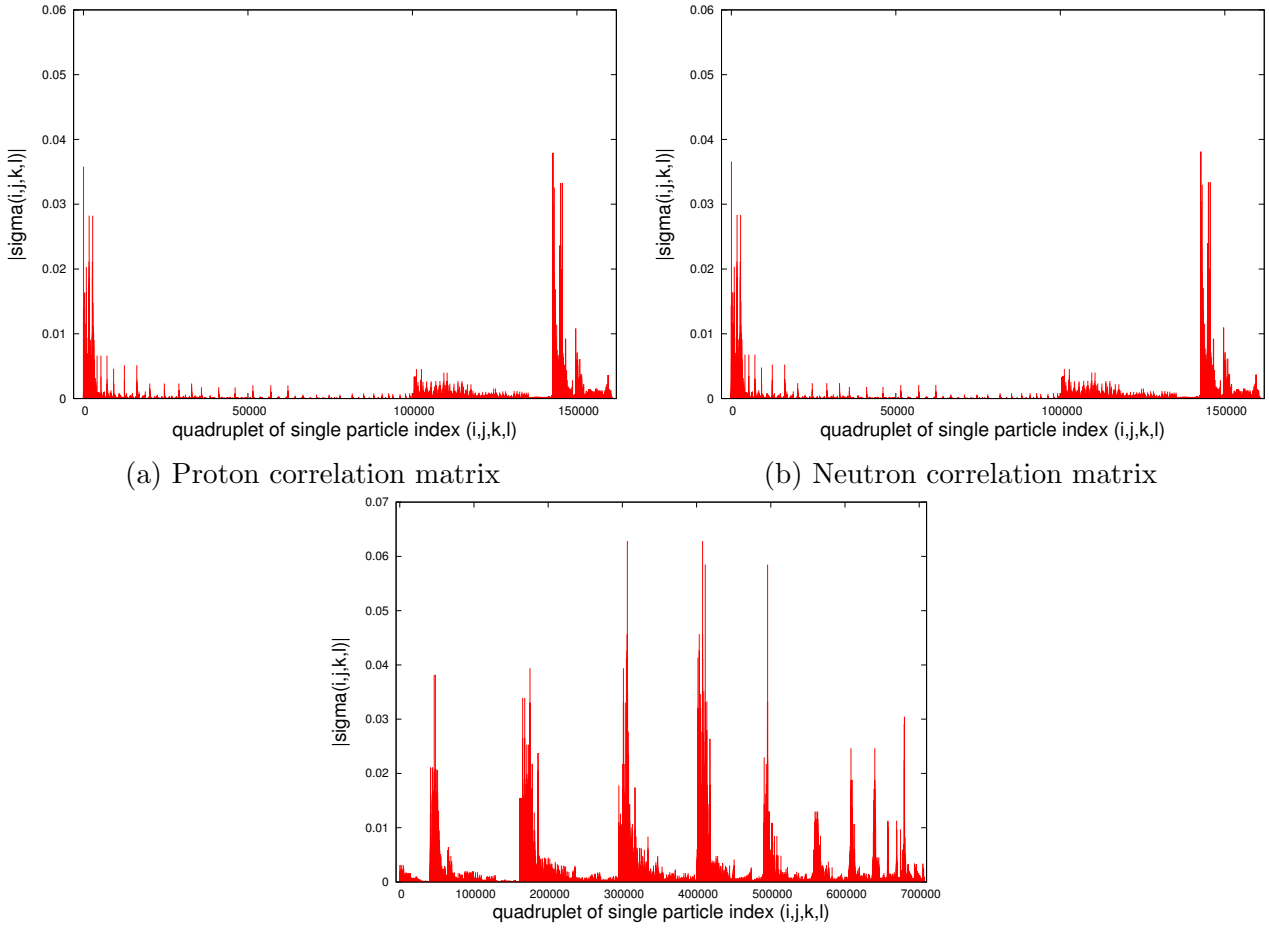

(a) Proton correlation matrix

(b) Neutron correlation matrix

(c) proton-neutron correlation matrix

Figure III.18: Correlation matrices when convergence is reached, at iteration $N = 14$.

to the previous truncation scheme. We show in the following table, the evolution of the Hartree-Fock state occupations at the beginning and end of the procedure.

	Protons		Neutrons	
Original Hartree-Fock sub-shell	Occupation at global iteration $N = 1$	Occupation at global iteration $N = 14$	Occupation at global iteration $N = 1$	Occupation at global iteration $N = 14$
$0s$	0.97	0.93	0.97	0.93
$0p_{3/2}$	0.90	0.78	0.90	0.77
$0p_{1/2}$	3.7×10^{-2}	9.2×10^{-2}	3.7×10^{-2}	9.2×10^{-2}
$0d_{5/2}$	2.1×10^{-2}	5.3×10^{-2}	2.1×10^{-2}	5.3×10^{-2}

Identical behaviors are obtained for both protons and neutrons. We observe a depopulation of the $0s$ shell that is of the order $\sim 4 \times 10^{-2}$. More importantly the $0p_{3/2}$ is emptied by more than 0.1. Conversely higher shells are filled.

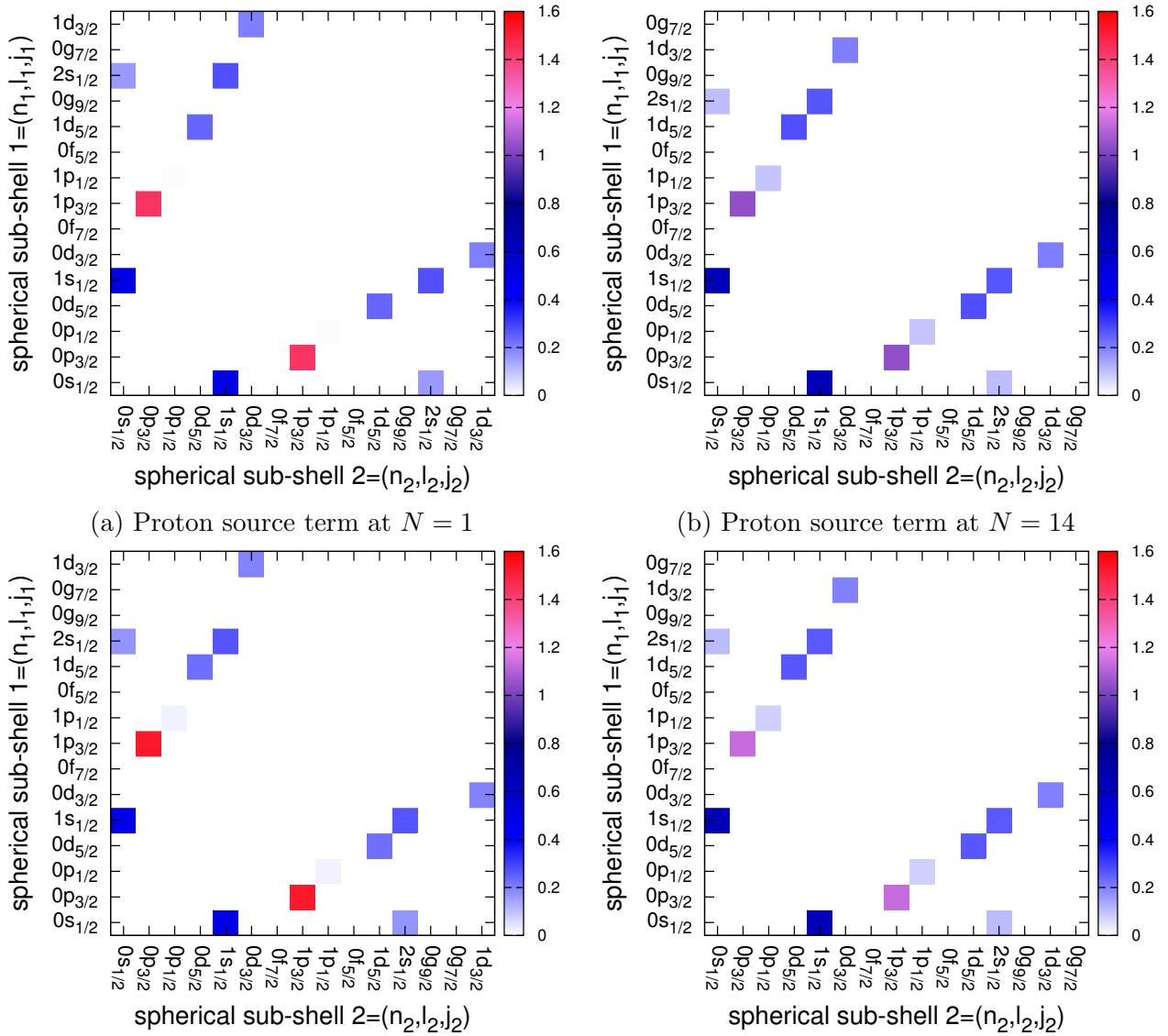

(a) Proton source term at $N = 1$

(b) Proton source term at $N = 14$

(c) Neutron source term at $N = 1$

(d) Neutron source term at $N = 14$

Figure III.19: Proton (up) and neutron (down) source terms at iterations $N = 1$ (left) and $N = 14$ (right).

Single-particle energies

The new single-particle energies are greatly affected by the renormalization procedure, as seen from Fig. (III.22). Most levels are shifted up compared to the Hartree-Fock spectrum. The biggest effect concerns again the $0s$ shell which is moved up by more than 6 MeV in the case of protons and neutrons. The gap at the Fermi level is also reduced by ~ 2 MeV in both cases.

Effect on the description of the ground-state

As previously we can study the effect of the orbital equation induced on e.g. the correlation energies as well as on the content of the ground state wave function. As seen from the following table, the correlation energies are increased by more than 50 MeV in all cases. This effect is

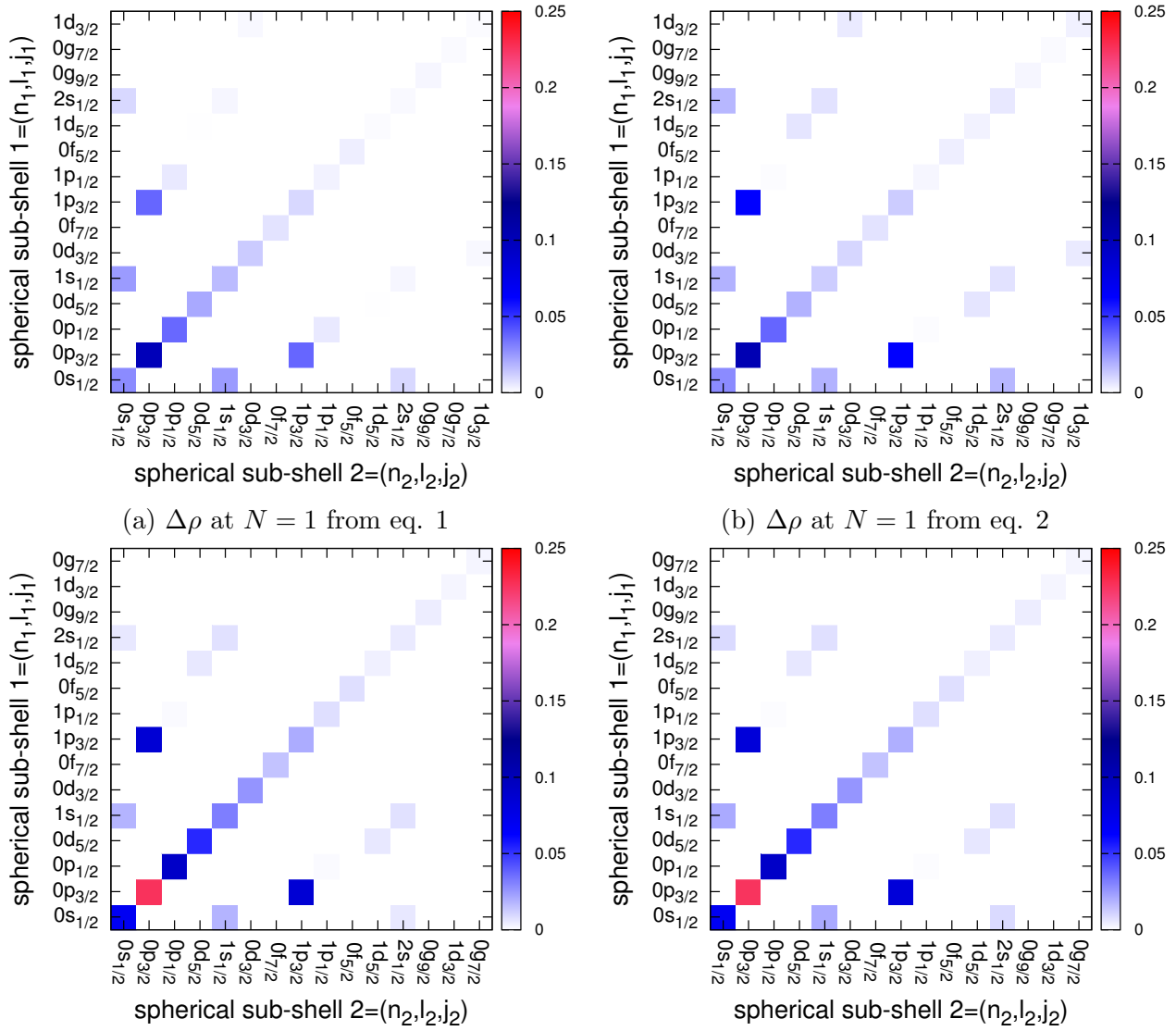

(a) $\Delta\rho$ at $N = 1$ from eq. 1

(b) $\Delta\rho$ at $N = 1$ from eq. 2

(c) $\Delta\rho$ at $N = 14$ from eq. 1

(d) $\Delta\rho$ at $N = 14$ from eq. 2

Figure III.20: One-body neutron density matrix in the Hartree-Fock basis from the first equation (left) and second equation (right) at iterations $N = 1$ (up) and $N = 14$ (down).

expected since the Gogny interaction has been fitted at the Hartree-Fock level. Considering only relative energies, we note however the reasonable gain of ~ 4.4 MeV in correlation energy when the full self-consistent process is applied.

Correlation energy (MeV)		
Eq. 1 with $R = 0$	Eq. 1 with $R \neq 0$	Eqs. 1 and 2 satisfied
58.15	61.77	62.54

Concerning the wave function composition, we note an important fragmentation already present at the non self-consistent stage. The Hartree-Fock component embodies less than a third of the total strength. This effect is reinforced by self-consistency effects which lower

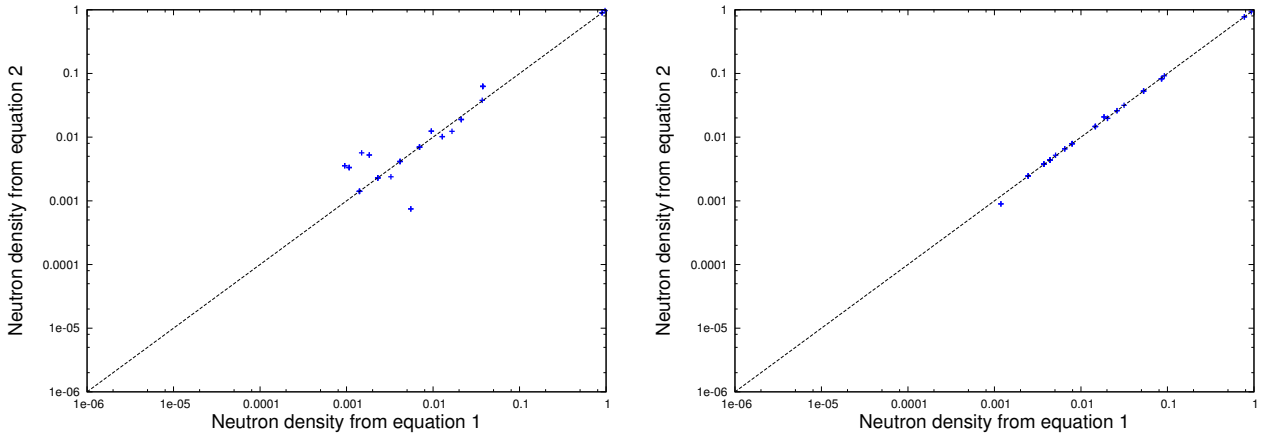

(a) Iteration $N = 1$.

(b) Iteration $N = 14$.

Figure III.21: Comparison between the neutron density matrices given by the first and second variational equations at the beginning and the end of the convergence process.

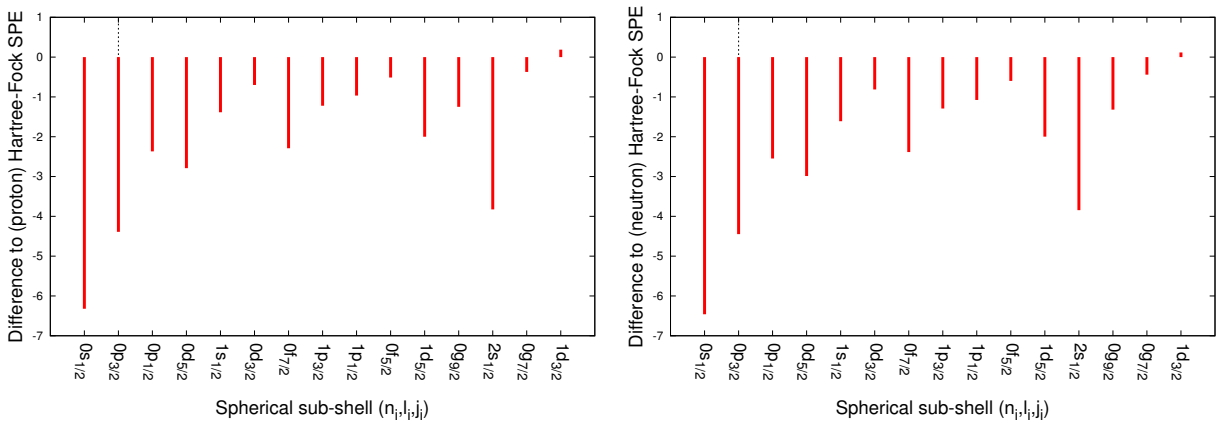

Figure III.22: Difference $\Delta\varepsilon = \varepsilon^{HF} - \varepsilon[\rho, \sigma]$ between single-particle energies taken as eigenvalues of the Hartree-Fock field and single-particle energies taken as eigenvalues of the mean-field $h[\rho, \sigma]$, for protons (left) and neutrons (right). The Fermi level is marked by a dashed line.

the HF component to $\sim 20\%$ only. Again let us note that the weight of the optimized 0p-0h component is slightly higher (22.33%).

Hartree-Fock component in the ground state wave function		
Eq. 1 with $R = 0$	Eq. 1 with $R \neq 0$	Eqs. 1 and 2 satisfied
29.29	21.46	20.39

Conclusion A few conclusions can be drawn from this comparative study. Firstly, we noticed that the number of global iterations needed to reach global convergence was similar when using both truncation schemes (~ 15). However it should be said that it was not possible to go beyond the convergence criterion $\eta = |\Delta\rho| = 10^{-4}$ using a truncation based on the excitation order of the configurations. The renormalization of orbitals appears to have a stronger effect

when a larger model space is used. This was illustrated on the evolution of e.g. occupations of Hartree-Fock states or fragmentation of the wave function. However this type of truncation scheme involves a rapid growth of the number of configurations. Indeed in this study of ^{12}C, increasing the model space from one to five oscillator shells enlarged the number of configurations from only 38 to more than 26 millions. Moreover as seen from the correlation energies obtained in this framework, the D1S Gogny interaction does not seem to be suited for this type of truncation, when the full single-particle space is explicitly considered (although results concerning the wave function are very reasonable). In the next chapter we go back to the first truncation scheme to perform a systematic study of ground and excited states in *sd*-shell nuclei.

Chapter IV

Description of sd-shell nuclei

In this chapter we perform a detailed study of *sd*-shell nuclei characterized by proton and neutron numbers $10 \leqslant (Z, N) \leqslant 18$. In the first section we investigate the ground-state properties of these nuclei, and analyze in more detail the features of a few benchmark cases with different correlation content. In particular, we are interested in the composition of the wave function providing information on the collectivity of the nuclei, as well as quantities such as correlation and binding energies, charge radii and neutron skin thickness. In the second section we expose the low-lying spectroscopy obtained with the multiparticle-multihole configuration mixing approach. Observables such as excitation energies, electric quadrupole and magnetic dipole moments, as well as electric and magnetic transition probabilities $B(E2)$ and $B(M1)$, are calculated and compared to experiment. This study is in the continuation of a previous work [63] that provided a description of ground and excited properties of *sd*-shell nuclei. However that investigation was only performed at the non self-consistent level i.e. performing a configuration mixing on frozen Hartree-Fock orbitals and without introducing rearrangement terms. Moreover the Hartree-Fock average potential did not include the exchange Coulomb field and $N_0 = 11$ major oscillator shells were used to expand the single-particle states.
In the present work, we investigate the effect induced by self-consistency on spectroscopic observables. Theoretical results are generally shown at three levels:

- At the non self-consistent stage, after the Hamiltonian matrix $H[\rho_{HF}]$ has been diagonalized without rearrangement terms (a Hartree-Fock density ρ_{HF} being introduced in the Gogny interaction).

- After solving the first variational equation consistently with rearrangement terms $R[\rho, \sigma]$, in order to quantify the effect induced by the medium. This is achieved by diagonalizing $\mathcal{H}[\rho, \sigma] = H[\rho] + R[\rho, \sigma]$ iteratively using the densities (ρ, σ) of the correlated ground-state, until the mixing coefficients have converged.

- After full self-consistency has been reached, that is, when both orbitals and mixing coefficients are optimized together. This is achieved using the double iterative procedure

described in section III.3.

In this way, we are able to quantify the effect of introducing the correlated density in the interaction, which is not justified *a priori*, and to appreciate the consequence of the orbital optimization. When only little change is induced by the rearrangement terms, we do not expose the corresponding results.

Technical framework This systematic study of *sd*-shell nuclei is performed is the following framework.

- The single-particle states are expanded on axially deformed harmonic oscillator states at the spherical point. In order to ensure convergence of the results we use $N_0 = 9$ major oscillator shells.

- The relevant many-body configurations included in the wave function are selected in a "shell-model manner", that is, by defining a filled core[1] of ^{16}O and allowing for all possible excitations of nucleons in the *sd*-shell. This is depicted on Fig. (IV.1). The nuclear state is thus written,

$$|\Psi\rangle = \sum_{\alpha} A_\alpha \, |\phi_\alpha\rangle \qquad \text{where,} \quad |\phi_\alpha\rangle = \prod_{i_\alpha \in sd\text{-shell}} a^\dagger_{i_\alpha} \, |^{16}O\rangle \ .$$

  Making use of the time-reversal invariance, the number of configurations spans from 418 in the case of ^{20}Ne (4 valence nucleons, excitations from 0p-0h to 4p-4h) up to 56 937 in the case of ^{28}Si (12 valence nucleons, excitations from 0p-0h to 12p-12h).

- The convergence criteria on the one-body density are taken equal to $\eta_1 = \eta_2 = |\Delta\rho_{ij}| = 1.0 \times 10^{-5}$, $\forall\, i, j$.

IV.1 Ground-state properties

Deformation properties of *sd*-shell nuclei predicted within mean-field approaches are very diverse. For instance, we show on Fig. (IV.2) axial potential-energy curves (PEC) and triaxial potential-energy surfaces (PES) of Neon isotopes, obtained within the Hartree-Fock-Bogolyubov (HFB) approach using the same D1S Gogny interaction. One observes a transition of shape from spherical to deformed as the number of neutrons N decreases. The heaviest isotopes appear spherical while the lightest ones are predicted oblate (^{24}Ne) or prolate ($^{20-22}$Ne). We also display on Fig. (IV.3) the PEC and PES of three other noteworthy nuclei of the *sd*-shell: ^{24}Mg, ^{28}Si and ^{32}S. The ^{24}Mg and ^{28}Si nuclei exhibit a large prolate deformation

[1] Again, this core will not remain inert through the convergence procedure.

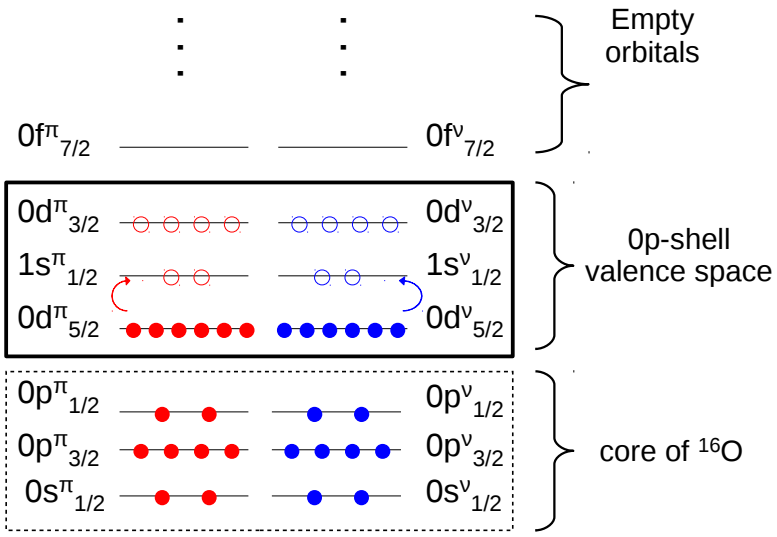

Figure IV.1: Separation of the single-particle states. The picture illustrates the case of ^{28}Si.

characterized by $\beta \sim 0.6$ and $\beta \sim 0.4$ respectively. The ^{32}S nucleus, although predicted spherical in its ground state, exhibits a super-deformed second minimum at $\beta \sim 1.2$ as seen from the potential energy curve (IV.3c).

IV.1.1 Correlation content

Correlation matrices

The collective deformation present (or absent) in these benchmark nuclei should reflect on the intensity of their two-body correlation matrices σ. We show on Fig. (IV.4) the calculated correlations for three Neon isotopes at the global iteration $N = 1$. If proton correlations appear quite analogous for all three nuclei (σ^{π} is a bit more fragmented for ^{20}Ne), correlations of neutron type are seen much more important and fragmented in the lighter nuclei. This is in accordance with the interpretation that the neutron collectivity increases as N decreases and drives the shape transition in this isotopic chain through the proton-neutron interaction. One also notes the importance of correlations between protons and neutrons, which is generally enhanced in nuclei with equal numbers of protons and neutrons, such as ^{20}Ne, since the two types of nucleons occupy the same orbitals and highly overlap spatially.
This effect is also illustrated on Fig. (IV.5) where we display the correlation content of the three other $N = Z$ benchmark nuclei. We also note the strength of pure neutron and proton correlations in ^{28}Si and ^{24}Mg, compared to other nuclei under study.

Source term

As explained in the previous chapter (in the study of ^{12}C), the source term $G[\sigma]$ couples

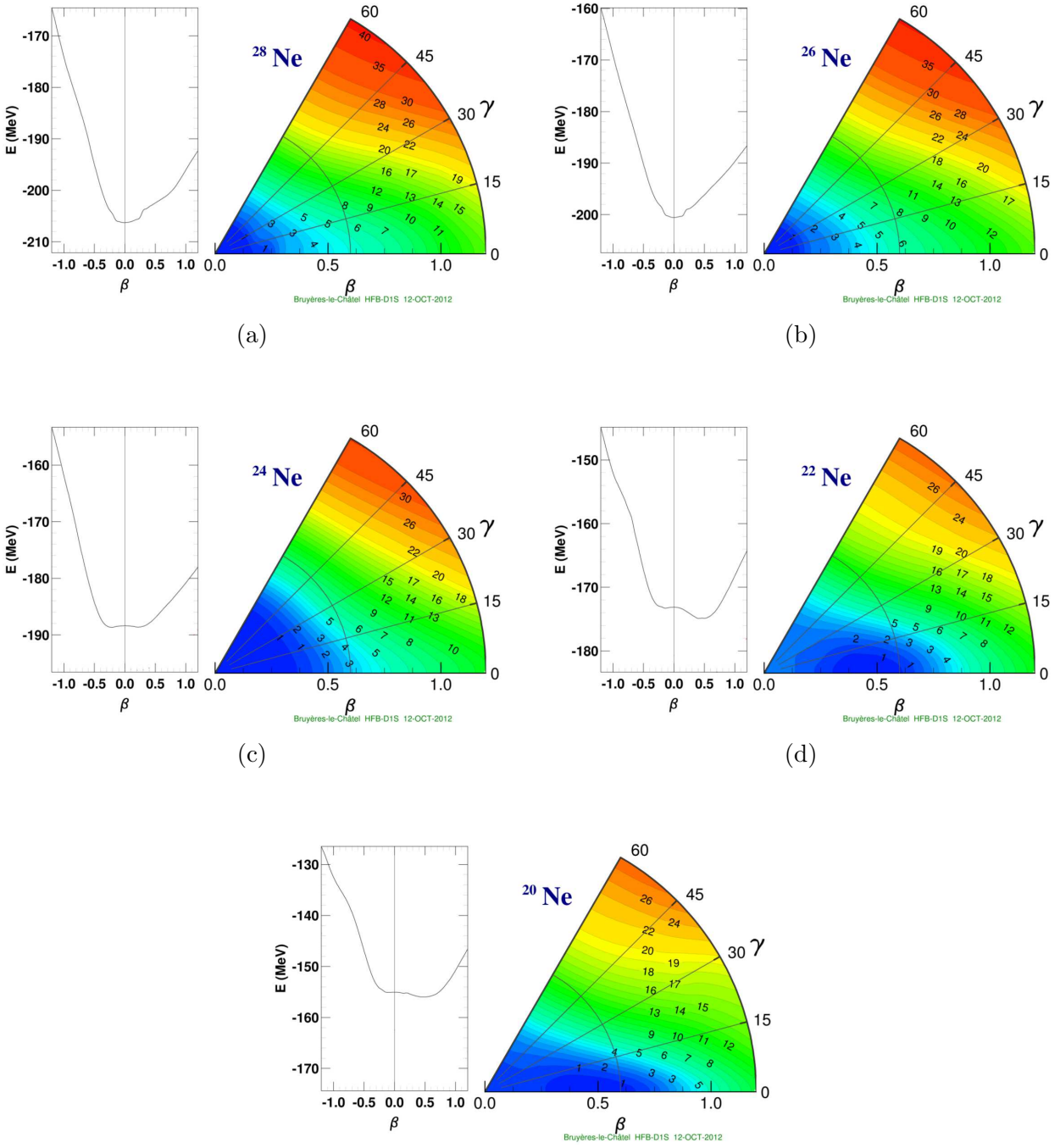

Figure IV.2: HFB PES and PEC of the Neon isotopes. The red curve is to be ignored. We observe a transition from spherical to deformed: $^{28-26}$Ne is predicted spherical while ^{24}Ne is oblate, and $^{22-20}$Ne prolate.

single-particle states in the valence space, to orbitals in the rest of the basis, characterized by same angular momentum j and parity π. Since we perform the present calculation using

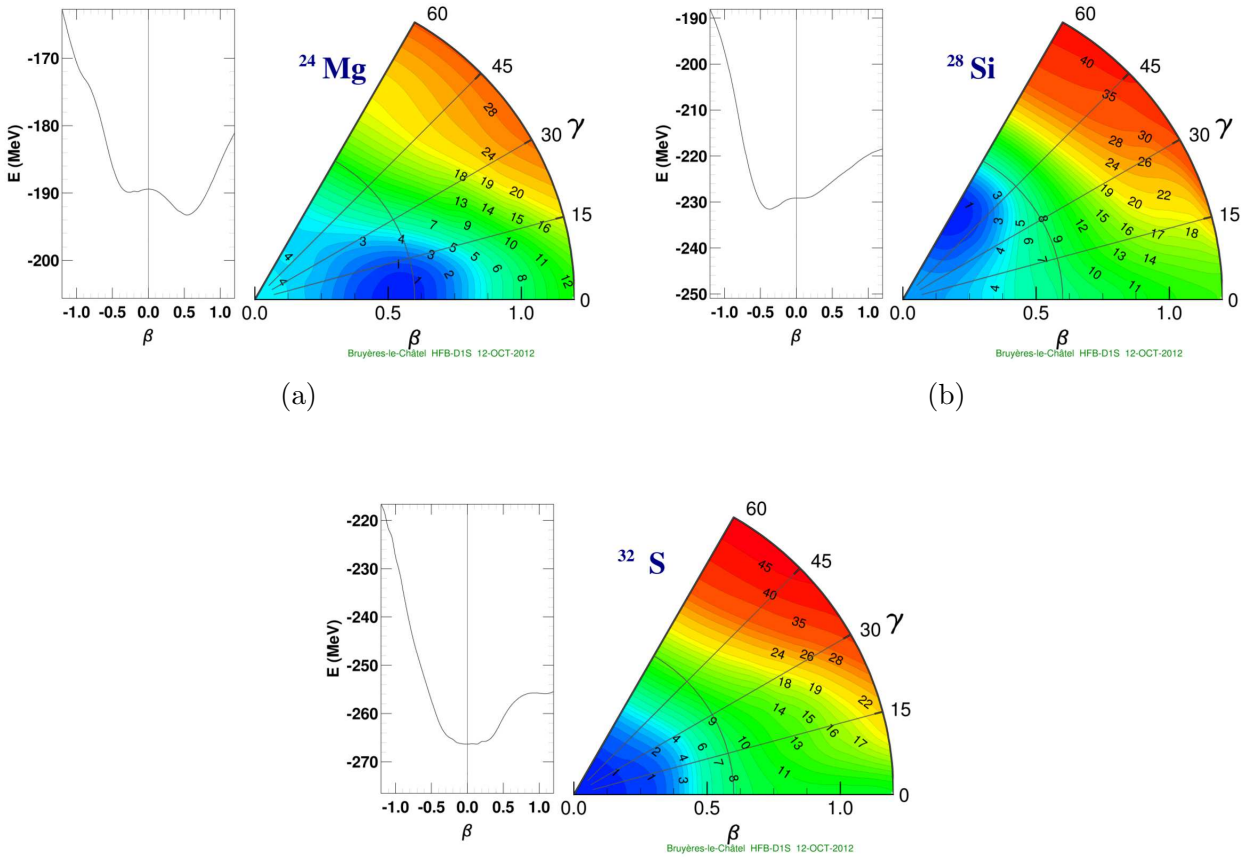

(a) (b)

(c)

Figure IV.3: HFB PES and PEC for ^{24}Mg (top left), ^{28}Si (top right) and ^{32}S (bottom). ^{24}Mg and ^{28}Si are both predicted with a strong axial deformation, prolate for the former and oblate for the latter. ^{32}S is predicted spherical with the existence of a super-deformed second minimum.

$N_0 = 9$ oscillator shells, the $0d_{5/2}$ sub-shell can couple to the $1d_{5/2}$, $2d_{5/2}$ and $3d_{5/2}$ empty sub-shells. The same happens concerning the $d_{3/2}$ sub-shells. In addition to the $2s$, $3s$ and $4s$ empty orbitals, the $1s$ shell can also couple to the filled $0s$ states of the core. Thus, we obtain a total of 10 couplings for each isospin. The corresponding values are displayed in table (IV.1) for the selected nuclei.
A few remarks can be done.

- Clearly some values of the source term are not negligible. In particular, we observe a systematic high value of the coupling between the $1s$ and the $0s$ shells (shown in bold) compared to other couplings. They are > 1 MeV in the nuclei described as the most deformed by mean-field calculations, and reach ~ 2 MeV in ^{24}Mg and ^{28}Si. Dynamical correlations related to the source term therefore seem to act toward a strong mixing of these shells.

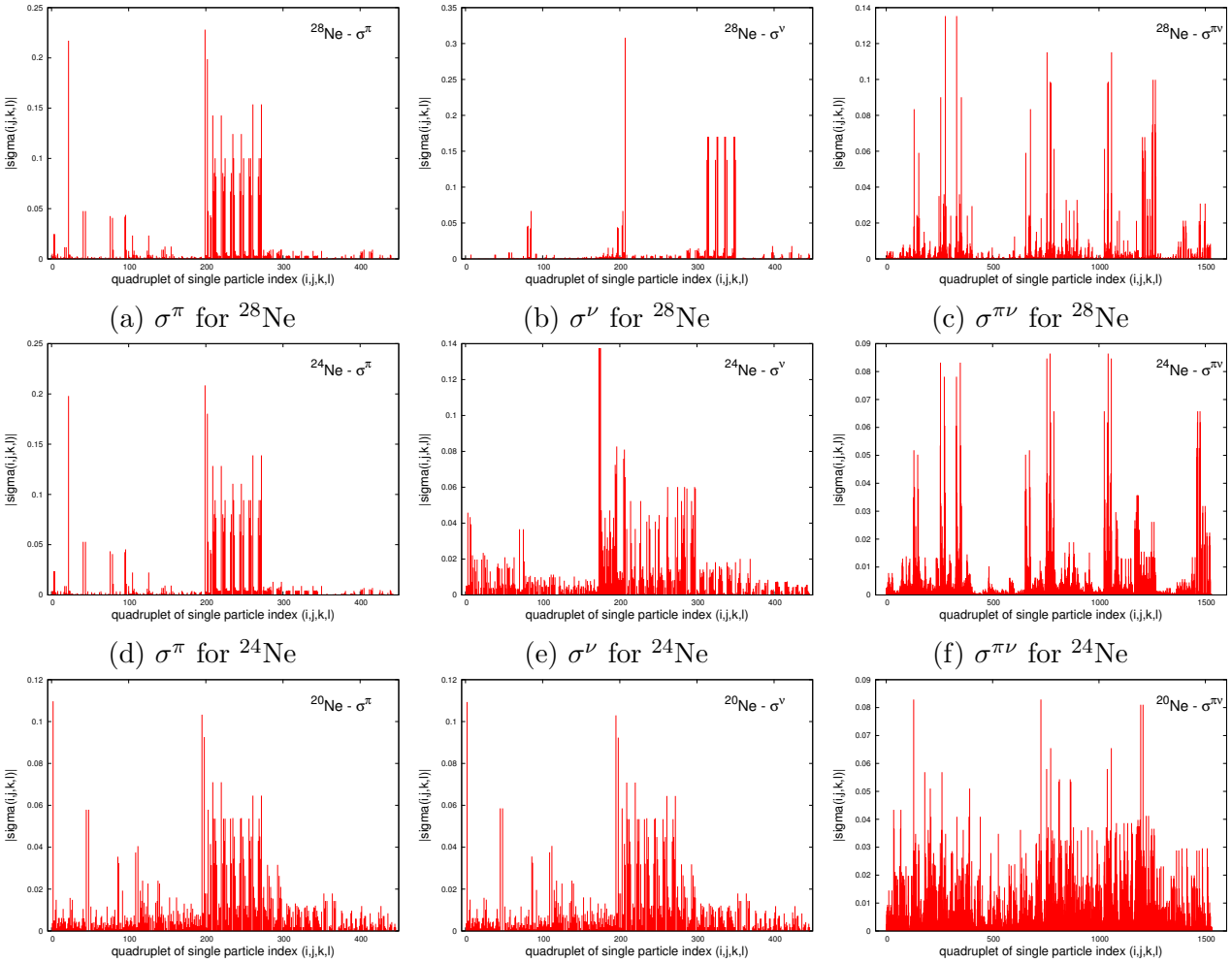

(a) σ^{π} for ^{28}Ne (b) σ^{ν} for ^{28}Ne (c) $\sigma^{\pi\nu}$ for ^{28}Ne

(d) σ^{π} for ^{24}Ne (e) σ^{ν} for ^{24}Ne (f) $\sigma^{\pi\nu}$ for ^{24}Ne

(g) σ^{π} for ^{20}Ne (h) σ^{ν} for ^{20}Ne (i) $\sigma^{\pi\nu}$ for ^{20}Ne

Figure IV.4: Proton correlations σ^{π} (left), neutron correlations σ^{ν} (center) and proton-neutron correlations $\sigma^{\pi\nu}$ (right), for ^{28}Ne, ^{24}Ne and ^{20}Ne. They are calculated at the global iteration $N = 1$.

- Regarding the Neon isotopic chain, the proton source term generally increases as the neutron number N decreases. Since the proton correlation content was similar for different isotopes (except for the very light ^{20}Ne nucleus), this behavior seems to be produced via the effect of proton-neutron correlations. Looking now at the behavior of the neutron source term, the interpretation is less clear. For instance, the coupling between the $0d_{3/2}$ and the $1d_{3/2}$ appears more important in the heavier Neon nuclei. This suggests a dependence of $G[\sigma]$ on the occupation of the shells. Indeed the $0d_{3/2}$ orbitals are much more occupied in ^{28}Ne than e.g. ^{20}Ne. This would also explain why $G^{\nu}[\sigma]$ is always slightly higher in ^{24}Ne than ^{20}Ne. Since the correlation field $Q[\rho, \sigma]$ divides the source term by the corresponding occupations this trend should be compensated. Indeed the corresponding values of e.g. $|Q_{0d_{3/2},1d_{3/2}}|$ appear equal to 0.550, 4.09 and 3.66 in ^{28}Ne, ^{24}Ne and ^{20}Ne respectively. In fact, similar occupations of the $0d^{\nu}_{3/2}$ are found for the

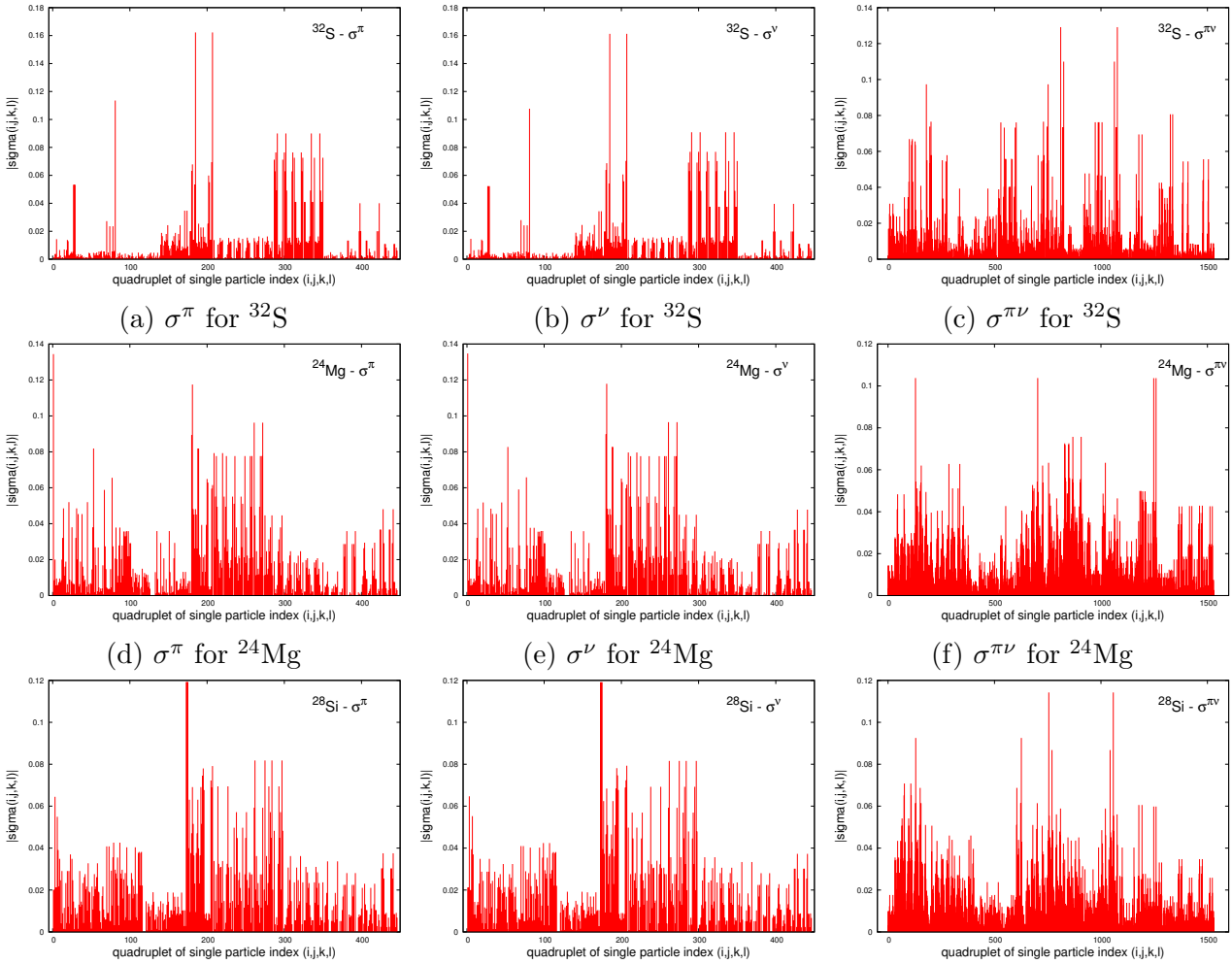

(a) σ^{π} for ^{32}S (b) σ^{ν} for ^{32}S (c) $\sigma^{\pi\nu}$ for ^{32}S

(d) σ^{π} for ^{24}Mg (e) σ^{ν} for ^{24}Mg (f) $\sigma^{\pi\nu}$ for ^{24}Mg

(g) σ^{π} for ^{28}Si (h) σ^{ν} for ^{28}Si (i) $\sigma^{\pi\nu}$ for ^{28}Si

Figure IV.5: Proton, neutron and proton-neutron correlation matrices, σ^{π}, σ^{ν}, $\sigma^{\pi\nu}$ respectively, for ^{32}S (up), ^{24}Mg (middle) and ^{28}Si (down). They are calculated at the global iteration $N = 1$.

^{28}Ne and ^{24}Ne isotopes.

- Finally, lets us look more carefully at the evolution of the couplings $G_{kl}[\sigma]$ with the single-particle energy difference $\Delta\varepsilon = |\varepsilon_k - \varepsilon_l|$. One would expect the values of $G[\sigma]$ to decrease while $\Delta\varepsilon$ increases. However, this behavior is not clear from the calculated values. Let us remind that these calculations are realized using a spherical mean-field. Thus if correlations associated to deformation are strong, important couplings to high energy orbitals can appear.

Correlation energy

Table (IV.2) displays the correlation energy, defined as the difference of the correlated ground

Sub-shells (α_k, α_l)	^{28}Ne	^{24}Ne	^{20}Ne	^{24}Mg	^{28}Si	^{32}S
$(0d_{\frac{5}{2}}, 1d_{\frac{5}{2}})$	0.0643	0.0328	0.0432	0.183	0.127	0.000156
$(0d_{\frac{5}{2}}, 2d_{\frac{5}{2}})$	0.253	0.439	0.593	0.543	0.399	0.170
$(0d_{\frac{5}{2}}, 3d_{\frac{5}{2}})$	0.299	0.272	0.405	0.505	0.542	0.211
$(1s, 0s)$	**0.263**	**0.281**	**1.248**	**1.913**	**2.210**	**1.256**
$(1s, 2s)$	0.0839	0.0830	0.526	0.749	0.827	0.637
$(1s, 3s)$	0.0337	0.0314	0.194	0.139	0.0983	0.112
$(1s, 4s)$	0.0523	0.0414	0.244	0.436	0.602	0.235
$(0d_{\frac{3}{2}}, 1d_{\frac{3}{2}})$	0.0463	0.0795	0.277	0.345	0.381	0.279
$(0d_{\frac{3}{2}}, 2d_{\frac{3}{2}})$	0.0198	0.0205	0.308	0.241	0.170	0.350
$(0d_{\frac{3}{2}}, 3d_{\frac{3}{2}})$	0.0303	0.0748	0.340	0.389	0.414	0.459

(a) Protons couplings $|G^{\pi}_{\alpha_k,\alpha_l}|$ (in MeV).

Sub-shells (α_k, α_l)	^{28}Ne	^{24}Ne	^{20}Ne	^{24}Mg	^{28}Si	^{32}S
$(0d_{\frac{5}{2}}, 1d_{\frac{5}{2}})$	0.0267	0.0681	0.0247	0.0976	0.050	0.0279
$(0d_{\frac{5}{2}}, 2d_{\frac{5}{2}})$	0.00578	0.177	0.610	0.572	0.427	0.177
$(0d_{\frac{5}{2}}, 3d_{\frac{5}{2}})$	0.0128	0.265	0.391	0.489	0.523	0.199
$(1s, 0s)$	**0.304**	**1.411**	**1.239**	**1.918**	**2.206**	**1.226**
$(1s, 2s)$	0.111	0.573	0.454	0.655	0.709	0.545
$(1s, 3s)$	0.0447	0.0143	0.219	0.184	0.166	0.0461
$(1s, 4s)$	0.0430	0.350	0.230	0.424	0.585	0.226
$(0d_{\frac{3}{2}}, 1d_{\frac{3}{2}})$	0.293	0.247	0.235	0.293	0.315	0.185
$(0d_{\frac{3}{2}}, 2d_{\frac{3}{2}})$	0.0613	0.144	0.319	0.261	0.201	0.397
$(0d_{\frac{3}{2}}, 3d_{\frac{3}{2}})$	0.252	0.276	0.331	0.382	0.406	0.448

(b) Neutrons couplings $|G^{\nu}_{\alpha_k,\alpha_l}|$ (in MeV).

Table IV.1: Proton (top) and neutron (bottom) source terms $|G^{\tau}_{\alpha_k,\alpha_l}|$ $(\tau = \pi, \nu)$ (in MeV) between the sub-shells of the valence space and other sub-shells (with same j^{π}) outside of the model space (at the first iteration $N = 1$).

energy E_0 with the energy of a spherical Hartree-Fock ground-state E_{HF},

$$E_{corr} = E_{HF} - E_0 \ , \tag{IV.1}$$

for the selected benchmark nuclei. We show here the results at three levels: without any self-consistency i.e. after diagonalizing the Hamiltonian matrix $H[\rho]$ without rearrangement terms; after solving the first variational equation with rearrangement terms $R[\rho, \sigma]$ i.e. by iterating the diagonalization of $\mathcal{H}[\rho, \sigma] = H[\rho] + R[\rho, \sigma]$; and after the full self-consistent procedure when both variational equations are satisfied.

As expected from the values of σ and $G[\sigma]$, the correlation energy of the Neon isotopes increases drastically for the lighter ones. At the non self-consistent level, among the presented nuclei,

	No self-consistency ($R = 0$)	1^{st} eq. with $R \neq 0$	Full self-consistency
^{20}Ne	10.93	11.54	13.30
^{22}Ne	10.48	10.90	12.12
^{24}Ne	5.75	6.23	6.98
^{26}Ne	0.41	0.88	1.55
^{28}Ne	1.15	1.28	1.58
^{24}Mg	14.24	15.06	16.04
^{28}Si	5.89	6.25	8.08
^{32}S	3.37	4.58	5.76

Table IV.2: Correlation energy $E_{corr} = E_{HF} - E_0$ for the Neon isotopes and other benchmark nuclei, in MeV.

^{24}Mg appears as the most correlated one. The introduction of rearrangement terms accounting for medium effects, allows to gain an energy $\Delta E_{corr} < 1$ MeV in all nuclei. The rest of the correlation energy is thus attributed to the renormalization of single-particle states. The most significant effect concerns the ^{28}Si for which optimizing the orbitals allows to gain additional 1.83 MeV. E_{corr} is increased by 1.76, 1.22, 1.18 and 0.98 MeV for ^{20}Ne, ^{22}Ne, ^{32}S and ^{24}Mg respectively. The effect is weaker in other nuclei under study.

Composition of the wave function

In order to obtain a more precise description of the amount of correlations in the ground-state, it is necessary to analyze the composition of the wave function in terms of the different configurations. We show in Table (IV.3) the main components of the wave function at the three stages explained at the beginning of the chapter, that is, (i) without any self-consistency (1^{st} variational equation with a Hartree-Fock density in the interaction), (ii) solving iteratively the 1^{st} variational equation with the correlated density in the interaction and thus, with rearrangement terms, (iii) when full self-consistency of correlations and orbitals is reached. In cases (i) and (ii), we show the weights of the most important configurations built on *Hartree-Fock single-particle states*, while in case (iii) the many-body Slater determinants are constructed on *optimized orbitals*.

- At the non self-consistent level, the Hartree-Fock 0p-0h state always appears as the major component, and absorbs most of the wave function in poorly correlated nuclei ($> 86\%$ in ^{28}Ne). The rest of the weight is distributed among many other configurations, mostly of 1p-1h and 2p-2h types.

- As already stated, configurations involving excitations of both protons and neutrons are more important in $N = Z$ nuclei, where their interaction is favored. The second main component in ^{28}Si is a $(2p-2h)_{\pi\nu} = (1p-1h)_\pi \otimes (1p-1h)_\nu$ excitation, with a weight $> 12\%$ while the Hartree-Fock states only embodies $\sim 26\%$ of the wave function.

Nucleus	Configuration	No self-consistency	Eq. 1 with rearrangements	Full self-consistency
^{28}Ne	**0p-0h**	**86.24**	**84.11**	**83.63**
	$(1\text{p-}1\text{h})_\pi$ $(0d_{5/2} \to 1s)$	3.49	3.19	2.85
	$(1\text{p-}1\text{h})_\nu$ $(1s \to 0d_{3/2})$	3.26	4.04	4.50
^{26}Ne	**0p-0h**	**77.11**	**70.88**	**69.62**
	$(1\text{p-}1\text{h})_\nu$ $(1s \to 0d_{3/2})$	6.02	7.28	7.59
	$(1\text{p-}1\text{h})_\nu$ $(0d_{5/2} \to 0d_{3/2})$	4.45	4.87	5.20
	$(2\text{p-}2\text{h})_{\pi\nu}$ $(1s^\nu \otimes 0d^\pi_{5/2} \to 0d^\nu_{3/2} \otimes 1s^\pi)$	2.27	2.75	2.38
^{24}Ne	**0p-0h**	**56.51**	**53.45**	**49.41**
	$(1\text{p-}1\text{h})_\nu$ $(0d_{5/2} \to 1s)$	17.81	17.48	17.81
	$(1\text{p-}1\text{h})_\nu$ $(0d_{5/2} \to 0d_{3/2})$	5.60	6.27	6.34
	$(2\text{p-}2\text{h})_\nu$ $(0d_{5/2} \to 1s)$	6.17	6.56	7.54
^{20}Ne	**0p-0h**	**45.36**	**43.05**	**33.05**
	$(2\text{p-}2\text{h})_{\pi\nu}$ $(0d^\pi_{5/2} \otimes 0d^\nu_{5/2} \to 1s^\pi \otimes 1s^\nu)$	8.15	6.80	8.86
	$(1\text{p-}1\text{h})_\pi$ $(0d_{5/2} \to 0d_{3/2})$	6.91	8.26	8.65
	$(1\text{p-}1\text{h})_\nu$ $(0d_{5/2} \to 0d_{3/2})$	6.94	8.30	8.58
	$(1\text{p-}1\text{h})_\pi$ $(0d_{5/2} \to 1s)$	5.29	4.44	5.08
	$(1\text{p-}1\text{h})_\nu$ $(0d_{5/2} \to 1s)$	5.40	4.50	5.13
	$(2\text{p-}2\text{h})_\pi$ $(0d_{5/2} \otimes 0d_{5/2} \to 1s \otimes 1s)$	2.32	1.89	2.46
	$(2\text{p-}2\text{h})_\nu$ $(0d_{5/2} \otimes 0d_{5/2} \to 1s \otimes 1s)$	2.44	1.95	2.52
^{24}Mg	**0p-0h**	**34.63**	**32.45**	**23.82**
	$(1\text{p-}1\text{h})_\nu$ $(0d_{5/2} \to 1s)$	8.31	7.13	6.49
	$(1\text{p-}1\text{h})_\pi$ $(0d_{5/2} \to 1s)$	8.08	6.98	6.37
	$(2\text{p-}2\text{h})_{\pi\nu}$ $(0d^\pi_{5/2} \otimes 0d^\nu_{5/2} \to 1s^\pi \otimes 1s^\nu)$	5.30	4.32	5.16
	$(1\text{p-}1\text{h})_\nu$ $(0d_{5/2} \to 0d_{3/2})$	4.43	4.83	3.94
	$(1\text{p-}1\text{h})_\pi$ $(0d_{5/2} \to 0d_{3/2})$	4.37	4.83	3.96
	$(2\text{p-}2\text{h})_\nu$ $(0d_{5/2} \otimes 0d_{5/2} \to 1s \otimes 1s)$	2.24	1.83	2.26
	$(2\text{p-}2\text{h})_\pi$ $(0d_{5/2} \otimes 0d_{5/2} \to 1s \otimes 1s)$	2.12	1.76	2.17
^{28}Si	**0p-0h**	**26.02**	**38.68**	**17.80**
	$(2\text{p-}2\text{h})_{\pi\nu}$ $(0d^\pi_{5/2} \otimes 0d^\nu_{5/2} \to 1s^\pi \otimes 1s^\nu)$	12.36	8.11	8.98
	$(2\text{p-}2\text{h})_\nu$ $(0d_{5/2} \otimes 0d_{5/2} \to 1s \otimes 1s)$	5.03	3.28	3.66
	$(2\text{p-}2\text{h})_\pi$ $(0d_{5/2} \otimes 0d_{5/2} \to 1s \otimes 1s)$	4.87	3.17	3.54
^{32}S	**0p-0h**	**60.30**	**47.23**	**26.20**
	$(2\text{p-}2\text{h})_{\pi\nu}$ $(1s^\pi \otimes 1s^\nu \to 0d^\pi_{3/2} \otimes 0d^\nu_{3/2})$	8.36	9.31	11.20
	$(2\text{p-}2\text{h})_\nu$ $(1s \otimes 1s \to 0d_{3/2} \otimes 0d_{3/2})$	3.80	4.38	5.47
	$(2\text{p-}2\text{h})_\pi$ $(1s \otimes 1s \to 0d_{3/2} \otimes 0d_{3/2})$	4.11	4.80	5.87

Table IV.3: Main components of the ground-state of different nuclei, expressed in percents (%).

- Accounting for medium effect via rearrangement terms allows to fragment the wave function by diminishing the 0p-0h component in most cases. The opposite phenomenon only occurs in ^{28}Si where the Hartree-Fock component is increased from ~ 26 to $\sim 39\%$.

- After self-consistency is reached the composition of the ground state wave function appears again considerably modified. The 0p-0h (reference state) component undergoes the biggest variation. In the Neon chain it decreases by a few percents in the heavier isotopes. The reduction is more important in the lighter ones such as ^{20}Ne where the weight of the reference state is lowered from $\sim$ 43 to $\sim$ 33%. The wave function of ^{24}Mg already appeared fragmented before self-consistency was introduced with a 0p-0h Hartree-Fock component of $\sim$ 35%. Still the self-consistency effects lead to an additional loss of $\sim$ 11% of the total strength. In ^{28}Si, the rise of the 0p-0h component due to rearrangement terms is now counterbalanced by the renormalization of single-particle states which bring it back down to only $\sim$ 18%. Finally the most striking effect is seen on ^{32}S for which the reference state component decreases from $\sim$ 60% to $\sim$ 45% with rearrangement terms and to only $\sim$ 26% after orbital optimization.

- Looking now at other components, we note that this systematic reduction of the 0p-0h configuration is not transmitted to one particular other configuration. The missing weight seems to be rather equally distributed on many components. This strong fragmentation seems to reflect an important increase of the collectivity of the wave function.

Finally, it is always informative to analyze the evolution of the pure Hartree-Fock component, that is the weight of the 0p-0h component built on *non-optimized Hartree-Fock orbitals* at the three stages (i), (ii) and (iii) of the mp-mh method. Following the procedure described in section III.4 to obtain this quantity after reaching self-consistency, we get the results shown in table (IV.4).

Nucleus	Without self-consistency	1^{st} eq. with $R \neq 0$	full self-consistency
^{26} Ne	77.11	70.89	61.50
^{28} Si	26.02	38.68	16.99
^{32} S	60.30	47.23	24.26

Table IV.4: Pure Hartree-Fock component in the correlated ground-state (i.e. weight of the 0p-0h configuration built on non-optimized Hartree-Fock orbitals), in percent.

Comparing them to the values showed in table (IV.3) after full self-consistency, we note that the weight of the optimized reference 0p-0h state (called ϕ) is systematically slightly higher than the weight of the Hartree-Fock state $|HF\rangle$, illustrating the fact that the new reference state always incorporates more physics and minimizes the effect of correlations. This phenomenon is however in competition with the tendency to fragment the wave function and the evolution of the single-particle spectrum. Indeed if gaps around the Fermi level are reduced, certain excitations may become more favorable and their weight might increase.

Single-particle energies

We present here the modification of single-particle energies (SPE) when the mean-field is

constructed consistently with the correlations present in the system. We show on Fig. (IV.6) the difference between Hartree-Fock SPE ε_{HF} and optimized SPE taken as eigenvalues ε_a of the mean-field,

$$h[\rho,\sigma]_{ab} = K_{ab} + \sum_{cd} \langle ac|\hat{V}[\rho]|\widetilde{bd}\rangle\, \rho_{dc} + \frac{1}{4}\sum_{cdc'd'} \langle cd|\frac{\partial \hat{V}[\rho]}{\partial \rho_{ba}}|\widetilde{c'd'}\rangle\, \langle\Psi|a_c^\dagger a_d^\dagger a_{d'} a_{c'}|\Psi\rangle \ ,$$

for the lightest and heaviest Neon isotopes.

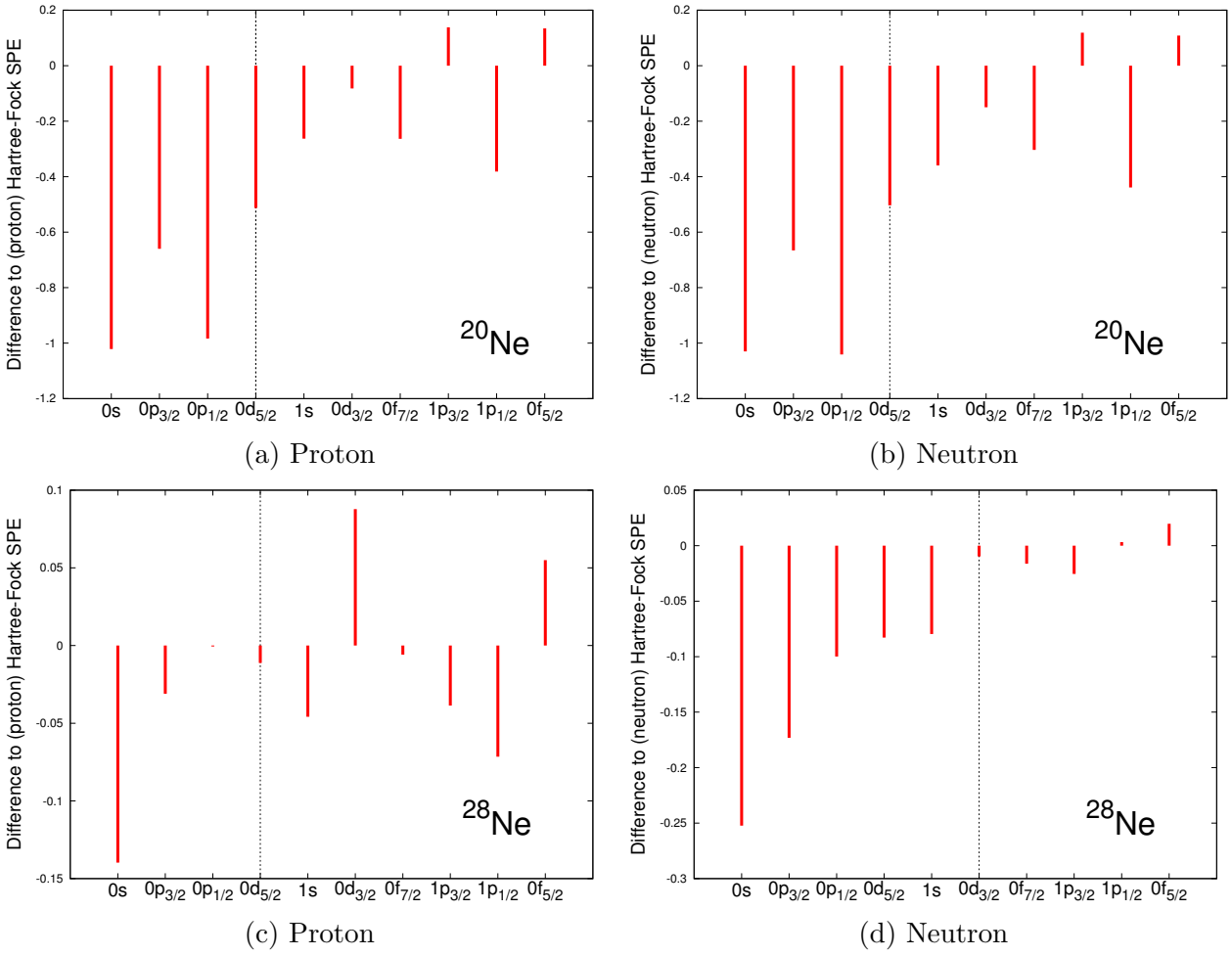

(a) Proton (b) Neutron

(c) Proton (d) Neutron

Figure IV.6: Differences $\Delta\varepsilon = \varepsilon_{HF} - \varepsilon$ between Hartree-Fock and self-consistent single-particle energies, expressed in MeV. The differences between proton SPEs are on the left and the neutron ones on the right. The Fermi level is marked by a dashed line.

The proton and neutron spectra appear very similar for the $N = Z$ nucleus ^{20}Ne. They are globally more compressed than the Hartree-Fock ones (by $\sim$ 1 MeV), and in particular the gaps under and above the Fermi level are decreased. The deepest shells $0s$ and $0p$ undergo the biggest modification and are shifted up by > 600 keV ($\sim$ 1 MeV for the $0s$ and the $0p_{1/2}$). The change is less important in ^{28}Ne where the biggest shifts are of order $\sim$ 250 keV. If a smooth compression of the neutron spectrum is observed, the behavior of the proton one

is a bit more chaotic and seems to indicate an important influence of the proton-neutron interaction. The gap at the Fermi level is actually slightly increased in this case (by $\sim$ 40 keV).

IV.1.2 Binding and separation energies

We plotted on Fig. (IV.7) the difference between experimental and theoretical binding energies $BE(N,Z) = \langle \Psi_0^{(N,Z)} | H[\rho] | \Psi_0^{(N,Z)} \rangle$ for the different isotopic chains.

	No self consistency	Eq. 1 with $R \neq 0$	Full self-consistency
$\langle \Delta BE \rangle$	8.342	8.914	9.837
$\sigma_{dev}(BE)$	0.821	0.793	0.789

Table IV.5: Average difference $\langle \Delta BE \rangle$ and standard deviation $\sigma_{dev}(BE)$ of binding energies compared to experiment (in MeV).

At the non-self consistent level, an average difference to experiment $\langle \Delta BE \rangle \sim 8.34$ MeV is found. This global shift is understood as due to the Gogny interaction that was fitted at the Hartree-Fock level, as already stated in [63]. This also explains the increase of $\langle \Delta BE \rangle$ from no to full self-consistency. On the contrary the standard deviation $\sigma_{dev}(BE)$ is slightly improved from 0.82 to 0.79 MeV.

Fig. (IV.8) now displays the difference between experimental and theoretical two-neutron and two-proton separation energies defined respectively as,

$$\begin{cases} S_{2n}(N,Z) = BE(N,Z) - BE(N-2,Z) \ , \\ S_{2p}(N,Z) = BE(N,Z) - BE(N,Z-2) \ . \end{cases} \tag{IV.2}$$

Little change is induced by self-consistency. The standard deviation is improved by $\sim$ 100 keV in both cases. The average difference in the proton case is also decreased by the same quantity, while it is increased by $\sim$ 80 keV in the neutron one. Globally these results are very satisfactory. Finally we obtain theoretical $S_{2p} < 0$ for ^{28}Ar, ^{30}Ar and ^{26}S. These nuclei are thus predicted unbound, which is in agreement with experiment.

IV.1.3 Charge radii and neutron skin-thickness

Charge radii

Charge radii are measurable quantities very sensitive to the correlation content of nuclei and related to nuclear deformation. The root mean-square charge radius r_c is expressed as,

$$r_c = \sqrt{r_p^2 + \frac{3}{2}(B^2 - b^2) - 0.1161\frac{N}{Z}} \ , \tag{IV.3}$$

where r_p denotes the proton root mean square radius,

$$r_p = \sqrt{\frac{\int d^3r \rho_\pi(r) r^2}{Z}} \,, \tag{IV.4}$$

with $\rho_\pi(r)$ the proton radial density. The charge radius r_c is corrected by $\frac{3}{2}(B^2 - b^2)$ where $B = 0.7144$ fm results from the proton form factor, and b is a center of mass correction. Finally $0.1161\frac{N}{Z}$ denotes a correction due to neutron electromagnetic properties.
We display on Fig. (IV.9) the charge radii calculated in the mp-mh approach at the three levels of the method. They are compared to experimental data taken from [3].

- At the non self-consistent stage, charge radii are either underestimated or lying in the experimental error bars, leaving room for unaccounted correlations. The worst discrepancy is encountered in the nuclei where collectivity is expected to be stronger. This behavior can be anticipated since the configuration mixing has been restricted to the *sd*-shell, and therefore "surface" orbitals with a larger spatial extension such as the $0f_{7/2}$ are not populated.

- The introduction of rearrangement terms slightly improves the theoretical values. Only ^{28}Si makes exception again.

- At the fully self-consistent level, when both coefficients and orbitals are optimized, the charge radii are (almost) systematically increased. The radii of the Argon isotopes, rather poorly correlated, are all improved. The radii of Sulfur nuclei are drastically augmented and in better accordance with experiment. Let us remind the important fragmentation introduced in the nucleus ^{32}S via the orbital renormalization. An important effect is also seen on the Silicon and Magnesium isotopes, although it appears too important in ^{26}Mg and ^{28}Si, leading to an overestimation of the radii and a wrong trend along the isotopic chains. Let us remind once again that the Gogny interaction used to perform the calculation is not *a priori* adapted to approaches such as the mp-mh configuration method which introduces all types of correlations. Moreover the use of the correlated density in the interaction may lead to uncontrolled over-counting effects. Concerning the Neon nuclei, the results without self-consistency already lied at the top of the error bars for $^{28-26-24}$Ne, and become now slightly overestimated. Very little effect is seen on the lighter and more correlated isotopes $^{20-22}$Ne, whose radii remain largely undervalued. Finally let us note that a good experimental trend is obtained from the Ne, S and Ar isotopes.

Neutron-skin thickness The neutron skin thickness $r_n - r_p$, difference between neutron and proton root mean square radius, can provide information on the relative distribution of

protons and neutrons in nuclei. We calculate this quantity for the Neon isotopes and show the results on Fig. (IV.10).
As expected, the neutron-skin thickness increases with the number of neutrons. No influence of the rearrangement terms is observed. However we note that the orbital renormalization has a tendency to slightly decrease the neutron thickness in neutron rich isotopes. Concerning the ^{24}Ne isotope this effect seems to be attributed to a slight increase of the proton radius. However, no clear attribution can be made in the case of $^{26-28}$Ne.

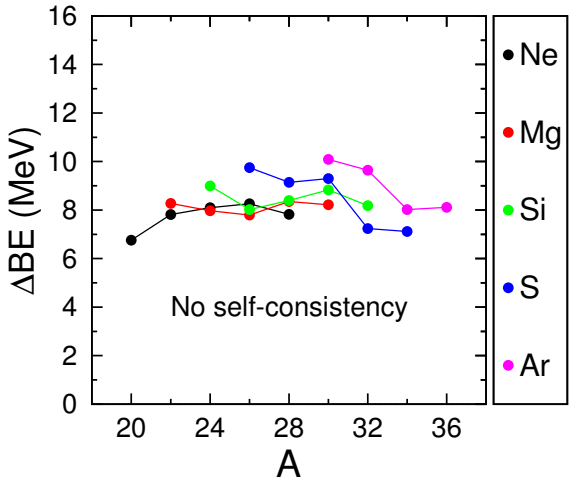

(a)

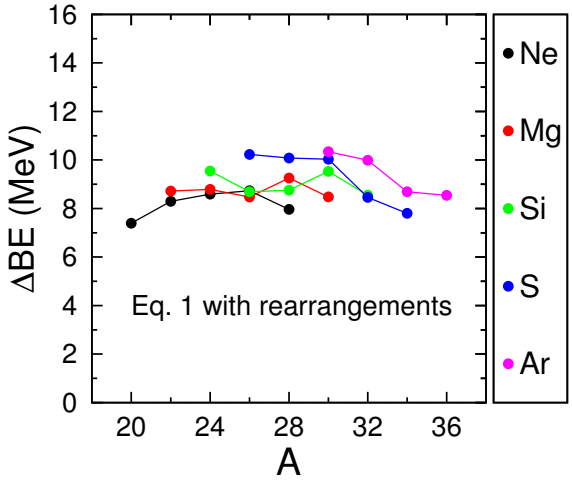

(b)

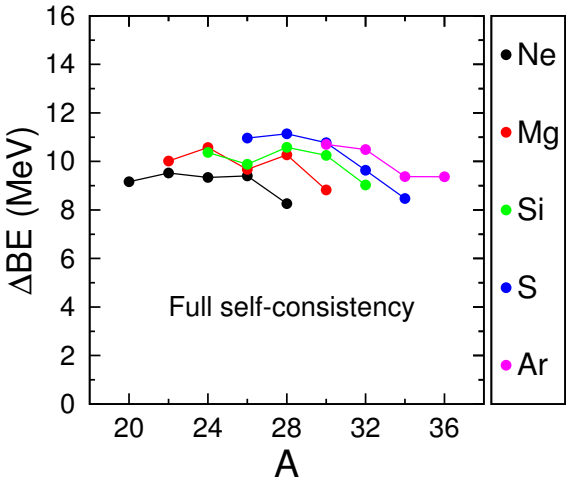

(c)

Figure IV.7: Difference between theoretical and experimental binding energies (in MeV) at the non-self consistent level (a), introducing rearrangement terms only (b), after full self-consistency is reached (c). Experimental data are taken from [104].

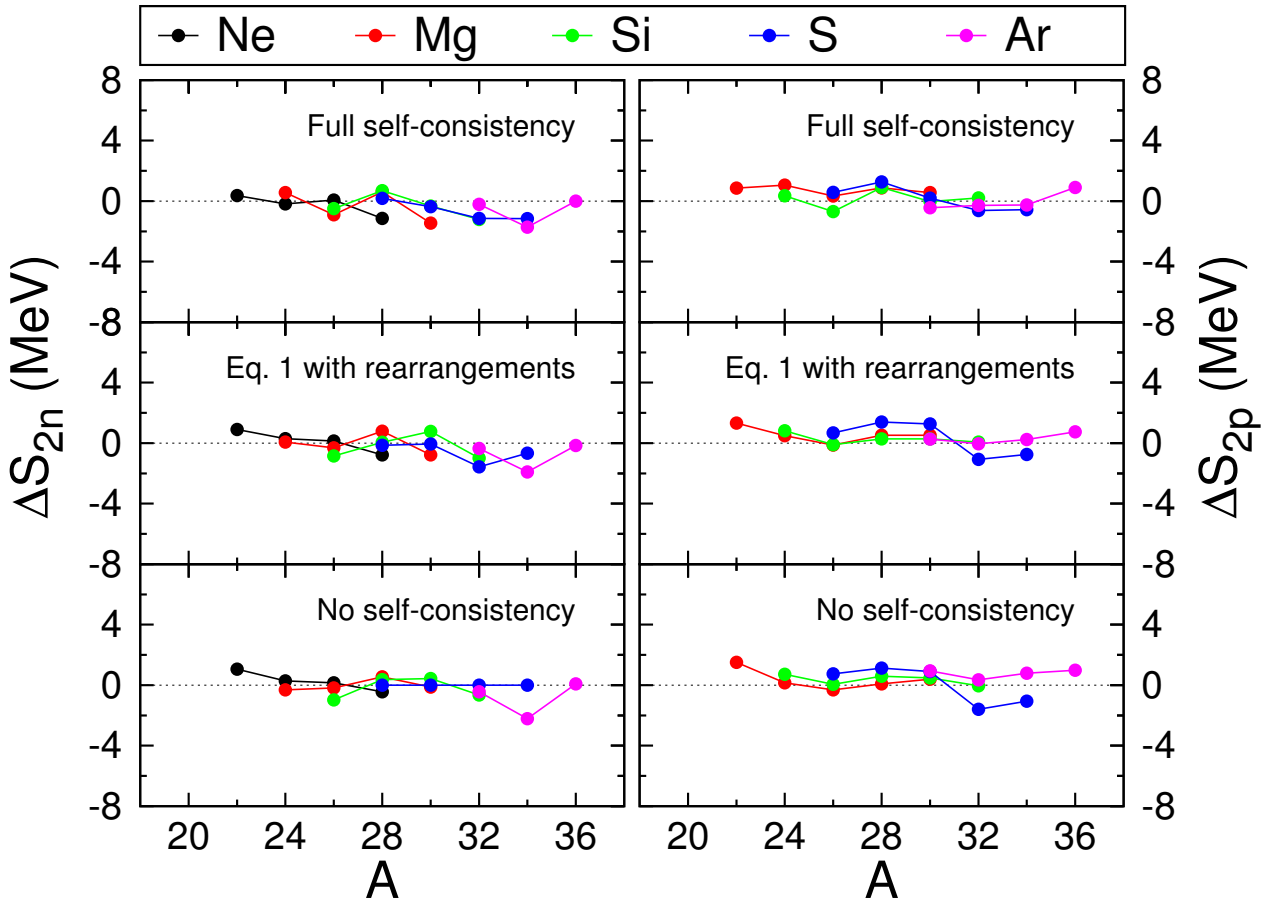

Figure IV.8: Difference between theoretical and experimental [104] two-neutron (left) and two-proton (right) separation energies (in MeV).

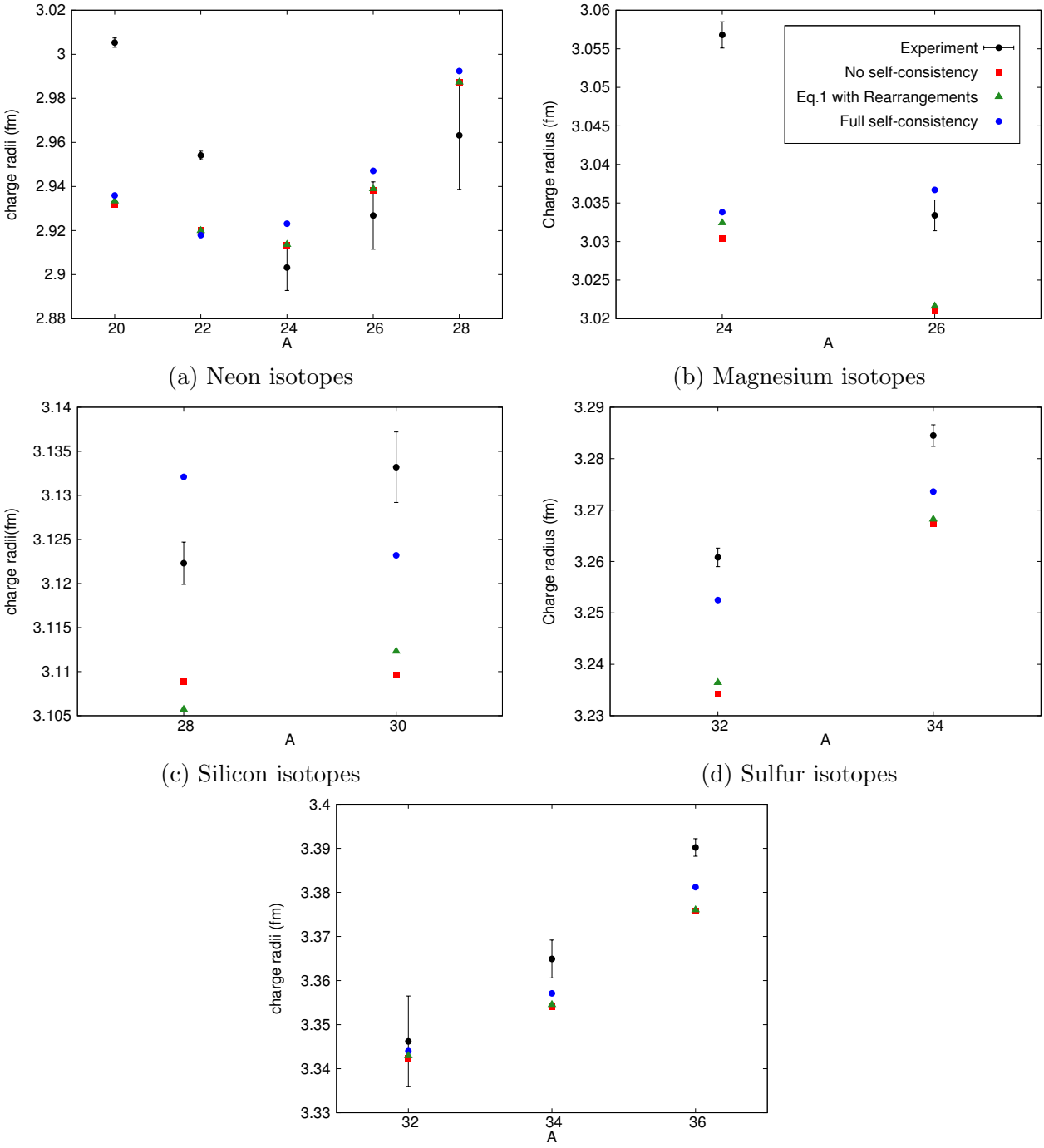

(a) Neon isotopes

(b) Magnesium isotopes

(c) Silicon isotopes

(d) Sulfur isotopes

(e) Argon isotopes

Figure IV.9: Comparison between experimental and mp-mh charge radii (in fm). Experimental values are taken from [3].

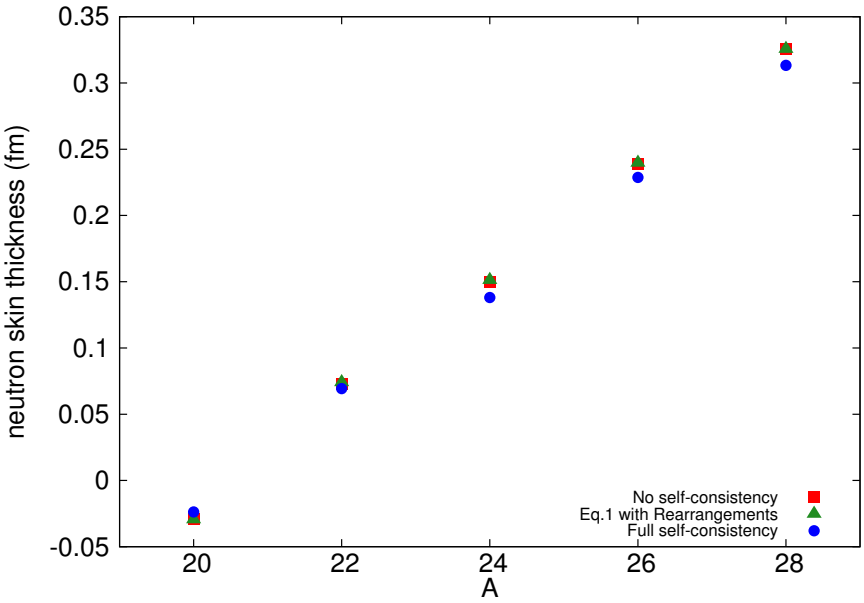

(a) Neon isotopes

Figure IV.10: Theoretical neutron skin thickness for Ne isotopes.

IV.2 Low-lying spectroscopy

In this section we study the properties of excited states in *sd*-shell nuclei. Observable quantities such as excitation energies and electromagnetic moments and transitions, are calculated and compared to experiment.

- At the non-self consistent stage, excited states are obtained by extracting several eigenstates of the Hamiltonian matrix $H[\rho_{HF}]$ with the Lanczos algorithm.
- When the first equation is solved iteratively with rearrangement terms, we iterate the diagonalization of $\mathcal{H}[\rho_{gs}, \sigma_{gs}] = H[\rho_{gs}]+R[\rho_{gs}, \sigma_{gs}]$, where ρ_{gs} and σ_{gs} denote the densities of the correlated ground-state. Once this procedure has converged, we extract several eigenvalues of $\mathcal{H}[\rho_{gs}, \sigma_{gs}]$ in order to obtain the excited states.
- Similarly, to achieve self-consistency, we perform the global iterative procedure described in section III.3 *at the ground state level*. In other words, the orbitals are optimized consistently with the mixing coefficients A^{gs}_{α} of the ground-state Ψ_0, by solving the second variational equation using the ground-state densities ρ_{gs} and σ_{gs}. Again, once this doubly-iterative procedure has converged, we extract several eigenvalues of $\mathcal{H}[\rho_{gs}, \sigma_{gs}]$ in order to obtain the excited states.

IV.2.1 Excitation energies

Excitation energies E^*_N are defined as the difference between the ground-state binding energy $E_0 = \langle\Psi_0|H[\rho_{gs}]|\Psi_0\rangle$ and the energy $E_N = \langle\Psi_N|H[\rho_{gs}]|\Psi_N\rangle$ of the excited state N,

$$E^*_N = E_N - E_0 \ . \tag{IV.5}$$

Since the configuration mixing is restricted to the *sd*-shell, the excited states are all characterized by a positive parity. We show in Table (IV.6) the theoretical excitation energy of the first three excited states in a few nuclei, and compare them to experiment.
Only little change is induced by the introduction of rearrangement terms (except in ^{28}Si). However the renormalization of orbitals clearly improves the predicted results in the majority of cases.
Looking in more detail, before modification of the single-particle states, one observes an overestimation of $\sim 1.5 - 2$ MeV of the energy spectra in ^{30}Si and ^{30}S, two mirror nuclei. This behaviour has already been identified and investigated in a previous study [86]. It has been found that this global shift is actually due to uncontrolled proton-neutron matrix elements of the Gogny interaction in the $T = 0$ channel. However, as illustrated in the previous section, the optimization of orbitals modifies the single-particle spectra and in particular the sizes of the gaps around the Fermi level. Solving the second variational equation is thus expected to

Nucleus	state J^π_n	isospin T	No self-consistency	Eq. 1 with rearrangements	Full self-consistency	Experiment
^{28}Ne	2^+_1	4.002	1.181	1.182	1.272	1.304 (3)
	4^+_1	4.002	2.392	2.392	2.658	(3.010 (6))
	2^+_2	4.002	3.149	3.149	3.401	?
^{24}Ne	2^+_1	2.003	1.769	1.848	1.925	1.9816 (4)
	4^+_1	2.003	3.515	3.503	3.867	3.972 (20)
	2^+_2	2.003	4.069	4.411	4.094	3.868 (4)
^{22}Ne	2^+_1	1.002	1.045	1.081	1.117	1.274577 (2)
	4^+_1	1.002	2.881	2.881	3.250	3.3577 (3)
	2^+_2	1.002	4.034	3.982	4.639	4.4558 (3)
^{20}Ne	2^+_1	0.002	1.630	1.694	1.880	1.633614 (15)
	4^+_1	0.002	3.360	3.312	4.441	4.2477 (11)
	2^+_2	0.002	5.543	5.410	7.507	7.4219 (12)
^{32}S	2^+_1	0.01	2.247	2.821	2.063	2.23057 (15)
	0^+_1	0.01	2.958	3.402	3.049	3.7784 (10)
	2^+_2	0.01	5.539	6.263	4.929	4.2818 (3)
^{30}S	2^+_1	1.004	3.894	3.935	3.294	2.2106 (5)
	2^+_1	1.004	4.902	4.915	4.344	3.4026 (10)
	0^+_2	1.004	6.566	6.407	5.793	5.2174 (7)
^{30}Si	2^+_1	1.003	4.145	4.184	3.478	2.235322 (18)
	2^+_1	1.003	5.219	5.218	4.673	3.49849 (3)
	0^+_2	1.003	7.073	6.977	6.167	3.78772 (4)
^{28}Si	2^+_1	0.006	1.771	2.536	1.963	1.779030 (11)
	0^+_2	0.006	4.460	4.891	5.284	4.97992 (8)
	4^+_1	0.006	5.060	6.033	5.420	4.61786 (4)
^{24}Mg	2^+_1	0.004	1.318	1.369	1.453	1.368672 (5)
	4^+_1	0.004	4.152	4.804	4.564	4.122889 (12)
	2^+_2	0.004	4.470	4.322	4.230	4.23824 (3)

Table IV.6: Energies of the three first excited states in a few nuclei (in MeV). Experimental data with error (*err*) are taken from [1].

modify the values of the matrix elements occurring in the Hamiltonian matrix to diagonalize, and hence to have an impact on the low-lying spectroscopy. Indeed we observe a downward shift of $\sim$ 600 keV in the spectra of ^{30}Si and ^{30}S. This effect is very encouraging but still insufficient to reach the experimental values. The rest of the discrepancy can now be more surely attributed to the D1S Gogny interaction that is used in the calculations.

Fig. (IV.11) now displays the theoretical excitation energies of the first excited $J^\pi = 2^+$ state as a function of experimental ones, for all *sd*-shell nuclei. Results are shown without and with full self-consistency.

Excluding the peculiar cases ^{30}S and ^{30}Si, a good agreement with experiment is found at the non self-consistent level for most nuclei. However we note a slight systematic underestimate

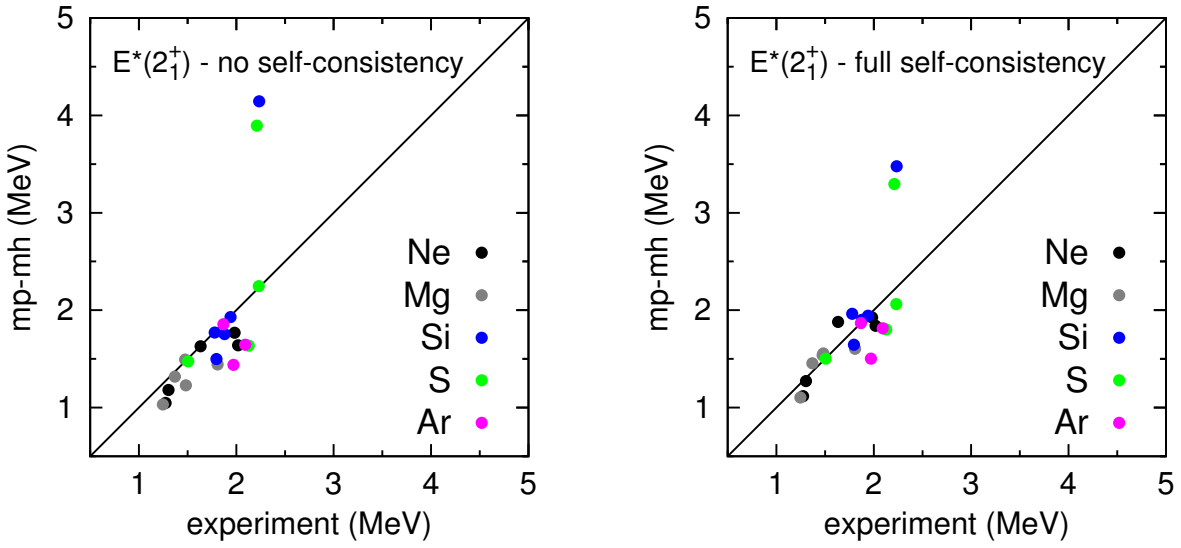

(a) (b)

Figure IV.11: Theoretical excitation energies of the 2_1^+ states compared to experiment. Experimental data are taken from [1]. Results are expressed in MeV.

of the experimental values, as the points always lie under the $y = x$ line. This discrepancy disappears after self-consistency is reached. Statistically, the average difference to experimental results is decreased from 191 to 142 keV and the standard deviation is lowered from 178 to 122 keV. Including now also 2_1^+ states of ^{30}S and ^{30}Si, the average difference to experiment of 383 keV obtained when no self-consistency is applied, is lowered to 281 keV when the full iterative procedure is performed. Similarly the standard deviation is modified from 670 to 496 keV. Overall results for excitations energies are in very good agreement with experiment.

IV.2.2 Electromagnetic properties of nuclei - reminder

◦ Transition probabilities

Electromagnetic transitions in nuclei result from the interaction of the nucleus with an external electromagnetic field. Interaction of radiation with matter is well known theoretically. We first remind a few aspects of the formalism and refer to e.g. [92] or [74] for more details. The total system nucleus+radiation is governed by $H = H_{nucl} + H_{field} + H_{int}$, sum of the nuclear Hamiltonian, the Hamiltonian of the free radiation field and the interaction between the nucleus and the field. Compared to the strong nuclear force, the electromagnetic interaction H_{int} can be regarded as a perturbation. The transition probability for the nucleus to decay by photon emission is thus given by the "Fermi Golden rule",

$$T_{fi} = \frac{2\pi}{\hbar} \left| \langle \Psi_i | \hat{H}_{int} | \Psi_f \rangle \right|^2 \rho(E_f) \ , \tag{IV.6}$$

where $\rho(E_f)$ denotes the density of available final states.
The interaction Hamiltonian is given by,

$$H_{int} = -\frac{1}{c}\int j_\mu A^\mu d^3r = \int \left(\rho(\vec{r},t)\Phi(\vec{r},t) - \frac{1}{c}\vec{j}(\vec{r},t).\vec{A}(\vec{r},t)\right) d^3r \ , \tag{IV.7}$$

where $\rho(\vec{r},t)$ and $\vec{j}(\vec{r},t)$ denote the charge and current density of the nucleus respectively. The scalar potential Φ couples the field to the nuclear density while the vector potential $\vec{A}$ couples to the current. In a general way, one can write the potential $(\Phi, \vec{A})$ as a multipole expansion $(\sigma, \lambda\mu)$ of two types of radiations (electric $\sigma = E$ and magnetic $\sigma = M$) expressed in terms of spherical harmonics. λ and μ denote the total angular momentum of the emitted photon and its projection respectively. After calculus (see e.g. [92]) one finally gets the following probability for emission of a photon with quantum numbers (σ, λ, μ) and energy E_γ,

$$T_{fi}(\sigma,\lambda\mu) = \frac{8\pi}{\hbar}\frac{\lambda+1}{\lambda[(2\lambda+1)!!]^2}\left(\frac{E_\gamma}{\hbar c}\right)^{2\lambda+1}\left|\langle\Psi_i|\hat{\mathcal{M}}(\sigma,\lambda\mu)|\Psi_f\rangle\right|^2 \ , \tag{IV.8}$$

where $\hat{\mathcal{M}}(\sigma,\lambda\mu)$ is the operator associated with the multipole radiation field $(\sigma,\lambda\mu)$.
Experimentally one usually does not differentiate different orientations of the angular momenta and measures quantities where all projections have been resumed. The total probability for a multipole transition is then given by,

$$T_{fi}(\sigma,\lambda) = \frac{1}{2J_i+1}\sum_{\mu,M_i,M_f} T_{fi}(\sigma,\lambda\mu) \ , \tag{IV.9}$$

where (J_i, M_i) and (J_f, M_f) characterize the angular momentum and projection of the initial and final nuclear state respectively. Since the multipole operators are spherical tensor operators one can make use of the Wigner-Eckart theorem [74] and write,

$$\langle J_i M_i|\hat{\mathcal{M}}(\sigma,\lambda\mu)|J_f M_f\rangle = (-)^{J_f-M-f}\begin{pmatrix} J_f & \lambda & J_i \\ -M_f & \mu & M_i\end{pmatrix}\langle J_i||\hat{\mathcal{M}}(\sigma,\lambda)||J_f\rangle \ , \tag{IV.10}$$

where the second term on the r.h.s of Eq. (IV.10) denotes the 3j-symbol and $\langle J_i||\hat{\mathcal{M}}(\sigma,\lambda)||J_f\rangle$ has lost any dependency on magnetic numbers. Inserting this into Eq. (IV.9) one finally gets,

$$T_{fi}(\sigma,\lambda) = \frac{8\pi}{\hbar}\frac{\lambda+1}{\lambda[(2\lambda+1)!!]^2}\left(\frac{E_\gamma}{\hbar c}\right)^{2\lambda+1} B(\sigma\lambda \ ; \ J_i \to J_f) \ , \tag{IV.11}$$

where $B(\sigma\lambda \ ; \ J_i \to J_f)$ are called *reduced transition probabilities* and are given by,

$$B(\sigma\lambda \ ; \ J_i \to J_f) = \frac{1}{2J_i+1}\langle J_i||\hat{\mathcal{M}}(\sigma,\lambda)||J_f\rangle \ . \tag{IV.12}$$

In order to practically calculate the reduced transition probabilities $B(\sigma\lambda\ ;\ J_i \to J_f)$, one usually performs the explicit calculation of one element $\langle J_i M_i|\hat{\mathcal{M}}(\sigma,\lambda\mu)|J_f M_f\rangle$ (the simplest one) and uses the Wigner-Eckart theorem (IV.10) to deduce the value of the reduced element $\langle J_i||\hat{\mathcal{M}}(\sigma,\lambda)||J_f\rangle$.

→ **Electric and magnetic operators:** As mentioned previously, two types of radiation appear in the multipole expansion of the field: electric (denoted $\sigma = E$) and magnetic (denoted $\sigma = M$) radiations. The electric and magnetic transition operators $\hat{\mathcal{M}}(E,\lambda\mu)$ and $\hat{\mathcal{M}}(M,\lambda\mu)$ can be generally derived in terms of spherical harmonics $Y_{\lambda,\mu}(\theta,\phi)$ and Bessel spherical functions j_λ. In the context of nuclear physics, the "long-wavelength limit" is generally assumed (i.e. the wavelength of the photon is considered large compared to the size of the nucleus), and one can expand the Bessel functions in term of the small kr parameter (k being the momentum of the photon).

- At first order, one obtains for the electric operator,

$$\hat{\mathcal{M}}(E,\lambda\mu) = \int \rho(\vec{r}) r^\lambda Y_{\lambda\mu}(\theta,\phi) d^3r + \frac{ik}{\lambda+1}\int (\vec{r}\times\vec{\mu}(\vec{r}))\vec{\nabla} r^\lambda Y_{\lambda\mu}(\theta,\phi) d^3r\ , \tag{IV.13}$$

  where $\rho(\vec{r}) = \sum_{j=1}^{A} e(j)\delta(\vec{r}-\vec{r}_j)$ is the charge density of the nucleus ($e(j) = e(\frac{1}{2} - t_z(j))$) and $\vec{\mu}(\vec{r})$ the density of magnetic moment. The second term in Eq. (IV.13) is usually neglected and one gets the following electric multipole operator,

$$\hat{Q}(\lambda\mu) \equiv \hat{\mathcal{M}}(E,\lambda\mu) = \sum_{j=1}^{A} e(j) r_j^\lambda Y_{\lambda\mu}(\theta_j,\phi_j)\ . \tag{IV.14}$$

- At first order in the long-wavelength limit, the multipole magnetic operator reads,

$$\hat{M}(\lambda\mu) \equiv \hat{\mathcal{M}}(M,\lambda\mu) = \mu_N \sum_{j=1}^{A}\left[\frac{2}{\lambda+1} g_l^{(j)}\vec{l}^{(j)} + g_s^{(j)}\vec{s}^{(j)}\right].\vec{\nabla}\left[r_j^\lambda Y_{\lambda\mu}(\theta_i,\phi_i)\right]\ . \tag{IV.15}$$

  In Eq. (IV.15), $\mu_N = \frac{e\hbar}{2m_p} = 0.10515\, c\, e$ fm is the nuclear magneton. g_l and g_s are the orbital and gyromagnetic factors respectively. They are equal to,

$$g_l = \left(\frac{1}{2} - t_z\right) = \begin{cases} 1 & \text{for protons}\,, \\ 0 & \text{for neutrons}\,, \end{cases} \tag{IV.16}$$

  and,

$$g_s = \begin{cases} g_p = 5.586 & \text{for protons}\,, \\ g_n = -3.826 & \text{for neutrons}\,. \end{cases} \tag{IV.17}$$

→ **Selection rules:**

- The transition probability $T_{fi}(\sigma\lambda) \sim \int_{-\infty}^{\infty} \Psi_i^* \mathcal{M}(\sigma,\lambda)\Psi_f$ is non-vanishing if the product of the parities $\pi(\Psi_i)\,\pi\left(\hat{\mathcal{M}}(\sigma,\lambda)\right)\,\pi(\psi_f) = +$. The multipole operators $\hat{Q}(\lambda\mu)$ and $\hat{M}(\lambda\mu)$ have parity $(-)^\lambda$ and $(-)^{\lambda+1}$ respectively[2]. Therefore the parity selection rule reads,

$$\pi(\Psi_i)\pi(\Psi_f) = \begin{cases} (-)^\lambda & \text{for an electric transition } E_\lambda \ , \\ (-)^{\lambda-1} & \text{for a magnetic transition } M_\lambda \ . \end{cases} \tag{IV.18}$$

- Moreover, the conservation of angular momentum leads to,

$$\begin{cases} |J_i - J_f| \leqslant \lambda \leqslant J_i + J_f \ , \\ \mu = M_f - M_i \ . \end{cases} \tag{IV.19}$$

○ Static multipole moments

Diagonal expectation values of the multipole operators in a nuclear state can provide information on the structure of nuclear wave function. In particular,

- the magnetic dipole moment defined as,

$$\mu \equiv \sqrt{\frac{4\pi}{3}}\,\langle J, J|\hat{M}(1,0)|J, J\rangle \ , \tag{IV.20}$$

  informs on the current densities in the nucleus, while

- the quadrupole electric moment (also called quadrupole spectroscopic moment),

$$Q_s \equiv \sqrt{\frac{16\pi}{5}}\,\langle J, J|\hat{Q}(2,0)|J, J\rangle \ , \tag{IV.21}$$

  provides insight into the charge repartition and this the shape associated to the nuclear state.

We refer to [62] for details about the practical calculation of electromagnetic transition probabilities and moments within the multiparticle-multihole configuration mixing method.

IV.2.3 Magnetic dipole properties

Magnetic dipole moments

We first investigate the magnetic dipole properties of the nuclei of interest. In Fig. (IV.12), we compare the theoretical magnetic dipole moments μ of the 2_1^+ states to available experimental data.

[2] $(-)^\lambda$ from the spherical harmonics and $(-)$ from $\vec{\nabla}$ in $M(\lambda,\mu)$

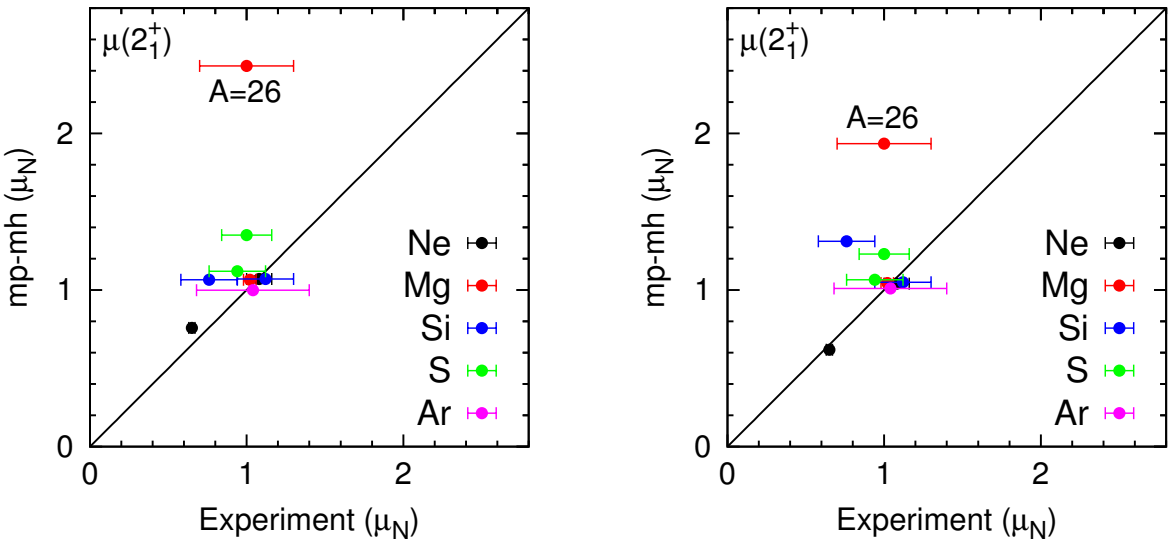

(a) No self-consistency

(b) Full self-consistency

Figure IV.12: Comparison of theoretical magnetic dipole moments $\mu(2_1^+)$ to experiment. Experimental data are taken from [1]. Results are expressed in units of the nuclear magneton μ_S.

Before self-consistency, a general good agreement is found for the majority of nuclei. Four nuclei lie outside the experimental error bars, including the peculiar ^{30}Si case. Regarding ^{26}Mg, as already stated in [63], the experimental value originally at 2.6 μ_N has been re-evaluated to 1.0 μ_N. We obtain at this stage an average difference to experiment of $\langle\Delta\mu\rangle = 0.31$ μ_N, and a standard deviation $\sigma_{dev}(\mu) = 0.47$ μ_N.
With self-consistency, the statistics is improved to $\langle\Delta\mu\rangle = 0.25$ μ_N and $\sigma_{dev}(\mu) = 0.33$ μ_N, as the results for ^{22}Ne, ^{34}S and ^{26}Mg get closer to experiment. However the magnetic moment of ^{30}Si worsens.

Magnetic dipole transitions

We present in Table (IV.7) magnetic transition probabilities $B(M1)$. The conclusion already drawn for the static magnetic moments roughly apply here.
Results at the first stage agree rather nicely with experiment and are slightly globally improved by self-consistency: $\langle\Delta B(M1)\rangle$ goes from 1.9×10^{-2} to 1.5×10^{-2} W.u. and $\sigma_{dev}(B(M1))$ from 2.9×10^{-2} to 1.7×10^{-2} W.u.. This behavior can be understood from the following arguments. Selection rules for a $B(M1)$ transition enforce the parities of the initial and final states to be identical: $\pi_i\pi_f = +$. Moreover transition characterized by angular momentum transfer $\lambda = 1$ can allow excitations between shells with $\Delta N_{shell} = 0, 1$, where N_{shell} denotes the major quantum number $N = 2(n-1)+l$ of the oscillator shell. $\Delta N_{shell} = 0, 1$ correspond to transition characterized by $\Delta E = 0, 1\hbar\omega$. $0\hbar\omega$ excitations are restricted within the *sd*-shell and hence, are already explicitly accounted for in the configuration mixing. $1\hbar\omega$ configurations would

Nucleus	Transition	Experiment	No self-consistency	Full self-consistency
^{24}Mg	$2_2^+ \to 2_1^+$	9×10^{-6} (8)	9.582×10^{-6}	5.043×10^{-6}
	$3_1^+ \to 2_1^+$	2.1×10^{-5} (1.1)	5.150×10^{-5}	2.363×10^{-7}
	$3_1^+ \to 2_2^+$	3.5×10^{-4} (1.7)	2.231×10^{-4}	5.371×10^{-5}
^{26}Mg	$2_2^+ \to 2_1^+$	9.7×10^{-2} (12)	6.698×10^{-2}	6.846×10^{-2}
	$3_1^+ \to 2_1^+$	1.02×10^{-3} (15)	5.003×10^{-3}	5.601×10^{-4}
	$3_1^+ \to 2_2^+$	1.59×10^{-2} (23)	2.125×10^{-2}	2.976×10^{-2}
	$3_2^+ \to 2_1^+$	6.7×10^{-3} (14)	4.596×10^{-3}	2.011×10^{-3}
	$3_2^+ \to 2_2^+$	3.2×10^{-2} (7)	5.509×10^{-2}	5.270×10^{-2}
^{26}Si	$2_2^+ \to 2_1^+$	1.0×10^{-1} (3)	6.367×10^{-2}	6.668×10^{-2}
^{30}Si	$2_2^+ \to 2_1^+$	9×10^{-2} (3)	1.905×10^{-1}	4.056×10^{-2}
^{34}S	$2_2^+ \to 2_1^+$	5.2×10^{-2} (3)	6.057×10^{-2}	4.811×10^{-2}
^{34}Ar	$2_2^+ \to 2_1^+$	5.8×10^{-2} (12)	3.175×10^{-2}	2.990×10^{-2}

Table IV.7: Transition probabilities $B(M1)$ in Weisskopf units (W.u.). Experimental data are extracted from [1].

correspond to 1p-1h excitations from *sd* to the *fp* shell or from the 0*p* to *sd* shell. However these would lead to a change of parity and are therefore forbidden. This would explain why the results at the non-self consistent level are already roughly in accordance with experimental values. This result also demonstrates that the D1S Gogny interaction exhibits good dipole magnetic properties.

IV.2.4 Electric quadrupole properties

We now investigate quadrupole electric features of *sd*-shell nuclei.

Quadrupole spectroscopic moments

Fig. (IV.13) shows the quadrupole static moment for the first excited state 2_1^+.
At the non self-consistent stage, clearly theoretical values badly agree with experiment. When the predicted sign is in agreement with the experimental one, the mp-mh approach always underestimates spectroscopic quadrupole moments (in absolute value). Self-consistency, and in particular orbital optimization, does not seem to induce a significant change on the results.

Electric quadrupole transitions

We now display in Fig. (IV.14) the reduced probabilities $B(E2)$ for the transition $2_1^+ \to 0_1^+$ in different isotopic chains.

- Without self-consistency (red squares), the behavior is similar to what we obtained for the static moments. That is, the probability calculated within the multiparticle-multihole approach largely underestimates the experimental values. This being said,

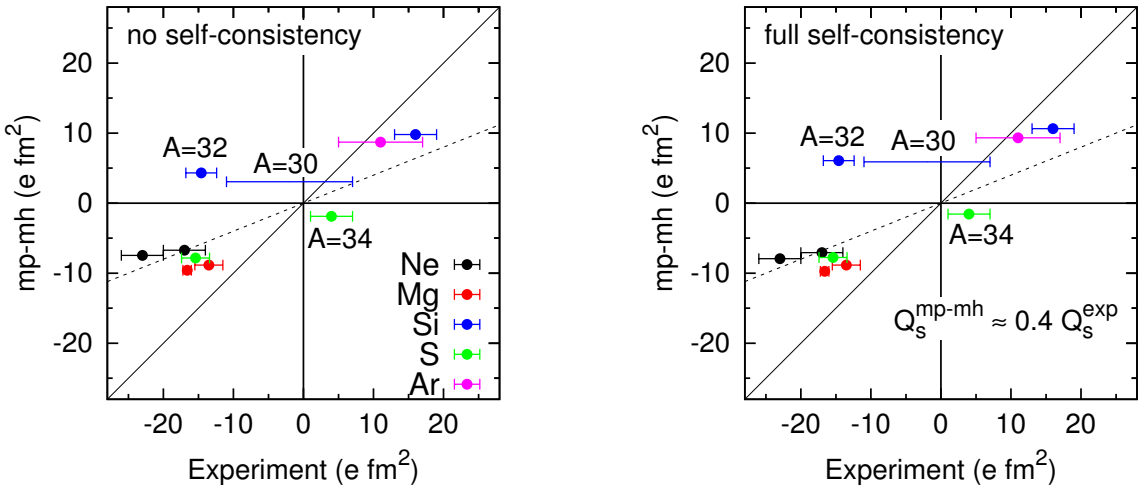

(a) (b)

Figure IV.13: Comparison of theoretical spectroscopic quadrupole moments $Q_s(2_1^+)$ with experiment. Experimental values are taken from [1]. Results are expressed in e.fm^2

one notes however that the experimental trends along isotopic chains are generally well reproduced (apart from a few cases). The multiplication of the theoretical $B(E2)$ by a global factor would lead to a nice agreement with experiment in most isotopic chains. At a closer look, a wrong behavior is seen in the light Silicon isotopes $A = 24, 26$. A discrepancy is also found in the Neon chain: the slope is predicted too small for $^{20-22}$Ne. Concerning the Sulfur isotopes, the small predicted value for $^{30-32}$S compared to $^{28-34}$S has been investigated in [63]. The main component in the 0_1^+ ground state ($\sim 60\%$ of 0p-0h as shown in Table IV.3) is found much higher than the weight of the most important configuration in the 2_1^+ state ($\sim 22\%$ of $(1\text{p-}1\text{h})_\nu + \sim 25\%$ of $(1\text{p-}1\text{h})_\pi$), leading to a small matrix element $\langle 0_1^+|\hat{Q}(2,0)|2_1^+\rangle$.

- With rearrangement terms in the first variational equation and Hartree-Fock orbitals kept frozen (forest green circles), the transition probabilities are essentially modified for the Silicon and Sulfur isotopes where $B(E2)$ are increased in most nuclei. Only ^{28}Si and ^{30}Si make exception and suffer a reduction of their electric quadrupole probability. This is in accordance with the increase of the Hartree-Fock 0p-0h component noted in the wave function of the 0_1^+ state in ^{28}Si (see previous section). Overall, all predicted $B(E2)$ stay largely lower than the experimental ones.

This systematic underestimate of the electric quadrupole properties is a well-known behavior which is due to the restriction of the configuration mixing to the *sd*-shell, unable to fully account for quadrupole collectivity. In shell-model studies, this issue is overcome by the introduction of effective charges e_p^{eff} and e_n^{eff} instead of $e_p = 1$ and $e_n = 0$ in the definition (IV.14) of the electric quadrupole operator $\hat{Q}(2,0)$. If effective charges arise naturally from the theory

of effective operators [77] used to compensate for Hilbert space truncation, the values of e_p^{eff} and e_n^{eff} utilized in shell-model calculations are usually fitted so to reproduce experimental data. Ref. [21] discusses this in detail and compares $E2$ matrix elements calculated with and without effective charges. Without effective charges, transition probabilities are found systematically smaller than the experimental data (factor ~ 0.6). The same behavior is observed for spectroscopic quadrupole moments.

In this work we aim to quantify the effect of the optimization of orbitals on transition probabilities, with no use of effective charges. As previously mentioned, solving the second variational equation introduces coupling between the valence space and the fully occupied core of ^{16}O as well as the empty states. The latter therefore do not remain frozen. In fact, as discussed in chapter II, this procedure allows to generate mp-mh excitations spanning on the entire starting single-particle basis, on top of the Slater determinants of the *sd*-shell. Part of the neglected Hilbert space is thus implicitly accounted for.
Let us examine in more detail what types of configurations are missing to improve the transitions $B(E2)$. The action of the electric quadrupole $E2$ operator on a state J^π is able to generate excitations characterized by $\Delta N_{shell} = 0, 1, 2$. Again, $0\hbar\omega$ ones are already accounted for in the *sd*-shell, and excitations $1\hbar\omega$ (1p-1h $sd \to fp$ or $p \to sd$) would involve a parity change which is forbidden in $E2$ transitions. Excitations $2\hbar\omega$ are however clearly missing when restricting the many-body mixing to the *sd*-shell. Such configurations can be generated by,

- 1p-1h excitations between shells differing by $\Delta N_{shell} = 2$.

  - The most important are expected to be excitations from the *sd* to the *sdg* shell or from the $0s$ to the *sd* shell. As seen from the previous section the $0s$ and *sdg* shells are largely influenced by the source term $G[\sigma]$. In particular, the coupling $sd - 0s$ is always very strong. Moreover, 1p-1h excitations are of one-body type and therefore can be generated through the optimization of orbitals (acting at the mean-field, thus one-body level). For these two reasons, the effect of the second variational equation should be maximal in this case, and should allow to partly account for this type of excitations.

  - At a weaker level, 1p-1h excitations from the p to the fp shells can also come into play in a $B(E2)$ transition. The source term does not couple to such negative parity states. The orbital equation will however allow to mix the single-particle orbitals from p sub-shells with same angular momentum j through $[h(\rho, \sigma), \rho] = 0$. A configuration
  $$|\phi_\alpha\rangle = ...a^\dagger_{k\in 0p_j}... |0\rangle$$

will transform as

$$|\phi_\alpha\rangle \rightarrow |\phi'_\alpha\rangle = ... \left(C_1 a^\dagger_{k\in 0p_j} + C_2 a^\dagger_{k\in 1p_j} + ... \right) ... |0\rangle \ .$$

The $1p_j$ ($j = 1/2$ or $3/2$) sub-shell from the fp shell thus become slightly occupied in Ψ, and some core-polarization effect is produced. It is important to remind that we are reasoning here in terms of the starting non-optimized orbitals. In practice these are taken as spherical Hartree-Fock states. Since the Hartree-Fock field already incorporates much physical information (compared to e.g. pure harmonic oscillator potential), the mixing between orbitals is usually weak.

- 2p-2h excitations between shells with $\Delta N_{shell} = 1$. The most important ones being excitations from sd to fp and p to sd. Because symmetries are explicitly conserved here, single-particle states from sd will never mix with orbitals from fp. More precisely, writing schematically the explicitly introduced many-body configurations as,

$$|\phi_\alpha\rangle = \prod a^\dagger_{k\in s} \prod a^\dagger_{l\in p} \prod a^\dagger_{m\in sd} |0\rangle \ ,$$

they transform as,

$$|\phi_\alpha\rangle \rightarrow |\phi_\alpha\rangle = \prod (C^1_k a^\dagger_{k\in s} + C^2_k a^\dagger_{k\in sd}) \prod (C^1_l a^\dagger_{l\in p} + C^2_l a^\dagger_{l\in fp}) \prod (C^m_l a^\dagger_{m\in sd} + C^2_l a^\dagger_{m\in s}) |0\rangle \ ,$$

where for the sake of simplicity, we only considered shells up to fp. Hence, we see that 2p-2h excitations $sd \rightarrow fp$ or $p \rightarrow sd$ can never be generated by the transformation of orbitals.

Let us now look at the transition probabilities from Fig. (IV.14) obtained when full self-consistency is applied. Although small, the effect induced by the orbital renormalization allows to systematically improve the $B(E2)$. The Silicon and Sulfur isotopes seem again to be the most sensitive to the transformation of single-particle states. In particular, a factor ~ 1.7 is gained in ^{30}Si, and ~ 1.3 in ^{28}Si and ^{32}S. In the Neon chain however, the difference with the non self-consistent case is hardly visible. According to our previous analysis, this would suggest that the $E2$ transition is mainly generated by 2p-2h excitations $sd \rightarrow fp$ or $p \rightarrow sd$. In order to verify this, we take ^{20}Ne as a test nucleus, and apply the mp-mh configuration mixing introducing the fp-shell in the valence space, creating thus explicit 2p-2h excitations $sd \rightarrow fp$. The effect on $B(E2)$ transition is shown on Fig. (IV.15). We already note an increase of the $B(E2)$ at the non-self consistent level reflecting the inclusion of additional explicit configurations. We also note that the self-consistency effects have increased in accordance.

In summary, this first systematic study of *sd*-shell nuclei within the fully self-consistent mp-mh approach was very satisfying. Most observables quantities that have been calculated are generally found in good agreement with experiment. This study also allowed to quantify the effect of the renormalization of single-particle states, which almost systematically improved the theoretical results. Although weak, the effect induced on transition probability $B(E2)$ was positive. However, it appeared that a truncation of the wave function in terms of valence space might not be the optimal selection criterion to exploit the maximum effect of the orbital optimization. This was confirmed by the modification of $B(E2)$ when adding the fp shell to the valence space in the case of ^{20}Ne.

Accounting for the missing quadrupole collectivity could in principle by achieved either by increasing the size of the model space, or, when such calculations are not tractable by current computational resources, by the construction of effective operators. In the former case, an analysis of the composition of deformed Hartree-Fock or HFB states, projected on a spherical basis, could be very useful. As deformed HF(B) often give an accurate quadrupole moment, such a study could provide an estimate of how large the model space needs to be in order to describe the quadrupole collectivity of the system. Enlarging the size of the space will however inevitably lead to an increase of the correlation energy which may become pathologically high, such as found in the study of ^{12}C in the previous chapter. This behaviour might however be corrected by the use of a fully finite range interaction. When such model spaces are too large to deal with, the construction of effective operators may be a good alternative. Such operators act within a restricted space $\mathcal{P}$ while accounting implicitly for the missing space $\mathcal{Q}$. Resulting consistent effective charges would also lead to an increase of the radii.

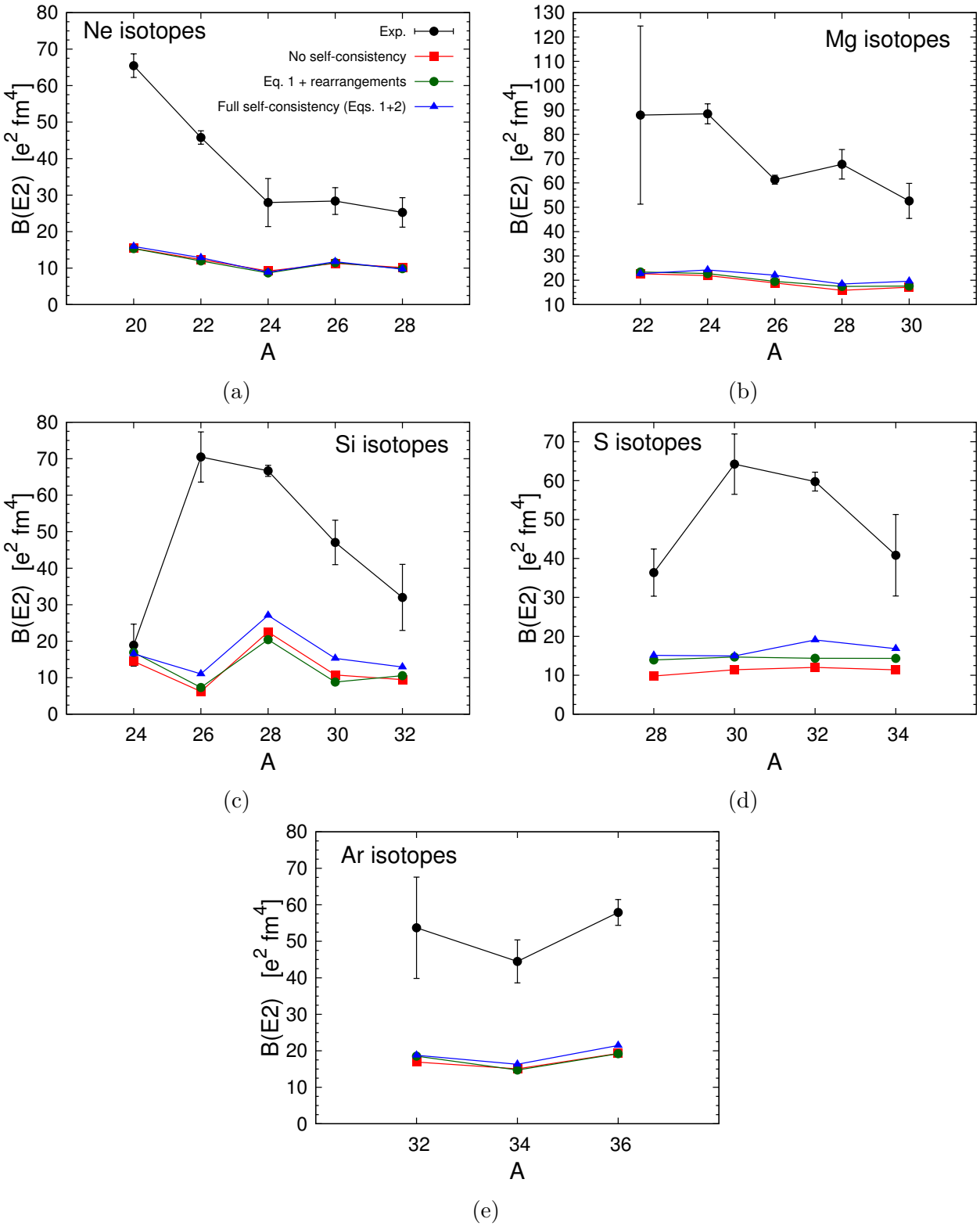

Figure IV.14: Comparison of quadrupole transition probabilities $B(E2; 2_1^+ \rightarrow 0_1^+)$ expressed in $e^2.fm^4$. The experimental data (in black) are taken from [1]. Results without and with full self-consistency are shown in red and blue respectively. We also display $B(E2)$ obtained with introducing rearrangement terms in the first variational equation (in green).

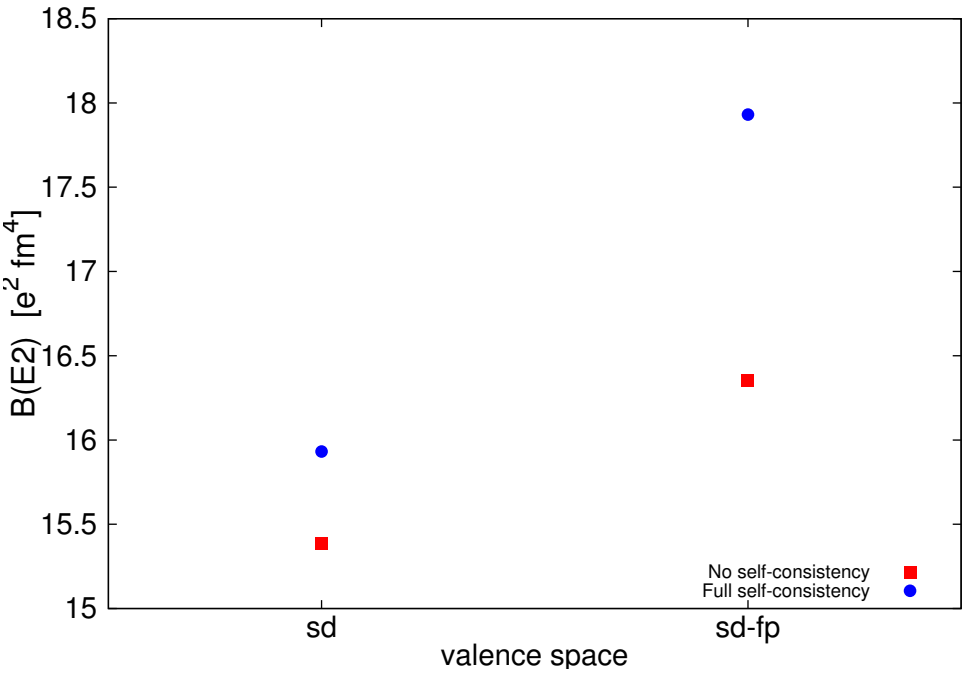

Figure IV.15: Modification of the transition probability $B(E2)$ when adding the fp-shell to the valence space. Results are shown for the ^{20}Ne nucleus.

Chapter V

First applications to reactions

In this last chapter, we use the structure description provided by the mp-mh approach for the study of reaction mechanisms on target nuclei. The field of nuclear reactions is very wide. Depending on the nature of the probe, many mechanisms can occur when a projectile strikes a nucleus. They spread from the long-time compound nucleus reactions involving the capture of the projectile by the target, to short time direct reactions involving nucleon exchange (transfer, pick-up...) or not (elastic or inelastic scattering).
In the following we are interested in inelastic scattering of protons and electrons from *sd*-shell nuclei, when the target nucleus is excited from its ground to a low-lying excited state.

V.1 Inelastic electron scattering on discrete states

Electrons are point-like particles which only interact electromagnetically with the target. Experimentally, the study of electron scattering can thus provide direct and clear information about the charge distribution of nuclei.

V.1.1 Formal aspects

The theoretical study of electron scattering is widely discussed in the literature. Hence, we only remind here of a few important results and refer to e.g. [28, 54, 32] for more detail.
Since the electromagnetic interaction is weak in comparison to the nuclear force, electron scattering can usually be treated in the context of the Plane Wave Born Approximation, as an exchange of a single virtual photon between the target and the electron described as a plane wave. In this approximation, the cross section for electron scattering from the target nucleus reads,

$$\frac{d\sigma}{d\Omega} = \left(\frac{d\sigma}{d\Omega}\right)_{\text{Mott}} R\left[|F_L(q)|^2 + \left(1 + \tan^2\frac{\theta}{2}\right)|F_T(q)|^2\right] , \tag{V.1}$$

where,

$$\left(\frac{d\sigma}{d\Omega}\right)_{\text{Mott}} = \frac{Z^2 e^4 \cos^2(\theta/2)}{4E_i^2 \sin^4(\theta/2)} \ , \tag{V.2}$$

is the Mott cross section for the scattering of an electron with incoming energy E_i, on a point-like target with charge Ze. θ denotes the scattering angle in the laboratory. The factor,

$$R = \left(1 + \frac{2E_f}{M_T}\sin^2(\theta/2)\right)^{-1} \ , \tag{V.3}$$

is the correction due to the recoil of the target with mass M_T. Finally the form factor $\left[|F_L(q)|^2 + \left(1 + \tan^2\frac{\theta}{2}\right)|F_T(q)|^2\right]$ is the correction to the Mott cross section due to the extended size of the nucleus.

- $|F_L(q)|^2$ is called the longitudinal form factor. It arises from the Coulomb interaction of the electron with the charge distribution of the nucleus. This form factor can be expanded into multipoles as,

$$|F_L(q)|^2 = \sum_{\lambda \geqslant 0} |F_{C,\lambda}(q)|^2 \tag{V.4}$$

  where,

$$F_{C,\lambda}(q) = \frac{4\pi}{Z^2}\sqrt{\frac{2J_f+1}{2J_i+1}}\int_0^\infty \rho_{tr}(r) j_\lambda(qr) r^2 dr \ . \tag{V.5}$$

  $\rho_{tr}(r) = \langle \Psi_f | \hat{\rho}_{ch}(r) | \Psi_i \rangle$ is the radial transition density between initial and final states.

- The transverse part $|F_T(q)|^2$ of the form factor is due to the interaction of the electron with electric and magnetic currents of the nucleus. It is composed of electric and magnetic multipoles,

$$|F_T(q)|^2 = \sum_{\lambda \geqslant 1} \left[|F_{E,\lambda}(q)|^2 + |F_{M,\lambda}(q)|^2\right] \ . \tag{V.6}$$

The transverse form factor is usually negligible compared to the Coulomb part [54]. It is neglected in the present study. Moreover, we study here transitions $0^+ \to J^+$ (target initially in its ground state). In this case, a unique angular momentum $\lambda = J$ is transferred and the longitudinal factor reduces to,

$$|F_L(q)|^2 = |F_{C,\lambda=J}(q)|^2 = \frac{4\pi}{Z^2}\sqrt{\frac{2J_f+1}{2J_i+1}}\int_0^\infty \rho_{tr}(r) j_\lambda(qr) r^2 dr \ . \tag{V.7}$$

The transition charge densities $\rho_{tr}(r) = \langle \Psi_f | \hat{\rho}_{ch}(r) | \Psi_i \rangle$ constitute the input provided by the multiparticle-multihole configuration mixing method.
Considering the finite size of the nucleons, the charge density $\rho_{ch}(r)$ is obtained by folding

the proton density with the distribution of the proton (which is normalized to unity). In the same way, the correction due to the internal structure of neutrons is added by convoluting the neutron density and the charge distribution of the neutron. The latter is now normalized to zero, as neutrons have zero global charge.

V.1.2 Results

Using transition densities calculated in the framework described in the previous chapter, we calculated form factors for scattering on nuclei of the *sd*-shell. They are shown on Fig. (V.1) to (V.6) and compared to experimental data taken from [56, 57, 58, 65, 111, 19, 109, 66]. Again we show the results at three levels: (i) without self-consistency (Hartree-Fock density in the interaction, no rearrangement terms, frozen Hartree-Fock orbitals), (ii) self-consistency in the first equation only (correlated density in the interaction, rearrangement terms are introduced, frozen Hartree-Fock orbitals) (iii) full self-consistency (both variational equations are solved, i.e. coefficients and orbitals are optimized at the same time, correlated densities and rearrangement terms are introduced everywhere). The black curves are the theoretical form factors. We show in red the curve obtained when multiplying these results by a global factor which allows to fit at best the experimental data. To interpret the results, we also show the theoretical transition densities.

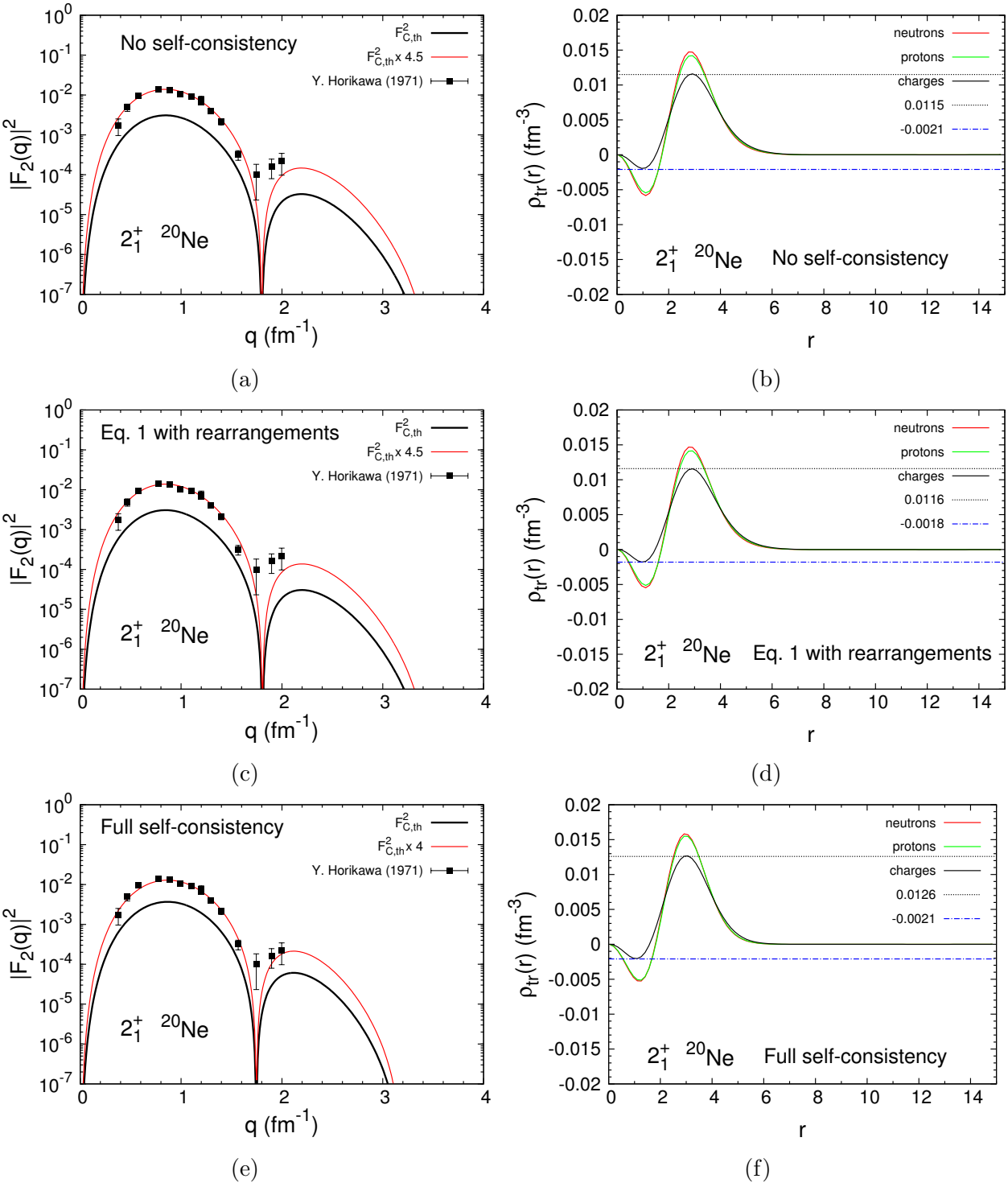

Figure V.1: Transition densities and Coulomb form factor for $\lambda = 2$ electron scattering from ^{20}Ne target.

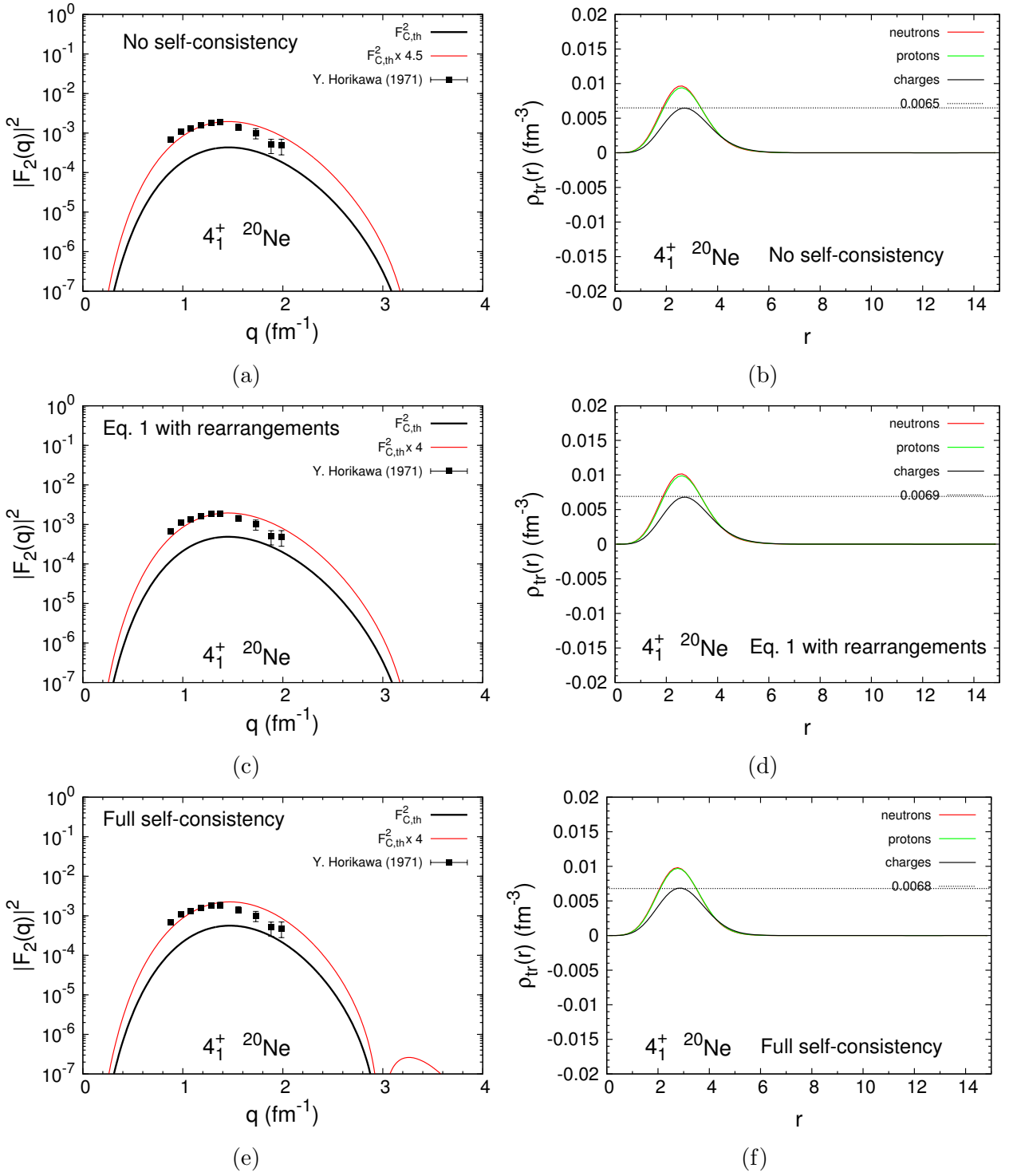

Figure V.2: Transition densities and Coulomb form factor for $\lambda = 4$ electron scattering from ^{20}Ne target.

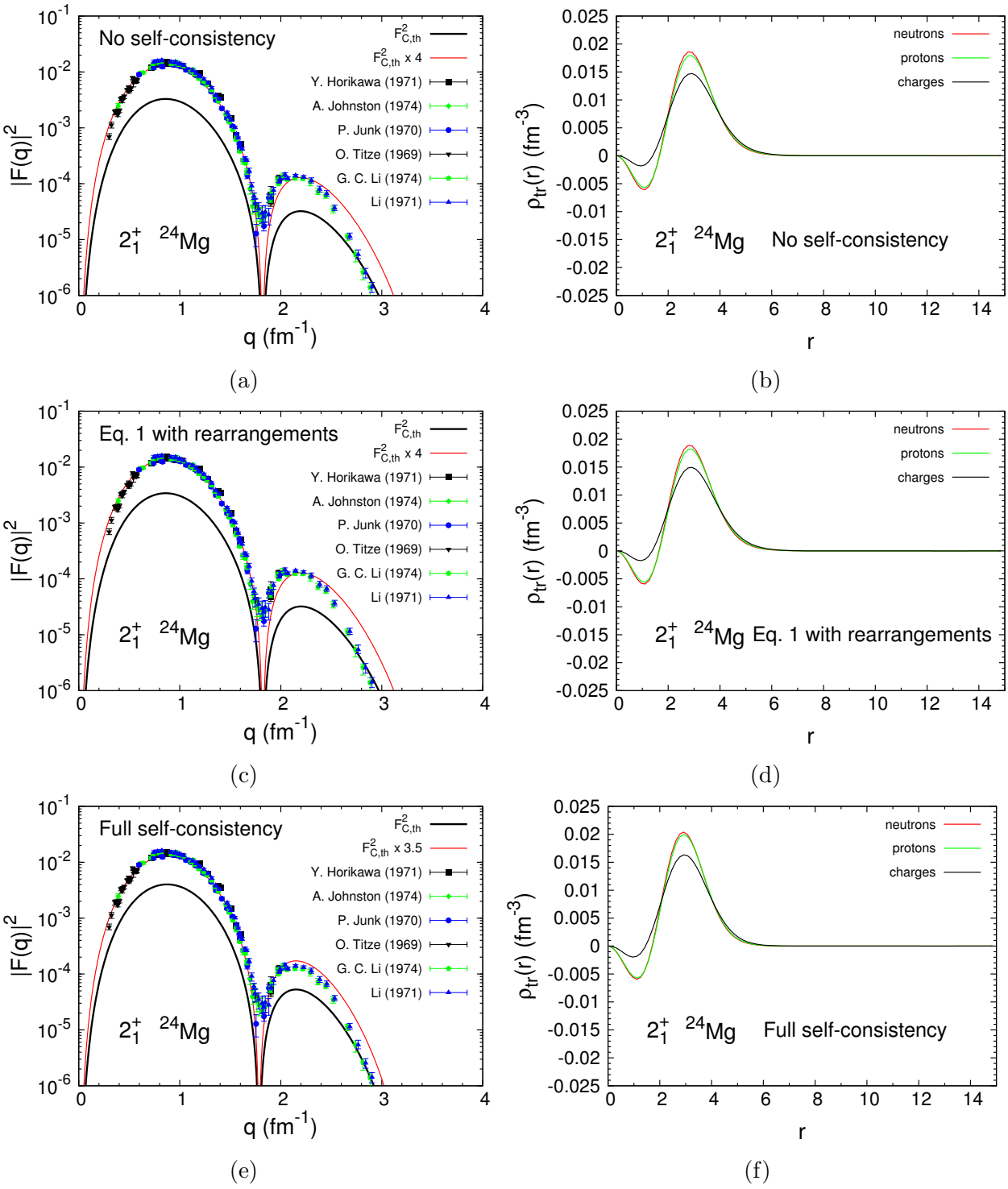

Figure V.3: Transition densities and Coulomb form factor for $\lambda = 2$ electron scattering from ^{24}Mg target.

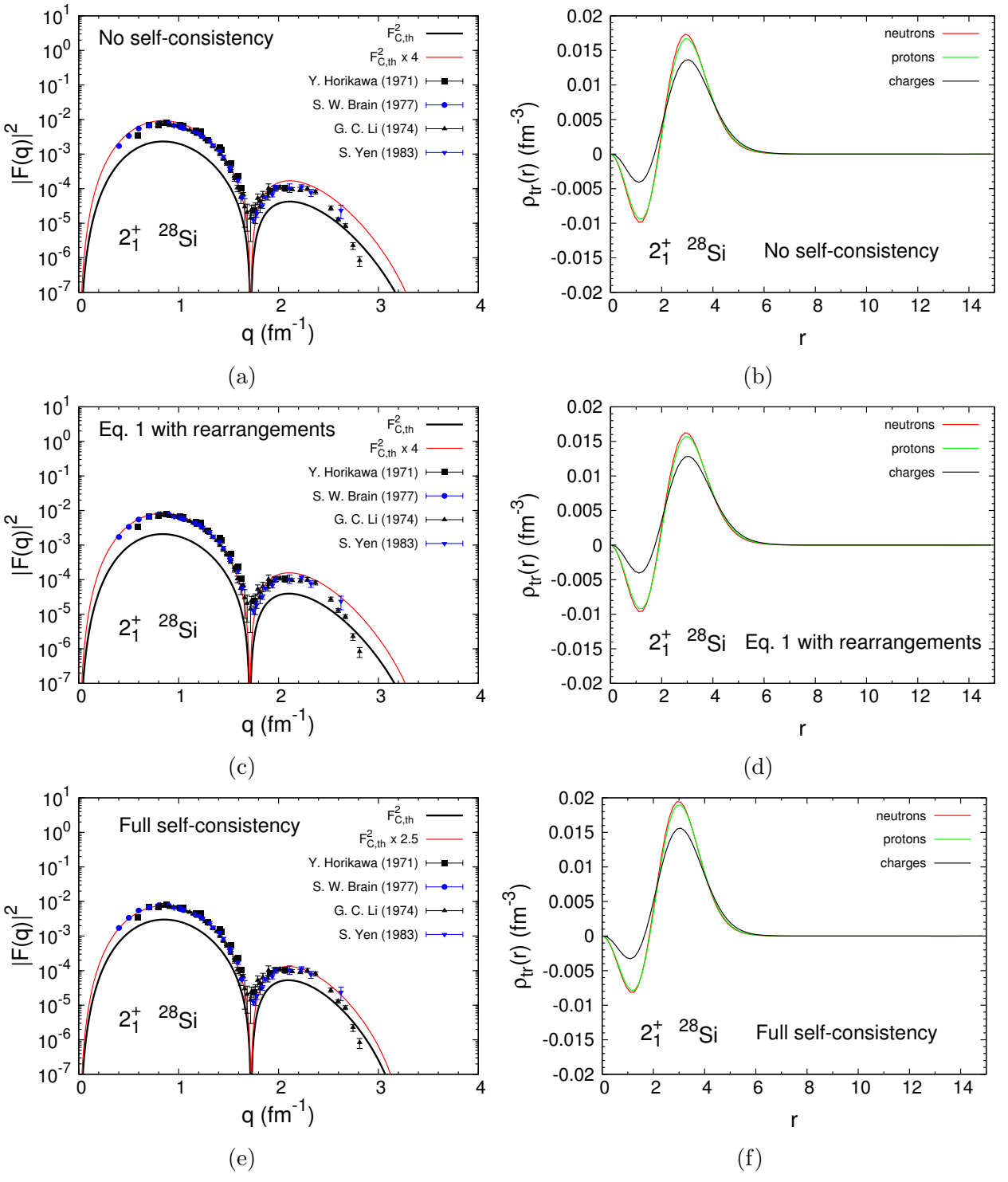

Figure V.4: Transition densities and Coulomb form factor for $\lambda = 2$ electron scattering from ^{28}Si target.

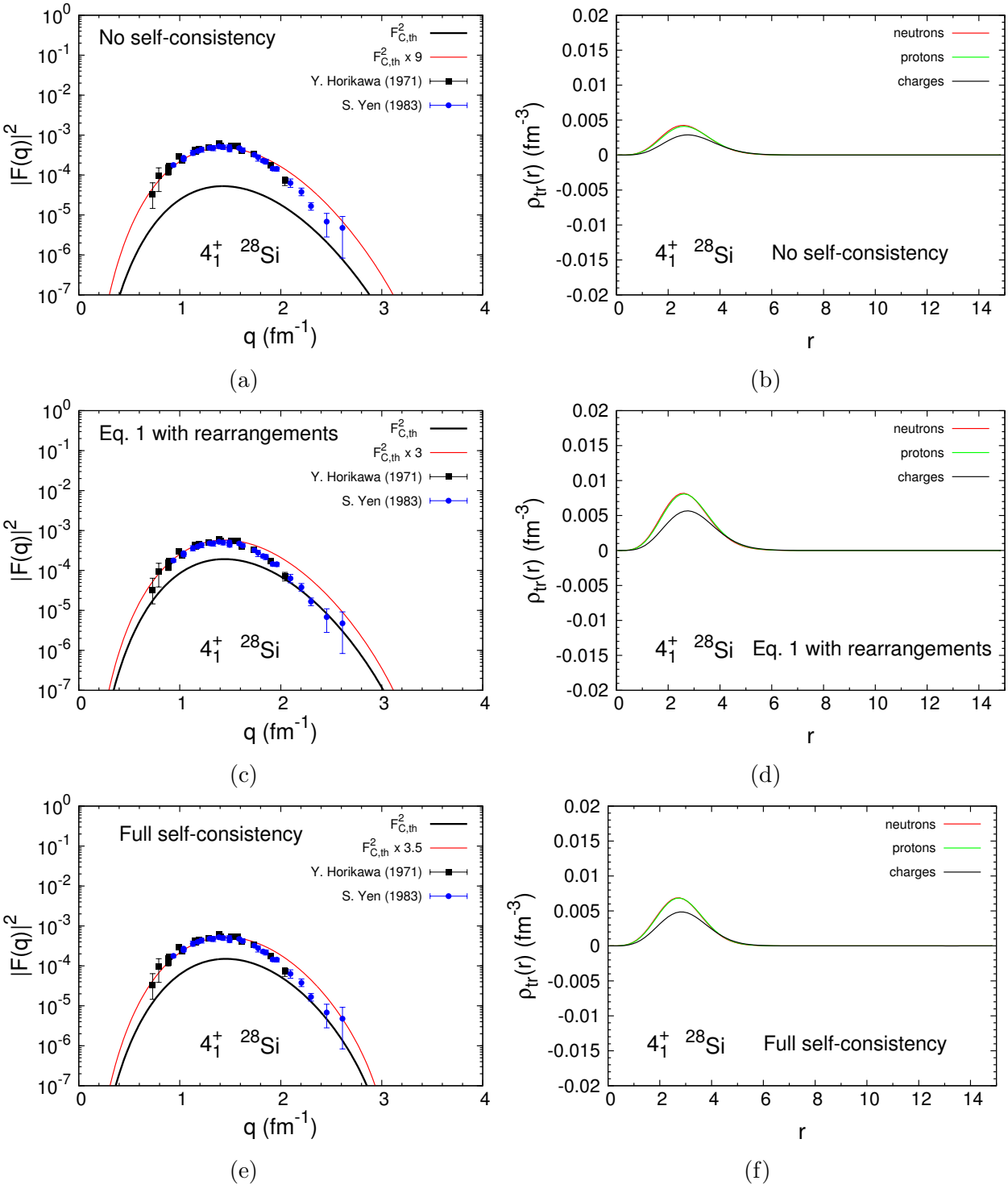

Figure V.5: Transition densities and Coulomb form factor for $\lambda = 4$ electron scattering from ^{28}Si target.

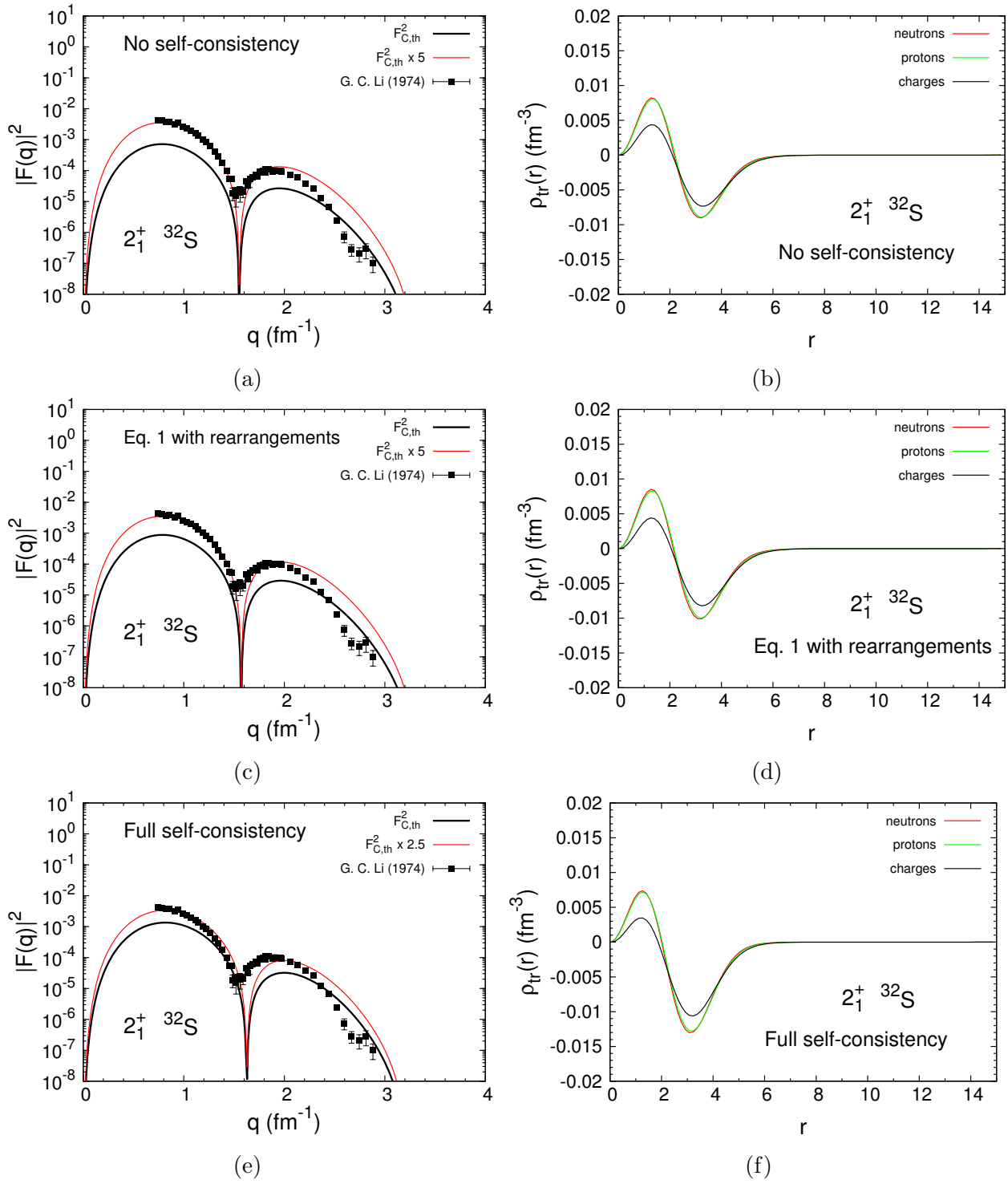

Figure V.6: Transition densities and Coulomb form factor for $\lambda = 2$ electron scattering from ^{32}S target.

The results are globally in accordance with the quadrupole transition probabilities $B(E2)$ calculated in the previous chapter. For instance, looking at the transition $0_1^+ \rightarrow 2_1^+$ in ^{20}Ne shown in (Fig. V.2), we observe a clear lack of magnitude on the form factor at the non self-consistent stage. We only note a small effect induced by self-consistency: the global factor applied to reach experiment decreases from 4.5 to 4. However one notes an improvement of the trend due to the orbital renormalization. More precisely, a displacement of the minimum of $|F_{C,2}|^2$ toward smaller momenta is observed. This shift leads now to a good agreement with the experimental minimum. We also observe a narrowing at the tail of the form factor. The latter reflects a slight spreading of the transition density toward higher distance r. This is in accordance with the interpretation of the orbital transformation which allows to partially populate single-particle states outside of the original *sd*-shell, characterized by larger spatial extensions. The conclusion from the $0_1^+ \rightarrow 2_1^+$ transition in ^{20}Ne (Fig. V.2) is similar.
Regarding ^{24}Mg, the global factor gained from no to full self-consistency is ~ 1.1, and corresponds to the value that was gained on the $B(E2)$ in the previous chapter. Again the experimental trend is slightly improved at the tail.
Looking at the transition $0_1^+ \rightarrow 2_1^+$ in ^{28}Si, we note an important increase in the charge density profile caused by the optimization of the single-particle states. The peak at $r \sim 3$ fm varies from a value ~ 0.13 fm^{-3} to ~ 0.16 fm^{-3}. The increase of the density at the surface is balanced by a decrease of the volume component at $r \sim 1.2$ fm. This reflects in a important gain of magnitude for the form factor $|F_{C,2}|^2$. Indeed the latter is improved by a factor $\sim \frac{4}{2.5} \sim 1.6$ in accordance with the results for the $B(E2)$ (~ 1.3). The transition $0_1^+ \rightarrow 4_1^+$ in ^{28}Si is more peculiar. At the non self-consistent level, an important lack of collectivity is noted (global factor 9). This lack of strength is largely corrected by the introduction of rearrangement terms which lower this factor to 3. We note however that the orbital equation acts slightly against this process and bring back up to ~ 3.5. Nevertheless, the second orbital equation narrows the form factor leading to a better trend.
Finally, regarding the $0_1^+ \rightarrow 2_1^+$ in ^{32}S, we note a displacement of the form factor minimum toward higher momenta q, when the full self-consistency is applied. It is related to a shrinking of the transition density toward smaller r. This leads to a disagreement with the experimental value of the minimum, although global magnitude is gained.

In conclusion, the renormalization of single-particle states generally improves the theoretical results. In particular, it involves a spreading of the radial density toward the surface, causing a shrinking of the tail of the form factor and a better agreement with the experimental trend. The minima are usually also improved (except in ^{32}S), and magnitude is gained.

Finally, let us look at the effect of the explicit introduction of the fp-shell in the valence space. Results are shown on Fig. (V.7) for ^{20}Ne. At the non self-consistent case, little change is observed compared to the *sd* valence space calculation. Self-consistency effects are how-

ever increased. The shift of the minimum toward smaller momenta q is found larger, and is accompanied by a global compression of the form factor (in particular at the tail). Global magnitude is also gained.

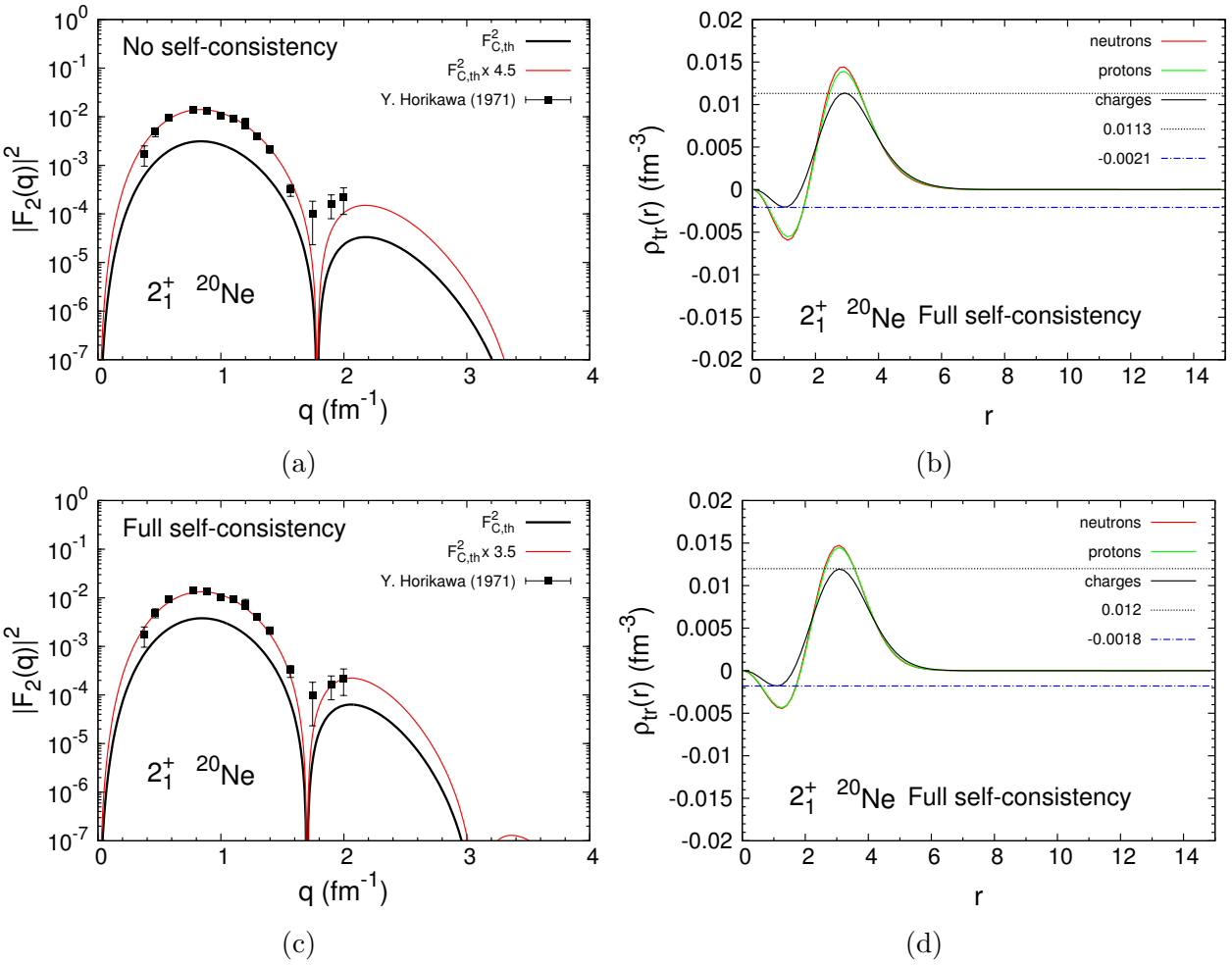

Figure V.7: Transition densities and Coulomb form factor for $\lambda = 2$ electron scattering from ^{20}Ne target. Results are obtained with $sd + fp$ valence space.

V.2 Inelastic proton scattering on discrete states

Hadron scattering can provide information on the distribution of protons and neutrons. In particular, due to the strength of the proton-neutron interaction between projectile and target, proton scattering is more sensitive to the contribution of neutron collectivity in transitions. Because of the complexity of the nuclear force, the transition operator $\hat{T}$ needed to calculate a transition probability $\langle \Psi_i | \hat{T} | \Psi_f \rangle$ from an initial to a final state is unknown. The model used here to approach this quantity is based on the Distorted Born Wave Approximation (DWBA), which describes the incident and scattered waves of the projectile as distorted by the field of the target nucleus. The latter is taken as an optical potential simulating the interaction between the proton and the nucleus. The calculations of resulting cross sections are realized in collaboration with Marc Dupuis (CEA,DAM,DIF).

V.2.1 Formal aspects of the model

We first recall briefly the main points of the theoretical framework, leading to the derivation of cross sections. More details can be found in [35].
One starts from the initial Schrödinger equation for the target+projectile system,

$$\hat{H} \, |\Psi\rangle = E\Psi \ , \tag{V.8}$$

where the wave function is written assuming discernibility between the projectile and the nucleons of the target. That is,

$$|\Psi\rangle = \sum_i |\psi_i\rangle \otimes |u_i\rangle \ , \tag{V.9}$$

where $\{|\psi_i\rangle\}$ form an orthonormal basis for the target states, while $\{|u_i\rangle\}$ characterizes the relative motion between the target and the projectile. We denote by $|\psi_0\rangle$ the ground state of the target, and $|u_0\rangle$ the center of mass in an elastic scattering state with energy E. The Hamiltonian can then be separated into,

$$\hat{H} = \hat{H}_A + T_0 + \hat{V} \ , \tag{V.10}$$

where $\hat{H}_A$ denotes the intrinsic Hamiltonian of the target nucleus, T_0 the relative kinetic energy, and $\hat{V} = \sum_{n=1}^{A} V_{0n}$ is the sum of the interactions between the projectile and each nucleon of the target. Inserting (V.10) and (V.9) into (V.8), one obtains the (*a priori* infinite) following system of coupled equations,

$$(E_k + T_0 - E + V_{kk}) \, |u_k\rangle = - \sum_{i \neq k} V_{ki} \, |u_i\rangle \ , \tag{V.11}$$

where we defined the one-body potential,

$$V_{ki} \equiv \langle \psi_k | \hat{V} | \psi_i \rangle \ . \tag{V.12}$$

Practically unsolvable, this problem has to be simplified with the use of approximations. When one wants to study one particular transition $\psi_i = \psi_0 \to \psi_f = \psi_N$, a good strategy is found in the Feshbach formalism [40, 41]. One thus defines $\mathcal{P}$ and $\mathcal{Q}$ spaces[1] with respective projectors,

$$\begin{cases} \hat{P} = |\psi_0\rangle \langle \psi_0| + |\psi_N\rangle \langle \psi_N| \ , \\ \hat{Q} = \hat{1} - \hat{P} \ . \end{cases} \tag{V.13}$$

The $\mathcal{P}$ subspace contains the elastic channel where the nucleus is left in its ground state ψ_0 as well as the particular inelastic channel under study, while $\mathcal{Q}$ includes the rest of the channels. Using projection techniques, one can show that the Schrödinger equation (V.8) for the wave function $|\Psi\rangle$ spanning the whole Hilbert space, can be recasted into an equation,

$$H_{eff} P |\Psi\rangle = E P |\Psi\rangle \ , \tag{V.14}$$

for the projection $P|\Psi\rangle$ of $|\Psi\rangle$ on $\mathcal{P}$. The action of the $\mathcal{Q}$ space is implicitly accounted for through the definition of the effective Hamiltonian H_{eff} acting within $\mathcal{P}$,

$$\begin{aligned} H_{eff} &= H_{PP} + H_{PQ} \frac{1}{E - H_{QQ} + i\eta} H_{QP} \\ &= T_0 + \underbrace{\left(V_{PP} + V_{PQ} \frac{1}{E - H_{QQ} + i\eta} H_{QP} \right)}_{V_{eff}} \ . \end{aligned} \tag{V.15}$$

Using the definition (V.13) for P and projecting (V.14) onto $|\psi_0\rangle$ and $|\psi_N\rangle$, one obtains the following set of two coupled equations,

$$\begin{cases} \left(E_{k_i} - T_0 + \langle \psi_0 | V_{eff} | \psi_0 \rangle \right) |u_0\rangle = \langle \psi_0 | V_{eff} | \psi_N \rangle |u_N\rangle & \text{(V.16)} \\ \left(E_{k_f} - T_0 + \langle \psi_N | V_{eff} | \psi_N \rangle \right) |u_N\rangle = \langle \psi_N | V_{eff} | \psi_0 \rangle |u_0\rangle \ . & \text{(V.17)} \end{cases}$$

The potentials $U_{NN} \equiv \langle \psi_N | V_{eff} | \psi_N \rangle$ and $U_{00} \equiv \langle \psi_0 | V_{eff} | \psi_0 \rangle$ are the one-body optical potentials acting in the space of the projectile states. Similarly, $U_{0N} \equiv \langle \psi_0 | V_{eff} | \psi_N \rangle$ and $U_{N0} \equiv \langle \psi_N | V_{eff} | \psi_0 \rangle$ are the transition potentials.
The approximation usually made to solve the system of Eqs. (V.16, V.17) consists in neglecting the term $\langle \psi_0 | V_{eff} | \psi_N \rangle$ in Eq. (V.16). This assumption amounts to assuming that the

[1] Obviously, different from the ones discussed in the context of the mp-mh method in chapter II.

elastic channel $|u_0\rangle \otimes |\psi_0\rangle$ is not perturbed by the particular inelastic process where the target is excited in the state $|\psi_f\rangle = |\psi_N\rangle$.
Calling now $|\chi^-_{k_f}\rangle$ and $|\chi^+_{k_i}\rangle$ the solutions of

$$\Big(E_{k_i} - T_0 + \langle\psi_0|V_{eff}|\psi_0\rangle\Big)\,|\chi^{+/-}_{k_{i/f}}\rangle = 0\ , \tag{V.18}$$

the transition probability for exciting the target from $|\psi_0\rangle$ to $|\psi_N\rangle$ is given, in the DWBA approximation, by

$$\begin{aligned} T_{fi} &= \langle\chi^-_{k_f}\psi_N|\hat{T}|u_0\psi_0\rangle \\ &\simeq \langle\chi^-_{k_f}\psi_N|\hat{V}_{eff}|\chi^+_{k_i}\psi_0\rangle \\ &= \langle\chi^-_{k_f}|U_{N0}|\chi^+_{k_i}\rangle\ . \end{aligned} \tag{V.19}$$

We note that the T-matrix has been expanded to first order in V_{eff}, hence the name "Born approximation". The differential scattering cross-section is then obtained from,

$$\frac{d\sigma_{fi}}{d\Omega} = \frac{\mu^2}{4\pi^2\hbar}\frac{k_f}{k_i}|T_{fi}|^2\ . \tag{V.20}$$

In second quantization, the optical and transition potential are obtained from the effective interaction V_{eff} as,

$$\begin{aligned} U_{NN'} &= \frac{1}{2}\sum_{\beta\delta kk'}\langle k'\beta|V_{eff}|\widetilde{k\delta}\rangle\,\langle\psi_N|a^\dagger_{k'}a_k a^\dagger_\beta a_\delta|\psi_{N'}\rangle \\ &= \frac{1}{2}\sum_{\beta\delta kk'}\langle k'\beta|V_{eff}|\widetilde{k\delta}\rangle\,\langle\psi_N|a^\dagger_\beta a_\delta|\psi_{N'}\rangle\,a^\dagger_{k'}a_k\ , \end{aligned} \tag{V.21}$$

where (k, k') denote states of the projectile nucleon, while (β, δ) are states for nucleons in the target. In order to determine the optical and transition potentials, one thus needs two input quantities:

- Firstly, one needs to know the effective interaction V_{eff}. In the present application, this interaction is taken as a G-matrix (the Melbourne G-matrix obtained from the Bonn realistic potential [2]).
- Secondly, one needs to know the transition densities of the target nucleus. These are calculated within the mp-mh approach.

V.2.2 Results

We show in Fig. (V.8) and (V.9) the theoretical cross sections for proton scattering on a ^{28}Si target. Fig. (V.8) displays the cross section for the $0^+_1 \to 2^+_1$ transition, while Fig. (V.9)

shows the cross section for the $0_1^+ \rightarrow 4_1^+$ transition. Again the black lines are the theoretical cross sections, while the red ones represent the theoretical value multiplied by a global factor adjusted to fit at best the experimental data. Qualitatively, the results are in accordance with the previous electron scattering study. Concerning the $0_1^+ \rightarrow 2_1^+$ transition, we observe a disagreement with the experimental trend at high angle. This discrepancy might be due to the reaction model. Comparing the theoretical results obtained at the three stages of the mp-mh approach, we note that the rearrangement terms do not produce a noticeable effect, while the optimization of orbitals globally improves the cross section by a factor ~ 1.25. Looking now at the $0_1^+ \rightarrow 4_1^+$ transition, we observe a nice agreement of the theoretical and experimental trends. As noted on electronic form factors, the rearrangement terms have a drastic effect in this case. They allow to reduce the global factor needed to reach experiment by a factor 3. This improvement is then slightly worsen by the orbital renormalization. Let us remind that in this nuclei, rearrangement terms and orbital optimization often act against each other. The deductions made from the electron scattering thus globally apply here. We are led to similar conclusions in other *sd*-shell nuclei.

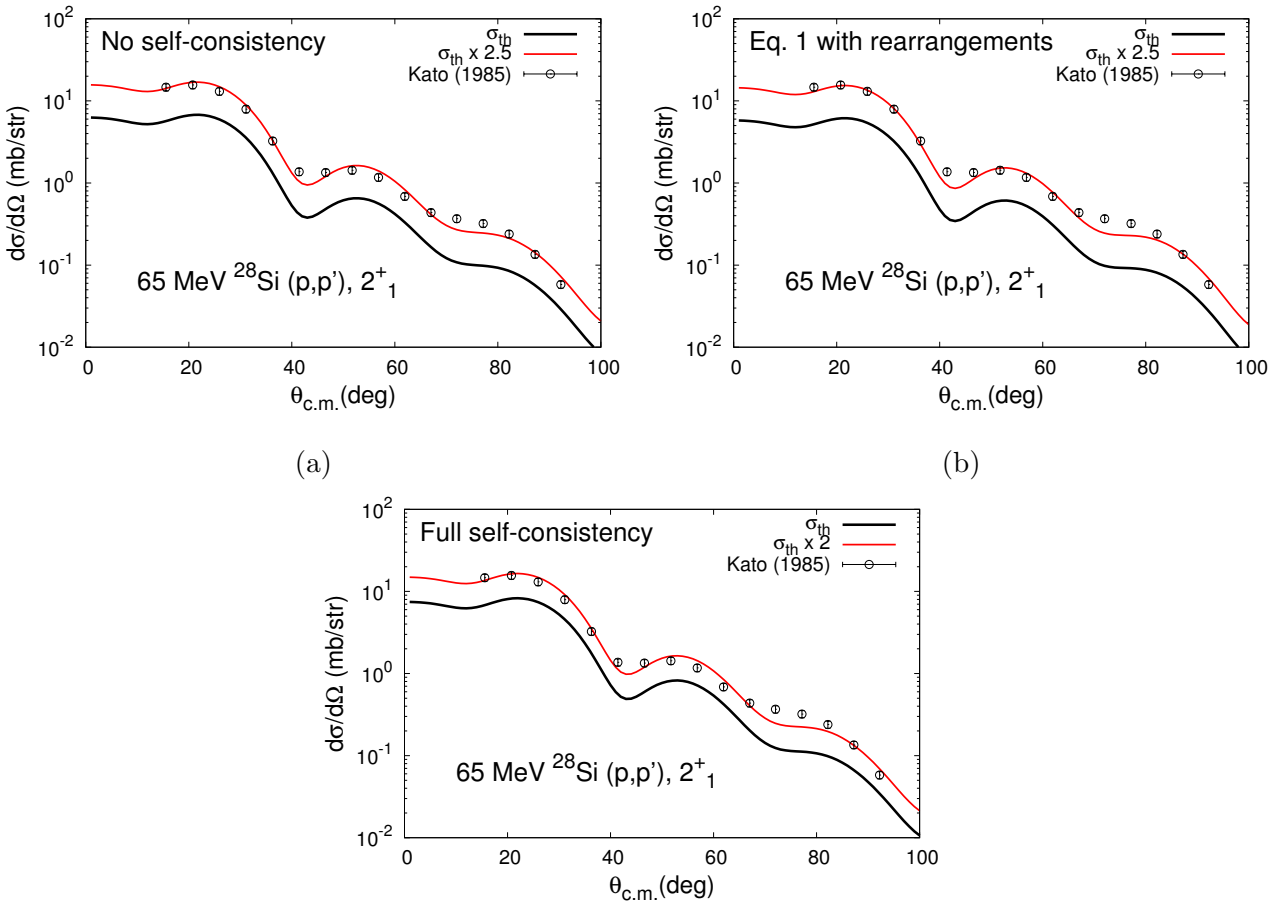

Figure V.8: Cross section for the $0_1^+ \to 2_1^+$ transition in proton scattering on a ^{28}Si target, with incident proton energy $E = 65$ MeV.

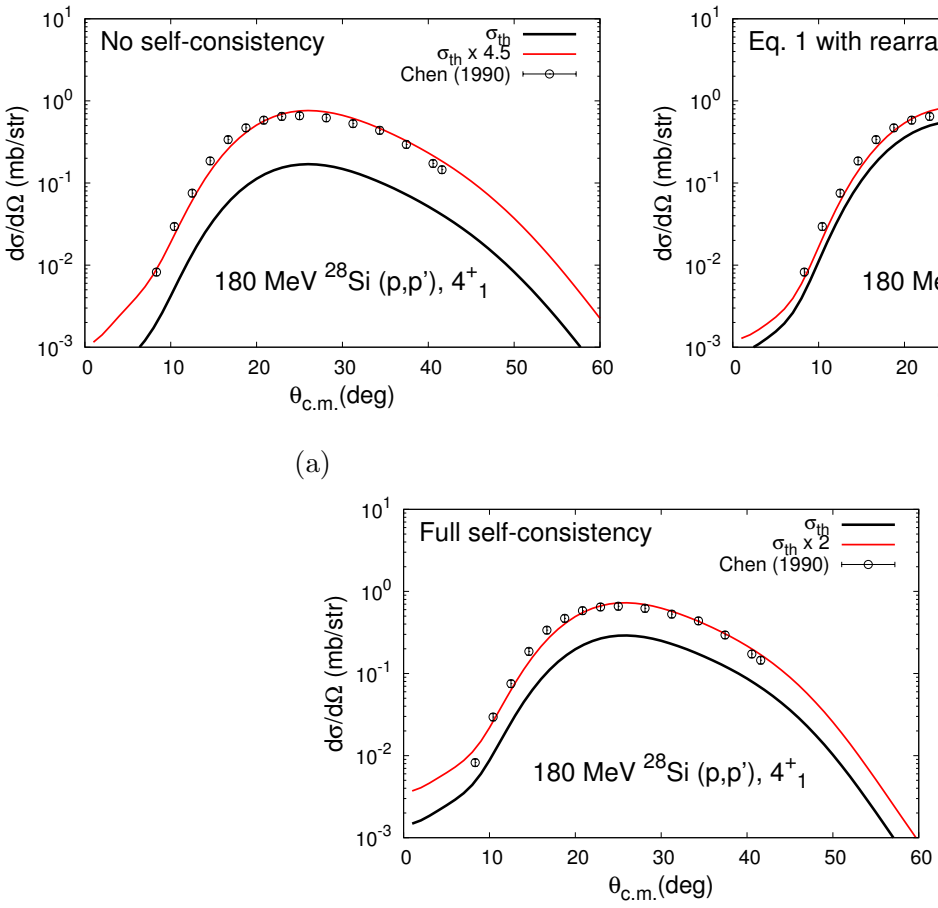

Figure V.9: Cross section for the $0_1^+ \to 4_1^+$ transition in proton scattering on a ^{28}Si target, with incident proton energy $E = 180$ MeV.

Chapter VI

Conclusion and outlook

This thesis work took part in the development of the multiparticle-multihole configuration mixing approach for the description of atomic nuclei. Based on a variational principle determining both the expansion coefficients of the nuclear wave function and the single-particle orbitals, this method establishes a natural link between Shell-Model and self-consistent mean-field approaches.

The formal analysis conducted in the first part of this document allowed us to improve our comprehension of the mp-mh method and more precisely to gain insight into the role of the orbital optimization. In particular, this study revealed the link between the variational equation determining the single-particle states and the Green's function formalism at equal times. It was shown that, while all static correlations can be incorporated into the general mean-field naturally defined by the orbital equation, the remaining dynamical correlations are related to the source term of this equation.
The rest of the present work was devoted to applications of the fully self-consistent mp-mh approach using the D1S Gogny interaction. Particular attention was paid to the effect induced by the orbital transformation. The systematic study of *sd*-shell nuclei conducted in chapter IV led to very satisfactory results. In particular, separation and excitation energies, as well as magnetic dipole properties were found in very good agreement with experimental data. A particularly positive effect was induced by the orbital equation on excited spectra as well as charge radii. The study of electric quadrupole transitions $B(E2)$ clearly suffered from a lack of collectivity when the mp-mh approach was applied at the non self-consistent level. This behavior was expected since the configuration mixing was restricted to the sd-shell and no use of effective charge was made. A global improvement of these results was obtained through the renormalization of single-particle states. Although the effect is systematically directed in the right direction, it appears very small for the majority of nuclei under study. This behavior was understood as due to the explicit symmetry conservation imposed in the method, which prevents the orbital equation from generating 2p-2h excitations from the positive parity valence

sd-shell to the surroundings negative parity shells. The inclusion of the fp shell in the valence space in the case of ^{20}Ne led to an improvement of the theoretical $B(E2)$ and to a larger effect of the orbital optimization. This result suggests that another type of selection criteria of the configurations according to e.g. their excitation order and taking into account the full available single-particle space could be more successful. The test study of ^{12}C performed in chapter III using this type of truncation scheme however led to unrealistically high correlation energies, confirming that the D1S Gogny interaction is not prepared for this kind of truncations. The global shifts observed in the excitation spectra of ^{30}Si and ^{30}S by $\sim$ 1.5 MeV compared to experiment, also reinforce the need for an interaction that is constrained in the $T = 0$ channel. Moreover, although pathological behaviors have not been encountered in the present work, the zero-range terms in the Gogny interaction (spin-orbit and density-dependent terms) may lead to ultra-violet divergences during the self-consistent procedure. To avoid such behaviors, a fully finite-range interaction is necessary. Work in this direction is in progress [26, 82].

Many perspectives can be considered concerning both applications and extensions of the formalism of the multiparticle-multihole configuration mixing method. For instance the description of collective excitations such as giant or Pygmy resonances would be of great interest. A comparison to the Random Phase Approximation approach which utilizes frozen Hartree-Fock orbitals and an uncorrelated ground state to calculate matrix elements (Quasi-Boson Approximation) could be conducted. This would allow to further quantify the effect of the renormalization of orbitals on observables and the importance of correlations in the ground state.

As illustrated during the study of ^{12}C in chapter III, the use of a selection criterion of the many-body configurations involving the whole single-particle space can become numerically very demanding as the number of particles increases. When this type of truncation is unfeasible, an alternative can be found in the definition of effective operators. One of the perspective of the mp-mh approach is to use the Feshbach formalism [40, 41] to renormalize the Hamiltonian within the space $\mathcal{P}$ of configurations that are explicitly treated. Such an effective Hamiltonian would account for the effect of the missing space that is left untreated by the renormalization of orbitals.

Finally, from the perspective of a unified treatment of all nuclei, applications of the method to odd nuclei are in progress. Also, motivated by the experimental progress achieved in the production of exotic nuclear systems, it appears necessary to extend the formalism of the mp-mh approach in order to account for the continuum of unbound states. Treating closed and open systems on an equal footing, such a formalism would contribute to a unification of both structure and reaction aspects.

Appendix A

Derivation of the orbital equation for two- and three-body Hamiltonians

We showed in section (II.1.2) that requiring the energy to be stationary with respect to orbital variations $\delta a_i^\dagger$ leads to the following "generalized Brillouin equation",

$$\langle \Psi | \left[\hat{H}, \hat{T} \right] | \Psi \rangle = 0 \, , \tag{A.1}$$

where $\hat{T}$ is the one-body hermitian operator parameterizing the variation.
In this appendix we derive the orbital equation for the general case of a three-body Hamiltonian,

$$\begin{aligned} \hat{H} &= \hat{K} + \hat{V}^{2N} + \hat{V}^{3N} \\ &= \sum_{ij} K_{ij} a_i^\dagger a_j + \frac{1}{4} \sum_{ijkl} \langle ij | \widetilde{V^{2N}} | kl \rangle \, a_i^\dagger a_j^\dagger a_l a_k + \frac{1}{36} \sum_{ijklmn} \langle ijk | \widetilde{V^{3N}} | lmn \rangle \, a_i^\dagger a_j^\dagger a_k^\dagger a_n a_m a_l \, , \end{aligned} \tag{A.2}$$

where $\hat{K}$ is the kinetic energy operator (including center-of-mass correction), and $\widetilde{V^{2N}}$ and $\widetilde{V^{3N}}$ are the antisymmetrized two- and three-body interactions respectively.
That is,

$$\begin{aligned} \widetilde{V^{2N}} &= (1 - P_{12}) V^{2N} \\ \widetilde{V^{3N}} &= (1 - P_{12} - P_{23} - P_{13} + P_{12}P_{23} + P_{13}P_{23}) V^{3N} \, , \end{aligned} \tag{A.3}$$

where $P_{ij} = P_{r_i r_j} P_{\sigma_i \sigma_j} P_{\tau_i \tau_j}$ denotes the exchange operator between particle i and j.

Injecting (A.2) into Eq. (A.1) we get,

$$0 = \sum_{rs} T_{rs} \Big(\underbrace{\sum_{ij} K_{ij} \langle \Psi | \left[a_i^\dagger a_j, a_r^\dagger a_s \right] | \Psi \rangle}_{①} + \underbrace{\frac{1}{4} \sum_{ijkl} \widetilde{V}^{2N}_{ijkl} \langle \Psi | \left[a_i^\dagger a_j^\dagger a_l a_k, a_r^\dagger a_s \right] | \Psi \rangle}_{②} + \underbrace{\frac{1}{36} \sum_{ijklmn} \widetilde{V}^{3N}_{ijklmn} \langle \Psi | \left[a_i^\dagger a_j^\dagger a_k^\dagger a_n a_m a_n, a_r^\dagger a_s \right] | \Psi \rangle}_{③} \Big) . \tag{A.4}$$

We can calculate ①, ② and ③ using the following anti-commutation properties of the creation and annihilation fermion operators,

$$\{a_i^\dagger, a_j\} = \delta_{ij}, \text{ and } \{a_i^\dagger, a_j^\dagger\} = \{a_i, a_j\} = 0 , \tag{A.5}$$

where $\{A, B\} = AB + BA$ is the notation for the anti-commutator.

Calculation of the first term We have,

$$\begin{aligned} \left[a_i^\dagger a_j, a_r^\dagger a_s \right] &= a_i^\dagger \underbrace{a_j a_r^\dagger}_{=\delta_{rj} - a_r^\dagger a_j} a_s - a_r^\dagger \underbrace{a_s a_i^\dagger}_{=\delta_{si} - a_i^\dagger a_s} a_j \\ &= \delta_{rj} a_i^\dagger a_s - \delta_{si} a_r^\dagger a_j - a_i^\dagger a_r^\dagger a_j a_s + \underbrace{a_r^\dagger a_i^\dagger a_s a_j}_{= a_i^\dagger a_r^\dagger a_j a_s} \\ &= \delta_{rj} a_i^\dagger a_s - \delta_{si} a_r^\dagger a_j . \end{aligned} \tag{A.6}$$

Injecting this into the expression of ①, we obtain,

$$\begin{aligned} ① &= \sum_{ij} K_{ij} \langle \Psi | \left[a_i^\dagger a_j, a_r^\dagger a_s \right] | \Psi \rangle \\ &= \sum_i K_{ir} \langle \Psi | a_i^\dagger a_s | \Psi \rangle - \sum_j K_{sj} \langle \Psi | a_r^\dagger a_j | \Psi \rangle \\ &= \sum_i \rho_{si} K_{ir} - \sum_j K_{sj} \rho_{jr} , \end{aligned} \tag{A.7}$$

where $\rho_{si} = \langle \Psi | a_i^\dagger a_s | \Psi \rangle$ is the one-body density matrix.
So that finally,

$$① = [\rho, K]_{sr} . \tag{A.8}$$

Calculation of the second term Using again the anti-commutation relations (A.5) we can express the commutator in ② as,

$$\begin{aligned}\left[a_i^\dagger a_j^\dagger a_l a_k, a_r^\dagger a_s\right] &= a_i^\dagger a_j^\dagger a_l a_k a_r^\dagger a_s - a_r^\dagger a_s a_i^\dagger a_j^\dagger a_l a_k \qquad (A.9)\\ &= \delta_{kr} a_i^\dagger a_j^\dagger a_l a_s - \delta_{lr} a_i^\dagger a_j^\dagger a_k a_s \\ &\quad -\delta_{is} a_r^\dagger a_j^\dagger a_l a_k + \delta_{js} a_r^\dagger a_i^\dagger a_l a_k \\ &\quad +a_i^\dagger a_j^\dagger a_r^\dagger a_l a_k a_s - \underbrace{a_r^\dagger a_i^\dagger a_j^\dagger a_s a_l a_k}_{=a_i^\dagger a_j^\dagger a_r^\dagger a_l a_k a_s} . \qquad (A.10)\end{aligned}$$

The two terms on the first line of Eq. (A.10) differ by the exchange $k \leftrightarrow l$. Using the property $\widetilde{V}^{2N}_{ijkl} = -\widetilde{V}^{2N}_{ijlk}$ of the antisymmetrized interaction we therefore see that they both bring the same contribution to ②. The same argument apply to both terms on the second line of (A.10), whereas the two terms on the third line cancel each other. As a result we have,

$$② = \frac{1}{2}\sum_{ijl} \widetilde{V}^{2N}_{ijrl} \langle\Psi|a_i^\dagger a_j^\dagger a_l a_s|\Psi\rangle - \frac{1}{2}\sum_{jkl} \widetilde{V}^{2N}_{sjkl} \langle\Psi|a_r^\dagger a_j^\dagger a_l a_k|\Psi\rangle \ . \qquad (A.11)$$

Using the definition of the two-body correlation matrix σ,

$$\begin{aligned}\rho^{[2]}_{1'1,2'2} &\equiv \langle\Psi|a_1^\dagger a_2^\dagger a_{2'} a_{1'}|\Psi\rangle \\ &= (1-P_{12})\rho_{1'1}\rho_{2'2} + \sigma_{11',22'} \ , \qquad (A.12)\end{aligned}$$

we obtain,

$$② = \sum_i \rho_{si} \underbrace{\left(\sum_{jl} \widetilde{V}^{2N}_{ijrl}\rho_{lj}\right)}_{\equiv\Gamma^{2N}[\rho]_{ir}} - \sum_k \underbrace{\left(\sum_{jl} \widetilde{V}^{2N}_{sjkl}\rho_{lj}\right)}_{\equiv\Gamma^{2N}[\rho]_{sk}} \rho_{kr} + \underbrace{\frac{1}{2}\left(\sum_{ijl}\sigma_{is,jl}\widetilde{V}^{2N}_{ijrl} - \sum_{jkl}\widetilde{V}^{2N}_{sjkl}\sigma_{rk,jl}\right)}_{\equiv G^{2N}[\sigma]_{sr}} , \qquad (A.13)$$

where we introduced the average potential $\Gamma^{2N}[\rho]$ and the source term $G^{2N}[\sigma]$ coming from the two-body interaction V^{2N}. As a result we have,

$$② = \Big[\rho, \Gamma^{2N}[\rho]\Big]_{sr} + G^{2N}[\sigma]_{sr} \ . \qquad (A.14)$$

Calculation of the third term Following the same procedure than previously, we deduce,

$$\begin{aligned}\left[a_i^\dagger a_j^\dagger a_k^\dagger a_n a_m a_l, a_r^\dagger a_s\right] &= \delta_{lr} a_i^\dagger a_j^\dagger a_k^\dagger a_n a_m a_s - \delta_{mr} a_i^\dagger a_j^\dagger a_k^\dagger a_n a_l a_s + \delta_{nr} a_i^\dagger a_j^\dagger a_k^\dagger a_m a_l a_s \\ &\quad -\delta_{si} a_r^\dagger a_j^\dagger a_k^\dagger a_n a_m a_l + \delta_{sj} a_r^\dagger a_i^\dagger a_k^\dagger a_n a_m a_l - \delta_{sk} a_r^\dagger a_i^\dagger a_j^\dagger a_n a_m a_l \ . \qquad (A.15)\end{aligned}$$

The first three terms on the right-hand side of Eq. (A.15) differ by permutations of (l,m,n). Thus because of the anti-symmetrization properties $\widetilde{V}^{3N}_{ijklmn} = -\widetilde{V}^{3N}_{ijkmln} = +\widetilde{V}^{3N}_{ijknlm}$, they bring the same contribution to the sum ③. Similarly the last three terms on the right-hand side of Eq. (A.15) contribute equally to ③. Consequently we get,

$$③ = \frac{1}{12}\sum_{ijkmn}\widetilde{V}^{3N}_{ijkrmn}\,\langle\Psi|a_i^\dagger a_j^\dagger a_k^\dagger a_n a_m a_s|\Psi\rangle - \frac{1}{12}\sum_{jklmn}\widetilde{V}^{3N}_{sjklmn}\,\langle\Psi|a_r^\dagger a_j^\dagger a_k^\dagger a_n a_m a_l|\Psi\rangle \ . \quad \text{(A.16)}$$

Expressing the three-body density matrix in terms of the two-body and three-body correlations matrices σ and χ,

$$\begin{aligned}\rho^{[3]}_{1'1,2'2,3'3} &\equiv \langle\Psi|a_1^\dagger a_2^\dagger a_3^\dagger a_{3'} a_{2'} a_{1'}|\Psi\rangle \\ &= (1-P_{12}-P_{13})(1-P_{23})\rho_{1'1}\rho_{2'2}\rho_{3'3} \\ &\quad +(1-P_{12}-P_{13})\rho_{1'1}\sigma_{22',33'} + (1-P_{12}-P_{23})\rho_{2'2}\sigma_{11',33'} + (1-P_{13}-P_{23})\rho_{3'3}\sigma_{11',22'} \\ &\quad +\chi_{11',22',33'} \ , \end{aligned} \quad \text{(A.17)}$$

injecting it into Eq. (A.16) and using again the anti-symmetrization properties of $\widetilde{V}^{3N}$ we obtain,

$$\begin{aligned} ③ \ = \ & \sum_i \rho_{si} \underbrace{\left(\sum_{jkmn}\widetilde{V}^{3N}_{ijkrmn}\left[\frac{1}{2}\rho_{mj}\rho_{nk}+\frac{1}{4}\sigma_{jm,kn}\right]\right)}_{\Gamma^{3N}[\rho,\sigma]_{ir}} - \sum_l \underbrace{\left(\sum_{jkmn}\widetilde{V}^{3N}_{sjklmn}\left[\frac{1}{2}\rho_{mj}\rho_{nk}+\frac{1}{4}\sigma_{jmkn}\right]\right)}_{\Gamma^{3N}[\rho,\sigma]_{sl}}\rho_{lr} \\ & \underbrace{\frac{1}{2}\left(\sum_{ijkmn}\sigma_{is,kn}\widetilde{V}^{3N}_{ijkrmn}\rho_{mj} - \widetilde{V}^{3N}_{sjkimn}\rho_{mj}\sigma_{ri,kn}\right) + \frac{1}{12}\left(\sum_{ijkmn}\chi_{is,jm,kn}\widetilde{V}^{3N}_{ijkrmn} - \widetilde{V}^{3N}_{sjkimn}\chi_{ri,jm,kn}\right)}_{G^{3N}[\rho,\sigma,\chi]_{sr}} , \end{aligned} \quad \text{(A.18)}$$

where we have introduced the average potential $\Gamma^{3N}[\rho,\sigma]$ and the source term $G^{3N}[\rho,\sigma,\chi]$ coming from the three-body interaction V^{3N}. This leads to,

$$③ = \Big[\rho, \Gamma^{3N}[\rho,\sigma]\Big]_{sr} + G^{3N}[\rho,\sigma,\chi]_{sr} \ . \quad \text{(A.19)}$$

Thus, adding ①, ② and ③, the variational equation (A.4) can be rewritten as,

$$\sum_{rs} T_{rs}\left(\Big[\rho, K+\Gamma^{2N}[\rho]+\Gamma^{3N}[\rho,\sigma]\Big]_{sr} + G^{2N}[\sigma]_{sr} + G^{3N}[\rho,\sigma,\chi]_{sr}\right) = 0 \ . \quad \text{(A.20)}$$

This needs to be verified for any variation of the orbitals, i.e. for all T_{rs}. Therefore the stationarity of the energy with respect to orbital variations can be expressed as,

$$\boxed{\left[\hat{h}[\rho,\sigma],\hat{\rho}\right] = \hat{G}[\rho,\sigma,\chi]\ ,} \tag{A.21}$$

where we defined the one-body mean-field Hamiltonian $\hat{h}[\rho,\sigma]$ whose matrix elements are,

$$\begin{aligned}
\hat{h}[\rho,\sigma]_{ij} &= K_{ij} + \Gamma^{2N}[\rho]_{ij} + \Gamma^{3N}[\rho,\sigma]_{ij} \\
&= K_{ij} + \sum_{kl} \widetilde{V}^{2N}_{ikjl}\rho_{lk} + \frac{1}{4}\sum_{klmn} \widetilde{V}^{3N}_{ikl,jmn} \langle\Psi|a_k^\dagger a_l^\dagger a_n a_m|\Psi\rangle \\
&= K_{ij} + \sum_{kl} \widetilde{V}^{2N}_{ikjl}\rho_{lk} + \frac{1}{2}\sum_{klmn} \widetilde{V}^{3N}_{ikl,jmn}\rho_{mk}\rho_{nl} + \frac{1}{4}\sum_{klmn} \widetilde{V}^{3N}_{ikl,jmn}\sigma_{km,ln}\ ,
\end{aligned} \tag{A.22}$$

and the source term $\hat{G}[\rho,\sigma,\chi]$ given by,

$$\begin{aligned}
G[\rho,\sigma,\chi]_{sr} &= G^{2N}[\sigma]_{sr} + G^{3N}[\rho,\sigma,\chi]_{sr} \\
&= \frac{1}{2}\left(\sum_{ijl}\sigma_{is,jl}\widetilde{V}^{2N}_{ijrl} - \sum_{jkl}\widetilde{V}^{2N}_{sjkl}\sigma_{rk,jl}\right) + \frac{1}{2}\left(\sum_{ijkmn}\sigma_{is,kn}\widetilde{V}^{3N}_{ijkrmn}\rho_{mj} - \widetilde{V}^{3N}_{sjkimn}\rho_{mj}\sigma_{ri,kn}\right) \\
&\quad + \frac{1}{12}\left(\sum_{ijkmn}\chi_{is,jm,kn}\widetilde{V}^{3N}_{ijkrmn} - \widetilde{V}^{3N}_{sjkimn}\chi_{ri,jm,kn}\right)\ .
\end{aligned} \tag{A.23}$$

This source term is generated by two- and three-body correlations beyond the mean-field $\hat{h}[\rho,\sigma]$. We easily notice that there exists an operator $\hat{F}[\rho,\sigma,\chi]$ such that $\hat{G} = \hat{F} - \hat{F}^\dagger$. Consequently, $\hat{G}[\rho,\sigma,\chi]$ is an anti-hermitian operator.

Appendix B

Two- and three-body correlation matrices

B.1 Wick's theorem

Several proofs of the Wick's theorem can be found in the literature [101, 42]. In this appendix we only state the fermionic time-independent Wick's theorem and apply it to two- and three-body operators.

The fermion particle creation and destruction operators annihilate the true vacuum $|0\rangle$ as,

$$a_i \left|0\right\rangle = \left\langle 0\right| a_i^\dagger = 0 \ , \forall i \ . \tag{B.1}$$

They satisfy the anti-commutation rules,

$$\begin{cases} \{a_i^\dagger, a_j\} \equiv a_i^\dagger a_j + a_j a_i^\dagger = \delta_{ij} \\ \{a_i^\dagger, a_j^\dagger\} = \{a_i, a_j\} = 0 \ . \end{cases} \tag{B.2}$$

Before stating Wick's theorem we need to introduce the concepts of normal ordering and contractions.

Normal product The normal product $N(...)$ (or : ... :) of creation and/or annihilation operators, with respect to the vacuum $|0\rangle$, is equal to the product of these operators reordered so that all creation operators $a_i^\dagger$ are on the left of all destruction operators a_i. It is affected by the sign of the permutation $\mathcal{P}$ required to bring the product to that form.
That is,

$$\begin{aligned} N(a_1^\dagger a_2 ... a_m a_{m+1}^\dagger a_{m+2}^\dagger .... a_n .... a_N^\dagger) &\equiv : a_1^\dagger a_2 ... a_m a_{m+1}^\dagger a_{m+2}^\dagger .... a_n .... a_N^\dagger ... : \\ &= (-)^{\mathcal{P}} (a_1^\dagger ... a_{m+1}^\dagger a_{m+2}^\dagger ... a_N^\dagger ...)(a_2 ... a_m ... a_n ...) \ . \end{aligned} \tag{B.3}$$

A very useful property arises from this definition: the vacuum expectation value of a normal product of operators is equal to zero.

$$\langle 0|N(A,B,C...)|0\rangle = \langle 0| : A,B,C... : |0\rangle = 0 \ , \tag{B.4}$$

where $A, B, C...$ can be any linear combinations of $a^\dagger$ and a's.

Contractions The contraction $\overbrace{AB}$ of two operators A and B is defined as,

$$\overbrace{AB} = AB - : AB : \ . \tag{B.5}$$

Clearly this quantity is a number either equal to 0 or $\{A, B\}$. Moreover since the vacuum expectation value $\langle 0| : AB : |0\rangle = 0$ we have,

$$\overbrace{AB} = \langle 0|AB|0\rangle \ . \tag{B.6}$$

In many-body theories, one often defines a reference state taken as the ground state of a first approximation non-interacting theory. In our case, this reference state is the Slater determinant $|\phi\rangle = \prod_{i=1}^{A} a_i^\dagger|0\rangle = \prod_h a_h^\dagger|0\rangle$ containing a filled Fermi sea (hole states h) and empty particle states p. Therefore if we define a new basis of operators b and $b^\dagger$ such that,

$$\begin{cases} b_h^\dagger = a_h \quad , \quad b_h = a_h^\dagger \\ b_p^\dagger = a_p^\dagger \quad , \quad b_p = a_p \ , \end{cases} \tag{B.7}$$

we have,

$$b_i \, |\phi\rangle = \langle\phi| \, b_i^\dagger = 0 \ , \forall i = p, h \ . \tag{B.8}$$

The state $|\phi\rangle$ is said to be a vacuum for these operators and therefore we can define the contraction and normal products with respect to this reference state [1]
For instance,

$$\begin{aligned} : a_h^\dagger a_p : \ &= \ +a_h^\dagger a_p \\ : a_p^\dagger a_{p'} : \ &= \ +a_p^\dagger a_{p'} \\ : a_h^\dagger a_{h'} : \ &= \ -a_{h'} a_h^\dagger \ . \end{aligned}$$

where $: ... :$ denotes now the normal ordering with respect to $|\phi\rangle$.

[1] In fact more generally any $b^\dagger$ and b's obtained by linear combination of $a^\dagger$ and a's conserve the anti-commutation rules (B.1) (canonical transformation). Therefore the new reference state obtained by filling the lowest b-states can be used to define contractions and normal products.

Wick's theorem:
We can now state the Wick's theorem as following.

For a given reference state, **any product of N creation and/or annihilation operators $A_1A_2...A_N$ is equal to the sum of all possible terms obtained by contracting p pairs of operators ($0 \leqslant p \leqslant N/2$), by normal ordering the remaining ones and by affecting each term by the sign of the permutation required to bring together the contracted operators.** That is,

$$\begin{aligned} A_1A_2...A_N &= :A_1A_2...A_N: \\ &+ \sum :A_1A_2...\overbrace{A_i...A_j}...A_N: \\ &+ \sum :A_1A_2...\overbrace{A_i...A_j...A_k...A_l}...A_N: \\ &+ \sum :A_1A_2...\overbrace{A_i...A_j...A_k...A_l...A_p...A_q}...A_N: \\ &+ \ldots . \end{aligned} \tag{B.9}$$

B.1.1 Wick's theorem for a two-body operator

Let us apply (B.9) to a two-body operator $a_i^\dagger a_k^\dagger a_j a_l$. Contraction and normal products are taken with respect to the reference state $|\phi\rangle = \prod_{i=1}^{A} a_i^\dagger|0\rangle = \prod_h a_h^\dagger|0\rangle$.

$$\begin{aligned} a_i^\dagger a_k^\dagger a_j a_l &= \overbrace{a_i^\dagger a_k^\dagger a_j a_l} - \overbrace{a_i^\dagger a_j a_k^\dagger a_l} + \overbrace{a_i^\dagger a_l a_k^\dagger a_j} \\ &+ \overbrace{a_i^\dagger a_k^\dagger}: a_j a_l: + \overbrace{a_j a_l}: a_i^\dagger a_k^\dagger: \\ &- \overbrace{a_i^\dagger a_j}: a_k^\dagger a_l: - \overbrace{a_k^\dagger a_l}: a_i^\dagger a_j: \\ &+ \overbrace{a_i^\dagger a_l}: a_k^\dagger a_j: + \overbrace{a_k^\dagger a_j}: a_i^\dagger a_l: \\ &+ : a_i^\dagger a_k^\dagger a_j a_l: \ . \end{aligned} \tag{B.10}$$

Since the Slater determinant $|\phi\rangle = \prod_{i=1}^{A} a_i^\dagger|0\rangle$ has a good particle number, we have,

$$\overbrace{a_i^\dagger a_j^\dagger} = \overbrace{a_i a_j} = 0 \ . \tag{B.11}$$

Thus, Eq. (B.10) reduces to,

$$\begin{aligned} a_i^\dagger a_k^\dagger a_j a_l \;=\; & - \overbracket{a_i^\dagger a_j} \overbracket{a_k^\dagger a_l} + \overbracket{a_i^\dagger a_l} \overbracket{a_k^\dagger a_j} \\ & - \overbracket{a_i^\dagger a_j} : a_k^\dagger a_l : \; - \overbracket{a_k^\dagger a_l} : a_i^\dagger a_j : \\ & + \overbracket{a_i^\dagger a_l} : a_k^\dagger a_j : \; + \overbracket{a_k^\dagger a_j} : a_i^\dagger a_l : \\ & + : a_i^\dagger a_k^\dagger a_j a_l : \; . \end{aligned} \tag{B.12}$$

B.1.2 Wick's theorem for a three-body operator

Let us now apply (B.9) to a three-body operator $a_i^\dagger a_j^\dagger a_k^\dagger a_n a_m a_l$. Again we use the fact that the particle number is a good quantum number.

$$\begin{aligned} a_i^\dagger a_j^\dagger a_k^\dagger a_n a_m a_l \;=\; & \overbracket{a_k^\dagger a_n} \overbracket{a_j^\dagger a_m} \overbracket{a_i^\dagger a_l} - \overbracket{a_k^\dagger a_n} \overbracket{a_j^\dagger a_l} \overbracket{a_i^\dagger a_m} - \overbracket{a_k^\dagger a_m} \overbracket{a_j^\dagger a_n} \overbracket{a_i^\dagger a_l} \\ & + \overbracket{a_k^\dagger a_m} \overbracket{a_j^\dagger a_l} \overbracket{a_i^\dagger a_n} - \overbracket{a_k^\dagger a_l} \overbracket{a_j^\dagger a_m} \overbracket{a_i^\dagger a_n} + \overbracket{a_k^\dagger a_l} \overbracket{a_j^\dagger a_n} \overbracket{a_i^\dagger a_m} \\ & + \overbracket{a_k^\dagger a_n} \overbracket{a_j^\dagger a_m} : a_i^\dagger a_l : \; + \overbracket{a_k^\dagger a_n} \overbracket{a_i^\dagger a_l} : a_j^\dagger a_m : \; + \overbracket{a_j^\dagger a_m} \overbracket{a_i^\dagger a_l} : a_k^\dagger a_n : \\ & - \overbracket{a_k^\dagger a_n} \overbracket{a_j^\dagger a_l} : a_i^\dagger a_m : \; - \overbracket{a_k^\dagger a_n} \overbracket{a_i^\dagger a_m} : a_j^\dagger a_l : \; - \overbracket{a_j^\dagger a_l} \overbracket{a_i^\dagger a_m} : a_k^\dagger a_n : \\ & - \overbracket{a_k^\dagger a_m} \overbracket{a_j^\dagger a_n} : a_i^\dagger a_l : \; - \overbracket{a_k^\dagger a_m} \overbracket{a_i^\dagger a_l} : a_j^\dagger a_n : \; - \overbracket{a_j^\dagger a_n} \overbracket{a_i^\dagger a_l} : a_k^\dagger a_m : \\ & + \overbracket{a_k^\dagger a_m} \overbracket{a_j^\dagger a_l} : a_i^\dagger a_n : \; + \overbracket{a_k^\dagger a_m} \overbracket{a_i^\dagger a_n} : a_j^\dagger a_l : \; + \overbracket{a_j^\dagger a_l} \overbracket{a_i^\dagger a_n} : a_k^\dagger a_m : \\ & - \overbracket{a_k^\dagger a_l} \overbracket{a_j^\dagger a_m} : a_i^\dagger a_n : \; - \overbracket{a_k^\dagger a_l} \overbracket{a_i^\dagger a_n} : a_j^\dagger a_m : \; - \overbracket{a_j^\dagger a_m} \overbracket{a_i^\dagger a_n} : a_k^\dagger a_l : \\ & + \overbracket{a_k^\dagger a_l} \overbracket{a_j^\dagger a_n} : a_i^\dagger a_m : \; + \overbracket{a_k^\dagger a_l} \overbracket{a_i^\dagger a_m} : a_j^\dagger a_n : \; + \overbracket{a_j^\dagger a_n} \overbracket{a_i^\dagger a_m} : a_k^\dagger a_l : \\ & + \overbracket{a_k^\dagger a_n} : a_i^\dagger a_j^\dagger a_m a_l : \; - \overbracket{a_k^\dagger a_m} : a_i^\dagger a_j^\dagger a_n a_l : \; + \overbracket{a_k^\dagger a_l} : a_i^\dagger a_j^\dagger a_n a_m : \\ & - \overbracket{a_j^\dagger a_n} : a_i^\dagger a_k^\dagger a_m a_l : \; + \overbracket{a_j^\dagger a_m} : a_i^\dagger a_k^\dagger a_n a_l : \; - \overbracket{a_j^\dagger a_l} : a_i^\dagger a_k^\dagger a_n a_m : \\ & + \overbracket{a_i^\dagger a_n} : a_j^\dagger a_k^\dagger a_m a_l : \; - \overbracket{a_i^\dagger a_m} : a_j^\dagger a_k^\dagger a_n a_l : \; + \overbracket{a_i^\dagger a_l} : a_j^\dagger a_k^\dagger a_n a_m : \\ & + : a_i^\dagger a_j^\dagger a_k^\dagger a_n a_m a_l : \; . \end{aligned} \tag{B.13}$$

B.2 Two-body correlation matrix σ

Let us show that there exists a matrix σ such that the two-body density $\rho^{[2]}$ can be written as,

$$\begin{aligned} \rho^{[2]}_{li,jk} &\equiv \langle\Psi|a_i^\dagger a_k^\dagger a_j a_l|\Psi\rangle \\ &= \rho_{li}\rho_{jk} - \rho_{lk}\rho_{ji} + \sigma_{il,kj} \end{aligned} \tag{B.14}$$

where $\rho_{li} = \langle\Psi|a_i^\dagger a_l|\Psi\rangle$ is the one-body density matrix.
Making use of Wick's theorem (B.12) with respect to $|\phi\rangle$, we obtain,

$$\begin{aligned} \rho^{[2]}_{li,jk} &\equiv \langle\Psi|a_i^\dagger a_k^\dagger a_j a_l|\Psi\rangle \\ &= - \overbrace{a_i^\dagger a_j}\overbrace{a_k^\dagger a_l} + \overbrace{a_i^\dagger a_l}\overbrace{a_k^\dagger a_j} \\ &\quad - \overbrace{a_i^\dagger a_j} : a_k^\dagger a_l : - \overbrace{a_k^\dagger a_l}\,\langle\Psi| : a_i^\dagger a_j : |\Psi\rangle \\ &\quad + \overbrace{a_i^\dagger a_l}\,\langle\Psi| : a_k^\dagger a_j : |\Psi\rangle + \overbrace{a_k^\dagger a_j}\,\langle\Psi| : a_i^\dagger a_l : |\Psi\rangle \\ &\quad + \langle\Psi| : a_i^\dagger a_k^\dagger a_j a_l : |\Psi\rangle \ , \end{aligned} \tag{B.15}$$

Since $\overbrace{a_i^\dagger a_j} = \langle\phi|a_i^\dagger a_j|\phi\rangle$ is a number, taking the expectation value of Eq. (B.5) in the correlated state $|\Psi\rangle$, leads to $\overbrace{a_i^\dagger a_j} = \langle\Psi|a_i^\dagger a_j|\Psi\rangle - \langle\Psi| : a_i^\dagger a_j : |\Psi\rangle$. We inject this expression into Eq. (B.15) to finally get,

$$\begin{aligned} \rho^{[2]}_{li,jk} &= \langle\Psi|a_i^\dagger a_k^\dagger a_j a_l|\Psi\rangle \\ &= \langle\Psi|a_i^\dagger a_l|\Psi\rangle\langle\Psi|a_k^\dagger a_j|\Psi\rangle - \langle\Psi|a_i^\dagger a_j|\Psi\rangle\langle\Psi|a_k^\dagger a_l|\Psi\rangle \\ &\quad + \langle\Psi| : a_i^\dagger a_k^\dagger a_j a_l : |\Psi\rangle - \langle\Psi| : a_i^\dagger a_l : |\Psi\rangle\langle\Psi| : a_k^\dagger a_j : |\Psi\rangle + \langle\Psi| : a_i^\dagger a_j : |\Psi\rangle\langle\Psi| : a_k^\dagger a_l : |\Psi\rangle \\ &\equiv \rho_{li}\rho_{jk} - \rho_{lk}\rho_{ji} + \sigma_{il,kj} \ , \end{aligned} \tag{B.16}$$

where,

$$\boxed{\sigma_{il,kj} = \langle\Psi| : a_i^\dagger a_k^\dagger a_j a_l : |\Psi\rangle - \langle\Psi| : a_i^\dagger a_l : |\Psi\rangle\langle\Psi| : a_k^\dagger a_j : |\Psi\rangle + \langle\Psi| : a_i^\dagger a_j : |\Psi\rangle\langle\Psi| : a_k^\dagger a_l : |\Psi\rangle} \tag{B.17}$$

is the two-body correlation matrix.
This can be written in a more compact way as,

$$\begin{aligned} \rho^{[2]}_{1'1,2'2} &\equiv \langle\Psi|a_1^\dagger a_2^\dagger a_{2'} a_{1'}|\Psi\rangle \\ &= (1 - P_{12})\rho_{1'1}\rho_{2'2} + \sigma_{11',22'} \ , \end{aligned} \tag{B.18}$$

with

$$\sigma_{11',22'} = \langle\Psi| : a_1^\dagger a_2^\dagger a_{2'} a_{1'} : |\Psi\rangle - (1 - P_{12}) \langle\Psi| : a_1^\dagger a_{1'} : |\Psi\rangle \langle\Psi| : a_2^\dagger a_{2'} : |\Psi\rangle \ . \tag{B.19}$$

B.3 Three-body correlation matrix χ

Similarly we can use Wick's theorem (B.13) for a three-body operator to show that,

$$\begin{aligned}
\rho^{[3]}_{li,jk} &\equiv \langle\Psi|a_i^\dagger a_j^\dagger a_k^\dagger a_n a_m a_l|\Psi\rangle \\
&= \rho_{nk}\rho_{mj}\rho_{li} - \rho_{nk}\rho_{mi}\rho_{lj} - \rho_{mk}\rho_{nj}\rho_{li} + \rho_{mk}\rho_{ni}\rho_{lj} - \rho_{ni}\rho_{mj}\rho_{lk} + \rho_{nj}\rho_{mi}\rho_{lk} \\
&\quad + \rho_{nk}\sigma_{il,jm} - \rho_{nj}\sigma_{im,kl} - \rho_{ni}\sigma_{kl,jm} \\
&\quad + \rho_{mj}\sigma_{il,kn} - \rho_{mi}\sigma_{jl,kn} - \rho_{mk}\sigma_{il,jn} \\
&\quad + \rho_{li}\sigma_{jm,kn} - \rho_{lj}\sigma_{im,kn} - \rho_{lk}\sigma_{jm,in} \\
&\quad + \chi_{il,jm,kn} \ ,
\end{aligned} \tag{B.20}$$

where,

$$\begin{aligned}
\chi_{il,jm,kn} &= 2\Big(\langle\Psi| : a_i^\dagger a_l : \Psi\rangle \langle\Psi| : a_j^\dagger a_m : |\Psi\rangle \langle\Psi| : a_k^\dagger a_n : |\Psi\rangle \\
&\quad - \langle\Psi| : a_i^\dagger a_l : \Psi\rangle \langle\Psi| : a_j^\dagger a_n : |\Psi\rangle \langle\Psi| : a_k^\dagger a_m : |\Psi\rangle \\
&\quad - \langle\Psi| : a_i^\dagger a_m : \Psi\rangle \langle\Psi| : a_j^\dagger a_l : |\Psi\rangle \langle\Psi| : a_k^\dagger a_n : |\Psi\rangle \\
&\quad - \langle\Psi| : a_i^\dagger a_n : \Psi\rangle \langle\Psi| : a_j^\dagger a_l : |\Psi\rangle \langle\Psi| : a_k^\dagger a_m : |\Psi\rangle \\
&\quad + \langle\Psi| : a_i^\dagger a_n : \Psi\rangle \langle\Psi| : a_j^\dagger a_l : |\Psi\rangle \langle\Psi| : a_k^\dagger a_m : |\Psi\rangle \\
&\quad + \langle\Psi| : a_i^\dagger a_m : \Psi\rangle \langle\Psi| : a_j^\dagger a_n : |\Psi\rangle \langle\Psi| : a_k^\dagger a_l : |\Psi\rangle \Big) \\
&\quad - \langle\Psi| : a_i^\dagger a_l : |\Psi\rangle \langle\Psi| : a_j^\dagger a_k^\dagger a_n a_m : |\Psi\rangle + \langle\Psi| : a_j^\dagger a_l : |\Psi\rangle \langle\Psi| : a_i^\dagger a_k^\dagger a_n a_m : |\Psi\rangle \\
&\qquad + \langle\Psi| : a_k^\dagger a_l : |\Psi\rangle \langle\Psi| : a_j^\dagger a_i^\dagger a_n a_m : |\Psi\rangle \\
&\quad - \langle\Psi| : a_j^\dagger a_m : |\Psi\rangle \langle\Psi| : a_i^\dagger a_k^\dagger a_n a_l : |\Psi\rangle + \langle\Psi| : a_k^\dagger a_m : |\Psi\rangle \langle\Psi| : a_i^\dagger a_j^\dagger a_n a_l : |\Psi\rangle \\
&\qquad + \langle\Psi| : a_i^\dagger a_m : |\Psi\rangle \langle\Psi| : a_j^\dagger a_k^\dagger a_n a_l : |\Psi\rangle \\
&\quad - \langle\Psi| : a_k^\dagger a_n : |\Psi\rangle \langle\Psi| : a_i^\dagger a_j^\dagger a_m a_l : |\Psi\rangle + \langle\Psi| : a_i^\dagger a_n : |\Psi\rangle \langle\Psi| : a_k^\dagger a_j^\dagger a_m a_l : |\Psi\rangle \\
&\qquad + \langle\Psi| : a_j^\dagger a_n : |\Psi\rangle \langle\Psi| : a_i^\dagger a_k^\dagger a_m a_l : |\Psi\rangle \\
&\quad + \langle\Psi| : a_i^\dagger a_j^\dagger a_k^\dagger a_n a_m a_l : |\Psi\rangle \ .
\end{aligned} \tag{B.21}$$

That is,

$$\begin{aligned}\rho^{[3]}_{1'1,2'2,3'3} &\equiv \langle\Psi|a_1^\dagger a_2^\dagger a_3^\dagger a_{3'}a_{2'}a_{1'}|\Psi\rangle \\ &= (1-P_{12}-P_{13})(1-P_{23})\rho_{1'1}\rho_{2'2}\rho_{3'3} \\ &\quad +(1-P_{12}-P_{13})\rho_{1'1}\sigma_{22',33'}+(1-P_{12}-P_{23})\rho_{2'2}\sigma_{11',33'}+(1-P_{13}-P_{23})\rho_{3'3}\sigma_{11',22'} \\ &\quad +\chi_{11',22',33'}\ , \end{aligned} \tag{B.22}$$

where

$$\begin{aligned}\chi_{11',22',33'} &= 2(1-P_{12}-P_{13})(1-P_{23})\,\langle\Psi|:a_1^\dagger a_{1'}:\Psi\rangle\,\langle\Psi|:a_2^\dagger a_{2'}:|\Psi\rangle\,\langle\Psi|:a_3^\dagger a_{3'}:|\Psi\rangle \\ &\quad -(1-P_{12}-P_{13})\,\langle\Psi|:a_1^\dagger a_{1'}:|\Psi\rangle\,\langle\Psi|:a_2^\dagger a_3^\dagger a_{3'}a_{2'}:|\Psi\rangle \\ &\quad -(1-P_{12}-P_{23})\,\langle\Psi|:a_2^\dagger a_{2'}:|\Psi\rangle\,\langle\Psi|:a_1^\dagger a_3^\dagger a_{3'}a_{1'}:|\Psi\rangle \\ &\quad -(1-P_{13}-P_{23})\,\langle\Psi|:a_3^\dagger a_{3'}:|\Psi\rangle\,\langle\Psi|:a_1^\dagger a_2^\dagger a_{2'}a_{1'}:|\Psi\rangle \\ &\quad +\langle\Psi|:a_1^\dagger a_2^\dagger a_3^\dagger a_{3'}a_{2'}a_{1'}:|\Psi\rangle\ . \end{aligned} \tag{B.23}$$

Appendix C

Practical calculations of the densities and the source term $G[\sigma]$

C.1 Construction of the many-body wave function in the mp-mh approach

In the mp-mh approach, the nuclear states $|\Psi\rangle$ are explicitly characterized by a good parity p, and projection J_z of the total angular momentum J on the symmetry axis. The rotational invariance is implicitly preserved by restricting the configuration mixing to Slater determinants ensuring the conservation of J as good quantum number. These Slater determinants are practically classified into blocks characterized by a certain projection J_z and parity p. In the present appendix, we focus on the description of the ground-state of even-even nuclei, characterized by $J = K = 0$. In this case, the blocks of configurations to be considered are the followings.

- **Block (0)** containing all the configurations $\alpha \equiv (\alpha_\pi \alpha_\nu)$ with $\boldsymbol{K(\alpha_\pi) = K(\alpha_\nu) = 0}$. In particular, this block groups configurations built from pairs of time-reversed single-particle states (BCS-type), as well as configurations built with more general pairs (HFB-type).

- **Blocks (−)** containing the configurations $\alpha \equiv (\alpha_\pi \alpha_\nu)$ characterized by $\boldsymbol{K(\alpha_\pi) < 0}$ and
  $K(\alpha_\nu) = -K(\alpha_\pi)$.

- **Blocks (+)** containing the configurations $\alpha \equiv (\alpha_\pi \alpha_\nu)$ characterized by $\boldsymbol{K(\alpha_\pi) > 0}$ and
  $K(\alpha_\nu) = -K(\alpha_\pi)$.

They are represented on Fig. (C.1).

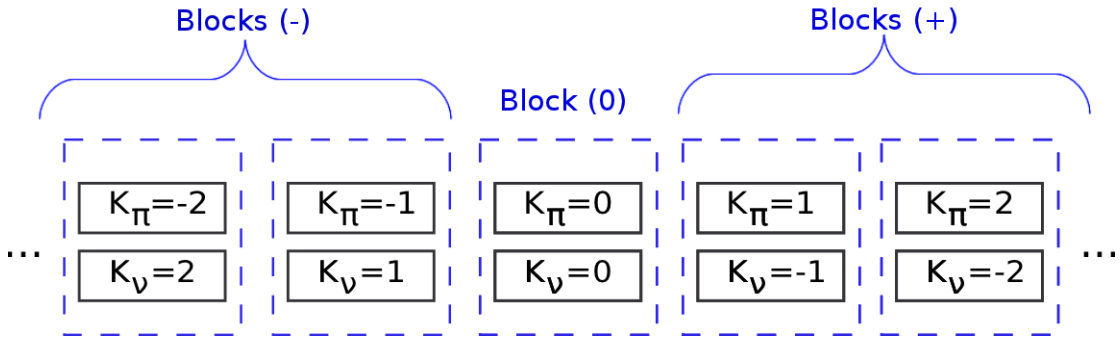

Figure C.1: Different configuration blocks for the case $K = K_\pi + K_\nu = 0$. Only blocks (0) and $(-)$ are explicitly constructed.

Practically all configurations belonging to the block (0) and to the blocks $(-)$ are explicitly constructed. In order to minimize at best the size of the matrix to diagonalize while solving the first variational equation, configuration blocks $(+)$ are never explicitly built. Indeed one can make use of time-reversal invariance to write the total wave function as,

$$\begin{aligned} |\Psi\rangle_{J=0,K=0,p} &= \sum_{\alpha\in(0)} A_\alpha |\phi_\alpha\rangle + \frac{1}{\sqrt{2}} \sum_{\alpha\in(-)} \left(A_\alpha |\phi_\alpha\rangle + \hat{T} A_\alpha |\phi_\alpha\rangle \right) \\ &= \sum_{\alpha\in(0)} A_\alpha |\phi_\alpha\rangle + \frac{1}{\sqrt{2}} \sum_{\alpha\in(-)} \left(A_\alpha |\phi_\alpha\rangle + A^*_\alpha \underbrace{\hat{T} |\phi_\alpha\rangle}_{\equiv |\overline{\phi_\alpha}\rangle} \right) . \end{aligned} \tag{C.1}$$

This wave function is time reversal invariant as it satisfies $\hat{T}|\Psi\rangle \equiv |\overline{\Psi}\rangle = |\Psi\rangle$. More precisely, in terms of proton and neutron configurations we have,

$$\begin{aligned} |\Psi\rangle_{J=0,K=0,p} = & \sum_{\substack{\alpha^0_\pi \\ K_{\alpha^0_\pi}=0}} \sum_{\substack{\alpha^0_\nu \\ K_{\alpha^0_\nu}=0}} A_{\alpha^0_\pi \alpha^0_\nu} |\phi_{\alpha^0_\pi}\rangle \otimes |\phi_{\alpha^0_\nu}\rangle \\ & + \frac{1}{\sqrt{2}} \sum_{\substack{\alpha_\pi \\ K_{\alpha_\pi}<0}} \sum_{\substack{\alpha_\nu \\ K_{\alpha_\nu}=-K_{\alpha_\pi}}} \left[A_{\alpha_\pi\alpha_\nu} |\phi_{\alpha_\pi}\rangle \otimes |\phi_{\alpha_\nu}\rangle + A^*_{\alpha_\pi\alpha_\nu} |\overline{\phi_{\alpha_\pi}}\rangle \otimes |\overline{\phi_{\alpha_\nu}}\rangle \right] . \end{aligned} \tag{C.2}$$

C.2 Calculation of the densities

Two types of densities are to be calculated:

- **Isospin-diagonal densities.**
  Let us write the wave function in a generic way [1] as $|\Psi\rangle = \sum_\alpha C_\alpha |\phi_\alpha\rangle$, and denote by $\tau = (\pi, \nu)$ the isospin. This type of density can be of one-body ($\rho_\tau^{[1]}$) or two-body ($\rho_\tau^{[2]}$) type. It can be expressed as,

$$\begin{aligned}\langle\Psi|\hat{\rho}_\tau^{[i]}|\Psi\rangle &= \sum_{\alpha\beta} C_\alpha^* C_\beta \langle\phi_\alpha|\hat{\rho}_\tau^{[i]}|\phi_\beta\rangle \\ &= \sum_{\alpha_\tau\alpha_{\tau'}}\sum_{\beta_\tau\beta_{\tau'}} C^*_{\alpha_\tau\alpha_{\tau'}} C_{\beta_\tau\beta_{\tau'}} \langle\phi_{\alpha_\tau}|\hat{\rho}_\tau^{[i]}|\phi_{\beta_\tau}\rangle \langle\phi_{\alpha_{\tau'}}|\phi_{\beta_{\tau'}}\rangle \\ &= \sum_{\alpha_\tau\alpha_{\tau'}}\sum_{\beta_\tau} C^*_{\alpha_\tau\alpha_{\tau'}} C_{\beta_\tau\alpha_{\tau'}} \langle\phi_{\alpha_\tau}|\hat{\rho}_\tau^{[i]}|\phi_{\beta_\tau}\rangle\end{aligned}$$

  where $i = (1, 2)$.
  The τ' configurations must therefore be identical. Since,

$$\begin{cases} K = K_{\alpha_\pi} + K_{\alpha_\nu} = K_{\beta_\pi} + K_{\beta_\nu} & \text{(C.3)} \\ p = p_{\alpha_\pi} \times p_{\alpha_\nu} = p_{\beta_\pi} \times p_{\beta_\nu}\ , & \text{(C.4)} \end{cases}$$

  this restricts the τ configurations to have identical projections $K_{\alpha_\tau} = K_{\beta_\tau}$ and parities $p_{\alpha_\tau} = p_{\beta_\tau}$. *Pure-proton and pure-neutron densities can therefore only couple Slater determinants belonging to the same block.*

- **Proton-neutron density.**
  Since the numbers of protons and neutrons are conversed, this type of density can only be of two-body type. Let us consider for instance,

$$\langle i_\pi j_\nu|\hat{\rho}^{[2]}_{\pi\nu}|k_\nu l_\pi\rangle = \langle\Psi|a^\dagger_{i_\pi}a^\dagger_{j_\nu}a_{k_\nu}a_{l_\pi}|\Psi\rangle = \sum_{\alpha_\pi\alpha_\nu}\sum_{\beta_\pi\beta_\nu} C^*_{\alpha_\pi\alpha_\nu} C_{\beta_\pi\beta_\nu} \langle\phi_{\alpha_\pi}|a^\dagger_{i_\pi}a_{l_\pi}|\phi_{\beta_\pi}\rangle \langle\phi_{\alpha_\nu}|a^\dagger_{j_\nu}a_{k_\nu}|\phi_{\beta_\nu}\rangle\ .$$

  We see that now both proton and neutron configurations in α and β can be different. Therefore $|\phi_\alpha\rangle$ *and* $|\phi_\beta\rangle$ *can belong to different configuration blocks.*

  Conditions (C.3) and (C.4) lead to,

$$\begin{cases} \underbrace{K_{\alpha_\pi} - K_{\beta_\pi}}_{\Delta_{K_\pi}} = -\ \underbrace{(K_{\alpha_\nu} - K_{\beta_\nu})}_{\Delta_{K_\nu}} & \text{(C.5)} \\ \underbrace{\dfrac{p_{\alpha_\pi}}{p_{\beta_\pi}}}_{\Delta_{p_\pi}} = \dfrac{p_{\beta_\nu}}{p_{\alpha_\nu}} = \underbrace{\dfrac{p_{\alpha_\nu}}{p_{\beta_\nu}}}_{\Delta_{p_\nu}}\ . & \text{(C.6)} \end{cases}$$

[1] C_α contains eventual $\frac{1}{\sqrt{2}}$ factors.

So that the only conditions to be fulfilled are,

$$\begin{cases} \Delta_{K_\pi} = m_{i_\pi} - m_{l_\pi} = m_{k_\nu} - m_{j_\nu} = -\Delta_{K_\nu} & \text{(C.7)} \\ \Delta_{p_\pi} = \dfrac{p_{i_\pi}}{p_{l_\pi}} = \dfrac{p_{k_\nu}}{p_{j_\nu}} = \Delta_{p_\nu} \ . & \text{(C.8)} \end{cases}$$

C.2.1 Conventions and notations

The single-particle states $a^\dagger_{i(j,k,l...)}$ (we omit the index τ) can be either states $a^\dagger_\mu = a^\dagger_{\kappa_\mu,m_\mu}$ with positive projection $m_\mu = j_{z_\mu}$ (κ_μ = other quantum numbers) or time-reversed states $\bar{a}^\dagger_\mu = (-)^{l_\mu+j_\mu-m_\mu} a^\dagger_{\kappa_\mu,-\mu}$.
Let us therefore define in a generic way $\widetilde{a}^\dagger_i$ as,

$$\widetilde{a}^\dagger_i = \begin{cases} \bar{a}^\dagger_\mu & \text{, if } i = \mu > 0 \\ a^\dagger_\mu & \text{, if } i = \bar{\mu} < 0 \ . \end{cases} \tag{C.9}$$

Practically, the configurations $|\phi_\alpha\rangle$ are built with the following conventions,

- The orbitals are ordered by increasing energies.
- If $|\phi_\alpha\rangle$ contains pairs of time-reversed single-particle states, the particle in the reversed state is created first.

For instance,

$$|\phi_\alpha\rangle = a^\dagger_{\mu_1} a^\dagger_{\mu_2} \overline{a}^\dagger_{\mu_2} a^\dagger_{\mu_3} |0\rangle \ . \tag{C.10}$$

The configuration obtained after applying a time-reversal transformation is,

$$\begin{aligned} |\overline{\phi_\alpha}\rangle \equiv \hat{T} |\phi_\alpha\rangle &= \left(\hat{T} a^\dagger_{\mu_1} \hat{T}^\dagger_s\right) \left(\hat{T} a^\dagger_{\mu_2} \hat{T}^\dagger_s\right) \left(\hat{T} \overline{a}^\dagger_{\mu_2} \hat{T}^\dagger_s\right) \left(\hat{T} a^\dagger_{\mu_3} \hat{T}^\dagger_s\right) \\ &= \left(\overline{a}^\dagger_{\mu_1}\right) \left(\overline{a}^\dagger_{\mu_2}\right) \left(-a^\dagger_{\mu_2}\right) \left(\overline{a}^\dagger_{\mu_3}\right) \ . \end{aligned} \tag{C.11}$$

If $\bar{N}_\alpha$ is the number of time-reversed states occupied in the configuration α, we note $\overline{\theta}_\alpha = (-)^{\bar{N}_\alpha}$ the phase obtained after applying time reversal transformation to $|\phi_\alpha\rangle$. (In the previous example, $\overline{\theta}_\alpha = (-)$).

Let us now define $|\widetilde{\phi_\alpha}\rangle$, the state obtained after time-reversal transformation of $|\phi_\alpha\rangle$ *without* the phase $\overline{\theta}_\alpha$. That is,

$$|\overline{\phi_\alpha}\rangle = \overline{\theta}_\alpha \, |\widetilde{\phi_\alpha}\rangle \ . \tag{C.12}$$

In the previous example,

$$\begin{aligned} |\overline{\phi_\alpha}\rangle &= (-) \underbrace{\overline{a}^\dagger_{\mu_1} \overline{a}^\dagger_{\mu_2} a^\dagger_{\mu_2} \overline{a}^\dagger_{\mu_3}} \\ &= (-) \, |\widetilde{\phi_\alpha}\rangle \ . \end{aligned} \tag{C.13}$$

In terms of i-states, if

$$|\phi_\alpha\rangle = a^\dagger_{i_1} a^\dagger_{i_2} ... a^\dagger_{i_N} |0\rangle \ , \tag{C.14}$$

then,

$$|\widetilde{\phi_\alpha}\rangle = \widetilde{a}^\dagger_{i_1} \widetilde{a}^\dagger_{i_2} ... \widetilde{a}^\dagger_{i_N} |0\rangle \ . \tag{C.15}$$

One notices that the pairs of reversed single-particle states $(\mu, \overline{\mu})$ in $|\widetilde{\phi_\alpha}\rangle$ are not ordered as in the conventions previously stated.

We therefore define,

$$|\widetilde{\phi_\alpha}^R\rangle = \theta^R_\alpha |\widetilde{\phi_\alpha}\rangle \ , \tag{C.16}$$

as the state corresponding to $|\widetilde{\phi_\alpha}\rangle$, with pairs that are correctly ordered. θ^R_α is the phase appearing when reordering the pairs.

In the previous example,

$$\begin{aligned} |\widetilde{\phi_\alpha}^R\rangle &= \overline{a}^\dagger_{\mu_1} a^\dagger_{\mu_2} \overline{a}^\dagger_{\mu_2} \overline{a}^\dagger_{\mu_3} \\ &= (-) \overline{a}^\dagger_{\mu_1} a^\dagger_{\mu_2} \overline{a}^\dagger_{\mu_2} \overline{a}^\dagger_{\mu_3} \\ &= (-) |\widetilde{\phi_\alpha}\rangle \ . \end{aligned} \tag{C.17}$$

In summary we have,

$$\boxed{\begin{aligned} \hat{T} |\phi_\alpha\rangle \equiv |\overline{\phi_\alpha}\rangle &= \overline{\theta}_\alpha |\widetilde{\phi_\alpha}\rangle \\ &= \overline{\theta}_\alpha \theta^R_\alpha |\widetilde{\phi_\alpha}^R\rangle \ . \end{aligned}}$$

C.2.2 Two-body density of same isospin

Let us consider for instance an element $\rho^{[2]}_{l_\pi i_\pi, k_\pi j_\pi} = \langle \Psi | a^\dagger_{i_\pi} a^\dagger_{j_\pi} a_{k_\pi} a_{l_\pi} | \Psi \rangle$ of the two-body proton density. Using expression (C.2) for the wave function, we get,

$$\begin{aligned} \langle \Psi | a^\dagger_{i_\pi} a^\dagger_{j_\pi} a_{k_\pi} a_{l_\pi} | \Psi \rangle \ = \ & \sum_{\substack{\alpha^0_\pi \\ K_{\alpha^0_\pi}=0}} \sum_{\substack{\beta^0_\pi \\ K_{\beta^0_\pi}=0}} \sum_{\substack{\alpha^0_\nu \\ K_{\alpha^0_\nu}=0}} \underbrace{A^*_{\alpha^0_\pi \alpha^0_\nu} A_{\beta^0_\pi \alpha^0_\nu} \langle \phi_{\alpha^0_\pi} | a^\dagger_{i_\pi} a^\dagger_{j_\pi} a_{k_\pi} a_{l_\pi} | \phi_{\beta^0_\pi} \rangle}_{(a)} \\ & + \frac{1}{2} \sum_{\substack{\alpha_\pi \\ K_{\alpha_\pi}<0}} \sum_{\substack{\beta_\pi \\ K_{\beta_\pi}=K_{\alpha_\pi}}} \sum_{\substack{\alpha_\nu \\ K_{\alpha_\nu}=-K_{\alpha_\pi}}} \\ & \left(\underbrace{A^*_{\alpha_\pi \alpha_\nu} A_{\beta_\pi \alpha_\nu} \langle \phi_{\alpha_\pi} | a^\dagger_{i_\pi} a^\dagger_{j_\pi} a_{k_\pi} a_{l_\pi} | \phi_{\beta_\pi} \rangle}_{(b)} + \underbrace{A_{\alpha_\pi \alpha_\nu} A^*_{\beta_\pi \alpha_\nu} \langle \overline{\phi_{\alpha_\pi}} | a^\dagger_{i_\pi} a^\dagger_{j_\pi} a_{k_\pi} a_{l_\pi} | \overline{\phi_{\beta_\pi}} \rangle}_{(c)} \right) \end{aligned} \tag{C.18}$$

When, for a given quadruplet $Q \equiv (i,j,k,l)$ (we omit the π sub-index), there exists a non-zero contribution $\langle\phi_{\alpha_\pi}|a_i^\dagger a_j^\dagger a_k a_l|\phi_{\beta_\pi}\rangle$ from (b) to $\rho^{[2]}(Q)$, the corresponding contribution $\langle\overline{\phi_{\alpha_\pi}}|a_i^\dagger a_j^\dagger a_k a_l|\overline{\phi_{\beta_\pi}}\rangle$ from (c) to $\rho^{[2]}(Q)$ is zero, and the couplings $\langle\phi_{\alpha_\pi^0}|a_i^\dagger a_j^\dagger a_k a_l|\phi_{\beta_\pi^0}\rangle$ from (a) are built explicitly if non zero.
However the coupling $\langle\overline{\phi_{\alpha_\pi}}|\widetilde{a}_i^\dagger\widetilde{a}_j^\dagger\widetilde{a}_k\widetilde{a}_l|\overline{\phi_{\beta_\pi}}\rangle$ can be non zero and will be ignored by the code since the time-reversed configurations are not explicitly built. If the contribution from (a) to $\rho^{[2]}(\widetilde{Q}) = \langle\Psi|\widetilde{a}_{i_\pi}^\dagger\widetilde{a}_{j_\pi}^\dagger\widetilde{a}_{k_\pi}\widetilde{a}_{l_\pi}|\Psi\rangle$ is non zero, this means that $\rho^{[2]}(\widetilde{Q})$ will be partially filled.
One therefore needs to implicitly take into account the contributions from (c). That is, for every coupling $\langle\phi_{\alpha_\pi}|a_i^\dagger a_j^\dagger a_k a_l|\phi_{\beta_\pi}\rangle = \varphi_{ijkl}^{\alpha\beta} \neq 0$ from (b) participating to $\rho^{[2]}(Q)$, one needs to add by hand the contribution from (c) to $\rho^{[2]}(\widetilde{Q})$. This contribution is equal to,

$$\begin{aligned}
& A_{\alpha_\pi\alpha_\nu}A^*_{\beta_\pi\alpha_\nu}\,\langle\overline{\phi_{\alpha_\pi}}|\widetilde{a}_i^\dagger\widetilde{a}_j^\dagger\widetilde{a}_k\widetilde{a}_l|\overline{\phi_{\beta_\pi}}\rangle \\
= \;& A_{\alpha_\pi\alpha_\nu}A^*_{\beta_\pi\alpha_\nu}\overline{\theta}_{\alpha_\pi}\overline{\theta}_{\beta_\pi} \underbrace{\langle\widetilde{\phi_{\alpha_\pi}}|\widetilde{a}_i^\dagger\widetilde{a}_j^\dagger\widetilde{a}_k\widetilde{a}_l|\widetilde{\phi_{\beta_\pi}}\rangle}_{\langle\phi_{\alpha_\pi}|a_i^\dagger a_j^\dagger a_{k_\pi}a_l|\phi_{\beta_\pi}\rangle \text{ (same ordering)}} \\
= \;& A_{\alpha_\pi\alpha_\nu}A^*_{\beta_\pi\alpha_\nu}\overline{\theta}_{\alpha_\pi}\overline{\theta}_{\beta_\pi}\varphi_{ijkl}^{\alpha\beta}\,. \qquad \text{(C.19)}
\end{aligned}$$

C.2.3 One-body densities

One-body densities being either of proton or neutron type, the same reasoning is applied for their calculation.

C.2.4 Two-body proton-neutron density

As shown previously, the situation gets more complicated when calculating the two-body density of proton-neutron type, since this type of operator can couple configurations belonging to different blocks.

Let us consider for instance the following element: $\langle\Psi|a_{i_\pi}^\dagger a_{j_\nu}^\dagger a_{k_\nu}a_{l_\pi}|\Psi\rangle$. Using expression (C.2)

for the wave function, we have,

$$\langle\Psi_{K=0}|a^\dagger_{i_\pi}a^\dagger_{j_\nu}a_{k_\nu}a_{l_\pi}|\Psi_{K=0}\rangle =$$

$$\frac{1}{2}\sum_{\substack{\alpha_\pi\\K_{\alpha_\pi}<0}}\sum_{\substack{\alpha_\nu\\K_{\alpha_\nu}=-K_{\alpha_\pi}}}\sum_{\substack{\beta_\pi\\K_{\beta_\pi}<0}}\sum_{\substack{\beta_\nu\\K_{\beta_\nu}=-K_{\beta_\pi}}} A^*_{\alpha_\pi\alpha_\nu}A_{\beta_\pi\beta_\nu}\,\langle\Phi_{\alpha_\pi}|a^\dagger_{i_\pi}a_{l_\pi}|\Phi_{\beta_\pi}\rangle\,\langle\Phi_{\alpha_\nu}|a^\dagger_{j_\nu}a_{k_\nu}|\Phi_{\beta_\nu}\rangle \tag{C.20a}$$

$$+\frac{1}{2}\sum_{\substack{\alpha_\pi\\K_{\alpha_\pi}<0}}\sum_{\substack{\alpha_\nu\\K_{\alpha_\nu}=-K_{\alpha_\pi}}}\sum_{\substack{\beta_\pi\\K_{\beta_\pi}<0}}\sum_{\substack{\beta_\nu\\K_{\beta_\nu}=-K_{\beta_\pi}}} A_{\alpha_\pi\alpha_\nu}A^*_{\beta_\pi\beta_\nu}\,\langle\overline{\Phi_{\alpha_\pi}}|a^\dagger_{i_\pi}a_{l_\pi}|\overline{\Phi_{\beta_\pi}}\rangle\,\langle\overline{\Phi_{\alpha_\nu}}|a^\dagger_{j_\nu}a_{k_\nu}|\overline{\Phi_{\beta_\nu}}\rangle \tag{C.20b}$$

$$+\frac{1}{2}\sum_{\substack{\alpha_\pi\\K_{\alpha_\pi}<0}}\sum_{\substack{\alpha_\nu\\K_{\alpha_\nu}=-K_{\alpha_\pi}}}\sum_{\substack{\beta_\pi\\K_{\beta_\pi}<0}}\sum_{\substack{\beta_\nu\\K_{\beta_\nu}=-K_{\beta_\pi}}} A^*_{\alpha_\pi\alpha_\nu}A^*_{\beta_\pi\beta_\nu}\,\langle\Phi_{\alpha_\pi}|a^\dagger_{i_\pi}a_{l_\pi}|\overline{\Phi_{\beta_\pi}}\rangle\,\langle\Phi_{\alpha_\nu}|a^\dagger_{j_\nu}a_{k_\nu}|\overline{\Phi_{\beta_\nu}}\rangle \tag{C.20c}$$

$$+\frac{1}{2}\sum_{\substack{\alpha_\pi\\K_{\alpha_\pi}<0}}\sum_{\substack{\alpha_\nu\\K_{\alpha_\nu}=-K_{\alpha_\pi}}}\sum_{\substack{\beta_\pi\\K_{\beta_\pi}<0}}\sum_{\substack{\beta_\nu\\K_{\beta_\nu}=-K_{\beta_\pi}}} A_{\alpha_\pi\alpha_\nu}A_{\beta_\pi\beta_\nu}\,\langle\overline{\Phi_{\alpha_\pi}}|a^\dagger_{i_\pi}a_{l_\pi}|\Phi_{\beta_\pi}\rangle\,\langle\overline{\Phi_{\alpha_\nu}}|a^\dagger_{j_\nu}a_{k_\nu}|\Phi_{\beta_\nu}\rangle \tag{C.20d}$$

$$+\frac{1}{\sqrt{2}}\sum_{\substack{\alpha_\pi\\K_{\alpha_\pi}<0}}\sum_{\substack{\alpha_\nu\\K_{\alpha_\nu}=-K_{\alpha_\pi}}}\sum_{\substack{\beta^0_\pi\\K_{\beta^0_\pi}=0}}\sum_{\substack{\beta^0_\nu\\K_{\beta^0_\nu}=0}} A^*_{\alpha_\pi\alpha_\nu}A_{\beta^0_\pi\beta^0_\nu}\,\langle\Phi_{\alpha_\pi}|a^\dagger_{i_\pi}a_{l_\pi}|\Phi_{\beta^0_\pi}\rangle\,\langle\Phi_{\alpha_\nu}|a^\dagger_{j_\nu}a_{k_\nu}|\Phi_{\beta^0_\nu}\rangle \tag{C.20e}$$

$$+\frac{1}{\sqrt{2}}\sum_{\substack{\alpha^0_\pi\\K_{\alpha^0_\pi}=0}}\sum_{\substack{\alpha^0_\nu\\K_{\alpha^0_\nu}=0}}\sum_{\substack{\beta_\pi\\K_{\beta_\pi}<0}}\sum_{\substack{\beta_\nu\\K_{\beta_\nu}=-K_{\beta_\pi}}} A^*_{\alpha^0_\pi\alpha^0_\nu}A_{\beta_\pi\beta_\nu}\,\langle\Phi_{\alpha^0_\pi}|a^\dagger_{i_\pi}a_{l_\pi}|\Phi_{\beta_\pi}\rangle\,\langle\Phi_{\alpha^0_\nu}|a^\dagger_{j_\nu}a_{k_\nu}|\Phi_{\beta_\nu}\rangle \tag{C.20f}$$

$$+\frac{1}{\sqrt{2}}\sum_{\substack{\alpha_\pi\\K_{\alpha_\pi}<0}}\sum_{\substack{\alpha_\nu\\K_{\alpha_\nu}=-K_{\alpha_\pi}}}\sum_{\substack{\beta^0_\pi\\K_{\beta^0_\pi}=0}}\sum_{\substack{\beta^0_\nu\\K_{\beta^0_\nu}=0}} A_{\alpha_\pi\alpha_\nu}A_{\beta^0_\pi\beta^0_\nu}\,\langle\overline{\Phi_{\alpha_\pi}}|a^\dagger_{i_\pi}a_{l_\pi}|\Phi_{\beta^0_\pi}\rangle\,\langle\overline{\Phi_{\alpha_\nu}}|a^\dagger_{j_\nu}a_{k_\nu}|\Phi_{\beta^0_\nu}\rangle \tag{C.20g}$$

$$+\frac{1}{\sqrt{2}}\sum_{\substack{\alpha^0_\pi\\K_{\alpha^0_\pi}=0}}\sum_{\substack{\alpha^0_\nu\\K_{\alpha^0_\nu}=0}}\sum_{\substack{\beta_\pi\\K_{\beta_\pi}<0}}\sum_{\substack{\beta_\nu\\K_{\beta_\nu}=-K_{\beta_\pi}}} A^*_{\alpha^0_\pi\alpha^0_\nu}A^*_{\beta_\pi\beta_\nu}\,\langle\Phi_{\alpha^0_\pi}|a^\dagger_{i_\pi}a_{l_\pi}|\overline{\Phi_{\beta_\pi}}\rangle\,\langle\Phi_{\alpha^0_\nu}|a^\dagger_{j_\nu}a_{k_\nu}|\overline{\Phi_{\beta_\nu}}\rangle \tag{C.20h}$$

$$+\sum_{\substack{\alpha^0_\pi\\K_{\alpha^0_\pi}=0}}\sum_{\substack{\alpha^0_\nu\\K_{\alpha^0_\nu}=0}}\sum_{\substack{\beta^0_\pi\\K_{\beta^0_\pi}=0}}\sum_{\substack{\beta^0_\nu\\K_{\beta^0_\nu}=0}} A^*_{\alpha^0_\pi\alpha^0_\nu}A_{\beta^0_\pi\beta^0_\nu}\,\langle\Phi_{\alpha^0_\pi}|a^\dagger_{i_\pi}a_{l_\pi}|\Phi_{\beta^0_\pi}\rangle\,\langle\Phi_{\alpha^0_\nu}|a^\dagger_{j_\nu}a_{k_\nu}|\Phi_{\beta^0_\nu}\rangle \tag{C.20i}$$

All contributions involving time-reversed configurations, i.e. contributions from terms (C.20b), (C.20c), (C.20d), (C.20g) and (C.20h) have to be treated implicitly.

Contribution (C.20b) As for the two-body density of same isospin, contributions from (C.20b) can be deduced from (C.20a). That is, for every

$$A^*_{\alpha_\pi\alpha_\nu}A_{\beta_\pi\beta_\nu}\langle\Phi_{\alpha_\pi}|a^\dagger_{i_\pi}a_{l_\pi}|\Phi_{\beta_\pi}\rangle\langle\Phi_{\alpha_\nu}|a^\dagger_{j_\nu}a_{k_\nu}|\Phi_{\beta_\nu}\rangle = A^*_{\alpha_\pi\alpha_\nu}A_{\beta_\pi\beta_\nu}\varphi^{\alpha\beta}_{i_\pi l_\pi}\varphi^{\alpha\beta}_{j_\nu k_\nu} \neq 0$$

contributing to $\rho^{[2]}_{l_\pi i_\pi,k_\nu j_\nu}$, we need to add by hand the contribution from (C.20b) to $\rho^{[2]}_{\tilde{l}_\pi\tilde{i}_\pi,\tilde{k}_\nu\tilde{j}_\nu}$. This contribution is equal to,

$$A^*_{\alpha_\pi\alpha_\nu}A_{\beta_\pi\beta_\nu}\varphi^{\alpha\beta}_{i_\pi l_\pi}\varphi^{\alpha\beta}_{j_\nu k_\nu}\overline{\theta}_{\alpha_\pi}\overline{\theta}_{\alpha_\nu}\overline{\theta}_{\beta_\pi}\overline{\theta}_{\beta_\nu}$$

.

Contribution (C.20c) To calculate couplings of the type $\langle\Phi_{\alpha_\pi}|a^\dagger_{i_\pi}a_{l_\pi}|\overline{\Phi_{\beta_\pi}}\rangle$, we act the operators $a^\dagger_{i_\pi}a_{l_\pi}$ on $\langle\Phi_{\alpha_\pi}|$. This returns a phase $\varphi^\alpha_{perm_{i_\pi l_\pi}}$ (corresponding to the number of permutations applied) and a Slater determinant $\langle\widetilde{\phi_{\beta_\pi}}^R|$ ordered in the same way than the states explicitly constructed in the code. That is, by orbitals of increasing energy and if it contains pairs of single-particle time-reversed states the time-reversed one is created first. Therefore we have,

$$\begin{aligned}\langle\Phi_{\alpha_\pi}|a^\dagger_{i_\pi}a_{l_\pi}|\overline{\Phi_{\beta_\pi}}\rangle &= \varphi^\alpha_{perm_{i_\pi l_\pi}}\langle\widetilde{\phi_{\beta_\pi}}^R|\overline{\phi_{\beta_\pi}}\rangle \\ &= \varphi^\alpha_{perm_{i_\pi l_\pi}}\overline{\theta_{\beta_\pi}}\,\theta^R_{\beta_\pi}\underbrace{\langle\overline{\phi_{\beta_\pi}}|\overline{\phi_{\beta_\pi}}\rangle}_{=1}\,. \end{aligned} \tag{C.21}$$

Contribution (C.20d) For each non-zero contribution

$$A^*_{\alpha_\pi\alpha_\nu}A^*_{\beta_\pi\beta_\nu}\langle\Phi_{\alpha_\pi}|a^\dagger_{i_\pi}a_{l_\pi}|\overline{\Phi_{\beta_\pi}}\rangle\langle\Phi_{\alpha_\nu}|a^\dagger_{j_\nu}a_{k_\nu}|\overline{\Phi_{\beta_\nu}}\rangle = \varphi^\alpha_{perm_{i_\pi l_\pi}}\overline{\theta_{\beta_\pi}}\,\theta^R_{\beta_\pi}\varphi^\alpha_{perm_{j_\nu k_\nu}}\overline{\theta_{\beta_\nu}}\,\theta^R_{\beta_\nu}$$

from (C.20c), to $\rho^{[2]}_{l_\pi i_\pi,k_\nu j_\nu}$, we add the contribution from (C.20d) to $\rho^{[2]}_{\tilde{l}_\pi\tilde{i}_\pi,\tilde{k}_\nu\tilde{j}_\nu}$. It is equal to,

$$\begin{aligned} & A^*_{\alpha_\pi\alpha_\nu}A^*_{\beta_\pi\beta_\nu}\langle\overline{\Phi_{\alpha_\pi}}|\widetilde{a}^\dagger_{i_\pi}\widetilde{a}_{l_\pi}|\Phi_{\beta_\pi}\rangle\langle\overline{\Phi_{\alpha_\nu}}|\widetilde{a}^\dagger_{j_\nu}\widetilde{a}_{k_\nu}|\Phi_{\beta_\nu}\rangle \\ = & A^*_{\alpha_\pi\alpha_\nu}A^*_{\beta_\pi\beta_\nu}\overline{\theta}_{\alpha_\pi}\overline{\theta}_{\alpha_\nu}\langle\widetilde{\overline{\Phi_{\alpha_\pi}}}|\widetilde{a}^\dagger_{i_\pi}\widetilde{a}_{l_\pi}|\Phi_{\beta_\pi}\rangle\langle\widetilde{\overline{\Phi_{\alpha_\nu}}}|\widetilde{a}^\dagger_{j_\nu}\widetilde{a}_{k_\nu}|\Phi_{\beta_\nu}\rangle \\ = & A^*_{\alpha_\pi\alpha_\nu}A^*_{\beta_\pi\beta_\nu}\overline{\theta}_{\alpha_\pi}\overline{\theta}_{\alpha_\nu}\varphi^\alpha_{perm_{i_\pi l_\pi}}\langle\phi^R_{\beta_\pi}|\phi_{\beta_\pi}\rangle\varphi^\alpha_{perm_{j_\nu k_\nu}}\langle\phi^R_{\beta_\nu}|\phi_{\beta_\nu}\rangle \\ = & A^*_{\alpha_\pi\alpha_\nu}A^*_{\beta_\pi\beta_\nu}\overline{\theta}_{\alpha_\pi}\overline{\theta}_{\alpha_\nu}\varphi^\alpha_{perm_{i_\pi l_\pi}}\theta^R_{\beta_\pi}\varphi^\alpha_{perm_{j_\nu k_\nu}}\theta^R_{\beta_\nu}\,. \end{aligned} \tag{C.22}$$

where we introduced $|\phi^R_{\beta_\pi}\rangle = \theta^R_{\beta_\pi}|\phi_{\beta_\pi}\rangle$ which corresponds to the Slater β_π with the pairs of time-reversed states in inversed order compared to the conventions of the code.

Contribution (C.20g) For each non-zero contribution

$$A^*_{\alpha_\pi\alpha_\nu}A_{\beta^0_\pi\beta^0_\nu}\langle\Phi_{\alpha_\pi}|a^\dagger_{i_\pi}a_{l_\pi}|\Phi_{\beta^0_\pi}\rangle\langle\Phi_{\alpha_\nu}|a^\dagger_{j_\nu}a_{k_\nu}|\Phi_{\beta^0_\nu}\rangle = A^*_{\alpha_\pi\alpha_\nu}A_{\beta^0_\pi\beta^0_\nu}\varphi^{\alpha\beta^0}_{i_\pi l_\pi}\varphi^{\alpha\beta^0}_{j_\nu k_\nu}$$

from (C.20e) to $\rho^{[2]}_{l_\pi i_\pi, k_\nu j_\nu}$, we add the contribution from (C.20g) to $\rho^{[2]}_{\tilde{l}_\pi \tilde{i}_\pi, \tilde{k}_\nu \tilde{j}_\nu}$ using,

$$\langle \overline{\phi_{\alpha_\pi}} | \widetilde{a}^\dagger_{i_\pi} \widetilde{a}_{l_\pi} | \phi_{\beta^0_\pi} \rangle = \overline{\theta_{\alpha_\pi}} \underbrace{\langle \widetilde{\phi_{\alpha_\pi}} | \widetilde{a}^\dagger_{i_\pi} \widetilde{a}_{l_\pi}}_{\langle \phi_{\beta^0_\pi} | \theta^R_{\alpha_\pi} \varphi^{\alpha\beta^0}_{i_\pi l_\pi}} | \phi_{\beta^0_\pi} \rangle = \overline{\theta_{\alpha_\pi}} \theta^R_{\alpha_\pi} \varphi^{\alpha\beta^0}_{i_\pi l_\pi} \ . \tag{C.23}$$

Contribution (C.20h) Finally, for each non-zero contribution from (C.20f) to $\rho^{[2]}_{l_\pi i_\pi, k_\nu j_\nu}$, we add the contribution from (C.20h) to $\rho^{[2]}_{\tilde{l}_\pi \tilde{i}_\pi, \tilde{k}_\nu \tilde{j}_\nu}$ using,

$$\underbrace{\langle \phi_{\alpha^0_\pi} | \widetilde{a}^\dagger_{i_\pi} \widetilde{a}_{l_\pi}}_{\langle \widetilde{\phi_{\beta_\pi}} | \varphi^{\alpha^0_\pi \beta\pi}_{il}} | \overline{\phi_{\beta_\pi}} \rangle = \theta^R_{\beta_\pi} \overline{\theta_{\beta_\pi}} \varphi^{\alpha^0\beta}_{i_\pi l_\pi} \ . \tag{C.24}$$

C.3 Calculation of the source term $G[\sigma]$

The source term is a one-body operator given by,

$$G[\sigma]^\tau_{kl} = F[\sigma]^\tau_{kl} - F[\sigma]^{\tau *}_{lk} \ , \tag{C.25}$$

where $\tau = (\pi, \nu)$ denotes the isospin and,

$$F[\sigma]^\tau_{kl} = \frac{1}{2} \sum_{imn} \langle im|V|\widetilde{nl_\tau}\rangle \, \sigma_{in,mk_\tau} \ , \tag{C.26}$$

where,

$$\sigma_{in,mk_\tau} = \langle \Psi | a^\dagger_i a^\dagger_m a_{k_\tau} a_n \rangle - \rho_{ni}\rho_{k_\tau m} + \rho_{nm}\rho_{k_\tau i} \ . \tag{C.27}$$

Here we assume all quantities to be real, so that,

$$G[\sigma]^\tau_{kl} = F[\sigma]^\tau_{kl} - F[\sigma]^\tau_{lk} \ , \tag{C.28}$$

Let us look more precisely at $F[\sigma]^\pi_{kl}$ (the neutron term being calculated similarly). The sum in Eq. (C.26) is over i, m, n of different isospin so that we have,

$$\begin{aligned}
F^\pi_{kl} &= \frac{1}{2} \sum_{imn} \langle im|V|\widetilde{nl_\pi}\rangle \, \sigma_{in,mk_\pi} \\
&= \frac{1}{2} \sum_{i_\pi m_\pi n_\pi} \langle i_\pi m_\pi|V|\widetilde{n_\pi l_\pi}\rangle \, \sigma_{i_\pi n_\pi, m_\pi k_\pi} + \frac{1}{2} \sum_{i_\nu m_\pi n_\nu} \langle i_\nu m_\pi|V|\widetilde{n_\nu l_\pi}\rangle \, \sigma_{i_\nu n_\nu, m_\pi k_\pi} \\
&\quad + \frac{1}{2} \sum_{i_\pi m_\nu n_\nu} \langle i_\pi m_\nu|V|\widetilde{n_\nu l_\pi}\rangle \, \sigma_{i_\pi n_\nu, m_\nu k_\pi} \\
&= \frac{1}{2} \sum_{i_\pi m_\pi n_\pi} \langle i_\pi m_\pi|V|\widetilde{n_\pi l_\pi}\rangle \, \sigma_{i_\pi n_\pi, m_\pi k_\pi} + 2 \times \frac{1}{2} \sum_{i_\nu m_\pi n_\nu} \langle i_\nu m_\pi|V|\widetilde{n_\nu l_\pi}\rangle \, \sigma_{i_\nu n_\nu, m_\pi k_\pi}
\end{aligned} \tag{C.29}$$

Using (C.27) this gives,

$$F^{\pi}_{kl} = \frac{1}{2}\sum_{i_\pi m_\pi n_\pi} \langle i_\pi m_\pi|V|\widetilde{n_\pi l_\pi}\rangle \langle\Psi|a^\dagger_{i_\pi} a^\dagger_{m_\pi} a_{k_\pi} a_{n_\pi}|\Psi\rangle \tag{C.30a}$$

$$-1 \times \sum_{i_\pi m_\pi n_\pi} \langle i_\pi m_\pi|V|\widetilde{n_\pi l_\pi}\rangle \langle\Psi|a^\dagger_{i_\pi} a_{n_\pi}|\Psi\rangle \langle\Psi|a^\dagger_{m_\pi} a_{k_\pi}|\Psi\rangle \tag{C.30b}$$

$$+1 \times \sum_{i_\nu m_\pi n_\nu} \langle i_\nu m_\pi|V|\widetilde{n_\nu l_\pi}\rangle \langle\Psi|a^\dagger_{i_\nu} a^\dagger_{m_\pi} a_{k_\pi} a_{n_\nu}|\Psi\rangle \tag{C.30c}$$

$$-1 \times \sum_{i_\nu m_\pi n_\nu} \langle i_\nu m_\pi|V|\widetilde{n_\nu l_\pi}\rangle \langle\Psi|a^\dagger_{i_\nu} a_{n_\nu}|\Psi\rangle \langle\Psi|a^\dagger_{m_\pi} a_{k_\pi}|\Psi\rangle \ . \tag{C.30d}$$

Let us note that σ being non-zero in the valence space only, all sums are restricted to i, m, n in this space. This restriction is implied in what follows.

C.3.1 Contribution from proton two-body densities

Let us look at the contribution (C.30a) from two-body proton densities. Here we omit the sub-index π since all indices are of same isospin.
Let us divide (C.30a) in three contributions using,

$$\sum_{imn} = \underbrace{\sum_{\substack{imn \\ (i,m,n,k) \text{ all different}}}}_{\text{(a)}} + \underbrace{\sum_{\substack{imn \\ 1 \text{ couple of indices equal among } (i,m,n,k)}}}_{\text{(b)}} + \underbrace{\sum_{\substack{imn \\ 2 \text{ couples of indices equal among } (i,m,n,k)}}}_{\text{(c)}} \tag{C.31}$$

Calculation of term a

We want to practically calculate,

$$\text{(a)} = \frac{1}{2} \sum_{\substack{imn \\ (i,m,n,k) \text{ all different}}} \langle im|V|\widetilde{nl}\rangle \langle\Psi|a^\dagger_i a^\dagger_m a_k a_n|\Psi\rangle \ . \tag{C.32}$$

In order to reduce the dimensions of the problem, we only explicitly calculate elements $\langle\Psi|a^\dagger_{m_1} a^\dagger_{m_2} a_{m_4} a_{m_3}|\Psi\rangle$ respecting the conditions,

- $m_2 > m_1$
- $m_4 > m_3$
- $m_1 > m_3$.

The difficulty comes from the fact that the sum in (a) is not over all indices. Therefore one needs to make use of permutation and hermiticity properties. Each element $\langle\Psi|a^\dagger_{m_1} a^\dagger_{m_2} a_{m_4} a_{m_3}|\Psi\rangle$ will then be contributing to $F(m_1, m_5)$, $F(m_2, m_5)$, $F(m_3, m_5)$ and $F(m_4, m_5)$,

Let us detail this procedure more specifically.
First, let us divide (a) as,

$$\begin{aligned}
\text{(a)} &= \frac{1}{2} \sum_{\substack{m_1 m_2 m_3 \\ (m_1,m_2,m_3,m_4) \text{ all different}}} \langle m_1 m_2 | V | \widetilde{m_3 m_5} \rangle \, \langle \Psi | a^\dagger_{m_1} a^\dagger_{m_2} a_{m_4} a_{m_3} | \Psi \rangle \\
&= \frac{1}{2} \sum_{m_3} \sum_{m_1} \left(\sum_{\substack{m_2 \\ m_2 > m_1}} + \sum_{\substack{m_2 \\ m_2 < m_1}} \right) \langle m_1 m_2 | V | \widetilde{m_3 m_5} \rangle \, \langle \Psi | a^\dagger_{m_1} a^\dagger_{m_2} a_{m_4} a_{m_3} | \Psi \rangle \ . \quad \text{(C.33)}
\end{aligned}$$

The sum being over both indices m_1 and m_2 it is easy to show that $\sum_{m_3} \sum_{m_1} \sum_{\substack{m_2 \\ m_2 < m_1}}$ gives the same contribution than $\sum_{m_3} \sum_{m_1} \sum_{\substack{m_2 \\ m_2 > m_1}}$ by permuting and renaming the dummy indices. We therefore get,

$$\text{(a)} = \sum_{m_3} \sum_{m_1} \sum_{\substack{m_2 \\ m_2 > m_1}} \langle m_1 m_2 | V | \widetilde{m_3 m_5} \rangle \, \langle \Psi | a^\dagger_{m_1} a^\dagger_{m_2} a_{m_4} a_{m_3} | \Psi \rangle \ . \quad \text{(C.34)}$$

One has to be more subtle regarding the other ordering conditions. Let us now divide $\sum_{m_3}$ in (a) as,

$$\sum_{m_3} = \sum_{\substack{m_3 \\ m_3 < m_4 \\ m_3 < m_1}} + \sum_{\substack{m_3 \\ m_3 < m_4 \\ m_3 > m_1}} + \sum_{\substack{m_3 \\ m_3 > m_4 \\ m_3 < m_1}} + \sum_{\substack{m_3 \\ m_3 > m_4 \\ m_3 > m_1}} \ . \quad \text{(C.35)}$$

The term,

$$\text{(a1)} \equiv \sum_{m_1} \sum_{\substack{m_2 \\ m_2 > m_1}} \sum_{\substack{m_3 \\ m_3 < m_4 \\ m_3 < m_1}} \langle m_1 m_2 | V | \widetilde{m_3 m_5} \rangle \, \langle \Psi | a^\dagger_{m_1} a^\dagger_{m_2} a_{m_4} a_{m_3} | \Psi \rangle \ , \quad \text{(C.36)}$$

already fulfills the ordering conditions (C.3.1). The external indices for this term are (m_4, m_5).

The term,

$$\text{(a2)} \equiv \sum_{m_1} \sum_{\substack{m_2 \\ m_2 > m_1}} \sum_{\substack{m_3 \\ m_3 < m_4 \\ m_3 > m_1}} \langle m_1 m_2 | V | \widetilde{m_3 m_5} \rangle \underbrace{\langle \Psi | a^\dagger_{m_1} a^\dagger_{m_2} a_{m_4} a_{m_3} | \Psi \rangle}_{\langle \Psi | a^\dagger_{m_3} a^\dagger_{m_4} a_{m_2} a_{m_1} | \Psi \rangle} , \quad \text{(C.37)}$$

can be written with conditions (C.3.1) by renaming the dummy variables, *as well as the external ones*. Thus we get,

$$\text{(a2)} = \sum_{\substack{m_1 m_3 m_4 \\ m_2 > m_1 \\ m_3 < m_4 \\ m_3 < m_1}} \langle m_3 m_4 | V | \widetilde{m_1 m_5} \rangle \, \langle \Psi | a^\dagger_{m_1} a^\dagger_{m_2} a_{m_4} a_{m_3} | \Psi \rangle \ , \quad \text{(C.38)}$$

where the external indices have become (m_2, m_5).

Similarly, using hermiticity and permutation properties,

$$\text{(a3)} \equiv \sum_{m_1} \sum_{\substack{m_2 \\ m_2>m_1}} \sum_{\substack{m_3 \\ m_3>m_4 \\ m_3<m_1}} \langle m_3 m_4|V|\widetilde{m_1 m_5}\rangle \, \langle\Psi|a^\dagger_{m_1} a^\dagger_{m_2} a_{m_4} a_{m_3}|\Psi\rangle \ , \tag{C.39}$$

can be written as,

$$\text{(a3)} = -\sum_{\substack{m_1 m_2 m_4 \\ m_2>m_1 \\ m_3<m_4 \\ m_3<m_1}} \langle m_1 m_2|V|\widetilde{m_4 m_5}\rangle \, \langle\Psi|a^\dagger_{m_1} a^\dagger_{m_2} a_{m_4} a_{m_3}|\Psi\rangle \ , \tag{C.40}$$

where the external indices have become (m_3, m_5).

And finally,

$$\text{(a4)} \equiv \sum_{m_1} \sum_{\substack{m_2 \\ m_2>m_1}} \sum_{\substack{m_3 \\ m_3>m_4 \\ m_3>m_1}} \langle m_3 m_4|V|\widetilde{m_1 m_5}\rangle \, \langle\Psi|a^\dagger_{m_1} a^\dagger_{m_2} a_{m_4} a_{m_3}|\Psi\rangle \ , \tag{C.41}$$

can be written as,

$$\text{(a4)} = -\sum_{\substack{m_2 m_3 m_4 \\ m_2>m_1 \\ m_3<m_4 \\ m_3<m_1}} \langle m_3 m_4|V|\widetilde{m_2 m_5}\rangle \, \langle\Psi|a^\dagger_{m_1} a^\dagger_{m_2} a_{m_4} a_{m_3}|\Psi\rangle \ , \tag{C.42}$$

where the external indices have become (m_1, m_5).

To sum up, in order to include the contribution of (a) to F, for each non zero element $\langle\Psi|a^\dagger_{m_1} a^\dagger_{m_2} a_{m_4} a_{m_3}|\Psi\rangle$ with condition (C.3.1), one needs to:

- add to $F(m4, m5)$ the contribution from (a1),
- add to $F(m2, m5)$ the contribution from (a2),
- add to $F(m3, m5)$ the contribution from (a3),
- add to $F(m1, m5)$ the contribution from (a4).

Calculation of term b

Let us now look at the term (b). We have,

$$\begin{aligned}
\text{(b)} &= \frac{1}{2} \sum_{\substack{imn \\ \text{1 couple of indices equal among } (i,m,n,k)}} \langle im|V|\widetilde{nl}\rangle \, \langle\Psi|a_i^\dagger a_m^\dagger a_k a_n|\Psi\rangle \\
&= \frac{1}{2}\left(\sum_{\substack{mn \\ i=k}} + \sum_{\substack{mn \\ i=n}} + \sum_{\substack{in \\ m=k}} + \sum_{\substack{in \\ m=n}}\right) \langle im|V|\widetilde{nl}\rangle \, \langle\Psi|a_i^\dagger a_m^\dagger a_k a_n|\Psi\rangle \\
&= \underbrace{\sum_{mn} \langle km|V|\widetilde{ln}\rangle \, \langle\Psi|a_k^\dagger a_m^\dagger a_n a_k|\Psi\rangle}_{\text{(b1)}} + \underbrace{\sum_{mn} \langle nm|V|\widetilde{nl}\rangle \, \langle\Psi|a_n^\dagger a_m^\dagger a_k a_n|\Psi\rangle}_{\text{(b2)}} ,
\end{aligned}$$

where we grouped equal contributions.
Again, ordering conventions are used in practice to calculate elements of the type $\langle\Psi|a_{m_1}^\dagger a_{m_2}^\dagger a_{m_3} a_{m_1}|\Psi\rangle$. These are: $m_2 < m_3$.
The term (b1) needs then to be written as,

$$\begin{aligned}
\text{(b1)} &= \sum_{m_2}\left(\sum_{\substack{m_3 \\ m_3<m_2}} + \sum_{\substack{m_3 \\ m_3>m_2}}\right) \langle m_1 m_2|V|\widetilde{m_4 m_3}\rangle \, \langle\Psi|a_{m_1}^\dagger a_{m_2}^\dagger a_{m_3} a_{m_1}|\Psi\rangle \\
&= \sum_{m_2}\sum_{\substack{m_3 \\ m_3>m_2}} \left(\langle m_1 m_2|V|\widetilde{m_4 m_3}\rangle + \langle m_1 m_3|V|\widetilde{m_4 m_2}\rangle\right) \langle\Psi|a_{m_1}^\dagger a_{m_2}^\dagger a_{m_3} a_{m_1}|\Psi\rangle \quad \text{(C.43)}
\end{aligned}$$

The external indices being (m_1, m_4).

The term (b2) is divided as,

$$\begin{aligned}
\text{(b2)} &= \underbrace{\sum_{m_1}\sum_{\substack{m_2 \\ m_2<m_3}} \langle m_1 m_2|V|\widetilde{m_1 m_4}\rangle \, \langle\Psi|a_{m_1}^\dagger a_{m_2}^\dagger a_{m_3} a_{m_1}|\Psi\rangle}_{\text{(b21)}} \\
&\quad + \underbrace{\sum_{m_1}\sum_{\substack{m_2 \\ m_2>m_3}} \langle m_1 m_2|V|\widetilde{m_1 m_4}\rangle \, \langle\Psi|a_{m_1}^\dagger a_{m_2}^\dagger a_{m_3} a_{m_1}|\Psi\rangle}_{\text{(b22)}} .
\end{aligned}$$

Indices in (b21) are already well ordered, the external ones are (m_3, m_4).
Using hermiticity property we find,

$$\text{(b22)} = \sum_{m_1} \sum_{\substack{m_3 \\ m_3 > m_2}} \langle m_1 m_3 | V | \widetilde{m_1 m_4} \rangle \, \langle \Psi | a^\dagger_{m_1} a^\dagger_{m_2} a_{m_3} a_{m_1} | \Psi \rangle \ . \tag{C.44}$$

The external indices are (m_2, m_4).

To sum up, in order to include the contribution of (b) to F, for each non zero element $\langle \Psi | a^\dagger_{m_1} a^\dagger_{m_2} a_{m_3} a_{m_2} | \Psi \rangle$ with $m2 < m3$, one needs to:

- add to $F(m1, m4)$ the contribution from (b1),
- add to $F(m3, m4)$ the contribution from (b21),
- add to $F(m2, m4)$ the contribution from (b22).

Calculation of term c

Finally let us consider now the term (c). We have,

$$\begin{aligned}
\text{(c)} &= \frac{1}{2} \sum_{\substack{imn \\ \text{2 couples of indices equal among } (i,m,n,k)}} \langle im | V | \widetilde{nl} \rangle \, \langle \Psi | a^\dagger_i a^\dagger_m a_k a_n | \Psi \rangle \\
&= \frac{1}{2} \left(\sum_{\substack{m \\ i=k \\ n=m}} + \sum_{\substack{i \\ m=k \\ n=i}} \right) \langle im | V | \widetilde{nl} \rangle \, \langle \Psi | a^\dagger_i a^\dagger_m a_k a_n | \Psi \rangle \\
&= \sum_m \langle km | V | \widetilde{ml} \rangle \, \langle \Psi | a^\dagger_k a^\dagger_m a_k a_m | \Psi \rangle \ ,
\end{aligned} \tag{C.45}$$

where we used the fact that both terms give the same contribution. No ordering being imposed here, for each non zero $\langle \Psi | a^\dagger_k a^\dagger_m a_k a_m | \Psi \rangle$, one needs to add to $F(k, l)$ the corresponding contribution from (c).

C.3.2 Contribution from products of proton one-body densities

Let us now turn to the contribution (C.30b) from one-body proton densities. Here we omit again the sub-index π since all indices are of same isospin.
One can again divide (C.30b)

$$\text{(C.30b)} = - \times \sum_{imn} \langle im | V | \widetilde{nl} \rangle \, \rho_{ni} \rho_{km} \ , \tag{C.46}$$

in three contributions using,

$$\sum_{imn} = \underbrace{\sum_{\substack{imn \\ n\neq m \\ k\neq i}}}_{\text{(a)}} + \underbrace{\sum_{\substack{imn \\ n=m \\ i\neq k}}}_{\text{(b)}} + \underbrace{\sum_{\substack{imn \\ n\neq m \\ i=k}}}_{\text{(c)}} + \underbrace{\sum_{\substack{imn \\ n=m \\ i=k}}}_{\text{(d)}} \tag{C.47}$$

In practice, non-diagonal elements $\rho_{m_1 m_2} = \langle a^\dagger_{m2} a_{m_1} \rangle$ of the one-body density are calculated for $m_1 < m_2$. Using similar reasoning as previously we finally obtain the following results.

Contribution from the term a For each product of non zero element $\rho_{m_1 m_2}\rho_{m_3 m_4}$ with $(m_1 < m_2)$ and $(m_3 < m_4)$, one needs to:

- add to $F(m4, m5)$ the contribution from

$$a1(m_4, m_5) = \sum_{\substack{m_1,m_2,m_3 \\ m_1<m_2 \\ m_3<m_4}} \left(\langle m_3 m_1 | V | \widetilde{m_2 m_5} \rangle + \langle m_3 m_2 | V | \widetilde{m_1 m_5} \rangle \right) \rho_{m_1 m_2} \rho_{m_3 m_4} \, . \tag{C.48}$$

- add to $F(m3, m5)$ the contribution from

$$a2(m_3, m_5) = \sum_{\substack{m_1,m_2,m_4 \\ m_1<m_2 \\ m_3<m_4}} \left(\langle m_4 m_1 | V | \widetilde{m_2 m_5} \rangle + \langle m_4 m_2 | V | \widetilde{m_1 m_5} \rangle \right) \rho_{m_1 m_2} \rho_{m_3 m_4} \, . \tag{C.49}$$

Contribution from the term b For each product of non zero elements $\rho_{m_1 m_1}\rho_{m_3 m_4}$ with $(m_3 < m_4)$, one needs to:

- add to $F(m4, m5)$ the contribution from

$$b1(m_4, m_5) = \sum_{\substack{m_1,m_3 \\ m_3<m_4}} \langle m_3 m_1 | V | \widetilde{m_1 m_5} \rangle \, \rho_{m_1 m_1} \rho_{m_3 m_4} \, . \tag{C.50}$$

- add to $F(m3, m5)$ the contribution from

$$b2(m_3, m_5) = \sum_{\substack{m_1,m_4 \\ m_3<m_4}} \langle m_4 m_1 | V | \widetilde{m_1 m_5} \rangle \, \rho_{m_1 m_1} \rho_{m_3 m_4} \, . \tag{C.51}$$

Contribution from the term c For each product of non zero elements $\rho_{m_1 m_2}\rho_{m_3 m_3}$ with $(m_1 < m_2)$, one needs to add to $F(m3, m5)$ the contribution from

$$c(m_3, m_5) = \sum_{\substack{m_1,m_2 \\ m_1<m_2}} \left(\langle m_3 m_1 | V | \widetilde{m_2 m_5} \rangle + \langle m_3 m_2 | V | \widetilde{m_1 m_5} \rangle \right) \rho_{m_1 m_2} \rho_{m_3 m_3} \, . \tag{C.52}$$

Contribution from the term d Finally, for each product of diagonal elements $\rho_{m_1m_1}\rho_{m_3m_3}$ one needs to add to $F(m3, m5)$ the contribution from

$$c(m_3, m_5) = \sum_{m_1} \langle m_3 m_1 | V | \widetilde{m_1 m_5} \rangle \, \rho_{m_1m_1}\rho_{m_3m_3} \ . \tag{C.53}$$

C.3.3 Contribution from proton-neutron two-body densities

Let us now look at the contribution (C.30c).

$$\begin{aligned} \text{(C.30c)} &= \sum_{i_\nu m_\pi n_\nu} \langle i_\nu m_\pi | V | \widetilde{n_\nu l_\pi} \rangle \, \langle \Psi | a^\dagger_{m_\pi} a^\dagger_{i_\nu} a_{n_\nu} a_{k_\pi} | \Psi \rangle \\ &= \Big(\underbrace{\sum_{\substack{i_\nu m_\pi n_\nu \\ n_\nu \neq i_\nu \\ m_\pi \neq k_\pi}}}_{\text{a}} + \underbrace{\sum_{\substack{i_\nu m_\pi \\ n_\nu = i_\nu \\ m_\pi \neq k_\pi}}}_{\text{b}} + \underbrace{\sum_{\substack{i_\nu n_\nu \\ n_\nu \neq i_\nu \\ m_\pi = k_\pi}}}_{\text{c}} + \underbrace{\sum_{\substack{i_\nu \\ n_\nu = i_\nu \\ m_\pi = k_\pi}}}_{\text{d}} \Big) \langle i_\nu m_\pi | V | \widetilde{n_\nu l_\pi} \rangle \, \langle \Psi | a^\dagger_{m_\pi} a^\dagger_{i_\nu} a_{n_\nu} a_{k_\pi} | \Psi \rangle \end{aligned} \tag{C.54}$$

Calculation of term a

Let us remind that, since parity p and projection K of the total angular momentum are good quantum numbers, the following relations must be fulfilled,

$$\begin{cases} \Omega(m_\pi) - \Omega(k_\pi) = \Omega(n_\nu) - \Omega(i_\nu) \equiv \Delta K & \text{(C.55)} \\ \dfrac{p(m_\pi)}{p(k_\pi)} = \dfrac{p(n_\nu)}{p(i_\nu)} \equiv \Delta p \ . & \text{(C.56)} \end{cases}$$

According the values of $(\Delta K, \Delta p)$, different ordering are imposed on the indices when calculating an element of the type $\langle \Psi | a^\dagger_{p_1} a^\dagger_{n_1} a_{n_2} a_{p_2} | \Psi \rangle$ (where p (n) refers to a proton (neutron) orbital). In all cases, the contribution of the term (a) requires the calculation of,

$$a1(p_2, p_3) = \sum_{\substack{p_1 n_1 n_2 \\ \text{ordering conditions}}} \langle n_1 p_1 | V | \widetilde{n_2 p_3} \rangle \, \langle \Psi | a^\dagger_{p_1} a^\dagger_{n_1} a_{n_2} a_{p_2} | \Psi \rangle \ , \tag{C.57}$$

and,

$$a2(p_1, p_3) = \sum_{\substack{p_2 n_1 n_2 \\ \text{ordering conditions}}} \langle n_2 p_2 | V | \widetilde{n_1 p_3} \rangle \, \langle \Psi | a^\dagger_{p_1} a^\dagger_{n_1} a_{n_2} a_{p_2} | \Psi \rangle \ . \tag{C.58}$$

Calculation of term b

Elements of the type $\langle \Psi | a^\dagger_{p_1} a^\dagger_{n_1} a_{n_1} a_{p_2} | \Psi \rangle$ being calculated for $(p_1 < p_2)$, the contribution from (b) involves the calculation of,

$$b1(p_2,p_3) = \sum_{\substack{p_1 n_1 \\ p_1<p_2}} \langle n_1 p_1|V|\widetilde{n_1 p_3}\rangle \langle\Psi|a^\dagger_{p_1}a^\dagger_{n_1}a_{n_1}a_{p_2}|\Psi\rangle \ , \tag{C.59}$$

and,

$$b2(p_1,p_3) = \sum_{\substack{p_2 n_1 \\ p_1<p_2}} \langle n_1 p_2|V|\widetilde{n_1 p_3}\rangle \langle\Psi|a^\dagger_{p_1}a^\dagger_{n_1}a_{n_1}a_{p_2}|\Psi\rangle \ . \tag{C.60}$$

Calculation of term c

Similarly, elements of the type $\langle\Psi|a^\dagger_{p_1}a^\dagger_{n_1}a_{n_2}a_{p_1}|\Psi\rangle$ being calculated for $(n_1 < n_2)$, the contribution from (c) involves the calculation of,

$$c(p_1,p_3) = \sum_{\substack{n_1 n_2 \\ n_1<n_2}} \left(\langle n_1 p_1|V|\widetilde{n_2 p_3}\rangle + \langle n_2 p_1|V|\widetilde{n_1 p_3}\rangle\right) \langle\Psi|a^\dagger_{p_1}a^\dagger_{n_1}a_{n_1}a_{p_2}|\Psi\rangle \ , \tag{C.61}$$

Calculation of term d

Finally, no ordering is imposed for the calculation of diagonal elements $\langle\Psi|a^\dagger_{p_1}a^\dagger_{n_1}a_{n_1}a_{p_1}|\Psi\rangle$, and therefore one can directly calculate,

$$d(p_1,p_3) = \sum_{n_1} \langle n_1 p_1|V|\widetilde{n_1 p_3}\rangle \langle\Psi|a^\dagger_{p_1}a^\dagger_{n_1}a_{n_1}a_{p_1}|\Psi\rangle \ . \tag{C.62}$$

C.3.4 Contribution from products of proton and neutron one-body densities

Finally let us look at,

$$\text{(C.30d)} \ = - \times \sum_{i_\nu m_\pi n_\nu} \langle i_\nu m_\pi|V|\widetilde{n_\nu l_\pi}\rangle \langle\Psi|a^\dagger_{i_\nu}a_{n_\nu}|\Psi\rangle \langle\Psi|a^\dagger_{m_\pi}a_{k_\pi}|\Psi\rangle \ . \tag{C.63}$$

Using similar reasoning as previously, we find that calculating this term implies the program-

ming of the following contributions,

$$
\begin{aligned}
a1(p2,p3) &= - \sum_{\substack{p_1 n_1 n_2 \\ \text{ordering conditions} \\ \text{fulfilled}}} \left(\langle n_1 p_1|V|\widetilde{n_2 p_3}\rangle + \langle n_2 p_1|V|\widetilde{n_1 p_3}\rangle\right) \langle\Psi|a^\dagger_{n_1} a_{n_2}|\Psi\rangle \, \langle\Psi|a^\dagger_{p_1} a_{p_2}|\Psi\rangle \ , \\
a2(p1,p3) &= - \sum_{\substack{p_2 n_1 n_2 \\ \text{ordering conditions} \\ \text{fulfilled}}} \left(\langle n_1 p_2|V|\widetilde{n_2 p_3}\rangle + \langle n_2 p_2|V|\widetilde{n_1 p_3}\rangle\right) \langle\Psi|a^\dagger_{n_1} a_{n_2}|\Psi\rangle \, \langle\Psi|a^\dagger_{p_1} a_{p_2}|\Psi\rangle \ , \\
b(p1,p3) &= \sum_{\substack{n_1 n_2 \\ \text{ordering conditions} \\ \text{fulfilled}}} \left(\langle n_1 p_1|V|\widetilde{n_2 p_3}\rangle + \langle n_2 p_1|V|\widetilde{n_1 p_3}\rangle\right) \langle\Psi|a^\dagger_{n_1} a_{n_2}|\Psi\rangle \, \langle\Psi|a^\dagger_{p_1} a_{p_1}|\Psi\rangle \ , \\
c1(p2,p3) &= \sum_{\substack{p_1 n_1 \\ \text{ordering conditions} \\ \text{fulfilled}}} \langle n_1 p_1|V|\widetilde{n_1 p_3}\rangle \, \langle\Psi|a^\dagger_{n_1} a_{n_1}|\Psi\rangle \, \langle\Psi|a^\dagger_{p_1} a_{p_2}|\Psi\rangle \ , \\
c2(p1,p3) &= \sum_{\substack{p_2 n_1 \\ \text{ordering conditions} \\ \text{fulfilled}}} \langle n_1 p_2|V|\widetilde{n_1 p_3}\rangle \, \langle\Psi|a^\dagger_{n_1} a_{n_1}|\Psi\rangle \, \langle\Psi|a^\dagger_{p_1} a_{p_2}|\Psi\rangle \ , \\
d(p1,p3) &= \sum_{n_1} \langle n_1 p_1|V|\widetilde{n_1 p_3}\rangle \, \langle\Psi|a^\dagger_{n_1} a_{n_1}|\Psi\rangle \, \langle\Psi|a^\dagger_{p_1} a_{p_1}|\Psi\rangle \ .
\end{aligned}
$$

Bibliography

[1] National Nuclear Data Center, Evaluated Nuclear Structure Data File, *http://www.nndc.bnl.gov/ensdf*.

[2] K. Amos, P. J. Dortmans, H. V. von Geramb, S. Karataglidis, and J. Raynal. *Adv. Nucl. Phys.*, **25**:275, 2000.

[3] I. Angeli. *Atomic Data and Nuclear Data Tables*, **87**:185, 2004.

[4] M. Baranger. *Nucl. Phys.*, **A149**:225, 1970.

[5] J. Bardeen, L. N. Cooper, and J. R. Schrieffer. *Phys. Rev.*, **108**:1175, 1957.

[6] J.-F. Berger. Private communications.

[7] J.-F. Berger, M. Girod, and D. Gogny. *Nucl. Phys.*, **A502**:85c, 1989.

[8] J.-F. Berger, M. Girod, and D. Gogny. *Comput. Phys. Commun.*, **63**:365, 1991.

[9] H. A. Bethe and J. Goldstone. *Proc. Roy. Soc.*, **A238**:551, 1957.

[10] J.-P. Blaizot and D. Gogny. *Nucl. Phys.*, **A284**:429, 1977.

[11] J.-P. Blaizot and G. Ripka. *Quantum Theory of Finite systems*. The MIT press, 1986.

[12] S. K. Bogner, R. Furnstahl, and R. J. Perry. *Phys. Rev. C(R)*, **75**:061001, 2007.

[13] S. K. Bogner, R. Furnstahl, and A. Schwenk. *Prog. Part. Nucl. Phys.*, **65**:94–147, 2010.

[14] S. K. Bogner, T. T. S. Kuo, and A. Schwenk. *Phys. Rep.*, **386**:1, 2003.

[15] S. K. Bogner, T. T. S. Kuo, A. Schwenk, D. R. Entem, and R. Machleidt. *Phys. Lett. B*, **576**:265, 2003.

[16] N. N. Bogoliubov. *Sov. Phys. JETP*, **7**:41, 1958.

[17] N. N. Bogoliubov. *Sov. Phys. Usp.*, **2**:236, 1959.

[18] L. Bonneau, P. Quentin, and K. Sieja. *Phys. Rev. C*, **76**:014304, 2007.

[19] S. W. Brain *et al. J. Phys. G Nuck. Phys*, **3**:821, 1977.

[20] L. Brillouin. *Act. Sci. Ind.*, **71**:159, 1933.

[21] B. A. Brown and B. H. Wildenthal. *Ann. Rev. Nucl. Part. Sci.*, **38**:29, 1988.

[22] K. A. Brueckner. *Phys. Rev.*, **97**:1353, 1955.

[23] J. Carlson. *Phys. Rev. C*, **36**:2026, 1987.

[24] E. Caurier, G. Martínez-Pinedo, F. Nowacki, A. Poves, and A. P. Zuker. *Rev. Mod. Phys.*, **77**:427, 2005.

[25] F. Chappert, M. Girod, and S. Hilaire. *Phys. Lett. B*, **668**:420, 2008.

[26] F. Chappert and N. Pillet *et al. Phys. Rev. C*, submitted.

[27] D. Day. *Rev. Mod. Phys.*, **39**:719, 1967.

[28] T. de Forest and J. D. Walecka. *Advances in Physics*, **15**:1–109, 1966.

[29] J. Dechargé and D. Gogny. *Phys. Rev.*, **C21**:1568, 1980.

[30] J.-P. Delaroche *et al. Phys. Rev. C*, **81**:014303, 2010.

[31] W. H. Dickhoff and C. Barbieri. *Prog. Part. Nucl. Phys.*, **52**:377, 2004.

[32] B. Dreher *et al. Nucl Phys.*, **A235**:219, 1974.

[33] T. Duguet and G. Hagen. *Phys. Rev.*, **C85**:034330, 2012.

[34] J. Dukelsky and P. Schuck. *Nucl. Phys.*, **A512**:466, 1990.

[35] M. Dupuis. *Modèles de réactions directes et de pré-équilibre quantique pour la diffusion de nucléons sur des noyaux sphériques*. PhD thesis, Université de Bordeaux I - Talence, 2006.

[36] E. Epelbaum. *Nuclear forces from chiral effective field theory: a primer*. Lacanau, France, Sept 27 - Oct 3 2009. Ecole Joliot Curie.

[37] E. Epelbaum, H. W. Hammer, and U. G. Meißner. *Phys. Rep.*, **503**:1–75, 2011.

[38] E. Epelbaum, H. Krebs, D. Lee, and U. G. Meißner. *Phys. Rev. Lett.*, **104**:142501, 2010.

[39] A. Faessler and A. Plastino. *Z. Phys.*, **220**:88, 1969.

[40] H. Feshbach. *Ann. Phys.*, **5**:357, 1958.

[41] H. Feshbach. *Ann. Phys.*, **19**:287, 1962.

[42] A. L. Fetter and J. D. Walecka. *Quantum Theory of Many-Particle Systems*. Courier Dover Publications, 2003.

[43] V. A. Fock. *Z. Phys.*, **61**:126, 1930.

[44] C. Froese-Fischer. *Comp. Phys. Comm.*, **1**:151, 1969.

[45] T. L. Gilbert. *J. Chem. Phys.*, **60**:3835, 1974.

[46] M. Girod, D. Gogny, and B. Grammaticos. In *Septième session d'études biennales de physique nucléaire*. Aussois, 14-18 Mars 1983.

[47] D. Gogny. In G. Ripka and M. Porneuf, editors, *Int. Conf. on Nuclear Self-Consistent Fields*, page 333. North Holland, Amsterdam, 1975.

[48] D. Gogny and R. Padjen. *Nucl. Phys.*, **A293**:365, 1977.

[49] S. Goriely, S. Hilaire, M. Girod, and S. Péru. *Phys. Rev. Lett.*, **102**:242501, 2009.

[50] J. J. Griffin and J. A. Wheeler. *Phys. Rev.*, **108**:311, 1957.

[51] D. Gross and F. Wilczek. *Phys. Rev. D*, **8**:3633, 1973.

[52] D. J. Gross and F. Wilczek. *Phys. Rev. Lett.*, **30**:1343, 1973.

[53] D. R. Hartree. *Proc. Camb. Phil. Soc.*, **24**:89, 1928.

[54] J. Heisenberg *et al. Phys. Rev. C*, **25**:2292, 1982.

[55] J. Hinze. *J. Chem. Phys.*, **59**:6424, 1973.

[56] Y. Horikawa *et al. Phys. Lett. B*, **36**:9, 1971.

[57] A. Hotta *et al. Phys. Rev. C*, **36**:2212, 1987.

[58] A. Johnston *et al. J. Phys. A: Math. Nucl. Gen.*, **7**:898, 1974.

[59] K. Kowalski, D. J. Dean, M. Hjorth-Jensen, T. Papenbrock, and P. Piecuch. *Phys. Rev. Lett.*, **92**:132501, 2004.

[60] S. Krewald, K. W. Schmid, and A. Faessler. *Z. Physik*, **269**:125, 1974.

[61] H. Laftchiev, J. Libert, P. Quentin, and T. L. Ha. *Nucl. Phys.*, **A845**:33, 2010.

[62] J. Le Bloas and N. Pillet. Overlap functions for nuclear structure and reactions. *CEA internal report*, 2013.

[63] J. Le Bloas, N. Pillet, M. Dupuis, J.-M. Daugas, L. M. Robledo, C. Robin, and V. G. Zelevinsky. *Phys. Rev. C (R)*, **89**:011306, 2014.

[64] B. Levy and G. Berthier. *Int. Journ. Quant. Chem.*, **2**:3, 1968.

[65] G. C. Li *et al. Phys. Rev. C*, **9**:1861, 1974.

[66] R. Lombard *et al. Nucl. Phys.*, **59**:398, 1964.

[67] J. K. L. MacDonald. *Phys. Rev.*, **43**:830, 1933.

[68] R. Machleidt. *Phys. Rev. C*, **63**:024001, 2001.

[69] R. Machleidt and D. R. Entem. *Phys. Rep.*, **503**:1–75, 2011.

[70] D. J. Marín-Lámbarri. *Phys. Rev. Lett.*, **113**:012502, 2014.

[71] P. C. Martin and J. Schwinger. *Phys. Rev.*, **115**:1342, 1959.

[72] R. D. Mattuck. *A guide to Feynman diagrams in the Many-Body Problem.* Courier Dover Publications, 2012.

[73] R. McWeeny. *Methods of molecular quantum mechanics, second edition.* Academic press, 1992.

[74] A. Messiah. *Mécanique quantique.* Dunod, Paris, 1964.

[75] J. C. Morrison and C. Froese-Fischer. *Phys. Rev. A*, **35**:2429, 1987.

[76] H. Nadja, P. Quentin, T. L. Ha, and D. Samsoen. *Phys. Rev. C*, **81**:044320, 2010.

[77] P. Navrátil, M. Thoresen, and B. R. Barrett. *Phys. Rev. C*, **65**:R573(R), 1997.

[78] P. Navrátil, J. P. Vary, and B. R. Barrett. *Phys. Rev. C*, **62**:054311, 2000.

[79] P. Navrátil, J. P. Vary, and B. R. Barrett. *Phys. Rev. C*, **84**:5728, 2000.

[80] A. Nogga, H. Kamada, and W. Glöckle. *Phys. Rev. Lett.*, **85**:944, 2000.

[81] R. Padjen and G. Ripka. *Nucl. Phys.*, **A149**:273, 1970.

[82] D. Peña Arteaga and N. Pillet. work in progress.

[83] S. C. Pieper, K. Varga, and R. B. Wiringa. *Phys. Rev. C*, **66**:044310, 2002.

[84] N. Pillet, J.-F. Berger, and E. Caurier. *Phys. Rev. C*, **78**:024305, 2008.

[85] N. Pillet, P. Quentin, and J. Libert. *Nucl. Phys. A*, **697**:141, 2002.

[86] N. Pillet, V. G. Zelevinsky, M. Dupuis, J.-F. Berger, and J.-M. Daugas. *Phys. Rev. C*, **85**:044315, 2012.

[87] H. D. Politzer. *Phys. Lett.*, **30**:1346, 1973.

[88] S. Péru, J.-F. Berger, and P. F. Bortignon. *Eur. Phys. J. A*, **26**:25, 2005.

[89] S. Péru, H. Goutte, and J.-F. Berger. *Nucl. Phys. A*, **788**:44, 2007.

[90] S. Péru *et al. Phys. Rev. C*, **83**:014314, 2011.

[91] P. Quentin, H. Laftchiev, D. Samsoen, I. N. Mikhailov, and J. Libert. *Nucl. Phys. A*, **734**:477, 2004.

[92] P. Ring and P. Schuck. *The Nuclear Many-Body Problem.* Spinger-Verlag, New-York, 1980.

[93] G. Ripka and J.-P. Blaizot. *Cours de Physique Nucléaire théorique.* CEA, Saclay, 1978.

[94] D. J. Rowe. *Rev. Mod. Phys*, **40**:153, 1968.

[95] M. J. Savage. *arXiv*, 1309.4752v1, 2013.

[96] K. W. Schmid, L. Satpathy, and A. Faessler. *Z. Physik*, **267**:345, 1974.

[97] I. Shavitt and R. J. Bartlett. *Many-body methods in Chemistry and Physics.* Cambridge University Press, 2009.

[98] T. H. R. Skyrme. *Phil. Mag.*, **1**:1043, 1956.

[99] T. H. R. Skyrme. *Nucl. Phys.*, **9**:615, 1959.

[100] D. J. Thouless. *Nucl. Phys.*, **22**:78, 1961.

[101] D. J. Thouless. *The Quantum mechanics of many-body systems.* Academic, New-York, 1961.

[102] K. Tsukiyama, S. K. Bogner, and A. Schwenk. *Phys. Rev. Lett.*, **106**:222502, 2011.

[103] N. Vinh Mau. *Quelques applications du formalisme des fonctions de Green à l'étude des noyaux.* Lecture notes, 1979.

[104] M. Wang *et al. Chin. Phys. C*, **36**:1603, 2012.

[105] S. Weinberg. *Phys. Lett. B*, **91**:51–55, 1980.

[106] H. J. Werner and W. Meyer. *J. Chem. Phys.*, **74**:10, 1981.

[107] R. B. Wiringa, V. G. J. Stoks, and R. Schiavilla. *Phys. Rev. C*, **51**:38, 1995.

[108] D. L. Yeager and P. Jørgensen. *J. Chem. Phys.*, **71**:2, 1979.

[109] S. Yen *et al. Phys. Lett. B*, **124**:471, 1983.

[110] H. Yukawa. *Proceeding Phys. Math. Soc. Japan*, **17**:48, 1935.

[111] H. Zarek *et al. Phys. Lett. B*, **80**:26, 1978.